AN EMPIRICAL STUDY OF FLOOD WAVE IMPACT PRESSURES

TO DETERMINE THE EFFECTIVENESS OF NEW SEAWALL DESIGNS

USING A DAM-BREAK APPROACH

PETER BABATUNDE ADEGOKE

A THESIS SUBMITTED IN PARTIAL FULFILMENT OF REQUIREMENTS OF LIVERPOOL JOHN MOORES UNIVERSITY FOR THE DEGREE OF DOCTOR OF PHILOSOPHY

FEBRUARY, 2014

ABSTRACT

Coastal flooding and erosion, a major consequence of coastal natural events can result in physical devastation, threats to human health and safety, detrimental effects on ecosystems, and severe economic losses to individuals and to society. These potentially devastating consequences are therefore justifying efforts to reduce both their occurrence and severity.

Seawalls of varying slopes with wave energy dissipaters to create various degrees of roughness on their surfaces have been proposed as a potential evolution in the design of coastal defences. This present study therefore aimed at investigating the energy dissipating ability, in terms of impact pressures, of newly designed seawalls which incorporate unique energy dissipaters, with the ultimate goal of predicting the effectiveness of these new designs.

To achieve these aims, a novel technique for generating floodwater waves has been developed and applied to new seawall models. A Low Cost Wave Tank (LCWT) with water release gate mechanism (dam-break method) was primarily designed and constructed for this purpose. Apart from the smooth surface wall model, geo-grid materials of varying textures and grit sizes have been used to model different degrees of surface roughness with each model subjected to varying wave heights and wall angles. The experimental tool and technique had been found to be effective and relatively economical while the gate release system represented a good approximation of instantaneous dam-break problem.

The innovative imaging system (IS) and the sensor signal capture (SSC) techniques used for estimating flow velocity were found to be in close agreement with the commonly used PIV method, thus, could be a useful laboratory scheme for analysing hydrodynamics model studies. The study has also found the location of maximum impact pressures for the vertically inclined smooth surface wall model, to be varied from that of sloping forms which is in agreement with the propositions of most previous researchers. The maximum impact pressures have been found to be about 1.4 to 40 times the hydrostatic pressure which is within the range previously suggested by other researchers. Also, angle 75^{o} appeared to be the best sloping position for the wall models investigated and in general, IMACTS wall seemed the most superior surface in terms of energy dissipation in vertical form. This implies that the harder the surface of the defence wall or/and the higher the degree of surface roughness the greater the energy of the floodwater waves that would be dissipated. Again, the predictive model equations proposed in

this study are useful for the purposes of assessment of the suitability of the seawalls and the mitigation against flood hazards.

ACKNOWLEDGEMENTS

First and foremost, I would like to acknowledge and thank my Directors of Studies, Dr William Atherton and Professor Rafid Al Khaddar for given me this rare opportunity in terms of funding. Without the funding from the University Research Funds which came through them I wouldn't have been able to progress this research in the first instance. Again, I am grateful to them for their input and guidance at every phase of the research.

I am also particularly grateful to my wife whose experience of being in the same position nine years ago makes her to understand the immensity of the work I am involved in. I am not only thankful to her for her understanding but also for her encouragement and valuable advice when needed. More importantly, for the profound LOVE she offers whenever the mission looks vague and I feel downcast. I will not but remember to appreciate my girls Shalom, Testimony and Goodness for their in-depth understanding of why I needed to pursue the degree at this time and for coping with my absences.

The contributions of Dr Geoff Cullen (Senior Research Assistant) and Malcoln Feegan (Senior Technical Assistant) cannot be over-emphasised. Geoff used his wealth of knowledge and experience to make the sensors and data loggers work while Malcoln also used his expertise and skill in the design and construction of the rig. Also, I would like to thank all my colleagues in the research hub who at one time or another helped in solving various computer problems.

Finally, I would like to acknowledge the financial help I received from the School of the Built Environment in terms of stipend in the final year of the programme.

GOD BLESS YOU ALL!

DEDICATION

This Thesis is dedicated to:

My Darling Wife, Dr (Mrs) Adetoro ADEGOKE and my wonderful girls Shalom, Testimony and Goodness ADEGOKE for giving me their LOVE, SUPPORT and ENCOURAGEMENT to make the DREAM realised.

LIST OF PUBLICATIONS

The research so far has produced and in the process of producing the following publications:

(1) Adegoke, B. P., Atherton, W. and Al Khaddar, R. M. (2011) "Effects of Tsunami on Coastal Waters: A New Hard Engineering Approach of Mitigation" **Extended Abstract,** *12th International Water Association UK Young Water Professional Conference Proceedings,* The University of Edinburgh, 13th – 15th April, 2011, pp 15-16

(2) Adegoke, B. P., Atherton, W. and Al Khaddar, R. M. (2011) "An experimental study of a new seawall design for the mitigation of Tsunami" **Full Paper,** *6th Annual Liverpool BEAN Conference Proceedings*, Liverpool John Moores University, 10th May, 2011

(3) Adegoke, P. B., Atherton, W. and Al Khaddar, R. M. (2012) "Seawall Design and Construction: Moving Toward A More Sustainable Method" **Full Paper,** *7th Annual Liverpool BEAN Conference Proceedings*, Liverpool John Moores University, 30th May, 2012

(4) Adegoke, P. B., Atherton, W. and Al Khaddar, R. M. (2013) "A Laboratory Investigation of the Effectiveness of New Seawall Designs for the Mitigation of Floodwater Waves using Dam-break Approach" **Extended Abstract,** *8th Annual Liverpool BEAN Conference Proceedings,* Liverpool John Moores University, 6th June, 2013

(5) Adegoke, P. B., Atherton, W. and Al Khaddar, R. M. (2014) "A review of effects of Tsunami on Coastal Waters and Hard Engineering Approach of Mitigation" **Full Paper,** *Water and Environment Journal,* Manuscript Number WEJ-5362-11 (**Under Review**)

(6) Adegoke, B. P., Atherton, W. and Al Khaddar, R. M. (2014) "Dam-break Flow: A Novel Simple Method for Measuring Flow Velocity" **Full Paper**, *4th International Conference on Flood, Recovery, Innovation and Response (FRIAR),* Poznan, Poland, 18 – 20 June 2014

(7) Adegoke, B. P., Atherton, W. and Al Khaddar, R. M. (2014) "A Simple Experimental Approach To Dam-break Problem – Surge Characteristics and Front Water Propagation Velocity" (**Preparation in progress**)

(8) Adegoke, B. P., Atherton, W. and Al Khaddar, R. M. (2014) "Prediction of wave pressures on vertically inclined smooth surface seawalls" (**Preparation in progress**)

(9) Adegoke, B. P., Atherton, W. and Al Khaddar, R. M. (2014) "Surface Roughness Effect of Vertical and Sloped Seawalls for Floodwater Waves" (**Preparation in progress**)

(10) Adegoke, B. P., Atherton, W. and Al Khaddar, R. M. (2014) "An Investigation of Floodwater Wave Pressures on Inclined Seawalls" (**Preparation in progress**)

CONTENTS

LIST OF FIGURES

LIST OF TABLES

ABBREVIATIONS/ACRONYMS

CIRIA – Construction Industry Research and Information Association

SWL – Still Water Level

DSWL – Downstream Water Level

MRA – Multiple Regression Analysis

RDEPTH – Initial Reservoir Depth

WSL – Wall Slope

SPSS – Statistical Package for Social Scientists

ANOVA – Analysis of Variance

P-P – Normal Probability Plot

Mhp – Minikin hydrostatic pressure

Fhp – Fukui et al. hydrostatic pressure

NF – Natural Frequency

PIV – Particule Image Velocimetry

LIST OF SYMBOLS

C	Wave celerity
G	Acceleration gravity
t	Time
v	Flood wave propagation velocity
A	Area
E	Energy
F	Force
F_I	Impact Force
F_r	Froude number
P	Pressure
P_{max}	Maximum impact pressure
P_h	Hydrostatic pressure
P_o	Atmospheric pressure
P_d	Dynamic pressure
P_i	Impact pressure
x	Distance/Length
%	Percentage
m	Meter
cm	Centimeter
s/sec	Second

S	Slope
V	Volume
D	Water depth
H	Flood wave height
H_s	Significant wave height
D_o	Initial reservoir depth
θ	Angle
ρ	Density
t_{op}	Gate opening time
H_{inc}	Incident wave height
H_{imp}	Wave height at impact
H_{ds}	Downstream water depth (wet-bed condition)
t_r	Rise time of maximum impact pressure
t_d	Duration of maximum impact pressure
Model-A	Smooth surface wall model
Model-B	Semi-smooth surface wall model
Model-C	IMACTS wall model
Model-D	IMICTS wall model

CHAPTER ONE

INTRODUCTION

1.1 General Introduction

For a society to develop in a sustainable manner, it has to cope with destabilizing influences such as natural and man-made disasters (Plate, 2000). Natural disasters are caused by extreme occurrences in nature for which society is unprepared. Such disasters occur when a natural hazard results in human death, injury or severe hardship, or damages public infrastructure, private property, land resources, or agricultural production. Weather-related disasters are exerting an increasing toll on developing and developed countries, destroying lives and livelihoods and hampering development processes (Zimmermann et al., 2010).

The challenges will be extended further through changes in climate. This will change profiles of natural hazards, alter underlying environmental risks and introduce new threats. Natural disasters are closely bound up with the development status of a region. They disrupt or impair development and, at the same time, a low level of development increases the chances of them occurring. A number of well documented studies (Plate, 2000, Garatwa and Bollin, 2002) show that there has been a significant increase in natural disasters over the last decade (Figure 1.1). The World Conference on Disaster Reduction emphasised that joint efforts are needed to prevent natural hazards from translating into disasters.

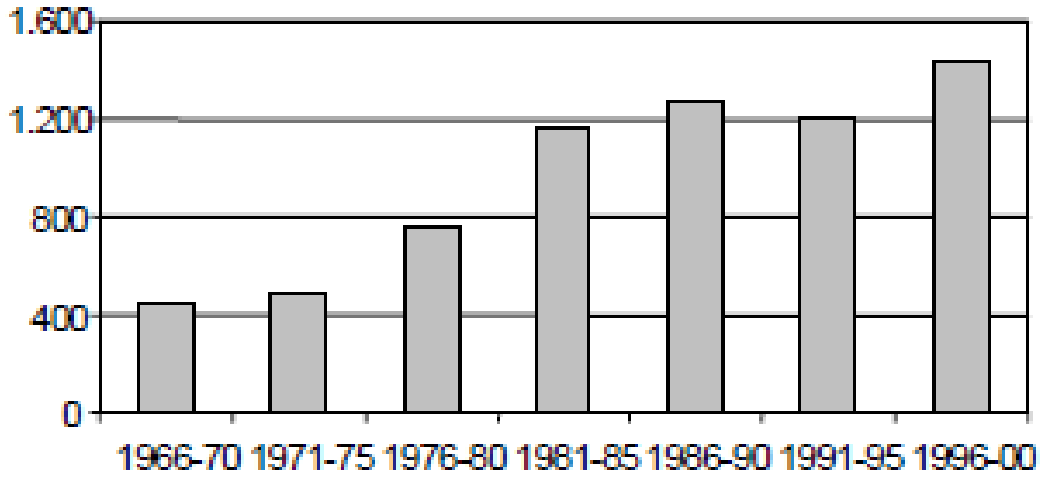

Figure 1.1: Total Number of Reported Natural Disasters Worldwide from 1966 to 2000

(Adapted from Plate, 2000)

1.2 Extent of Coastal Problem

The coastal zone is a dynamic area of natural change and of increasing human use. It is among the world's most densely populated and most industrialised areas (Vallinga and Klein, 1993). They occupy less than 15% of the Earth's land surface; yet accommodate more than 60% of the world population (Mylonas and Vordonis, 2004). It is estimated that 3.1 billion people live within 200 kilometres of the sea (Herrington, 2004) and that three-quarters of the world population is expected to reside in the coastal zone by 2025 (Mylonas, 2007). Coastal zones contain rich resources to produce goods and services and are home to most commercial and industrial activities. Human activities originating from this small land area will impose an inordinate amount of pressure on the global system. For instance, in the European Union, almost half of the population now lives within 50 kilometres of the sea and coastal zone resources produce much of the Union's economic wealth. The fishing, shipping and tourism industries all compete for vital space along Europe's estimated 89 000 kilometres of coastline and coastal zones contain some of Europe's most fragile and valuable natural habitats (European Union, 2002).

Major threats for large stretches of European coasts are erosion and flooding and about one-fifth of the coastline of the European Union is presently eroding away (Martinelli et al., 2010). Coastal flooding and erosion are the results of natural events such as earthquakes, hurricanes or tornadoes, landslides, volcanic eruptions, sandstorms and tsunamis. Other events which may also cause coastal or riverine flooding and erosion include:

1. open water (regional) floods, resulting from river capacities being exceeded due to increased runoff from snowmelt and/or heavy precipitation,

2. flash floods, occurring with little warning due to the runoff response of a watershed to high intensity tidal surge and/or storm force,

3. channel jams, due to the accumulation of broken ice, debris, mud, rocks or logs in a channel, resulting in a reduction in flow conveyance capacity,

4. riverine surges, from the failure of an upstream obstruction to flow such as a dam, ice jam, or debris jam, etc.

Although natural events such as earthquakes, hurricanes or tornadoes, landslides, volcanic eruptions, sandstorms and tsunamis are peculiar for catastrophic coastal flooding however, there are many human activities such as deforestation, land reclamation and resource over-exploitation etc. that could result in a global increase in temperature as well as an increase in greenhouse gas emissions which serve as underlying factors of climate change (IPCC, 2001). Climate change has been linked with most occurring natural disasters and more importantly climate change has been reported to be a major factor for riverine, pluvial, and coastal flooding (WHO, 2002).

A tsunami is a wave train, or series of waves, generated in a body of water by an impulsive disturbance that vertically displaces the water column, which could be a consequence of earthquake natural disaster. They have a long history of causing coastal flooding resulting in devastating damage and loss of life along low-lying coastal areas around the world. Tsunamis may inundate the shoreline as turbulent bores similar to the bores and surges resulting from flash floods and dam failures (Ramsden, 1996). Hence, the bores generated in the events of dam-breaks may be considered for the study of the terminal effects of tsunamis although a

complete study of the tsunami phenomenon could also involve a series of sub-topics of fundamental importance both from a geological and hydrodynamic point of view.

A dam breach (dam-break) is the result of a sudden release of fluid in a channel which may happen in various forms and generates a highly unsteady flow motion, called a dam-break wave (Chanson, 2008). According to Biscarini et al. (2010), it is the partial or catastrophic failure of a dam which leads to an uncontrolled release of water resulting in the development of a flood wave and such events have been responsible for the loss of numerous lives in the riverside and coastal areas (Chanson, 2009). With increasing populations and the construction of infrastructure in coastal zones, the effect of these waves has become a major concern (Langford et al., 2006).

Coastal flooding and erosion can result in physical devastation, threats to human health and safety, detrimental effects on ecosystems, and severe economic losses to individuals and to society. Concern is therefore growing worldwide regarding the extensive and catastrophic flooding being experienced in different parts of the world. For example, flood disasters in general account for about one third of all natural catastrophes in the world (by number and economic loss) and are responsible for about one half of the fatalities (Berz, 2000). In the 1990s alone, there were two dozen floods that caused more than 1,000 fatalities or one billion dollars (US) in material damages (Kundzewicz and Takeuchi, 1999). Besides, China has a long and terrible history of flooding with 1092 serious floods known to have occurred in China from 206 B.C. to 1949 A. D. (Zhang, 2002). Bangladesh has been characterised by (Chowdhury, 2000) as a state at permanent flood risk due to the unique topography, which includes a large delta and a shoreline that heightens coastal flooding. Europe incurred major flood events in 1993 (France, Italy and Switzerland), 1995 (Germany, France, Belgium and the Nertherlands), and 2002 (Germany). In 1953 a deep depression off the coast of the UK caused a tidal surge to build up in the Atlantic. The surge caused extensive flooding along the East coast of Britain, killing 307 people and making 40,000 homeless. Recent flood disaster that destroyed people, properties and infrastructures in England again illustrates the need for further research in this area. King (2004) stated that for the UK, future predictions indicate that, by 2080, floods that are now expected every 100 years will occur on average every three years.

1.3 Coastal Defence and Defence Options

This section explains the meaning and general understanding of coastal defence. It also describes the most common types of coastal defences that have been used in the UK and elsewhere around the world.

1.3.1 *Coastal Defence: What is it?*

Coastal defence is the general term used to cover all aspects of defence against coastal hazards, which includes schemes that are designed to prevent flooding and erosion of coastal regions under extremes of wave and water level serving to protect an existing coastline. Approaches to the design of coastal defence schemes include mimicking natural defence mechanisms with the potential for achieving economies while minimizing environmental impacts (this is generally known as soft solution approach). Another approach involves the construction of structures on the coastline to resist the energy of waves and tides and are referred to as hard engineering methods (Chadwick et al., 2004) while the third approach is referred to as urban planning practices.

1.3.2 *Soft Engineering Approaches*

The soft solution/engineering approaches involve the use of natural coastal ecosystems and relying on natural elements such as sands, dunes and vegetation to prevent wave forces from reaching the backshore. This technique includes the use of coral reefs, beach nourishment, sand dune stabilization, and effective use of coastal vegetation such as mangrove forest.

- ***Beach Nourishment or Replenishment***

Beach nourishment or replenishment is one of the most popular soft engineering techniques of coastal defence schemes. Beach nourishment and shingle recharge have been successfully employed along the coasts of Europe for some time mostly at Dungeness, south east England, where two nuclear power stations are protected against erosion by beach feeding although it has not received universal support by planners, engineers and the general public (Ballinger R. and Smith H., 1994).

- ***Coral Reefs***

Coral reefs are vitally important coastal ecosystems, providing local communities with a range of valuable social and economic goods and services. In addition, many reports have claimed that intact and healthy coral reefs shielded coastal communities from the worst of the tsunami's wrath (Environmental Justice Foundation, 2004, FAO, 2007). In the Maldives, for example, the extensive coral reefs surrounding the islands reportedly saved lives as they caused the wave to break offshore, dissipating much of its energy.

- ***Mangrove Forest***

The term mangrove refers to a diverse group of salt-tolerant trees and other plant species that are found along sheltered tropical and subtropical shores and estuaries. Mangroves prevent coastal erosion, and act as a barrier against typhoons, cyclones, hurricanes, and tsunamis, helping to minimize damage to property and life. Mangrove tree species that inhabit lower tidal zones can block or buffer wave action with their stems, which can measure 30m high and several metres in circumference (Environmental Justice Foundation, 2004). However, numerous field surveys and scientific studies in India, Indonesia, Japan, Malaysia, Maldives, Myanmar, Sri Lanka, and Thailand of the 2004 tsunami and other tsunami events elsewhere reported considerable evidences that coastal forests can reduce the force, depth and velocity of a tsunami. It was also revealed that coastal forest can minimise damage to property and reduce loss of life (Environmental Justice Foundation, 2004, FAO, 2007).

Development of Earthquake and Tsunami Disaster Mitigation Technologies and Their Integration for the Asia-Pacific Region (EqTAP Project) recommended the use of a coastal green belt to protect homes, as it was said to be sustainable and much cheaper than artificial barriers. Similar studies in Vietnam also demonstrate the usefulness of mangrove forests in coastal protection. Analytical models have further shown that 30 trees per 100 metre square in a 100 metre wide belt may reduce tsunami flow rates by as much as 90%. (Environmental Justice Foundation, 2004).

1.3.3 *Hard Engineering Approaches*

The Romans were the first dredgers in the Netherlands to maintain the harbour at Velsen through what we now refer to as hard engineering methods (Oleson et al., 2004). Structural or hard engineering techniques involve the use of permanent concrete and rock constructions to "fix" the coastline and protect the assets located behind it, thereby mitigating the impact of water wave. They include all defence mechanisms for shoreline protection such as seawalls, breakwaters, dikes, revetments etc. Such structures are used in coastal defence schemes with the objective of preventing shoreline erosion and flooding of the hinterland. The technique consists of interposing a static structure between the sea and the land to prevent erosion and/or flooding.

- ***Embankments***

Embankments are often mounds of earth built in low energy environments where there is minimal wave energy reaching the structure. Flood embankments are often called dykes or bunds and are constructed to prevent inundation of low-lying land by high sea levels caused by extreme tides, surges and/ or storm activity. They are probably the cheapest forms of linear coastal defence techniques. Their main purpose is to act as an impermeable barrier to the water. Examples of embankments can be found to the north of Southport where the primary and secondary defences located at Marshside are earth embankments (Sefton Council, 2007).

- ***Groins***

Groins are designed to either reduce the rate of transport of sand along a specific reach of shoreline or to completely block the alongshore movement of sand beyond a certain point. Groins are shore perpendicular protection structures often constructed in successions forcing the sand to fill to a specified level on one beach before allowing sand to be transported to the next beach in the field.

Groins are constructed with a number of different materials depending on availability, cost, and longevity. In high-energy environments, groins are typically constructed of granite, basalt

or pre-cast concrete interlocking units that resist movement. In lower energy environments, groins can be constructed of timber sheeting, poured or pre-cast concrete, metal sheeting, plastic sheeting, pilings, rock filled wire baskets (gabions), and sand filled geotextile tubes (Guo-Lin et al., 2010). Groins are often constructed of two or more materials to improve performance and cost-effectiveness. Groins are extremely cost-effective coastal defence measures, requiring little maintenance, and are one of the most common coastal defence structures.

Groins also vary in the shape of the cross-shore profile, depending on the intended function of the structure. According to Guo-Lin et al. (2010), groins can be constructed with low profile sections along the beach berm to allow the wind and storm tides to transport sand across the structure. Groins can be serrated and lowered down to the mean water level in sections along the beach foreshore and surf zone to allow breaking waves and wave run-up to transport sand across the structure. Groins can also be tapered at the offshore end to allow for unimpeded sand transport offshore of the structure (Guo-Lin et al., 2010). The size of the voids in the structure (the porosity) can also be altered to allow a certain percentage of sand to move through the structure. However, groins are increasingly viewed as detrimental to the aesthetics of the coastline, and face strong opposition in many coastal communities (Burcharth and Hughes, 2003).

- ***Breakwaters***

Breakwaters are built to reduce wave action in an area in the lee of the structure. Wave action is reduced through a combination of reflection and dissipation of incoming wave energy. Detached breakwaters dissipate waves or absorb the energy of waves so as to prevent the intrusion of waves onto the land and also help to prevent beach sand from being transported offshore so as to accumulate sand behind them. Submerged detached breakwaters are used in some cases because they do not spoil the view, but they do represent a serious non-visible hazard to boats and swimmers (Burcharth and Hughes, 2003).

- ***Water gates or Sluiceways***

Water gates or Sluiceways are disaster prevention facilities constructed across rivers, drainage channels and canals to protect the hinterland from storm surges and tsunamis. Of the water gates, sluiceways are water conveyance facilities to drain the target areas by use of tidal action.

- ***Levees***

Levees are structures or facilities constructed by a mound of soil with concrete or other surface material. They also prevent inland intrusion of storm surges, high waves and tsunamis and the erosion of coasts by waves.

- ***Gabions***

An unconfined flow of water causes erosion and may result in costly damage to most hydraulic structures used in coastal defences. In order to prevent this potential danger, gabion boxes and mattresses may be used to guide the flow of water. Gabion retaining walls are built as gravity structures and can withstand harsh environmental and climatic conditions. Flexible gabion structures used in the construction of retaining walls are a simple functional solution (Guo-Lin et al., 2010).

Gabions can be used for the construction of hydraulic structures. For instance, recharge dams to augment groundwater, and flood control dams for flood routing can be constructed economically using Gabions (Figure 1.2). Basic design principles of using gabion boxes and mattresses maximise the environmental benefits of construction works. The natural appearance, flexibility and low cost of gabions make them ideal for a wide range of environmental applications. These include housing developments, river management, coastal defence, road building, erosion prevention on degraded land etc. Gabions often have the benefit of allowing the retention of existing features which would otherwise be destroyed by sloping banks. When used in the sea, gabions can create artificial reefs and help expand fish breeding areas (Guo-Lin et al., 2010).

Special polyvinyl coated wires, highly resistant to corrosion and other environmental effects are used in the manufacture of gabions for marine works. Beach protection, marinas, retaining walls, ramps, piers and especially small jetties can be built at great speed with the minimum of cost. Gabions allow wave energy to be dissipated thus conserving beaches and preventing erosion. Other important features and structures on the shoreline can also be protected. Gabions may be used to build dykes and groins as well as guiding and regulating water flow in river and marine structures. Gabions are widely used for channel lining works to control and guide the course of water through channels and prevent erosion of the banks. Due to the flexibility and permeability of these structures, they permit the natural movement of ground water. In most cases, as time goes, voids may be filled by vegetation and silt which will reinforce the structure and give extra strength (Guo-Lin et al., 2010).

Gabions have been used successfully in mountainous areas to prevent and repair landslides. The gabion mesh rolls can be laid down the cliff face to prevent rocks falling. The gabion mesh obstructs rock fall and protects infrastructures. Gabions are used on a small scale and are wire mesh baskets filled with cobbles or crushed rock. They are flexible and porous forms of defences which can absorb some wind and wave energy by reducing scour that can often cause problems with impermeable sea defences such as sea walls. These are used in a small area on the Sefton Coast at Crosby in front of the Coastguard station (Sefton Council, 2007).

The design principle, functions and material properties of groins and gabions were utilised in the present study to investigate the behaviour of these materials in terms of dissipation of the energy of the waves when incorporated into the surface of seawalls. This may enhance the performance of the seawall by carrying out the dual functions of dissipating the energy of the waves and prevention of scour at the base of the wall. However, geo-grid materials which have similar characteristics of groins and gabions were used in the present study as these are most feasible for the experimental setup.

Figure 1.2: **Gabions used for scour protection along embankment**

- ***Rock Armour and Gabion Headlands***

The main difference between rock armour and seawalls is that rock armour is permeable. It is this permeability that allows it to dissipate the energy of storm waves and prevent erosion. A similar effect may be created through the use of precast concrete units that are designed to be permeable. An example of rock armour can be seen at Seaforth docks (Figure 1.3). Precast concrete units can be seen in use at Blackpool where they are used in combination with seawalls (Sefton Council, 2007).

Figure 1.3: Rock Armour at Seaforth Docks, Crosby

(Adapted from Coastal Defence Sefton Council, 2007)

- ***Revetments and Sea Walls***

In some cases the distinction between revetments and seawalls is not clear-cut, with different people using different terminology. Many new seawalls are said to be more accurately termed revetments since they consist of an embankment core covered by a protective surface layer (McConnell, 1998). Seawalls, however, typically have the following features; a beam along the toe of its seaward face often supported on piles, a rear wall and the crest (see section 2.2.3 – structural design concept of seawall). Seawalls are impermeable structures designed to provide a defence against the action of the sea. They are often made of concrete or rock and vary in shape depending on the local conditions. They are built at the base of a cliff or at the back of a beach, used to protect a settlement against the attack of waves, erosion or flooding. They are onshore structures built parallel to the shoreline as a reinforcement of a part of the coastal profile with the principal function of preventing or alleviating overtopping and flooding of the land and the structures behind due to storm surges and waves. Revetments are wooden slanted or upright blockades, built parallel to the sea on the coast, usually towards the back of the beach to protect the cliff or settlement beyond. Since the wall greatly absorbs the energy instead of reflecting, it erodes and destroys the revetment structure and that means it requires major maintenance within a moderate time of being built; this is greatly determined by the material the structure was built with and the quality of the product (Burcharth and Hughes, 2003).

Some will have a vertical wall that tends to result in spray coming over the wall and can have a detrimental effect upon the beach by reducing its height. Others will have a slope leading up to a curved wall that is designed to reduce the size of the wave reaching the wall and then to reflect it back out to sea. Older style vertical seawalls reflected all the energy of the waves back out to sea, and for this purpose were often given re-curved crest walls which also increase the local turbulence and thus increase entrainment of sand and sediment (Burcharth and Hughes, 2003). Modern seawalls aim to destroy most of the incident energy, resulting in low reflected waves and much reduced turbulence and thus take the form of sloping revetments. Seawalls are probably the second most traditional method used in coastal defence and management (Burcharth and Hughes, 2003). The difference in approaches to design can be clearly seen when

comparing the seawall at Crosby (Figure 1.4) built in the sixties with the seawall at Southport built 1997 to 2002 (Figures 1.5 and 1.6).

Figure 1.4: Crosby Seawall

(Adapted from Coastal Defence Sefton Council, 2007)

Figure 1.5 : Sloping concrete revetment in front of the sea wall at Southport

(Adapted from Coastal Defence Sefton Council, 2007)

Figure 1.6 : Seawall at Southport completed in 2002

(Adapted from Coastal Defence Sefton Council, 2007)

1.3.4 *Urban Planning Practices*

The achievement of any holistic framework of coastal defence is heavily dependent on the integrated coastal zone management and urban planning approaches to prevent development in erosion- or flood-prone areas. Urban planning involves measures which promote successful evacuation from coastal hazards such as tsunamis or earthquake which could cause flooding of the coastal communities. It includes simple warning systems, hazard vulnerability and risk maps, evacuation routes and major structures and flood resistant buildings. Today, the importance of planning techniques as a means of controlling development which threatens the natural resources of the coastal zone cannot be overestimated. Planning techniques are recognised as valid measures for coping with risks from natural hazards along the coastal zone, so it is vital that conservation of this zone is incorporated into planning.

Planning authorities have realised that 'hard' solutions are not permanent or reliable and that the soundest approach to coastal protection and sea defence relies on increasing co-ordination between planners and engineers, particularly at local levels. The UK Government has produced draft policy guidance on coastal planning and commissioned a 2 year study on planning policy for the coast and earth science information in support of coastal planning (Ballinger and Smith, 1994). A major item in urban planning is the land-use regulation. Important facilities such as town offices, police and fire stations as well as facilities such as hospitals, homes for the aged and nursery schools should not be located in the flood- or tsunami-prone low land. The flood-resistant building zone, i.e. alignment of substantial buildings along the shoreline is a hopeful countermeasure.

Studies have revealed that building survivability varies with construction type and flood or tsunami run-up height (Yeh, 2007). In recent evidence of the 2004 Indian Ocean tsunami, it was found that for a given tsunami height, wood frame construction experienced considerably more damage and was frequently destroyed, while reinforced concrete structures generally sustained only minor structural damage (FEMA, 2008). Hence, a good number of the earthquake-resistant reinforced concrete buildings could withstand tsunamis and protect the wooden houses behind in properly planned coastal areas. Elevating structures a few feet above the maximum potential water level provides a buffer against future sea level rise and long-term shoreline recession. Stronger connections of roof, wall plates and storm shutters harden the building against the on-coming wave. The Federal Emergency Management Agency in

the USA (FEMA) Act – Public Law 106-390 highlights the importance of communities planning for disasters before they occur. It emphasizes pre-disaster infrastructure mitigation planning to reduce disaster losses and the streamlining of federal disaster programs to promote mitigation (United Nations Educational Scientific and Cultural Organization (UNESCO), 2009). The Crescent City/Del Norte County Hazard Mitigation Plan in California also outlines long-term planning that should be fulfilled prior to disasters, to help reduce the impacts of natural hazards and increase the community‘s resilience through awareness and implementation of mitigation measures (Crescent City Planning Department, 2010).

The concept of retrofitting as defined by FEMA (2008) can be seen as one of the urban planning practices. FEMA defined retrofitting as any combination of adjustments or additions to features of an existing structure that are intended to eliminate or reduce the possibility of flood damage. They include: (1) Elevating a structure in a way that the lowest floor is at or above the designated flood protection level to prevent floodwaters from reaching damageable portions (2) Relocating the structure to a place that is less prone to flooding and flood-related hazards (3) Dry flood-proofing, which involves sealing that portion of a building that is below the flood production level, making that lower level water tight (4) Wet flood-proofing, which involves modifying a structure to allow floodwaters inside the building in a way that minimizes damage to the structure and its contents (5) Floodwalls and Leeves, which are barriers that are constructed between the building and the source of the flooding to block floodwaters.

Nonetheless, the decision to choose a strategy or an option is site-specific and depends on patterns of relative sea-level change, geo-morphological setting, sediment availability and erosion, as well as a series of social, economic and political factors. However, it is important to point out here that it is rare for any single type of defence to be installed on its own; a combination of techniques often provides the best solution. Hence, on many occasions the three components (soft solution approach, hard engineering approach and urban planning approach) can be adopted in parallel to develop well-integrated hybrid solutions satisfying environmental concerns. The establishment of a sustainable coastal zone management therefore involves the use of effective and appropriate coastal defence schemes that meet economic, environmental and social criteria. But, the construction of solid structures such as seawalls, groynes, detached breakwaters, and revetments has been employed all over the world and represents a significant share (more than 70%) of the protected shoreline in Europe (European Union, 2002).

1.4 Research Background

It is generally recognised that the risk to a system is a function of both exposure to the hazards and of the resilience of the system. In the coastal systems, risk will depend on the resilience of systems to the immediate impacts of coastal hazards, for example the quality of physical infrastructure, the preparedness of communities, and the ability of the system to recover from damage associated with coastal hazards while recovery is aided by the availability of financial and other resources. Conversely, for coastal systems risk is heavily influenced by environmental and geographical factors such as elevation above mean sea level, distance from the shoreline, and the effectiveness of artificial coastal defences in dissipating the energy of the hazards such as storm surges.

But, under existing management regimes such natural and artificial barriers are unlikely to provide adequate defence particularly against long-term sea level rise (SLR). Sutherland and Gouldby (2003) stated that climate change would alter wave and water level conditions and hence affect the vulnerability of coastal defence structures. Sutherland and Gouldby research results indicated that by 2075 there would be considerable increases in overtopping rates if present-day flood defences and beaches were unchanged. The potentially devastating consequences of flooding and erosion events therefore justify efforts to reduce both their occurrence and severity. Hence, an effective coastal defence would play a significant role in reducing the level of exposure of coastal communities to any potential coastal hazards such as flooding and erosion.

Seawalls have been seen as the most common form of coastal defence because by presenting a physical barrier between land and sea, they prevent any erosion of the hinterland and protect it from flooding. Their use is worldwide and can be found on a range of coastal types (Linham and Nicholls, 2010). In spite of few limitations, hard defences such as seawalls still remain the preferred response to coastal problems in many situations. This arises for a variety of reasons:

1. Perceived security – people tend to feel safer behind a seawall than a built-up beach, even though, scientifically, the safety benefits may be the same

2. High values of the hinterland – resort areas or industrial installations need a significant physical barrier between them and the sea.

Seawall provides a high degree of protection against coastal flooding and erosion. Most coastal management authorities have resorted to shore armouring by wave-resistant seawalls of various types when justified by the economic or aesthetic value of the property to be protected (United States Army Corps of Engineers (USACE), 2003). Seawalls have the advantage of providing protection against water levels up to the design height which in the past was often based on the highest known flood level (Pilarczyk, 1998). Seawalls also have a much lower space requirement than other defences such as dikes, especially if vertical seawall designs are selected thereby reducing the overall costs of construction. Seawalls can be adapted to climate change by progressively upgrading or increasing the height of the structure in response to SLR provided the upgrade does not compromise the integrity of the structure. They are potentially long-lived structures provided they are appropriately designed and adequately maintained.

Nevertheless, the problem of structural stability under wave attack, scour in front of structures, reduction of transmitted wave energy, etc. has long been a concern for this choice of shoreline protection. A wave which is breaking or near breaking when it hits a structure can cause large peaks in pressure. These pressures, though often of very short duration (1ms in the laboratory, 10-50ms in prototype) are sometimes substantial enough to cause damage to the structure (Wood, 1997, Kirkgoz and Mamak, 2004). The research into wave pressure impact on the structure to reduce such impact as much as possible is therefore of particular importance for its design.

Vertical seawalls have been widely used around the world as shore protection structures and may come in different forms, shapes and sizes and are constructed from a variety of materials, most commonly used materials are reinforced concrete, boulders, steel, or gabions. Other seawall designers use materials such as vinyl, wood, aluminium, fibreglass composite along with large biodegradable sandbags made of jute and coir. The choice of which type of seawall is most suitable is complex and depends on many factors such as position, tidal range, depth of water, prevailing conditions of the coastal area, availability of materials and financial restrictions.

Vertical seawalls have the disadvantage of increasing the water particle kinematics in front of the structure due to significant wave reflection (Neelamani and Sandhya, 2003) by setting up a

short-crested wave system adjacent to the wall, doubling the wave heights which results in increased wave loads on the seawall and potentially causing severe erosion action on the sea bed. Recent seawalls are designed to alleviate some of the problems associated with vertical seawalls by giving them a sloping face to reduce reflection. Sloped seawalls are good energy dissipaters when compared to vertical seawalls, especially when the slope of the seawall is mild. Sloped seawalls cause phase lag of reflected waves and induce waves to break on the slope and hence dissipate a part of the incident wave energy. The amount of wave energy dissipation depends greatly on the slope provided. If the slope of the seawall is mild, then a greater number of waves break by spilling which is beneficial for force and water particle kinematic reduction (Neelamani and Sandhya, 2005). However, such seawalls are expensive to construct and the efficacy of the initial design has to be tested by physical modelling before the design is finalized.

Seawalls of varying slopes with surface energy dissipaters in the form of dentated and serrated blocks have therefore, been proposed as a potential evolution in the design of coastal defences (Neelamani and Sandhya, 2005). A less expensive steep sloped seawall with energy dissipaters distributed on its surface is then expected to hydro-dynamically replace the expensive mild sloped seawall in dissipating the incident wave energy and hence is further expected to reduce the wave reflection, wave load on the seawall, wave run-up and run-down along with toe scour. As far as wave-structure interactions and mitigation of flood wave damage are concerned, a precise understanding of flooding effects around structures is critical for accurate force and scour predictions. This knowledge can be combined with run-up height predictions as well as reflection characteristics to devise measures for limiting exposure to flood damage.

This present study is therefore aimed at investigating the effectiveness of newly design seawalls which incorporate various energy dissipaters on its surface to curtail the devastating influence of flooding and erosion of the coastal environment. This study is particularly motivated by research on tsunamis and dam break flood waves due to coastal flooding disaster caused by these phenomena. Thousands of lives have been lost in tsunami disasters in addition to the extensive damage to coastal installations and buildings. Recent tsunami incidents in Japan only strengthen the argument for further research and development in this area. As a result, the performance of coastal structures against such events has become a major concern and an important aspect of coastal management and engineering has been brought into question.

1.5 Study Justification and Originality

Literature has revealed that tsunamis may inundate the shoreline as turbulent bores similar to the bores and surges resulting from flash floods and dam failures (Ramsden, 1996). As a result, the bores generated in the events of dam-breaks may be considered for the study of the terminal effects of tsunamis. This present study adopts the dam-break method to generate floodwater waves and particularly investigates the effects of these waves on new seawall designs. The unique method of generating floodwater waves in this study allows it to be related to terminal effects of tsunami waves as suggested by Ramsden (1996) and also closely represent the real sea state at the storm zone. Sea waves are characterised as irregular, short crested and steep containing a large range of frequencies and directions. This is a novel study as newly design seawalls which incorporate unique surface-energy dissipaters are being investigated against floodwater wave generated in an exclusive way.

Moreover, it has been reported that introducing a number of dents or serrations (square or rectangular, triangular, circular or any other shape) or a degree of roughness on the surface of seawall may dissipate more wave energy than the plane or smooth surface seawalls (Neelamani and Sandhya, 2005). A review of the available literature including the works of Fukui et al. (1963), Cross (1967), Nakamura and Tsuchiya (1973), Liu et al. (2008), Synolakis (1987) and others however, suggests that no investigations have been carried out on these newly proposed designs for wave pressure loads, wave reflection, run-up and run-down. Again, the wide range of seawall slopes covered in this study also form its uniqueness as opposed limited wall slopes covered by previous studies (see section 2.3.3).

Again, most researchers who studied wave pressure loads, reflection characteristics or run-ups used random or regular waves as well as solitary waves generated with wave-makers while those who used the method of dam-break to generate waves were only interested in the measurements of the dam break flow features/hydrographs after the dam burst but not the pressure force on defence structures. This study specifically used dam-break to generate the flood waves and focus on the study of wave pressure loads on newly proposed defence structural designs. The designs have been suggested to be operative and cost-effective so it is therefore crucial that the order of wave energy dissipation and the resultant change in hydrodynamic performance of these designs at both vertical and varying slopes be extensively investigated experimentally.

1.6 Overall Study Aim and Objectives

The previous sections highlighted areas where further research into vertical and sloped structures could improve the knowledge for devising measures in limiting exposure to flood damage. The ultimate goal for this particular study is to predict the energy dissipation ability of various seawall designs against the floodwater waves generated by dam-break events. The study focused on the physical modelling of seawall structures with simple shaped energy dissipaters on their surfaces exposed to a passing of floodwater wave or a tsunami-like wave modelled by a turbulent bore generated through dam-breaks. Measurements were made of the floodwater levels at various locations, floodwater propagation speed as well as impact pressures acting on the model structures. The aim is to further the understanding of the interaction between the bore and the structure, i.e. the structure's effect on the bore as well as the bore's effect on the structure and to predict the location and magnitude of the dynamic pressure on the structures during the impact and passage of floodwater waves.

The realisation of the above overall aim therefore, requires the pursuit of the following objectives.

1. To build a laboratory facility to perform simulations of catastrophic failure of dam to generate floodwater waves in a way which is also applicable to the study of terminal effects of tsunami wave.

2. To assess and validate the performance of the constructed rig.

3. To critically observe and analyse floodwater flow characteristics as it occurs in the channel for comparison with previous studies.

4. To compute the propagation velocity and/or celerity of the floodwater in the channel at varying reservoir depths using various methods and validate the results with previous studies.

5. To examine the location and magnitude of the maximum impact pressure of the floodwater on the seawall models under investigation.

6. To examine the influence of wave heights at impact by varying initial reservoir depth on the structural integrity of the designs.

7. To investigate the effects of the surface roughness (i.e energy dissipaters) and the slopes of the wall on the dissipation of the energy of the floodwater waves.

8. To examine the validity of the experimental data obtained in this study with existing theoretical and empirical formula and develop predictive equations of wave impact pressure when wall slope and initial reservoir depth are varied.

1.7 Research Approach and Extent of the Literature Review

Following the aims and objectives set out in section 1.6, a systematic approach for this research was engineered so that it could steadily and efficiently lead to achievement of the goals of the project. To start with, a rigorous review of literature was undertaken so that a fundamental background and knowledge of wave-structure interaction could be achieved. At the same time, relevant ideas and concepts on how to solve similar problems to the quests for this research were also collected and analysed. As part of a comprehensive literature review, information on the wave pressures impinging defence structures was sought through computer aided search of publications. The computer search was carried out under general headings such as; wave forces, wave pressures, wave measurements, seawalls, etc which produce several publications for review.

Even though the project set out to focus on the wave pressure loads on structures and the laboratory modelling of the flooding phenomenon, mathematical background to the stages through which these happened is also highly important and relevant. The information gathered or data obtained in physical modelling can certainly be used as input for the numerical or computational modelling. Therefore, a brief demonstrative knowledge of theoretical and mathematical development of wave structure impact was reviewed and explained. Having reviewed various publications on the subject, appropriate methodological approach was chosen and the project moved to designing the experimental rig to achieve the research objectives.

A brief discussion on previous studies and design formula of defence structures in terms of reflection characteristics and run-up and overtopping were deliberately included in the

literature review chapter. This is because as far as wave-structure interactions and mitigation of floodwater wave damage are concerned, a precise understanding of flooding effects around structures is critical for accurate force and scour predictions. This knowledge can be combined with run-up height or overtopping predictions as well as reflection characteristics to devise measures for limiting exposure to flood damage.

1.8 Structure of the Thesis

This thesis reports the extensive literature review, methodological approach as well as research findings on the subject matter. It is mainly divided into seven chapters. The first chapter is an introduction which gives a general overview of the subject, outlines the background of the study and clearly states the aim and objectives of the research project.

Chapter 2 is an extensive literature review which includes the mechanisms of wave actions on coastal structures, a review of seawall structural design concept as well as design and construction considerations which led to the assessment of various equations for estimating wave impact pressures and forces on walls, an evaluation of previous studies on wave impact pressures and forces on defence structures, a brief account of the theoretical background of breaking and non-breaking waves against coastal structures and finally a description of various existing methods of velocity measurements in dam-break flow and the concept of wave celerity.

Chapter 3 looks at various forms of the governing equations which include: a consideration of shallow water equations and its applicability to dam-break flood waves, an appraisal of the theoretical concepts of dam-break flow and finally an analysis of impulse-momentum relationship.

Chapter 4 addresses the methodological approach for the study which detailed the design and construction of the experimental rig including instrumentation, experimental programme and procedures as well as systems for data acquisition and analysis.

Chapter 5 covers data analysis and results. In this chapter, some of the main features of the flow structure were described and few qualitative and quantitative observations about the flow were analysed. These include the wave heights generated within the channel as initial reservoir

depth is varied, the front water propagation velocities, the impact pressure on the wall and the behaviour/characteristics of wave impacts on various wall orientations and surfaces.

Chapter 6 is the discussion of the results with emphasis on some of the major findings in the present study.

Chapter 7 is the concluding chapter which highlights the original contribution of this study to the body of knowledge and also includes discussion on the progress made as well as difficulties encountered during the investigations. This chapter also summarises the expected future work and recommendations to progress the research.

1.9 Summary

This chapter has discussed the extent of coastal problem and in particular coastal flooding and erosion. Coastal flooding and erosion has been attributed to the occurrence of natural events such as earthquakes, hurricanes or tornadoes, landslides, volcanic eruptions, sandstorms and tsunamis. It might also be the results of man-made activities such as deforestation, land reclamation and resource over-exploitation etc. More importantly, climate change has been linked with most occurring natural disasters. However, due to the damage caused by tsunami and dam-break in the past throughout the world and being the most occurring events that are responsible for coastal and/or riverine flooding and erosion, the chapter has emphasized more on these two phenomena. Moreover, the approach of the present study is to generate the waves developed as a result of these events.

The chapter also discussed the meaning and general understanding of coastal defence schemes. It also described the most common types of defences against coastal flooding and erosion. Approaches in the categories of soft engineering, hard engineering and urban planning practices were itemized. However, the importance as well as the problem of seawall defence scheme was stressed.

The problem of seawall defence schemes in terms of structural stability under wave attack, scour in front of structures and reduction of transmitted wave energy, which has been a major concern for this defence option, was mentioned in the chapter. Previous research works to alleviate some of the problems associated with this option were revealed and the need for

further research is emphasized in the chapter. The ultimate goal of the present study as well as various objectives to achieve this goal was identified. The chapter finally discussed the study approach and the way the entire thesis is structured.

CHAPTER TWO

LITERATURE REVIEW

2.1 Wave Actions On Defence Structures

2.1.1 *Introduction*

Wave action is a major consideration in the detailed assessment of the relative suitability of coastal defence structures. It is central for the evaluation of the hydraulic performance of any shoreline structure for example, seawall. Significant consideration should be given to the interaction of the wall with the propagation of waves. Thomas and Hall (1992) pointed out that waves reaching a seawall will reflect, dissipate, overtop or be subjected to a combination of the three actions. In essence, the purpose of the wall is to alter the balance of these three processes, and in so doing to reduce the amount of wave action reaching the land behind it. An evaluation of the mechanism of these three processes is therefore central to the design of any seawall structure. Thus, the following sections (sections 2.1.2 to 2.1.4) discuss the general mechanisms of these wave-structure interactions with emphasis on the three main phenomena that are of great importance to the present study.

Nevertheless, subsequent sections in this chapter also presented a review of seawall design concepts as well as design and construction considerations and also various methods/ formulae of estimating wave pressure, a detailed evaluation of previous studies on wave impact pressures and forces, the theory and studies on breaking and non-breaking waves and finally a description of various methods of velocity measurements in dam-break flow and the concept of wave celerity.

In general, wave action often leads to the generation of a number of forces, and flow conditions, requiring calculation by the designer. However, the primary hydraulic and structural parameters for which values may require calculations include: wave reflection**,** wave run-up and overtopping, wave impact pressures and forces, wave run-down for scour protection etc. It should be noted that this list cannot be exhaustive but occurrences that are only relevant to this study are stressed and discussed in the following sections.

2.1.2 *Wave Reflection Characteristics*

As earlier discussed wave energy arriving at a coastal structure may experience a number of processes of concern to the designer. The main processes include absorption or dissipation, transmission by overtopping and reflection. The estimation, or measurement, of wave reflections, and some of the effects of reflected wave action on the defence structures are discussed in this section.

All seawalls reflect waves, and reflections can have a significant impact on the coastal regime. The increase in reflections from the shore as a result of building a seawall will increase the amount of wave energy seaward of the wall. Wave incident on a vertical impermeable wall will be reflected almost totally giving rise to a reflected wave, approximately equal in height to the incident wave (Melito and Melby, 2002). The resulting wave pattern can produce increase run-up of waves and a severe deterioration in boating/swimming conditions seaward of the wall. As a result of reflections, wave action in front of the seawall will be increased which thus increases the risk of local scour, reduces the foreshore level and undermines the seawall. Reflected wave action on shoreline structure often leads to standing wave patterns produced by the interaction of incident and reflected waves which appear as a confused sea in front of the seawall.

Many of the available studies on the estimation of reflection characteristics of walls are based on regular waves, and often assume the use of linear wave theory (Goda and Suzuki, 1976, Isaacson, 1991). In most instances the reflection performance of a structure is described in terms of a reflection coefficient, K_r. This may be defined in terms of the total incident wave energy, E_i, and the total reflected by the structure, E_r, thus:

$$K_r = \left(\frac{E_r}{E_i}\right)^{\frac{1}{2}} \quad \ldots\ldots 2.1$$

Equation 2.1 is equivalent to the ratio of the reflected to incident wave heights in a regular wave train. For random wave conditions, K_r, may be defined in terms of the incident and reflected energy densities, S_i and S_r respectively:

$$K_r = \left(\frac{S_r}{S_i}\right)^{\frac{1}{2}} \quad \ldots\ldots 2.2$$

The prediction of the level of reflected wave energy is addressed by various researchers, using different approaches (Allsop and Hettiarachchi, 1988, Kajima, 1969). Both analytical and experimental techniques are reported. In general, however, most methods rely on model tests to determine values of the empirical coefficients used. Methods for the measurement and analysis of incident and reflected waves were discussed by Kajima (1969), Goda and Suzuki (1976) and Thornton and Calhoun (1972). In addition, Mallayachari and Sundar (1994) developed a computational method of measuring and analysing both incident and reflected waves using the original approach of Kajima.

2.1.3 *Wave run-up and overtopping*

Coastal structures, such as seawalls subject to wave attack, will experience wave run-up. If the structure crest is lower than the maximum run-up level reached in a particular storm, the structure will suffer overtopping. Wave overtopping is defined as the amount of water flowing over the crest of a coastal structure such as a seawall, a dike, or a breakwater, due to wave action. This may in turn lead to flooding and/or damage to the structure. In the planning and design of coastal structures, especially seawalls, wave run-up and overtopping are often the primary factors dictating the crest level of the wall hence a clear understanding of the processes of wave run-up and overtopping is essential to the optimum and economic design of such structures. Among the physical processes of wave-structure interaction, wave run-up and overtopping are two of the major complex phenomena (Shankar and Jayaratne, 2003) that influence the design of seawalls exposed to wave attack.

Historically, the designers of seawalls and breakwaters have often attempted to design the crest level high enough to prevent overtopping. This is done by calculating the maximum run-up level and setting the crest level above it. However, with a fuller understanding of the random nature of wave climate, it has become clear that overtopping cannot always be wholly prevented, although the mean expected overtopping discharge for a design event may be reduced to negligible proportions. Furthermore, for many structures it may be uneconomical to design a crest level above the maximum expected run-up level. The design approach for seawalls has therefore been altered to one of designing for various levels of tolerable discharge under the extreme events considered.

In seawall or breakwater design, the maximum wave run-up height is a key parameter in the design of seawall or breakwater height, while the mean overtopping rate is a key parameter for the design of seawall or breakwater crest (Allsop et al., 2005). Reports have indicated that wave run-up and the resulting overtopping events not only lead to flooding, of which the disastrous consequences are well known, but extreme overtopping events throw water over the crest with considerable velocities imposing serious hazards to both people and infrastructure (Allsop et al., 2005, Shankar and Jayaratne, 2003). The design of coastal structures therefore, should include a crest level design which takes into account an acceptable amount of overtopping. Both socio-economical and safety arguments determine this amount, for example, a high crested coastal structure with no overtopping is completely safe, but is extremely expensive to build. Moreover, such structures impose visual obstructions where the view of the sea is an important tourist attraction with a considerable economic value. However, when designing structures with a lower crest level, these structures should provide safety for people and vehicles on and behind the structure and limit damage to the structure itself as well as damage to properties behind the structure.

In an effort to provide guidelines for designing coastal structures that can withstand such aforementioned occurrences, numerous flume and basin tests of run-up and overtopping have been performed and formulae and design curves for estimating maximum run-up and average overtopping rates constructed. However, many of the attempted methods have been summarised in the Shore Protection Manual (SPM) (1984). The work presented in Shore Protection Manual (SPM) (1984) on wave run-up and overtopping is an historical work. Further review of methods of calculating wave run-up levels on smooth or sloped seawall under random wave action was presented by Ahrens et al. (1993) while more recent equations on run-ups on steep slopes have been presented by Van der Meer and Janssen (1995) and Srivastava and Sivakumar Babu (2009).

Wave run-up is often indicated by $R_{u2\%.}$ This is the run-up level, vertically measured with respect to the still water level (SWL), which is exceeded by two per cent of the incoming waves. The relative run-up is given by $R_{u2\%/Hs}$, with H_s, being the average value of the highest 1/3 part of the wave heights. H_s is the significant wave height at the toe of the structure (Van der Meer and Janssen, 1995). The relative run-up is usually given as a function of the surf similarity parameter or breaker parameter which is defined as:

$\zeta_{op} = tan\alpha / \sqrt{s_{op}}$ 2.3

ξ_{op} = breaker/surf similarity parameter

α = shoreline slope angle (generally the structure slope)

s_{op} = wave steepness = $2\pi / gT_p^2$

g = acceleration due to gravity

H_s = significant wave height near toe of the slope

T_p = peak period of the wave spectrum

When $\xi_{op} < 2$ the waves tend to break on the dike or seawall slope. The general design formula that can be applied for wave run-up on dikes is then given as:

$$\frac{R_{u2\%}}{H_s} = 1.6\gamma_b\gamma_f\gamma_\beta\varepsilon_{op} \ (with\ a\ maximum\ of\ 3.2\gamma_f\gamma_\beta \ldots\ldots 2.4$$

Where, γ_b = reduction factor for a berm, γ_f = reduction factor for slope roughness and γ_β = reduction factor for oblique wave attack. The method was developed for the Netherlands by Van der Meer and Janssen (1995) for estimating storm wave run-up and overtopping on sea dikes. The method has general applicability and is based on extensive laboratory measurements. This method, however, again distinguishes between breaking and non-breaking wave conditions, as identified by the surf similarity, ε_{op}, or breaker parameter.

The formula recommended by Srivastava and Sivakumar Babu (2009) for the estimation of wave run-up on the wall is given as:

$$\frac{Rg}{C^2} = 1.467(H/h)^{-0.0504} \ldots\ldots 2.5$$

C is the celerity of the water wave, *H* is the wave height and *h* is the still water depth at distance of 5*H* from the structure.

2.1.4 *Wave Absorption by Dissipation*

Waves impinging on a seawall may give rise to severe pressures against the wall, the magnitude of which is determined by the characteristics of the incoming wave, the history of previous waves, and the shape and construction of the wall. Waves impinging on a wall will lose energy as a result of dissipation (Thomas and Hall, 1992) primarily due to turbulence. Turbulence is induced, in the case of sloping walls, by causing the wave to break on the slope. Rough walls, such as stepped seawalls, disrupt the flow of water up and down the wall. In general terms, sloping, porous and rough walls will dissipate more energy than vertical, non-porous and smooth walls. In order for rough or porous walls to affect a substantial degree of dissipation the roughness/porosity element of the wall must be of significant thickness with respect to the proportions of the wave (Thomas and Hall, 1992). The focus of the present study is the absorption of wave energy by dissipation. The study therefore, aimed at investigating the dissipating ability of various surfaces of modelled seawalls at varying slopes. Thus, an extensive review of previous work done on this subject matter in respect to wave impact pressures and forces is dealt with separately in section 2.3. However, the following section reviews the general design, characteristics and construction of the seawall.

2.2 Seawall Structural Design Concept and Design and Construction Considerations

2.2.1 *Introduction*

Seawalls are designed to calm down the turbulent waves of the sea. Hence, most accounts of the design are given to hydraulic performance and structural issues to minimize the wave reflection and enhance the structural stability. This is because water waves attack seawalls over years and induce severe stress on the structures. The establishment of design criteria then becomes the first important step in identifying the characteristics of the seawall. Seawall design considerations should therefore cover various operational, functional, and navigational requirements, environmental and site conditions, and physical and regulatory constraints. Also, in the development phase of the engineering design, special attention should be paid to materials and structural integrity of seawalls, in order to reduce the cost for engineering

maintenance. The details that facilitate engineering maintenance such as the inspection access, maintenance easement, replacement of structural members, procedure/schedule of maintenance, etc. need to be incorporated in the engineering design (Hydraulic Research, 1987).

Moreover, a number of studies have reported lack of availability and accessibility of proper design and construction guidelines as a major contributing factor for seawall catastrophic failures (Linham and Nicholls, 2010, Department of Environment Climate Change and Water (DECCW), 2010). It is therefore necessary to provide more worldwide uniformity and effectiveness in design approaches which would be vital for the overall improvement of reliability of coastal structures. This section therefore provides a review of the important guidelines and precautions in satisfying seawall design and construction requirements. However, the criteria covered in this section should only serve as general design guideline. Appropriate literature needs to be sorted by relevant authorities and design professionals to meet their specific needs.

2.2.2 *Design Philosophy*

A prerequisite for determining design criteria is the selection of the overall standards, i.e. the required life of the seawall and the acceptable risk of being overwhelmed by exceptional waves or tides. The choice of design life requires careful consideration and regard for the marine environment in which it will function. It is usual for the design life chosen to be the economic optimum solution by which the functional requirements can be met. The Code of Practice for Maritime Structures gives recommended minimum design life for shore-protection works and breakwaters as 60 years and for sea defence works as 100 years (Allsop, 1986). However, the engineer should consider carefully the design lives that are realistically attainable both practically and cost-effectively, taking due note of such aspects as abrasion and corrosion.

The central philosophy of approach to seawall design is therefore to consider possible modes of failure and design against them. In the case of sea defences, the main modes of failures which might lead to flooding are flow under or through the seawall, flow over the seawall, and damage to the front face leading to breaching of the seawall, geotechnical instability and slope instability. The design of seawall must therefore consider all of these events to prevent flooding occurring.

2.2.3 *Structural Design Concept*

A seawall can be regarded as having elements which need to be combined to produce a coherent structure. Thomas and Hall (1992) defined the structural elements of seawall to consist of the body (which includes the front face and the core), the toe and the crest (which include the back face). The core of the seawall is often a significant part of the seawall, hence when fill is required it must be of good quality. Faces exposed to wave action are likely to require revetment or armouring and the crests will require protection if overtopping is expected.

The toe of the seawall terminates the base of the wall on its seaward face. Report has indicated that toe erosion is the most common cause of seawall failure and emphasized the importance of toe design (Mimura and Num, 1998). The primary purpose of the toe is to prevent undermining of the wall and to protect the beach or sub-strata in front of the wall against scour. The toe is also meant to improve the hydraulic performance of the wall, prevent or restrict seepage and provide structural support to the wall against sliding or toppling forward.

The crest provides the interface between the seawall and the land behind. In flood defences, it has been taken to include the back face of a flood embankment or dyke. An analysis of failure modes by CIRIA (1996) has indicated that partial crest failure is the second most common type of seawall damage leading to overtopping. The primary function of the crest is to prevent this overtopping to avoid flooding of the land behind.

2.2.4 *Design and Construction Considerations*

- ***Environmental and Safety Considerations***

With an ever-increasing array of environmental laws, regulations and requirements, more efforts are necessary to maintain compliance. As a standard procedure for the establishment of an environmental management system (EMS,) ISO 14001 covers environmental aspects of any development in terms of identification of key parameters and their overall evaluation (Yip et al., 2002). Inherently, engineers should be able to systematically improve the degraded ecosystem, reduce the marine pollution, prevent the soil erosion and sustain the economic development in coastal areas.

In respect to seawall design and construction, the major environmental aspects to be considered may include: (1) environmental benefits for the seawall installation (traditional usage, economic activities); (2) environmental elements likely to be affected (near-shore fisheries, coastal erosion); (3) potential losses or damage to natural habitats; (4) visual impacts to the landscape (channel width, tourism); (5) mitigation measures to minimize the environmental disturbance and nuisance during construction (noise); (6) measures to control debris (e.g., empty barrels, litter); and (7) associated port facilities (e.g., housing, roads, sewage).The potential environmental impact of seawall construction, like other forms of development, is assessed from two time scales: (i) short-term effect – during the construction and (ii) long-term effect – after the construction is completed (Yip et al., 2002).

This should represent good practice for all seawall proponents in ensuring that seawalls provide a safe, secure and healthy environment. Experience has shown that the establishment of environmental and safety considerations at a design stage can offer significant benefits to the consequent operations and maintenance. Early planning can make compliance with legal and technical requirements achievable without unnecessary cost and/or schedule impacts.

- ***Foundation and Material of Construction***

Generally, seawalls are gravity structures constructed of quarry stone rubble or massive concrete, constructed against land. Therefore, the earth pressure is a main design concern. These structures depend on their weight to resist overturning and to develop sufficient friction with the underlying soil to maintain their position. A seawall foundation must therefore be adequate to prevent settlement and the resulting loss of the seawall's height and structural integrity. The bases of seawalls may be widened to spread their load on the underlying soil and massive concrete seawalls may be placed on foundation piles to gain additional lateral support allowing stability against wave forces (USACE-CETN-III-8, 1981). Quarry stones of suitable size and structural properties are commonly used in seawall construction where available as they provide good habitat for marine organisms (USACE-CETN-III-8, 1981). Concrete seawalls are also common where aggregates for concrete are available. Concrete seawalls have the advantage of being built in a variety of shapes to suit their function and specific site conditions. The choice of material may depend on the consideration of other factors. According to Srivastava and Sivakumar Babu (2009) the depth of foundation (D_f) can be obtained from the Rankine formula:

$$D_f = \frac{p}{\gamma}\left[\frac{1-sin\emptyset}{1+sin\emptyset}\right]^2 \quad \dots\dots 2.6$$

Where p is the earth pressure coefficient, γ is the unit weight of water and $\emptyset$ is the angle of internal friction.

- ***Water Levels and Wave Characteristics***

The maximum water level is needed to estimate the maximum breaking wave height at the structure, the amount of run-up to be expected and the required crest elevation of the structure. Minimum expected water levels play an important role in anticipating the amount of toe scour that may occur and the depth to which the armour layer should extend. Wave heights and periods should be chosen to produce the most critical combination of forces on a structure with due consideration of the economic life, structural integrity and hazard potential for events that

may exceed the design conditions. Wave analyses may have to be performed for extreme high and low design water levels and for one or more intermediate levels to determine the critical design conditions.

Available wave information is frequently given as the energy-based height of the zeroth moment, H_{mo}. In deep water, H_s and H_{mo} are about equal; however, they may be significantly different in shallow water due to shoaling. The following equation may be used to equate the significant wave height, H_s from energy-based wave parameters:

$$\frac{H_s}{H_{mo}} = exp\left[c_0\left(\frac{d_s}{gT_p^2}\right)^{-c_1}\right] \ldots \quad 2.7$$

where T_p is the period of the peak energy density of the wave spectrum, d_s is the water depth at the toe of the structure, H_s is the significant wave height, g is the acceleration of gravity and c_o and c_1 are regression coefficients equal to 0.00089 and 0.834, respectively. This equation should not be used when $d/gT_p^2 < 0.0005$ or there is substantial wave breaking (USACE, 1995). Wave period for spectral wave conditions is typically given as the period of the peak energy density of the spectrum, T_p. However, it is not uncommon to find references and design formulae based on the average wave period or the significant wave period.

- ***Toe Protection***

Toe protection is supplemental armouring of the beach or bottom surface in front of a structure which prevents waves from scouring and undercutting it. Factors that affect the severity of toe scour include wave breaking (near the toe), wave run-up and backwash, wave reflection and grain size distribution of the beach or bottom material (USACE, 1995).

Toe stability is essential because failure of the toe will generally lead to failure throughout the entire structure. Design of toe protection for seawalls must consider geo-technical as well as hydraulic factors. Using hydraulic considerations, the toe apron should be at least twice the

incident wave height for sheet-pile walls and equal to the incident wave height for gravity walls. From the geotechnical point of view, the minimum width of the apron can be obtained using Rankine theory provided in USACE (1995) and it should be more than the product of the height of the apron and the Rankine passive earth pressure coefficient.

- ***Estimation of Wave Pressures and Forces for vertical wall***

Prediction of wave pressure forces on vertical and sloped seawalls is required for the design of walled structures in coastal waters. A number of methods are currently employed to estimate the magnitude and distribution of wave loading pressure exerted on vertical walls. The three most commonly used methods are: Goda's method which is outlined in the Japanese Design Guidelines and is used in both Japan and Europe, Minikin's method which is outlined in the Shore Protection Manual and used in the US, and Blackmore and Hewson's method which is outlined in BS 6349 and used in the design of UK structures. The development and validation of these three methods as well as the resulting design equations as described by Crawford (1999) are briefly discussed in this section.

(a)The Goda Design Method

Figure 2.1 shows the structure configuration for which the Goda method is applied and illustrates the linear pressure distribution on the wall face due to wave impact. The equations are said to be applicable to either breaking or non-breaking wave conditions Goda (1985).

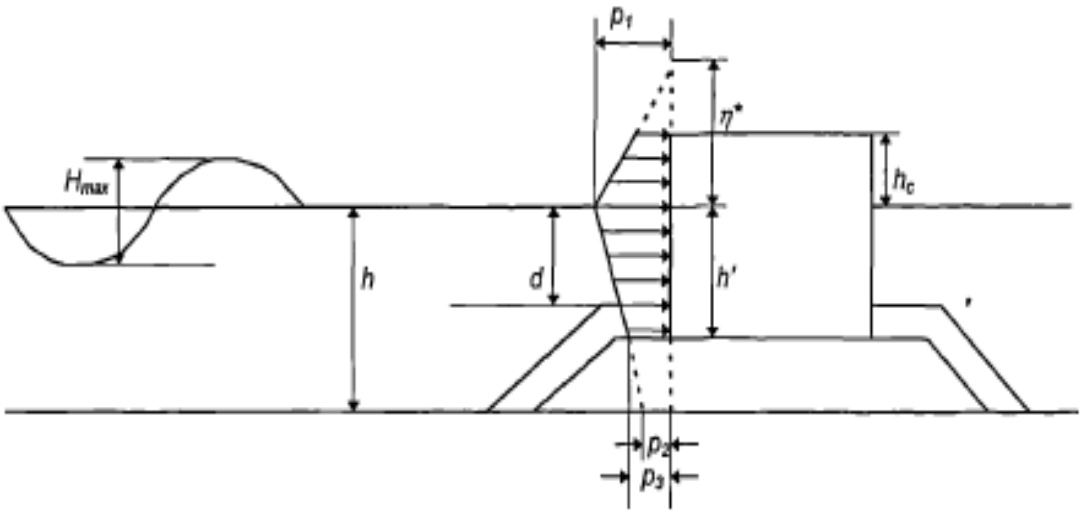

Figure 2.1 : Distribution of wave pressure on the upright section of a vertical breakwater according to Goda (1985)

The Goda method is widely adopted by the Technical Standards for Ports and Harbour Facilities in Japan even though however, it is used with caution due to the underestimation of the wave force. The principle behind this method is that the breakwaters or seawalls should withstand the force of the greatest single wave which is expected during its service life. Thus, pressure is estimated for a single extreme wave height which is usually estimated for a fifty or one hundred year return period.

The resultant formulae, developed by Goda (1985) are summarised by the equations below, with parameters as indicated in Figure 2.1

The wave pressures on the front of the vertical breakwater are estimated from:

$$p_1 = \frac{1}{2}(1 + \cos\beta)(\alpha_1 + \alpha_2 cos^2\beta)w_o H_{max} \dots\dots\dots\dots\dots\dots\dots\dots\dots\dots\dots\dots\dots\dots\dots\dots\dots\dots 2.8$$

$$p_2 = \frac{p_1}{cosh\left(\frac{2\pi h}{L}\right)} \ldots\ldots 2.9$$

$$p_3 = \alpha_3 p_1 \ldots\ldots 2.10$$

Where, w_o is the specific weight of the sea water (1030kg/m^3), β is the angle which the wave crest makes with the wall (Figure 2.1). The parameters $\alpha_1, \alpha_2, \alpha_3, L, H_{max}$ are explicitly defined in detail with various equations (Goda, 1985).

(b)The Minikin Design Method

The standard procedure followed by most harbour and coastal engineers, particularly in US is the Minikin method documented in detail in the Shore Protection Manual (SPM) (1984) though caution is given to users about the extremely high wave forces associated with this method. Crawford (1999) explained Minikin's formula as a development of Bagnold's piston model, calibrated with results from the Dieppe field measurements. Bagnold's model assumes that a wave initially encloses a pocket or lens of air and compresses it adiabatically at the moment of impact. For ease of calculation this principle was approximated to a piston model (Figure 2.2).

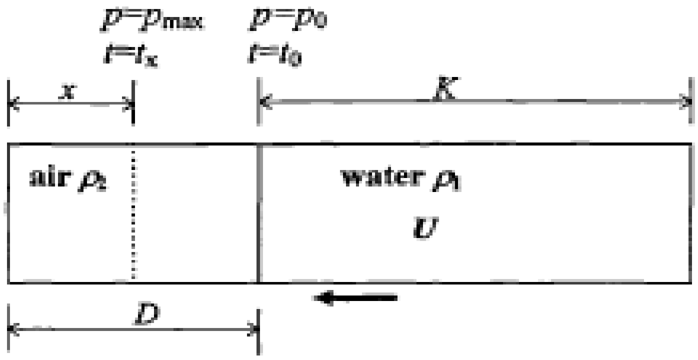

Figure 2.2 : Piston model of an entrapped air pocket according to Bagnold (1939)

The method assumed that the momentum destroyed per unit area of the air pocket is ρUK, where ρ is the density of the water, K is the effective length of the air pocket, and U is the initial velocity of the fluid as air starts to be compressed. This destroyed momentum was then expressed by Bagnold in terms of an impulse per unit area and a solution was found for predicting wave impact pressures from the wave amplitude, water velocity and width of the entrapped air pocket. Minikin further developed the Bagnold model for the prediction of maximum peak wave pressures from typical wave impact events for the design of composite breakwaters and produced the following design equation to estimate maximum pressures (Minikin, 1963).

$$p_{max} = \pi \rho g \frac{H}{L}\frac{d}{D}(D + d) \quad \ldots\ldots 2.11$$

where p_{max} is in tons (force) per square foot, ρ is the water density (in lbs/ft^3), g is the acceleration due to gravity (in ft/s^2), d is the depth of the bern (in feet), D is the water depth offshore of the structure berm (in feet), L and H are wavelength and wave height (in feet).

The above Minikin equation was again slightly modified by the Coastal Engineering Research Centre (CERC) to make it more applicable for vertical caissons and breakwaters without a substructure and also updated in convenient metric units of kPa (kN/m^2) as:

$$p_{max} = 101.1 w \frac{H_b d_s}{L_d D}(D + d_s) \quad \ldots\ldots 2.12$$

The total dynamic force acting on the wall was then found by integrating the pressure vertically up the wall with assumption that there is little variation in pressure horizontally and this is expressed as:

$$F_{max} = \frac{p_{max} H_b}{3} \left(in \frac{kN}{m^2} \right) \quad \text{...............} 2.13$$

(c) The Blackmore and Hewson Design Method

According to Crawford (1999), the British Standard Procedures (BS6349) to determine impact pressures and their distributions on breakwaters and seawalls were developed by Blackmore and Hewson (1984). The model is semi-empirical and was calibrated with results from field measurements from four seawalls in South West England. The derivation of the design pressure equations was based upon the momentum impulse relationship and takes into account the aeration using an empirical factor that depends on foreshore roughness.

Blackmore assumed that the total wave momentum was destroyed by the time the maximum impact was achieved which implies that the remaining pressure impulse after the peak pressure was hydrostatic. It was also assumed that there was little horizontal variation in pressure and that the total impact force on the wall acted uniformly over a height h_i and that h_i is approximately equal to the characteristic height H_b. The amount of air entrained in the process was also accounted for and from calibration with the field results the following design equation was developed:

$$p_p = ב \rho T C_b^2 \quad \text{...............} 2.14$$

Where, p_p is the dynamic pressure, ב is the aeration factor, and T and C_b are related to the characteristic length, $L_n = \frac{T}{C_b}$

The dynamic pressure, $p_p,$ was assumed to act uniformly over the impact area and to add to the hydrostatic pressure to give the total force per metre run (Figure 2.3).

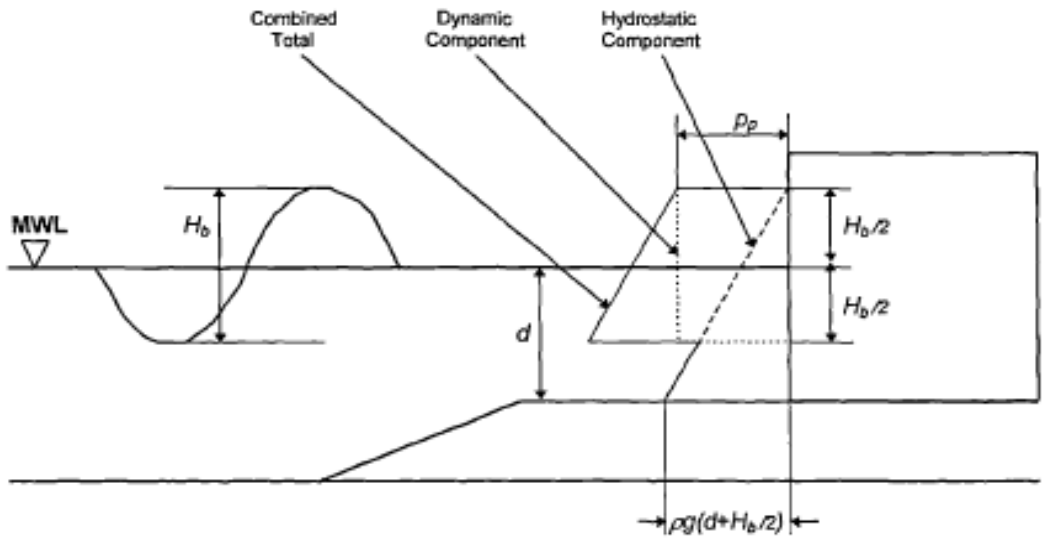

Figure 2.3 : Wave pressure distribution on a vertical seawall or breakwater according to Blackmore and Hewson (1984)

There are other analytical, experimental and numerical solutions for estimating the hydrodynamic pressure force due to wave attack on the coastal structures in the literature (Ramsden, 1996, Hamzah et al., 2000).

Ramsden (1996) presented empirical relationships for estimating the hydrodynamic force (F) on the vertical seawall type barrier as:

$$\frac{F}{F_1} = 1.325 + 0.347\left(\frac{H}{h}\right) + \frac{1}{58.5}\left(\frac{H}{h}\right)^2 + \frac{1}{7160}\left(\frac{H}{h}\right)^3 \quad \ldots\ldots\ldots\ldots\ldots\ldots\ldots\ldots\ldots\ldots\ldots\ldots\ldots\ldots 2.15$$

The equation is applicable for the range of values $0.62 \leq H/h \leq 30$ and can be used to estimate the maximum force due to bore impact. F_1 is the linear force scale (assuming hydrostatic distribution for the wave run-up equal to two times the wave height) which is used to normalize F. The value of F_1 can be calculated as below:

$$F_1 = \frac{1}{2}\gamma b(2H + h_w)^2 \quad \text{......} \quad 2.16$$

h_w is the water depth at the wall, γ is the unit weight of the water and b is the width of the wall.

- ***Empirical Equations for Wave Pressure Forces for Vertical and Sloped Walls***

Most books on coastal engineering give various methods of estimating wave impact pressures. They are usually found by calculating a maximum (design) wave for a given return period (Shore Protection Manual (SPM), 1984). The total pressure for this design wave is then calculated from one of the many available empirical equations based on the type of wave (breaking or non-breaking), the wall orientation (vertical or sloped) and many other conditions. Thus, engineers are faced with a multitude of equations for estimating wave impact pressures; the choice depends on the prevailing conditions of the area in question and the judgement of making suitable assumptions. Previous sections have dealt with the most commonly use standard design methods available for estimating wave impact pressures for vertical walls. However, this section intends to present some other important empirical equations that may also be used possibly for either vertical or sloped walls as well as the principle governing their application.

(a) Impact Pressure as a Function of Stagnation Pressure

Perhaps the most frequently used approach to explain breaking wave impact pressures assumes that a breaking wave is similar to a jet of water of uniform cross-section with velocity striking a vertical wall (Blackmore, 1982). The maximum resulting impact pressure will then be the stagnation pressure given by:

$$P_s = \frac{1}{2}\rho v^2 \quad \text{......} \quad 2.17$$

Apparently, a breaking wave does not have a uniform velocity gradient or act over a constant area, therefore a coefficient f is often added to the equation above to take account of this. Rearranging equation *2.16* into a velocity and pressure head gives;

$$\frac{P_{max}}{\rho g} = \frac{f v^2}{2} \dots \dots \dots \dots \dots \dots \dots \dots \dots \dots \dots \dots \dots \dots \dots \dots \dots \dots \dots \dots \dots \dots \dots \dots \dots \dots \dots \dots \dots \dots \dots \dots \dots . 2.18$$

where P_{max} is the maximum impact pressure from the breaking wave, and velocity *v* is often taken as the propagation speed or wave celerity *C*. The coefficient *f* ranged from 1.6 (Millar et al, 1974) to 80 (Kirkgoz, 1978). According to Blackmore (1982) this approach was first adopted by Gaillard (1904) and has been used by many investigators since at both full and model scale. This approach along with that of Bagnold (1939) assumed wave impact pressures were due to the adiabatic compression of a thin lens of air trapped between wave front and seawall. The assumptions brought about some of the most popular model equations used at present to predict wave impact pressures.

Hayashi and Hattori (1958) demonstrated how 13 independent wave pressure formulae could be reduced to the form of equation *2.17*. In their experiments using model seawalls it was found that *f* = 4 is a suitable constant for estimating the wave impact pressure using equation *2.17*. However, they concluded that impact pressures did not fit equation *2.17* well but the hydrostatic pressure closely followed the *f* = 4 line.

(b) Bagnold's Wave Impact Pressure Model

Bagnold assumed that wave impact pressures were generated by the compression of an air cushion trapped between the wave front and the seawall. Bagnold's innovative equation from his original model (see Minikin design method in section 2.4) is given as:

$$(p_{max} - p_o) = 2.7\frac{\rho v^2 L}{D} \quad \ldots\ldots 2.19$$

D is the thickness of the enclosed air cushion and *L* is the length of hypothetical piston. Bagnold found *L* was proportional to wave height (*H*), and assumed *L* = *H*/5, thus Bagnold's original equation can be written as:

$$p_i = A\rho C^2\frac{H}{D} \quad \ldots\ldots 2.20$$

Where $p_i = (p_{max} - p_o)$ (impact pressure), *C* = wave celerity, *A* = unknown

The impact pressure (p_i) is seen to vary inversely with the thickness of the enclosed air cushion (*D*), which in turn is dependent upon the surface roughness of the seawall. Equation *2.19* then suggests that if the air cushion were absent then infinite pressures would result. However, Bagnold found from his research that this was not the case, and in fact negligible pressures were produced when the air cushion was absent. Therefore, he concluded that for each seawall there must be a minimum air cushion thickness for which a maximum impact pressure results. The air cushion thickness was said to be governed by the physical properties of the seawall such as surface roughness, profile etc., and of the smoothness of the wave front. Thus for similar seawalls in similar environments the value of D_{min} (i.e minimum air cushion thickness) will probably be of the same magnitude hence suggested that when considering the maximum wave impact pressure on real seawalls it should be possible to assume D_{min} is a constant.

Therefore equation *2.19* will become;

$$p_{imax} = B\rho C^2 H \ldots\ldots 2.21$$

Where $B = \frac{A}{D_{min}}$

(c) Impact Pressure as a Function of Wave Height

A linear relationship between impact pressure and wave height was first proposed by (Hiroi, 1920). Hiroi proposed the following equation for estimating the maximum impact pressure:

$$p_{imax} = F\rho g H \ldots\ldots 2.22$$

Where F *is a constant = 1.5*, $\rho = mass\ density\ of\ water$, *g = gravity acceleration; H = wave height on the wall*

An equation of this type was also proposed by (Muraki, 1966) as follows:

$$p_i = F^1 H_o \ldots\ldots 2.23$$

Where F^l is an empirical coefficient ranging from 1 to 1.43; H_o = initial wave height

It is worthy of concluding the entire section 2.2 by reiterating the fact that many seawalls have been damaged due to the action of waves. However, a diligent construction is as important as

a sound design for the integrity and stability of seawall structures. Thus, the section has effectively dealt with the aspect of design and construction considerations of seawall defence. However, the challenges of devastating destruction of wave action on seawall has therefore instigated the current research programme which aimed at investigating the effectiveness of a new seawall design that is expected to curtail the destructive effects of such wave attacks. On the other hand, it is appropriate to review the work that has been carried out by previous researchers on this particular subject matter. Therefore, the following section (section 2.3) provides the summary of previous studies on wave energy dissipation by seawalls by absorption in terms of measurement of wave impact pressures and forces.

2.3 Summary of Previous Investigations

2.3.1 *Introduction*

Breaking waves cause shock (impact) pressures on vertical bodies which are extremely high in magnitude and short in durations compared with the pressures caused by non-breaking waves. Knowledge of the severity of breaking waves in producing these intensive loads is presumably as old as the first coastal structures, but until Stevenson (1874) recorded pressures of up to 318.8 kN/m^2 exerted by breaking waves on a vertical face, no detailed data had been available. Before then, "rules of thumb" had previously dominated the design and construction of marine structures.

As rapid economic growth began to take place in Europe and elsewhere, demand for the development of harbours was greatly increased at the beginning of the 20th Century. As a result, the ability of engineers to design breakwaters and seawalls to withstand the forces exerted by breaking waves became increasingly important and, after the destruction of a number of breakwaters by storms (e.g., Genoa Breakwater in 1920), serious investigation of the problem began (Kirkgoz, 1978).

The absence of the necessary laboratory equipment compelled early investigators to measure the force in full-scale experiments. Spring-type dynamometers were used as the pressure measuring devices but they were incapable of responding to impacts of very short duration. However, these early experiments did provide guidance to later investigators on the magnitude of impact pressures to be expected.

A major breakthrough came in the years 1933 – 1937 in the study by the French engineers Rouville, Besson and Petry. They carried out full-scale experiments at Dieppe using very delicate measuring apparatus. They measured pressures of 686.7 kN/m^2 acting on a small area and having duration of 1/200-th of a second; this was substantially different from what had been obtained previously as regards both magnitude and duration (Kirkgoz, 1978).

From 1937 onwards numerous investigators in both the laboratory and the field have collected data to determine the magnitude and duration of impact pressures. Early investigators, in particular, tended to work in the field. However, following the developments of highly sensitive miniature pressure transducers, model investigations became more popular since these allowed the various parameters which were of interest to be changed in a controlled way. The following sections (sections 2.3.2 and 2.3.3) therefore presented a detailed overview of both field and laboratory investigations stressing what was already known about the subject.

2.3.2 *Field Investigations*

Stevenson (1874) after having visually observed the damage done by breaking waves on shores over many years, started a series of field observations in 1843 at Skerryvore. In subsequent years he carried out the same type of observations at Bell Rock and Dunbar. A specially designed spring-type marine dynamometer was used and pressures up to 367.9 kN/m^2 were measured. He reported that the results could no doubt be much higher. He also gave the approximate wave heights. As an important conclusion the action of breaking waves was likened to the impact of a hard body.

Luiggi (1922) carried out some experiments at Genoa between 1882 and 1892 when he had to build a breakwater more than 1 km long in water depths of between 22 and 28m exposed to waves 6 to 7m high. He discharged conical heaps of materials of various sizes ranging from small stones weighing less than 1 kg up to 28t concrete blocks. He was able to determine the size of material which provided sufficient resistance to withstand storm waves that washed over it. Luiggi devised a diagram that could be used to predict the maximum pressures against a breakwater under the conditions of Genoa harbour. He claimed that the diagram could be applied to any height, H, of wave by multiplying the pressures by the ratio H/7. The Luiggi diagram has been used for the design of many structures. The results almost certainly do not

represent the pressures of breaking waves completely obstructed by vertical walls and composite-type breakwaters. However, Luiggi came up with the following conclusions:

(1) The maximum pressure occurs at SWL

(2) There is rapid diminution of pressure from just below SWL to the base of the wall; but above SWL, the intensity of pressure diminishes slowly with height.

Gaillard (1905) investigated wave pressures with a spring dynamometer on the Great Lakes in the years 1901 -1902. He observed the largest pressures at about SWL and found a decrease upwards to the top of the impinging wave. He pointed out that when the breaking wave is of considerable size, a large mass of water impinges with nearly constant velocity for an appreciable length of time. Therefore, it would seem that the ordinary hydrodynamic formula for the pressure of a current on a plane surface normal to the direction of flow should apply, at least approximately. Hence, Gaillard gave the pressure formula as:

$$p_{dyn} = \frac{k\gamma}{2g}(u + C)^2 \quad \text{2.24}$$

where the horizontal velocity of the motion, at impact, consists of the combined velocity of wave propagation, *C*, and the maximum orbital velocity, *u*, of a surface particle at the crest of the wave. *k* is a constant determined experimentally. The mean value of *k* was evaluated as 1.31 but the limiting value of it was found to be 2. He concluded that:

(1) The impact of a wave does not resemble that of a solid body

(2) The pressures, indicated by the dynamometers, conform to the hydro-dynamic laws governing the action of a current flowing normally against a submerged plane.

Hiroi (1920) carried out some observations using a number of spring dynamometers at Otaru harbour in the years 1905 – 1908. He offered the formula:

$$\overline{p} = 1.5H\gamma \quad \text{......} \quad 2.25$$

Where H is the height of wave at the site of the breakwater and $\overline{p}$ is the mean pressure on the wall. Hiroi suggested that equation 2.24 corresponds to a dynamic pressure exerted on a vertical wall by the fall of the wave crest on the wall at an angle of 45^{o} to the still water surface. The main conclusions were:

(1) the greatest intensity of wave pressure is found near SWL, and

(2) it acts on a comparatively small area

Molitor (1935) made some observations in connection with the seawalls and breakwater of Toronto harbour on Lake Ontario in 1915. The pressures were recorded by spring dynamometers mounted on a solid crib situated about 21m offshore in about 2.4m of water. He adopted equation 2.23 for the maximum pressure expression to define the position of the maximum impact pressure. He suggested that k in equation 2.23 could be taken as 1.8 for ocean storms. The elevation of the maximum impact pressure, h_1, above SWL was given as:

$$h_1 = 0.12H_b \quad \text{......} \quad 2.26$$

Molitor compared the computed pressure values using equation 2.23 with the observations obtained mostly by Gaillard. It was found that the computed and observed data were closely in agreement. He also reported that this method of analysis had been successfully applied to several existing breakwater structures on the Great Lakes. It should be noted, however, that the formula predicts pressures which are low compared to many results. This is almost certainly

because of the bed slope at the location of the experiments as bed slope has been found to have a considerable effect on impact pressures. Mild slopes were reported to produce relatively low pressures.

Till 1938 the most sophisticated pressure measuring device employed in the field was the spring dynamometer. Such dynamometers were incapable of responding to sudden pressure variations; hence the results of those investigations were regarded only as time-averaged pressures, not as the maximum pressures of structural significance. However, full scale investigations published by Rouville, Beson and Petry in 1938 at Dieppe during the years 1933 – 1937 and reported by Kirkgoz (1978) brought new insight into the impact pressure phenomenon both in terms of pressure magnitude and duration. The piezo-electric apparatus they used was capable of responding at a frequency of 1000Hz. Their pressure records showed that breaking waves were capable of generating exceptionally high pressures concentrated on small areas amounting to 686.7kN/m^2 and having durations of 0.005 seconds. This investigation clearly demonstrated the existence of exceptional pressure transients.

Kirkgoz (1978) also reported the study conducted by Cot between 1951– 1953 and published in 1954. Kirkgoz explained in the report that the study was a field investigation of wave pressure impact on the breakwater of the Port of Le Havre. Three out of five pressure cells were arranged vertically in the experiments. It was shown that the pressure rise is very abrupt being within 1/100-th of a second and that the peak pressure is followed by a long pressure oscillation of much lower value which is of a hydrostatic nature. His peak pressures varied between 49.1 – 98.1 kN/m^2.

Kuribayashi et al. (1959) investigated the wave forces on Haboro breakwater in Japan in an attempt to measure both the wave impact pressures on the vertical face of a composite-type breakwater and the resulting structural damage. They obtained a variety of pressure records which included those from a wave which broke on the breakwater. The maximum pressure measured was 147 kN/m^2.

Miller et al. (1974) carried out field investigations at Cape Cod. Measurements were obtained by placing a 1.8m long aluminium flat plate, backed by a cylinder, in the surf zone. Five sensors were placed at 0.3m intervals on the flat. They were subjected to several breaker types owing to the rising and falling tide. As a result, a variety of vertical simultaneous pressure distribution diagrams and graphs of pressures against $U^2/2g$ and H_b could be drawn (where U is the velocity

of the fluid at impact and H_b is the height of the breaking wave). The relationship between the maximum pressure head, $\frac{P_{max}}{\gamma}$ and the kinetic of the fluid, $\frac{U^2}{2g}$, at impact was found as:

$$\frac{P_{max}}{\gamma} = \frac{2U^2}{2g}\ (for\ plunging\ breakers) \ldots\ldots\ldots\ldots\ldots 2.27$$

Miller et al. (1974) concluded as follows:

(1) The largest impact pressures were generated by a bore, followed in decreasing order by plunging, spilling and collapsing waves.
(2) The largest impact pressures were recorded at or near the top of the structure, except for the bore where the reverse occurred
(3) The time-pressure pattern is characterised of the type of breaker
(4) Extreme shock pressure due to entrapped air did not occur because of the geometry of the sensor structure

Selected details of the various field investigations are summarised in Table 2.1

Table 2.1: A list of the field investigations

(adapted from Kirkgoz, 1978)

Author	Year	Pressure measuring apparatus	Beach slope	H_o (m)	P_{max} (kN/m^2)	$P_{max}/\gamma H_o$
Stevenson, T	1874	Spring dynamometer	-	≈ 6	367.9	6.3
Luiggi, L	1921	-	1/2	7	321.8	4.6
Gaillard, D. D.	1904	Spring dynamometer	-	5.5	114.8	2.1
Hirio, I	1920	Spring dynamometer	-	-	345.3	-
Molitor, D. A.	1935	Spring dynamometer	1/87	2.8	33.4	1.2
Rouville, M. A., Besson, P. and Petry, R.	1938	3 Piezoelectric pressure cells (NF=1000Hz)	1/5	1.8	676.9	38.3
Cot, P. D.	1954	5 Piezoelectric pressure cells (NF=10000Hz)	-	-	98.1	3
Kuribayashi, T., Muraki, Y. and Udai, G.	1959	4 Electric resistance pressure gauge (NF=22Hz)	1/3	-	147.2	-
Miller, R. L., Leverette, S., and O'Sullivan, J.	1974	5 Pressure cells	1/20 and 1/250	0.9	48.1	5.5

NF= Natural Frequency

2.3.3 *Laboratory Investigations*

Kirkgoz (1978) again summarised the results of the study conducted and published by Larras in 1937. Kirkgoz explained that subsequent to the full scale measurements by Rouville, Besson and Petry, Larras was probably the first to study in the laboratory the shock pressures exerted by breaking waves on vertical walls. He carried out tests with beaches having slopes of 1/10, 1/13.5 and 1/20 and measured the pressures by means of piezo-electric pickups capable of sensing pressures exerted for a minimum duration of 1/1000-th second. He concluded that the pressure history produced by waves breaking on a vertical wall was considered to be composed of two parts:

(1) The first part, called the "gifle", is a very short elastic shock which is extremely severe and transient and has the following characteristics:
   (a) the pressure peak is always extremely short compared with the wave period
   (b) the intensity of the pressure peak diminishes considerably if the waves do not break exactly on the wall.
   (c) the transient pressure head is spread almost uniform over a large zone in the vicinity of SWL and may have values up to 2.5 to 3 times the wave height. This seems to be in agreement with Stevenson's observations.

(2) The second part of the pressure history, called the "bourrage", is a slower transformation of kinetic energy into pressure and has the following characteristics:
   (a) the level of pressure intensity always lasts for a significant proportion of the wave period
   (b) the pressure level diminishes only a little when the wave does not break exactly on the wall
   (c) the pressure on the wall increases with depth
   (d) the pressure of the bourrage increases with period of the wave, and appeared not to depend on breaker height, breaker depth, slope and roughness of the bottom.

Bagnold (1939) started model experiments in 1937 and, to some extent they were complementary to the elaborate full-scale measurements undertaken by the French engineers

Rouville, Besson and Petry. Experiments were conducted with solitary waves of 0.25m height. In this way it was hoped that in the model tank, with wave production under control environment, it would be possible to correlate the pressure maxima with the observed characteristics of the waves. Bagnold assumed that the shock pressure exerted by a breaking wave is due to the violent simultaneous retardation of a certain limited mass of water which is brought to rest by the action of a thin cushion of air. With this theory, he observed pressures of up to 549.4kN/m^2 using a piezo-electric measuring device. The majority of shock pressures did not exceed 68.7kN/m^2, although very occasionally pressures of 245.3kN/m^2 were observed. Bagnold again came up with the formula for the maximum pressure as:

$$p_{max} - p_o = 0.54 \frac{qU^2H_b}{D} \quad \text{2.28}$$

where p_{max} is the máximum pressure; p_o is the atmospheric pressure of the enclosed air; q is the mass of water; U is the initial velocity of the flow; and D is the initial thickness of the enclosed air. Bagnold drew the following conclusions:

(1) The shock pressures occur only when the shape of the advancing wave is such as to enclose an air cushion between the wave front and the wall
(2) The great variation in the pressure maxima from impact to impact, even when all waves are identical, must be due to a variation in the mean thickness of the air cushion arising from random irregularities in the relief of the concave water face as it meets the wall.
(3) The peak pressures happen only over the zone occupied by the air cushion. This zone extends from the wave crest to a depth of 0.4H below it (where *H* is the breaker height). No shock pressure is imposed on the wall above the crest, and below the bottom edge of the air cushion the pressure falls off rapidly. Near the bottom of the wall pressures are hydrostatic only
(4) It seems reasonable to suppose that the portion of the pressure-time curve between its beginning and its peak corresponds to the destruction of the original momentum of the mass of water involved in the impact.

(5) The whole duration of the compression approximates, for high peak pressures, to the time taken by the water front to travel the distance D at the initial wave speed, U.

Denny (1951) carried out further experiments in support of the work done by Bagnold who had concluded that the air pocket between the wave and the wall played a dominant role in the generation of shock pressures. His conclusions were:

(1) The shock pressures occur regularly when the wave front is approximately plane and parallel to the wall.
(2) The pressures, when examined statistically, are found to be in direct proportion to the height of the waves.
(3) The maximum pressure, corresponding to any given wave, is determined by the flatness of the surfaces of both the wave and the wall.
(4) The pressure appears to be constant over the area covered by the air pocket but falls to a very small value below the air-covered area.

Ross (1955) conducted model investigations of breaking wave pressures on bulkheads sited on beaches with different slopes. His tests covered a wide range of oscillatory waves. The obtained results varied considerably and somewhat similar to those of Bagnold and Denny.

Hayashi and Hattori (1958) investigated the pressure of breaking waves both theoretically and experimentally. They suggested that the maximum dynamic pressure of waves could be expressed as:

$$\frac{P_{max}}{\gamma} = \frac{kU^2}{2g} \quad \ldots\ldots 2.29$$

where $\frac{P_{max}}{\gamma}$ is the dynamic pressure head, $\frac{U^2}{2g}$ is the velocity head of the water at impact and k is a coefficient. Their theoretical value of 4 for constant k gave only poor agreement between

the formula and the measured shock pressures which again varied enormously from test to test. However, they found that the greatest shock pressures occurred on the 1/11.5 slope and that pressures decrease with decreasing bottom slope.

Mitsuyasi (1966) conducted model experiments on the wave forces acting against a wall by employing a force transducer of comparatively low natural frequency (200 Hz in water). Four kinds of regular and oscillatory waves were tested on beaches with slopes of 1/15, 1/30, 1/50. He also measured the pressures acting at the foot of the wall. He drew the following conclusions:

(1) When a wave impinges against a wall, the total wave force increases rapidly and soon reaches the first peak. After that it decreases with the rise of the wave up the face of the wall and comes to the minimum value when the wave attains its maximum run-up. Then the wave force increases slightly and attains the second peak while the wave is running down.
(2) When the wall is situated at a comparatively deep place on the beach ($d/H_o > 1.8$), the wave arrives at the wall without breaking, a standing wave is produced and the wave force is not as large as when breaking occurs
(3) If the wave impinges against the wall with a vertical front, a shock force of great intensity occurs

Richert (1968) investigated experimentally the shock pressures of breaking waves preceded by non-breaking waves. Shocks of the comprehensive type were considered throughout the experiment, that is, shocks which occur when an air cushion is trapped between the wave and the wall. No correlation was found between the wave dimensions and the shock pressures. Richert then concluded as follows:

(1) The air cushion plays an important role in the pressure variation. The variation is oscillatory and can be explained as an adiabatic compression and expansion of the entrapped air.
(2) The largest pressure always occurs where the entrapped air cushion was initially situated

(3) The greatest shock pressures occur with a bottom slope of 1/10 in front of the wall
(4) The shock pressures against the test wall in no case decreased to zero at the bottom of the wall and this differs from what has frequently been stated by other authors. The apparent discrepancy can be explained by the differences in test procedures and hence in the ways in which the waves broke against the structures.

A number of studies on different hydrodynamic aspects of vertical as well as plane sloped seawalls have again been reported in the literature with the enthusiasm for improvement in their design. Neelamani and Sandhya (2005) gave a detailed list of various researchers who have studied wave reflection from seawalls (Shuto, 1982, Twu et al., 2000, Liu et al., 2002) those where their investigations were related to wave run-up and run down (Ahrens, 1989, Van der Meer and Janssen, 1995, Van der Meer, 1997, Liu et al., 2002) as well as those that looked at wave pressures (Minikin, 1963, Goda, 1974, Kirkgoz, 1995, Neelamani et al., 1999). These researchers used plane vertical or sloped seawalls in their investigations. Wood (1997) revealed the inadequacy of the earlier observational research work on wave impact on structures due to unavailability of electrical recording systems which made it difficult to resolve rapid changes in the pressures and particularly the peak pressures, and suggested state of the art measurement techniques.

Theoretical and experimental works to evaluate the performance of wave barriers in terms of wave energy dissipation with respect to transmission and reflection are the works of Ursell in 1947, Wiegel in 1960, Liu and Abbaspour in 1982, Losada and Roldan in 1992, Kribel, Sollitt and Gerken in 1998 as reported by Liu and Al-Banaa (2004). Most of these researchers considered periodic waves and presented information on wave forces acting on the barriers, which is an important element in the design of the structures.

Hattori et al. (1994) also realised the need for more detailed physical study on the wave-impact process for the establishment of physical models that can predict the impact pressures. Hence, they conducted laboratory experiments on flip-through and plunging wave collisions on a vertical wall with focus on the examination of the aerodynamic contributions of air bubbles to the generation of the impact pressure. The study concluded that when a small amount of air is entrapped between the breaking wave and the wall at the collision, the impact pressure increases considerably. They reported also that the highest pressure, of very short duration, was observed when a vertical wave front strikes the wall while trapping a small amount of air in

the form of either bubbles or a thin lens-shaped pocket. They explained that the impulse pressure occurred in the vicinity of the still water level and transmitted downwards through the water body with the sound velocity.

Kirkgoz and Mamak (2004) again proposed a theoretical analysis of the response characteristics of a vertical caisson plate of composite breakwaters under wave action. The theoretical impact pressures are determined using the experimental values of impact pressure rising time. The study found that the computational results of the impact pressures from the pressure impulse model are found to agree well with the experimental data of an early study and concluded that breaking waves on coastal structures caused high magnitude impact pressures which may be important for the structural stability.

The UK Health and Safety Executive (Health and Safety Executive (HSE), 2005) reported that in the event of a catastrophic failure of a storage tank, the quantity of fluid that can be lost into the environment can be as much as 70% of the stored material even when the bund wall remains intact. They further explained that the currently used bund wall cannot withstand the impact of such a release because of the dynamic pressures being nominally up to six times greater than those the bunds are generally designed to withstand. Further research work on this phenomenon brought about the development of MOTIF (Mitigation Of Tank Instantaneous Failure) and COAST (Catastrophic Overtopping Alleviation of Storage Tanks) by the same authors. MOTIF is a modification to the design of the storage vessel while COAST incorporates a specially designed deflector fitted to the top of the bund wall capable of withstanding any wave impact. The results of the physical modelling studies conducted at Liverpool John Moores University (LJMU) on this subject indicated that incorporating these modifications to the existing bund would marginally increase the overall capacity of the bund wall (Atherton et al., 2008).

Similar study to the UK Health and Safety Executive (HSE) work is the research conducted by Liu et al. (2008). Hydrodynamic loads on the arc crown wall were studied numerically and experimentally when overtopping occurs (Liu et al., 2008). The numerical model is validated in terms of wave force on a vertical wall using linear wave theory. Both numerical simulation and experimental data confirmed that the characteristics of the loads/wave forces on an arc crown wall using a sloped seawall are of two peak patterns. The first peak of the horizontal wave force was reported to appear when the returning jet is generated and then decreases till the jet touches the free surface of the major water while the second peak of the horizontal force

was generated after a short time during the running down of the contact point of the free surface and the crown wall.

Shuto (2009) published data on the degree of damage to coastal structures in terms of the inundation depth and concluded that a wooden structure can withstand the impact if the inundation depth is smaller than 1m and conversely, it is completely washed away if the inundation depth is larger than 2m. Iizuka and Matsutimi (2000) expressed quantitatively the damage conditions in terms of inundation depth, current velocity and/or hydrodynamic force and concluded that a wooden structure will be destroyed if the inundation depth is over 2 m, if current velocity is over 4.9m/s, or if hydrodynamic force is over 27kN/m. The research undertaken by Koshimura (2002) concluded that the structures were significantly vulnerable when the local inundation depth exceeds 2 or 3m, the current velocity exceeds 2.5m/s or hydrodynamic load on a structure exceeds 5kN/m.

Fukui et al. (1963) for example, measured the pressures generated on walls due to the reflection of bores. The bores were generated by suddenly releasing a reservoir of water using the dam-break method. The incident bore profile, the bore celerity, the pressures at three vertical stations along the wall and the run-up height were all measured. The test regime varied the slope of the wall from 34° to 90° and the incident bores ranged in relative wave height from H / h = 0.5 to H / h = 3.0, where H is the wave height of the incident bore above the still water surface and h is the still water depth. Fukui et al. (1963) differentiated between the "impulsive" pressure obtained soon after the bore strikes the wall and the "continuous" pressure which corresponds to the hydrostatic pressure at the wall once the reflected bore has propagated away from the wall. The study proposed the impulsive pressure as the fourth power of the incident wave celerity. Their expression for the maximum impulsive pressure, p, was:

$$P = \frac{K_o c^4}{gh\rho} \quad \text{2.30}$$

where K_o was an experimentally determined constant which was equal to 0.5 for the vertical wall experiments. It was also proposed that a linear relationship existed between the impulsive

pressures and the depth along the wall. From the experimental results it was concluded that the maximum run-up height was equal to 3.3 times the velocity head computed from the incident bore.

Cross (1967) investigated the properties of incident surges propagating over smooth and roughened bases and the forces caused by their impact on a vertical wall. Bores were generated using the dam-break method in a tank which had a negative slope of 0.002 in the direction of wave propagation. The following expression for the force time history, F(t), on the wall was proposed:

$$F(t) = \frac{1}{2}\gamma b\delta(t)^2 + \rho C_F(t) b\delta(t)c^2 \dots \quad 2.31$$

where γ is the weight of water per unit volume, *η(t)* = the water surface time history which would occur at the wall if the wall were not there, *c*= the surge celerity, and b = the width of the wall.

Ramsden (1993) investigated the interaction of tsunamis with a vertical wall. He used a physical model to look at bores and surges propagating on dry bed as well as solitary waves. His measurement included both force and run-up measurements. He found that the force computed from the maximum measured run-up, assuming hydrostatic condition, exceeded the maximum measured force. He also found that the model of Cross (1967) under-predicted the measured forces due to bore on dry bed by 30–50 %.

Nakamura and Tsuchiya (1973) studied the pressures on composite structures caused by the impact of surges propagating over a horizontal bed. The surges were generated by the dam-break method with initial reservoir depths of 30cm, 40cm, and 50cm. Large pressure heads of relatively short duration just after impact were recorded, followed by relatively constant pressures due to the nearly hydrostatic condition once the bore propagated away from the wall. The maximum measured pressure head reported was 46 cm with a rise time of 50msec obtained from a pressure cell located 2.5cm off the bottom of the tank. This maximum pressure was only

50% larger than the maximum hydrostatic pressure developed on the wall which was reported to occur approximately five seconds after the surge initially struck the wall.

Study on wave run-up included the work of Synolakis (1987) who presented an approximate theory for non-breaking solitary waves and derived an empirical equation for the maximum run-up in a series of laboratory experiments. The study found that the linear theory predicts the maximum run-up satisfactorily and that the non-linear theory describes the climb of solitary waves equally well. Yeh et al. (1989) also performed experimental investigations of bore propagation near the shoreline and the transition from bore to wave run-up. In the study, a single bore was generated by lifting a thick (12.7mm) aluminium plate gate which initially separates the quiescent water on the beach from the deeper water behind the gate. The study found that owing to momentum exchange process (that is collision of the bore against the initially quiescent water along the shoreline) a single bore motion degenerates into two successive run-up water masses; one involves a turbulent run-up water motion followed by the original incident wave motion.

In order to approximate the impact of a tsunami, Cumberbatch (1960) presented a solution for the impact of a two-dimensional fluid wedge on a flat surface. He assumed a constant wedge angle before impact, an inviscid fluid and irrotational flow where the velocities throughout the wedge before impact are equal to the constant approach velocity. He used a no-flux boundary condition at the wall and fully nonlinear free surface boundary conditions. Since gravity was neglected in the problem formulation, the theory was intended to model the dynamics soon after impact, before the gravitational acceleration begins to affect the flow along the wall. Water surface profiles and pressure distributions along the wall were presented for wedge angles of 22.2 degrees and 45 degrees. Cumberbatch (1960) defined a force coefficient which relates the force on the wall to the momentum flux which would occur at the wall location if the wall were not present, as follows:

$$F = \rho C_F b h C^2 \quad \ldots \quad 2.32$$

where C_F is the force coefficient which was shown to be a function of only the incident wedge angle , ρ is the density of the fluid, b is the width of the wall, h is the water level at the wall location and C is the celerity.

Neelamani and Sandhya (2003, 2005) conducted physical model studies on the hydrodynamic performance of vertical and sloped plane/smooth, dentated and serrated seawalls. Regular and random waves of wide range of heights and periods were used. Tests were carried out for different inclinations of the seawall for a constant initial water depth of 0.7m. The wave reflection, run-up and run-down and wave pressures were measured to assess the dissipation character of the seawalls. It was observed that the serrated seawall was superior to the plane and dentated seawall in reducing the wave reflection. The improved performance in terms of reduction of wave reflection, run-up and run-down and wave pressures of the serrated seawall was elucidated. The serrated seawall was found to be about 20 – 40% better than a plane seawall for reducing wave reflections as well as run-up and run-down. Based on the measurements, predictive equations were proposed for wave reflection characteristics for the regular waves on smooth, impermeable vertical and sloped seawalls. The derived equations were suggested to be of practical applications. A summary of various laboratory investigations is given in Table 2.2.

Table 2.2 : A list of laboratory investigations

(adapted from Kirkgoz, 1978)

Author	Year	Pressure measuring apparatus	Beach slope	Location of maximum pressure	Rising time of shock pressure (sec)	$(P_{max}/_{\gamma}H_o)$ (Maximum)
Larras, M.J.	1937	1 Piezoelectric cell (NF=1000Hz)	1/10, 1/13.5 and1/20	Vicinity of SWL	0.001	-
Bagnold, R.A.	1939	1 Piezoelectric cell (NF=2000Hz)	1/6.5	$0.4H_b$ upper part of the wave	0.0005	220
Denny, D.F.	1951	1 electro-magnetic cell (NF=2000Hz)	Steep	$0.4H_b$ upper part of the wave	0.001	100
Ross, C.W.	1953	2 Piezoelectric cell (NF=1000Hz)	1/5.5, 1/6.9, 1/10.6 & 1/13	Between near the top of wave and well below	0.0014	116
Hayashi, T.M. and Hattori, M.	1958	5 Pressure transducers (NF=3000Hz)	1/11.5, 1/14.4 & 1/22.5	Between wave crest and SWL	0.001	45
Rundgren, L.	1958	5 Pressure transducers (NF=475 &700Hz)	1/9.4	Below SWL	0.001	-
Nagai, S.	1960	3 Pressure transducers (NF=300Hz)	1/2, 1/3 and 1/5	Below SWL and bottom	0.002	20
Mitsuyasu, H.	1966	2 Pressure transducers (NF=10000Hz)	1/15	Below and in the vicinity of SWL	0.002	35
Richert, G.	1968	3 Pressure transducers (NF=5500Hz)	1/3, 1/6, 1/10 &1/25	1.25 h_b above the bottom	0.001	100
Weggel, J.R. and Maxwell, W.H.C.	1970	6 Pressure transducers (NF=10000Hz)	1/20	0.8 h_b	0.0005	≈28

NF=Natural frequency; H_o=deep water wave height; h_b=height above the bed of the breaker crest at impact

It worth mentioning here that, some laboratory investigations conducted by previous researchers used primitive measuring instruments. For instance, the instruments used by Larras, Bagnold, Denny and Ross (Table 2.2) ranged from Piezoelectric cells to electro-magnetic cells while the present study used modern pressure measuring instruments capable of responding to fast and turbulent flow experienced in the real sea state.

There are some previous researchers who used modern pressure measuring devices such as pressure transducers. For example Hayashi and Hattori, Rundgren, Nagai Mitsuyasu, Richet and others (Table 2.2) but most of these researchers used solitary waves generated with wave-makers as against the dam-break waves used in the present study. In addition, most of their studies covered slopping beaches ranging from 5.71^o (1/10) to 1.45^o (1/50) (see Table 2.2) as against the horizontal dry-bed investigated in this study. Nakamura and Tsuchiya (1973) studied the effects of solitary waves on horizontal beds but only focused on the effects of these waves on vertical walls, whereas this study covers a wide range of wall slopes.

There are few previous investigators who used dam-break methods to generate waves in their study however; the focus is mainly the effect of these waves on vertical smooth-surface defence walls. These include the work of Cross (1967), Ramsden (1996) and others. Fukui et al. (1963) who studied the effect of these waves on both vertical and slopping walls only compared a wall slope of 34^o to that of the vertical, whereas the present study covers the effect of these waves on a range of wall slopes (45^o, 60^o 75^o and 90^o). Although the work of Neelamani and Sandhya (2005) is based on the effect of ocean waves on both smooth and rough surfaces (dentated and serrated surfaces) they used only regular and random waves which were generated using wave-makers as opposed to the use of dam-break waves in the present study. The present investigation also looked at the effect of these waves on a wide range of unique wall surfaces (see section 4.4.2).

2.4 Wave Theory, Wave Generation and Wave Breaking Phenomenon

This section briefly gives an overview of the theories of waves by providing a descriptive outline of the small- and finite- amplitude wave theories. This includes wave generation with specific examples of physically generated waves using wave-makers as opposed to the use of dam-break waves as well as wave transformation with a focus on wave breaking and non-breaking phenomenon on coastal structures.

2.4.1 *Basic Wave Theory and Characteristics*

Linear Wave Theory (LWT) or Short-amplitude Wave Theory (SWT) is the core theory of ocean surface waves used in ocean and coastal engineering and naval architecture (Reeve et al., 2012). The sine function defines the characteristics of a regular wave. A regular wave is characterised by the amplitude, the wavelength and period. For full specification however, the propagation direction and phase at a given location and time will also be required. Therefore, any wave may be described in terms of height, length and frequency or period and may change shape, size and form as the waves interact with matter (sand or rock or defence structure on the beach). Linear Wave Theory forms the basic theoretical rationale behind the wave generation methods used in this study. Knowledge of the mechanics of short waves in particular, is essential for a good understanding of experiments conducted in wave flumes and successful interpretation of wave flume data in general, depends upon a fundamental understanding of wave theory and characteristics.

Ocean surface waves are mainly generated by the action of wind on water. According to Reeve et al. (2012), the waves are formed initially by a complex process of resonance and sharing action, in which waves of differing wave height, length and period are produced and travel in various directions. In the storm zone generation area, high frequency wave energy is dissipated and transferred to lower frequencies which make the waves travel at different speeds. The low-frequency waves travel more quickly than the high-frequency waves resulting in a swell sea condition as opposed to the storm sea condition, the term known as wave dispersion. As waves approach a shoreline, their height and wavelength are altered by the processes of refraction and shoaling before breaking on the shore. Where coastal structures are present, waves may also be diffracted and reflected resulting in additional complexities in the wave motion (Reeve et al., 2012).

Dean and Dalrymple (1991) revealed that the first mathematical description of intermittent progressive waves is that attributed to Airy in 1845. Airy wave theory is strictly only applicable to conditions in which the wave height is small compared to the wave wavelength and the water depth, commonly referred to as linear or first-order wave theory. The derivations followed the concepts of two-dimensional ideal fluid flow which is a reasonable starting point for ocean waves using basic sinusoidal wave theory. In order to form a controllable solution to short-amplitude wave theory, the following simplifying assumptions are made:

- The water is of constant depth, d and wave length, L (or period, T).
- The wave motion is two-dimensional, which leads to long crested waves with constant height along the crests.
- The waves are of constant form, that is, they do not change with time.
- The fluid (water) is incompressible.
- Effects of viscosity, turbulence, and surface tension are neglected.
- The wave height, H is small compared to the wave length, L and the water depth, d (i.e. H/L « 1 and H/d « 1).

However, there are some limitations which these assumptions place on the resulting theory, for instance the linear wave theory assumed that the wave height was so small that the dynamic and kinematic boundary conditions at the free surface could be applied at the still water level (SWL). Despite the apparently restrictive simplifying assumptions associated with this theory, its range of application is extensive.

There are, however, some applications where the simplifying assumptions of linear wave theory (LWT) become significant. In such cases it is necessary to resort to the use of a non-linear or finite amplitude wave theory. As opposed the Airy wave theory, finite amplitude wave theory was first developed by Stokes in 1847. It is applicable to steep waves in deep and transitional water depths. Following Stokes, Korteweg and de Vries developed a shallow-water finite amplitude wave theory in 1895. Both theories relaxed the linearity assumptions made in Airy theory deriving solutions up to and including the nth order and are termed Cnoidal wave theory which is analogous to the sinusoidal Airy wave theory (Reeve et al., 2012, Dean and Dalrymple, 1991, Falnes, 2002). There are a number of different finite amplitude wave theories which have been proposed, but the two most commonly adopted theories are: Stokes' Wave

Theory and Cnoidal Wave Theory. Stokes' theory is applicable in deep water whereas Cnoidal theory applies in finite depth situations. Despite the sophistication of finite amplitude wave theory, it still predicts waves which are of essentially a single period. There is a clear wave period and length. In reality, this seldom occurs in the ocean. Successive waves typically vary in height, period and propagation direction. Therefore, even high order finite amplitude theory is limited in such cases (Reeve et al., 2012).

The mathematical derivation of all these theories is beyond the scope of this thesis, however, it is useful here to provide some information on the circumstances under which these wave theories can be applied. According to Reeve et al. (2012), the range of validity of linear theory is reassuringly wide, covering all of the transitional water depths for most wave steepness encountered in practice. However, for engineering design purposes, the main implication of using linear theory outside its range of validity is the incorrect estimation of wave celerity and wave length.

Physically the difference between linear and finite amplitude theories is that finite amplitude theories consider the influence of the wave itself on its properties. Therefore, in contrast to linear theory, the phase speed, wave length, water surface profile and other properties are functions of the actual wave height. Linear wave theory predicts that the crest and trough heights of the wave are equal. That is, the wave is evenly distributed about the still water level. In contrast, finite amplitude theories predict waves with peaked crests and flat troughs. The crests are further above the still water level than the troughs are below this level. Hence, in applications such as determining the deck elevation of an offshore structure, the use of finite amplitude wave theory would be important. Linear wave theory predicts that water particles move in closed orbits. Hence, there is no net transport of fluid. In contrast, finite amplitude theory predicts a small net fluid transport in the direction of wave propagation (Cruz, 2008).

Many structures are exposed to severe environmental conditions where the sum effects on the structure are the results of continuous and intermittent wave spectra. These include structures such as bulk carriers, oil and gas drilling and production platforms, pipeline and sea bed mining structures as well as coastal defence structures. Knowledge gained from the generation of short amplitude waves as well as long waves in a laboratory wave flume can have practical applications in the study of tsunamis, storms surges, floodwater waves and other short or long free-surface waves.

2.4.2 *Wave Generation*

There is nothing new in the idea of generating artificial waves in flumes or tanks. Wave-making machines have been used for many years in tanks, for the testing of ships' models. According to Biesel and Suquet (1951), a laboratory wave generator can be used to test the stability and efficiency of ship hull design. Experimentation with ship models under varying wave conditions outputs data which can be used for analysis in the area of computational fluid dynamics (Maguire, 2011). While full-scale measurements of waves and their effects are essential, it is likely that the use of laboratory wave generators will more quickly advance our understanding and knowledge of the performance of model structures.

Engineers use wave tank facilities to assess the design, safety and economic feasibility of ships, coastal structures and wave energy devices. Wave-makers are a central component to such facilities. A wave flume is one of the most important professional and educational tools which have found wide applications in coastal and offshore engineering. A wave flume is a long tank with a wave-maker at one end and a wave absorbing unit at the other. Water waves generated by the wave-maker propagate along the tank and are utilised in the physical modelling of various wave-related phenomena.

The wave-making machinery may be used to produce sinusoidal or cnoidal waves, sequences of waves with desired spectral properties, and model reproduction of wave sequences. Mechanical type wave-makers which are utilised in laboratory wave studies include movable wall type generators and plunger type wave-makers. Examples include: hinged type generator, piston type generator, wedge generator and plunger type generator. Machine-generated waves can be varied from long, standing or random waves using appropriate types of the wave-makers.

Maguire (2011) revealed that at the initial stages of the generation, the input into the electric motor which runs the wave paddle will be from a functional generator. Once it is established that the paddle is functioning effectively and is capable of creating a variety of waves with different characteristic then the function generator will be removed as the input. It is then replaced with a computer running a program which incorporates feedback from the wave flume. Ideally the sizes, shapes and frequencies of individual waves at the working section were sensed and compared with desired values with a consequent error-eliminating action. The need for accuracy over a wide frequency ranges and for production of a wide variety of wave shapes

and sizes are the main reasons for the computer program. Frequently used software includes Motionlink and Matlab.

For the machine-generated wave system, wave absorption has important applications to reducing the cost of wave flume design and of planning and running experiments in physical wave flumes. Effects peculiar to wave channels, such as reflection from both ends are minimised through wave absorption techniques. This is particularly important due to consequences unwanted reflected waves can have on experimental data. As a result, machine-generated wave systems produce the following advantages:

- Avoidance of spurious reflections from the waver-maker which could spoil the target incident waves.
- Prevention of resonant oscillations in the facility which reduce the maximum test duration time.
- Substantial reduction in the flume stilling time between tests by quick removal of the slowly damped low-frequency oscillations.
- Making the experimental results less sensitive to the placing of artificial boundaries constituted by the wave-maker, and thus making them easier and more unambiguous to interpret.
- Avoidance of false wave-maker reflections of free long waves in connection with second-order wave generation.

When generating waves in a flumes or tanks, it is important to be able to control both the frequency and the amplitude of the test waves. The frequency of the monochromatic test waves is relatively simple as it is the same as the frequency of oscillation as the wave-maker. However, the more complicated parameter is the displacement amplitude of the wave-board and the concept used for that is the theory proposed in McMahon (2008), who reasoned that the volume of water displaced by the wave-maker should be equal to the volume of water in the crest of the propagating wave. Modern wave generators are capable of simulating regular or random wave sequences with a pre-determined wave energy spectrum in the case of two-dimensional investigations. Active absorption of reflected waves can also be incorporated to ensure that the generated incident waves are not contaminated by re-reflected waves from the generator.

Experimental wave tanks (EWT) provide an excellent opportunity for engineers to assess their designs and analyse its characteristic response in a controlled environmental setting. In contrast to the ocean however, the size of EWT facilities are limited and, as such, the boundaries and

walls of EWTs cause wave reflections which result in an unrealistic representation of the boundless ocean. This is a major issue in EWTs because, if waves are continuously reflecting off solid boundaries, over a period of time the wave reflections can build and contaminate the test domain thus shortening the test duration. This is being controlled in the design of machine-generated wave systems in many EWTs by incorporating some forms of wave absorption mechanisms at the boundaries of the EWT.

Experimental wave tanks (EWT) which incorporates waves generating systems (wave-makers) have been, and still are, an indispensable tool for any engineer working within coastal and ocean engineering. However, they are expensive facilities in both capital expenditure and operational expenditure terms. Computers are now capable of providing an analogue to the experimental wave tank with wave generating systems - the numerical wave tank (NWT). The NWT is beneficial to the engineers compared to the experimental facility, mainly through cost and space saving. The NWT also has the advantage of being able to provide a vast array of parametric point measurements all over the test domain. However, the objectives of using an NWT fall into two categories: reproduce physical wave tanks as closely as possible or to reproduce real sea conditions as closely as possible (Tanizawa, 2000).

It is obvious, however, that the natural waves of the sea are not monotonous. They are always somewhat irregular in height and form, and the inclination at which they approach the shore varies considerably. For this reason, a dam-break wave generating system is considered to be closely reproducing the real sea conditions for generating floodwater waves. This is in contrast to the machine-generated waves. Due to mode of generation, dam-break-generated waves are complex, incorporating many superimposed components of wave periods as a result of turbulence making the practicality of estimating some vital wave records difficult. Such records may include the wave period, wavelength, frequency etc. Dam-break wave generating systems may represent the situation in the storm zone of the sea as the resulting flood waves consist of random periodic fluctuations as opposed machined-generated waves. A detailed principle of dam-break flow, design of the experimental wave tank (EWT) with dam-break wave generating system as well as the mode of generation are discussed in chapter 4.

2.4.3 *Breaking and Non-breaking Waves*

Introduction

In considering the pressures or forces on seawalls a distinction is often made between the effects of breaking and non-breaking waves. The pressure exerted by non-breaking waves is taken to be predominately hydrostatic, and varies relatively slowly. In contrast breaking waves exert a dynamic force, due to the effects of wave momentum, water turbulence and entrapment of compressed air, which may be very much greater than the hydrostatic forces, but may last for much shorter durations. In particular, a breaking wave may produce a pressure of very high intensity and short duration, known as a shock (or impact) pressure, followed by a longer period of less intense pressure. The product of the force due to the shock pressure and its duration is usually referred to as impulse, which is a measure of the change in momentum of the wave as it strikes the wall.

Many different criteria have been proposed for predicting wave breaking. Although, none is universally accepted as correct for waves in shoaling water but McCowan's well-known expression, $H_b/d_b = 0.78$ for the limiting height of a solitary wave moving over a horizontal bed, has been frequently used in design for predicting the heights of breaking oscillatory waves. Consequently, a number of assumptions are usually made in deriving breaking criteria:

(a) A breaking wave is the highest possible wave for the specified conditions;
(b) Breaking occurs if the maximum horizontal water-particle velocity (at the wave crest) exceeds the wave celerity;
(c) Breaking occurs if the vertical pressure gradient beneath the crest falls below zero

McCowan (1894) analysed the maximum breaking elevation of a solitary wave by assuming the condition of zero relative horizontal water-paticle velocity at the crest (i.e., u = C). He gave a theoretical estimate of the maximum height to which a solitary wave might grow as $H_b \approx 0.87d_b$ and also carried out some experiments which gave $H_b \approx 0.75d_b$. McCowan (1894) later found an exact theoretical value for the limiting height of the solitary wave as;

$$H_b = 0.78d_b \quad \text{......} \quad 2.33$$

Where H_b *is wave height and* d_b *is the water depth.*

Breaking Waves On Vertical And Sloped Walls

For many situations, a seawall may be exposed to breaking rather than non-breaking waves at some point in the tidal cycle. A wave breaking on a vertical wall may exert short duration shock pressures which are considerably higher than the forces due to non-breaking waves. Over many years, authors have considered the problem of predicting these forces and pressures using theoretical and experimental means. The Shore Protection Manual (SPM) (1984) mentioned some of the very early work done in this area. Notable is the work of Bagnold (1939) who conducted experiments to investigate the shock pressures of breaking waves, and proposed a formula for their calculation (see section 2.2). Bagnold's theory predicted infinitely high shock pressures if it is assumed that no air is trapped by the breaking wave on impact.

Iribarren and Nogales (1949) proposed a formula for the calculation of shock pressures which does not assume that air must be trapped by the breaking wave. If air is present, its effect is to damp the pressure, and in this situation both Iribarren's and Bagnold's formulae predicted similar pressures. Bagnold's work was followed up by Denny (1951) who also conducted a series of experiments to measure the intensity and duration of shock pressures for breaking waves. Denny (1951) conducted extensive model tests to assess the effects of water depth, wave period and bed slope on shock pressures.

Both the Shore Protection Manual (SPM) (1984) and BS 6349 (1991) suggested that when calculating forces on a vertical wall due to breaking waves, the method of Minikin (1963) should be used. Minikin based his design procedure on field observations and the experimental results obtained by Bagnold. The SPM, however, notes that Minikin's formula may predict forces which are extremely high and should be used with caution. Horikawa and Kuo (1966) also indicates that Minikin's formula predicts a relatively high value for the mean shock pressure and suggests that the fairly simple wave pressure formula proposed by Hiroi (1920) often produces results in good agreement with the mean pressure intensity calculated from experimental and field data.

Kamel (1970) presented the results of an extensive study into the factors affecting the magnitude of wave pressures on vertical walls. Both theoretical and experimental works previously done by a number of authors were reviewed. Kamel then derived his own formula, for calculating shock pressures due to breaking waves based entirely on analytical considerations. The formula was compared with the results of a series of experiments and

proposed a theory which was found to predict higher value of the shock pressure than those measured experimentally. A numerical model for the calculation of the pressure distribution due to breaking waves on a vertical wall is proposed by Weggel and Maxwell (1970) based on the earlier work by Bagnold. The results were compared with pressures measured in a series of physical model tests with pressures measured simultaneously at several adjacent points. Comparisons were made between the numerical and experimental pressure distributions and were found to be in reasonable agreement. It would then be seen that progress on the prediction of pressures and forces due to breaking waves on seawalls can be advanced on several fronts. In particular the mechanism of waves breaking is still not sufficiently well understood and the theory of breaking waves still needed to be extended.

A number of seawalls have sloping front faces. This is particularly so in low-lying or agricultural areas, where the seawall bank is often an embankment structure formed of local materials. Such slopes may be armoured with stone or concrete revetment blocks, or concrete slabs or other materials. The Shore Protection Manual (SPM) (1984) gives an adaptation of the work of Minikin which enables the forces and pressures due to breaking waves to be calculated on sloping forces which are nearly vertical. More recently Li and Raichlen (2002) had reported the results of field observations and physical model tests on the effect of shock pressure and run-up on sloping sea dykes due to solitary waves. In particular, the study presented an analysis of the damage caused to the sea dykes on the north German coast by storm waves with special reference to shock pressure effects. The physical model tests are intended to investigate shock pressure forces and their effect on the core of the dyke. The study concluded that the maximum shock pressures are sustained about a wave height below the SWL, that high shock pressures are more likely to occur on steeply inclined slope and that the shock pressures decrease continuously through the core but suggests that full scale model tests would be useful in any attempt to derive a model law.

Non-breaking Waves On Vertical And Sloped Walls

Seawalls are often situated where the water depth is such that some waves may break against the structure. However, in certain situations, where the wall is located in deep water, the structure may be subjected to non-breaking waves. Therefore a means of calculating the pressures and/or forces due to such conditions is required. For non-breaking waves, the incoming wave is reflected by the vertical wall, forming a standing wave in front of it.

Horikawa and Kuo (1966) provided a series of useful illustrations of pressure/time curves showing the transition from non-breaking to breaking wave pressures. Other useful summaries are given by Goda (1972) and Nagai (1960).

The Shore Protection Manual (SPM) (1984) cited the work of Sainflou done in 1928, Miche carried out in 1944 and Rundgren in 1958. The SPM presented that Sainflou proposed method for calculating the pressure distribution on vertical walls due to non-breaking waves based on trochoidal wave theory. Details of development of Sainflou theory and its simplification are given by Horikawa and Kuo (1966). Whilst the expression given by Sainflou is reasonably easy to apply, it was found by Rundgren (1958) to overestimate the wave forces on a vertical wall for steep waves.

It was again stated (Shore Protection Manual (SPM), 1984) that Miche in 1944 derived a second order theory for calculating the pressure distribution on vertical walls which was found to give better agreement with experimental results. Rundgren (1958) extended the work of Miche to include the wave reflection coefficient of the structure. The SPM presented a series of design curves based on the work of Miche and Rundgren which may be used to calculate the forces on vertical walls due to non-breaking waves. BS 6349 (1984, 1991) also suggested that the wave pressure distribution on vertical seawalls should be calculated using Sainflou or Miche-Rundgren. The Shore Protection Manual (SPM) (1984) again reviewed the work of Goda done in 1972 and that of Kakizaki carried out in 1966 and concluded that their results give a fourth order approximation to the standing wave pressure on a vertical wall. Goda (1972) compared the results for pressure obtained from his approximation with measurements from a series of regular wave tests and found them to be in reasonably good agreement. Goda also found that Sainflou's formula generally tends to give an overestimate of the wave pressures and presented design diagrams based on his theory, with some modifications made for the total wave forces using his experimental results.

Nagai (1960) also reviewed the theories of standing waves in both deep and shallow water. He compared the calculated pressure distributions and maximum simultaneous pressures at the wall using the theories with his own experimental results for various water depths and wave steepness. The comparison of the theory and the experiment led him to suggest ranges of applicability of the theoretical wave pressure formulae, based on the values of wave steepness, H/L, and relative depth, d/L. He presented formulae which may be used to calculate the

maximum simultaneous pressure and the force/unit length due to non-breaking waves on vertical walls for both shallow and deep water regions.

2.5 Velocity Measurements In Dam-break Flow

2.5.1 Introduction

The need to predict the motions of the water in breaking waves is essential if a detailed understanding of sediment movement on beaches is ever to be attained. Likewise, knowledge of these motions is important in predicting forces on the wide variety of structures built in the breaker zone. A number of different methods of measuring water-particle kinematics have been tried in previous investigations.

Fluid-granular flows involve the movement of a fluid and/or a set of particles. Such flows of disperse phases are encountered in a wide variety of situations of scientific and engineering interest. Such particulate flows include liquid-entrained gas bubbles, aerosols, dry granular flows, fluidised beds of particles and liquid-saturated particulate currents. Purely fluid flows, on the other hand, may often be visualised by diluting seeding particles that act as tracers of the flow field, either within the fluid itself (neutrally buoyant particles) or at the free surface, if any (floaters).

2.5.2 Water -Particle Propagation Velocity

The use of digital imaging for qualitative and quantitative characterisation of fluid flows is not new. In recent years however, with the rapid development of powerful digital cameras at affordable prices and the advances in robust and fast image processing techniques, this tool has become very popular.

A typical set-up represented a flow seeded with particles which could be imaged from above or through a transparent side-wall. The particles are roughly identical and should appear brighter than the surrounding fluid on the digital images. The flow could be imaged from a

single camera or from two cameras in a stereoscopic arrangement (Douxchamps et al., 2004). When the imaged scene is immersed in a liquid and seen from the outside through a transparent wall, the image formation can be strongly influenced by refractive effects. Each interface separating materials of different refractive indexes will bend light rays according to Snell's law. Besides, particle positions information on the particle velocities is of great interest in fluid-particle applications.

The particle velocities are obtained as inter-frame displacements from the particle positions using various methods. These methods include Particle Tracking Velocimetry (PTV), Particle Image Velocimetry and Particle Streak Velocimetry (PSV). The PIV system consists of different optical components. Particle in the fluid are illuminated in a plane by a light source. The light scattered by the particles is recorded by a camera on a sequence of frames. In PIV, the average velocity vectors are obtained for a cloud of particles based on image cross-correlation techniques whereas for PTV the individual particle motions are resolved, and full sets of particle trajectories can be reconstructed by following one and the same particle over many successive frames (Capart et al., 2002). For further details on PIV, literature such as Raffel et al. (1998) or Adrian (1989) may be reviewed.

Chegini (1997) who had used both techniques explained that Particle Tracking Velocimetry (PTV) requires individual particles to be located in an image and successive images to be recorded on successive frames. The system analyses pairs of single exposed digital images to produce whole field maps of velocity vectors. Particle images at different times exist on the separate frames. He reported that there was no directional ambiguity in the calculated vectors and the direction of particle motion was easily found and that there was no lower limitation on particle motion between frames. PTV technique was said to accurately determine the position of a particle in an image frame and could compare this location at a known short time interval later (i.e in a successive frame). The distance travelled by an individual particle is then calculated and the velocity found knowing the time interval between images.

The application of Particle Streak Velocimetry (PSV) in fluid mechanics has been used for qualitative flow visualisation as illustrated in Van Dyke (1982). Seeding particles in the fluid medium may be recorded on a single frame of photographic or video film by using a relatively long exposure time. Particle streak images can be digitalised for development into the quantitative measuring technique known as Particle Streak Velocimetry (PSV). This method is

usually used when the medium fluid has a seeding particle concentration less than that of PTV. This method does not require individual streak images to be overlapped and distinguished from each other. PSV enables accurate individual streak lengths to be determined and then analysed. As the exposure time is known, it becomes possible to obtain the velocity associated with a particle streak. The image analysis for locating streak images and measuring their lengths with known exposure time to obtain the velocity field has been demonstrated in a wide variety of flow situations (Raffel et al., 1998, Chegini et al., 2004).

Many investigators who have used PIV or its adaptations have employed the use of coloured droplets having specific gravities close to unity (e.g , a mixture of carbon tetrachloride, xylene and zinc oxide) suspended in a wave channel at the points where measurements are to be taken. The movements of these particles are then recorded on a cine film as waves pass down the channel. Frame-by-frame analysis of the motions of the particles allows the water-particle kinematics to be estimated. Iversen (1952), Morison and Crooke (1953), Ippen and Kulin (1954), Adeyemo (1970), Iwagaki et al. (1971) and Sawaragi and Iwata (1974) have used some of these methods or its adaptations in various studies. However, in this study, water-particle velocity measurements were made using a different adaptation of PIV. The time variations of the horizontal components of the front edge of the floodwater were traced and located at various positions from which the propagation velocities of the floodwater wave were obtained using various methods (see chapter four for more detail about the adapted PIV technique used in the present study).

2.5.3 Wave Celerity

The celerity of wave's propagation in water of constant depth may be predicted to a high degree of accuracy using one of the varieties of existing wave theories. The most commonly used expression for wave celerity is that resulting from linear theory since it is both simple and may also be applied at any relative water depth. However, Goda (1972) in his experimental study of breaking waves, pointed out that linear theory may give erroneous results for waves propagating over a sloping sea-bed.

Morison (1951) examined the wave-steepness effect on celerity using an expression originally developed by Stokes in 1847. Morison concluded that the wave steepness effect would be negligible and that the Airy or linear theory expression for celerity would be good enough for practical purposes. Kirkgoz (1978) again reported that Larras's investigation conducted in 1952 also found that Airy's theory was suitable for predicting the wave celerity up to the breaking point.

The wave breaking phenomenon in shoaling water is sometimes considered to result directly from the differences in the local wave propagation velocities. This is the case for shoaling long waves in which the continuous change of form is caused by these differences. According to Kirkgoz (1978), Airy, in 1845 first pointed out that in long waves, different parts travel with different speeds depending on the local water depth. Stoker (1957) showed that it was possible to rearrange the equations of the shallow water theory so that they were analogous to the fundamental differential equations of gas dynamics for the case of a compressible flow involving only one space variable, x. He then confirmed the speed variations or the celerity at any point along the water surface as:

$$C = \sqrt{g(d(x) + \eta(x,t))} \quad \text{2.34}$$

Where *d(x)* is the local still-water depth and $\eta(x, t)$ is the surface elevation measured from still water level (SWL). Kirkgoz (1978) pointed out that it seems reasonable to expect that actual wave celerities in the breaker zone will fall between those values predicted by linear theory and the values of the solitary and long wave theories. Some experimental data on the front water propagation velocities for the present experiments were given in section 5.3. These data tend to support the use of equation 2.33.

2.6 Summary

The first section in this chapter has reviewed the mechanisms of wave action on coastal defence structures as this is central for the evaluation of the hydraulic performance of any shoreline structure. The section discussed the general mechanisms of wave-structure interactions with emphasis on the three main phenomena; reflection, dissipation and overtopping that are of great interest to the present study.

Subsequent sections in the chapter also offered a review of seawall design concepts as well as design and construction considerations. The chapter discussed various methods/ formulae for estimating wave pressure as well as the theory and studies on breaking and non-breaking waves. More importantly, the chapter presented detailed evaluation of previous studies on wave impact pressures and dissipation of wave energy by defence structures. Both detailed summaries of previous field and laboratory studies on this subject matter were presented. Finally a description of various methods of velocity measurements in dam-break flow and the concept of wave celerity were offered. The next chapter further reviewed the theoretical backgrounds as well as derivation of important governing equations that are related to dam-break flow and wave impact problems.

CHAPTER THREE

THEORETICAL CONSIDERATIONS

3.1 Introduction

The governing equations which present the movement of a fluid particle are the Navier-Stokes and the continuity equations. If viscous effects are negligible the flow is said to be inviscid and the corresponding equations are known as the Euler equations (widely used in compressible aerodynamics). Detailed explanations of these equations of motion are given in Hughes (1979), Anderson (1995), Ligget (1994) and Dean and Dalrymple (1994) for more details.

According to the above literature considering an inviscid incompressible fluid, the equations of motion in the vertical plane is given by:

$$\frac{\partial u}{\partial x} + \frac{\partial w}{\partial z} = 0 \quad \ldots\ldots 3.1$$

$$\frac{\partial u}{\partial t} + u\frac{\partial u}{\partial x} + w\frac{\partial u}{\partial z} = f_x - \frac{1}{\rho}\frac{\partial p}{\partial x} \quad \ldots\ldots 3.2$$

$$\frac{\partial w}{\partial t} + u\frac{\partial w}{\partial x} + w\frac{\partial w}{\partial z} = f_z - \frac{1}{\rho}\frac{\partial p}{\partial z} \quad \ldots\ldots 3.3$$

where u and w denote the velocity components in the x and z Cartesian coordinate directions respectively t, is the time, ρ is the mass density and p is fluid pressure. The terms f_x and f_z indicate body force per unit volume acting on the fluid element.

In many environmental fluid mechanics problems, the water depth (D) is considered to be much smaller than the horizontal length scales. In particular, there are a number of wave phenomena in nature in which the water-depth to wave length ratio is small and the vertical accelerations

of the fluid particles are unimportant (since the vertical displacement of the particles are small compared with their horizontal displacements). As mentioned by Kirkgoz (1978) amongst such cases are the tides in the oceans, solitary waves, breaking waves on sloping beaches, flood waves in rivers or dams and surges in open channels. Such motions are often considered to be best represented theoretically by non-linear shallow water equations. Although the governing equations for such phenomena are the equations of Navier-Stokes, due to the complexity and difficulty of the solution of the Navier-Stokes equations, they may be reduced to Shallow-water or Saint-Venant equations by relevant assumptions. Hence, an approximation of common practice for the calculation of dam-break floods is the utilization of the shallow water equations (Chanson, 2005).

3.2 Shallow Water Wave Equation

Shallow water equations are approximations of the free surface gravity flow problems, with viscosity and surface tension effects neglected. The important assumption contained in these equations is that the vertical component of the acceleration of the water particles has a negligible effect on the pressure, or equivalently that the pressure is hydrostatic. These equations assume a small ratio of the water depth relative to other length associated with the horizontal direction. The equations of shallow water can be obtained in a number of different ways. Perhaps the most basic is to begin with the hydrodynamics equations which are presented by Arnason (2005) as follows:

Conservation of mass or continuity for incompressible fluid in 2 dimensions (x; z) states that:

$$\bar{V}.u = \frac{\partial u}{\partial x} + \frac{\partial w}{\partial z} = 0 \ldots\ldots\ldots\ldots\ldots 3.4$$

A fluid domain with a flat nonporous bottom yields a no-flow condition at z = 0 or

$$w|_{z=0} = \cdots\ldots\ldots\ldots\ldots\ldots 3.5$$

At a free surface at $z = h(x; t)$ the kinematic condition is:

$$w|_{z=h} = \frac{Dh}{Dt} = \frac{\partial h}{\partial t} + u|_{z=h}\frac{\partial h}{\partial x} \quad \text{......} 3.6$$

and the dynamic condition is:

$$P|_{z=h} = 0 \quad \text{......} 3.7$$

where P represents pressure.

Integrating Equation 3.4 with respect to z and making use of Equations 3.5 and 3.6 yields:

$$\int_0^h \frac{\partial u}{\partial x} dz + \frac{\partial h}{\partial t} + u|_{z=h}\frac{\partial h}{\partial x} = \frac{\partial h}{\partial t} + \frac{\partial}{\partial x}\int_0^h u dz = 0 \quad \text{......} 3.8$$

Shallow water theory assumes that the fluid acceleration in the z-direction has a negligible effect on the pressure P, which means that the pressure is hydrostatic hence:

$$P = \rho g(h - z) \quad \text{......} 3.9$$

where ρ the fluid density and g is the acceleration of gravity.

Note that:

$$\frac{\partial P}{\partial x} = \rho g \frac{\partial h}{\partial x} \quad \ldots\ldots 3.10$$

is independent of z therefore, the x-component of the fluid acceleration is also independent of z and if at any time u is independent of z it will be so at any time. Equation 3.8 can then be written as:

$$\frac{\partial h}{\partial t} + \frac{\partial (uh)}{\partial x} = \frac{\partial h}{\partial t} + h\frac{\partial u}{\partial x} + u\frac{\partial h}{\partial x} = 0 \quad \ldots\ldots 3.11$$

The momentum principle or Newton's second law of motion states the total force on a fluid particle equals its mass times its acceleration. Assuming the significant forces are pressure and gravity, i.e. ignoring both turbulent and viscous shear, this can be written as:

$$\rho \frac{Du}{Dt} = \rho\left(\frac{\partial u}{\partial t} + (u.\overline{V})u\right) = -\overline{V}(P + \rho g z) = -\overline{V}(\rho g h) \quad \ldots\ldots 3.12$$

The x component, divided by ρ is then:

$$\frac{\partial u}{\partial t} + u\frac{\partial u}{\partial x} + w\frac{\partial u}{\partial z} = -g\frac{\partial h}{\partial x} \quad \ldots\ldots 3.13$$

and the shallow water assumption leaves:

$$\frac{\partial u}{\partial t} + u\frac{\partial u}{\partial x} + g\frac{\partial h}{\partial x} = 0 \quad \ldots\ldots 3.14$$

Now, with the introduction of the propagation speed:

$$C = \sqrt{gh} \quad \ldots\ldots 3.15$$

Equations 3.11 and 3.14 can be rewritten in terms of *u* and *c* rather than *u* and *h*, yielding:

$$2\frac{\partial c}{\partial t} + c\frac{\partial u}{\partial x} + 2u\frac{\partial c}{\partial x} = 0 \quad \ldots\ldots 3.16$$

and;

$$\frac{\partial u}{\partial t} + u\frac{\partial u}{\partial x} + 2c\frac{\partial c}{\partial x} = 0 \quad \ldots\ldots 3.17$$

These equations comprise what are known as the shallow water equations. It again worth pointing out that the derivation of the shallow water equations shows that simplifying assumptions are made. The shallow water equations based on Euler's equations neglect amongst others viscous stresses. These are of interest concerning dissipation of energy and thus

loss of momentum. Furthermore, a hydrostatic pressure distribution is assumed. Considering that dam-break induces flood waves, this assumption does not hold in the wave front and in the initial phase. Due to the limited stream line curvature which is assumed, also turbulence cannot be accounted for.

The shallow water equations modelled waves with small ratios H/L where H denotes the wave height and L its length. This signifies that waves of small lengths may not be resolved. Also, it is of common practice to assume that the dam breaches instantaneously and completely. However, in reality it will take some minutes for a dam wall to fail and even part of it would block the flow. Although some of these assumptions are unrealistic, studies have shown that SWE give quite good results for dam breaks so their use is justified coupled with the fact that the worst-case scenario of dam-break is being simulated with the equations (Chanson, 2004).

3.3 Theoretical Concepts of Dam-break Flow

After a dam breaks, two waves known as negative and positive waves are generated. The negative waves move in the upstream direction whilst the positive waves move downstream. Generally, the dam-break flow produces a hydraulic bore and/or irregular oscillation. However, though the dam break flow generates wave formation, it is not a proper wave which can be determined from the main wave parameters such as wave length, height and period.

A number of experimental investigations of one dimensional unsteady open channel flow and in particular dam break flows has been reported in the past and some important results have been obtained (Dressler, 1954, Su and Barnes, 1970, Sakkas and Strelkoff, 1973, Fread, 1977, Katopodes and Strelkoff, 1978, Bellos and Sakkas, 1987). For this reason, several theoretical and mathematical models have been developed to predict the problem. Dressler (1954) also obtained experimental data of dam break flows in a horizontal, rectangular and straight open channel. The Waterways Experiment Station (WES) of the U. S. Army Corps of Engineers in 1960 conducted a series of experiments in a rectangular, one dimensional flume with a small bottom slope. In this experiment, as reported by Kamel (1968) the partial or total collapse of a dam was carried out instantaneously using specific flow conditions for the application of shallow water equations.

Generally, the shallow water equations form a set of coupled, non-linear partial differential equations (PDEs) which must be solved within an irregular domain subject to various initial and boundary conditions (Chanson, 2005). This set of equations cannot usually be solved analytically; however they may be solved in certain relatively simple cases. The analytical approach for these equations in a particular case may be the characteristic method. Stoker (1957) presented one of the most attractive investigations using the characteristic method. An exact solution would provide the values of the flow-field variables continuously at any of the infinite number of points throughout the domain.

However, before Stoker's work Ritter (1892) had already introduced a theoretical description of the two dimensional dam break problem for an inviscid fluid for a dry bed by solving the non-linear shallow-water equations. The solution gives a parabolic water surface profile which is concave upward. The front travels downstream with the wave celerity $c = 2\sqrt{gh_1}$ where g is acceleration due to gravity and h_1 is the initial quiescent water depth behind the dam. Upstream of the dam a negative wave travels upstream with $c = \sqrt{gh_1}$ which corresponds to the shallow water wave celerity.

In the shallow front region of the flow, neglecting resistance from bed friction is not realistic as bed friction has considerable influence on the propagation speed. Dressler (1952) added a Chézy resistance term of the form $C(u/c)^2$ to the momentum equation and obtains a first order approximation of the location of the water front as a function of time. However, Whitham (1955) argued that near the surge front the effect of friction is to pile up the fluid so the water surface slope is steep, where the depth becomes small. Noting that the acceleration terms would remain finite, Whitham (1955) reasoned that the friction and the pressure gradient terms in the horizontal momentum equation should balance each other as they become large near the tip of the surge. If the acceleration terms in the equation of motion is neglected while using a friction model which is quadratic, then the flow velocity results in a parabolic water surface profile for the surge tip which is concave downward.

According to Chanson (2005), for an unsteady open channel flow, the continuity and momentum equations yield a system of two differential equations in terms of the depth-average velocity and flow depth. For a rectangular prismatic channel, the equations may be expressed in dimensionless terms as:

$$\frac{\partial d}{\partial t} + d\left(\frac{\partial v}{\partial x}\right) + v\left(\frac{\partial d}{\partial x}\right) = 0 \ldots\ldots\ldots\ldots\ldots\ldots\ldots\ldots\ldots\ldots\ldots\ldots\ldots .3.18$$

$$\frac{\partial v}{\partial t} + v\left(\frac{\partial v}{\partial x}\right) + \frac{\partial d}{\partial x} + \left(S_f - S_0\right) = 0 \ldots\ldots\ldots\ldots\ldots\ldots\ldots\ldots\ldots\ldots\ldots .3.19$$

where d is the dimensionless flow depth (d = D/D$_o$), D is the flow depth, D$_o$ is the initial reservoir height, t is the dimensionless time (t = T√g/D$_o$), T is the time, g is the gravity acceleration, x is the dimensionless distance from the dam wall (x = X/D$_o$), X is the stream wise co-ordinate, v is the depth-average velocity, S_o is the bed slope (S_o = sinθ), θ is the angle between the bed and the horizontal and S_f is the friction slope.

Equations 3.18 and 3.19 are called the Saint-Venant equations. They cannot be solved analytically usually because of non-linear terms (e.g S_f). A mathematical technique to solve them is the method of characteristics which again yields a characteristic system of equations.

According to Chanson (2004, 2005) there are three well-known analytical solutions of instantaneous dam break waves: Ritter (1892) solution for an ideal fluid flow on a horizontal channel with a semi-infinite reservoir, Whitham (1955) development for a real-fluid flow on a horizontal channel with a semi-infinite reservoir, and HUNT (1982,1984) solution for a real-fluid flow down a sloping channel. All these analytical solutions assume an instantaneous dam break such an approximation that is often reasonable for concrete dam failures.

Chanson (2005) reported that for an ideal dam break surging over a dry river bed, the method of characteristics may be applied to solve completely the wave profile as first proposed by Ritter in 1892. For an ideal dam-break over a dry horizontal two-dimensional channel with a semi-infinite reservoir as shown in Figure 3.1, the basic equations were presented as:

$$\frac{D}{Dt}(V + 2C) = S_0 - S_f \;\; (forward\ characteristic) \ldots\ldots\ldots\ldots\ldots\ldots\ldots\ldots ..3.20a$$

$$\frac{D}{Dt}(V - 2C) = S_0 - S_f \ (backward\ characteristic) \ldots\ldots\ldots\ldots\ldots\ldots\ldots\ldots\ldots\ldots\ldots\ldots\ldots 3.20b$$

Along with:

$$\frac{dx}{dt} = V + C \ (for\ forward\ characteristic) \ldots\ldots\ldots\ldots\ldots\ldots\ldots\ldots\ldots\ldots\ldots\ldots\ldots\ldots\ldots 3.21a$$

$$\frac{dx}{dt} = V - C \ (for\ backward\ characteristic) \ldots\ldots\ldots\ldots\ldots\ldots\ldots\ldots\ldots\ldots\ldots\ldots\ldots\ldots 3.21b$$

where *C* is the dimensional celerity of a small disturbance. Equations 3.20 and 3.21 mean that (*V + 2C*) and *(V – 2C)* are constants.

The instantaneous dam-break creates a negative wave propagating upstream into a fluid at rest with known water depth. In the (x, t) plane, the initial negative wave characteristic has a slope $dt/dx = -1/C_o$ where $C_o = \sqrt{(gd_o)}$ for a rectangular channel. On the initial backward characteristic, V = 0 and C = C_o everywhere. In the particular case of a frictionless dam break in a wide horizontal channel, equations 3.20 and 3.21 may be solved analytically following Ritter's principle. Figure 3.1 shows the sketch of Ritter's solution.

The propagation speed of the dam break wave front or the wave front celerity then equals:

$$U = 2\sqrt{gd_o} \ldots\ldots\ldots\ldots\ldots\ldots\ldots\ldots\ldots\ldots\ldots\ldots\ldots\ldots\ldots\ldots\ldots\ldots\ldots\ldots\ldots\ldots\ldots\ldots\ldots\ldots\ldots 3.22$$

At any given time, the free-surface profile between the leading edge of the negative wave and the wave front is a parabola given as:

$$\frac{x}{t}\sqrt{gd_o} = 2 - 3\sqrt{\frac{d}{d_o}} \quad \ldots\ldots 3.23$$

At the origin (x=0), constant water depth is given as:

$$\frac{d_{(x=0)}}{d_0} = \frac{4}{9} \quad \ldots\ldots 3.24$$

Similarly the velocity at the origin is deduced as:

$$\frac{V_{(x=0)}}{\sqrt{gd_0^3}} = \frac{8}{27} \quad \ldots\ldots 3.25$$

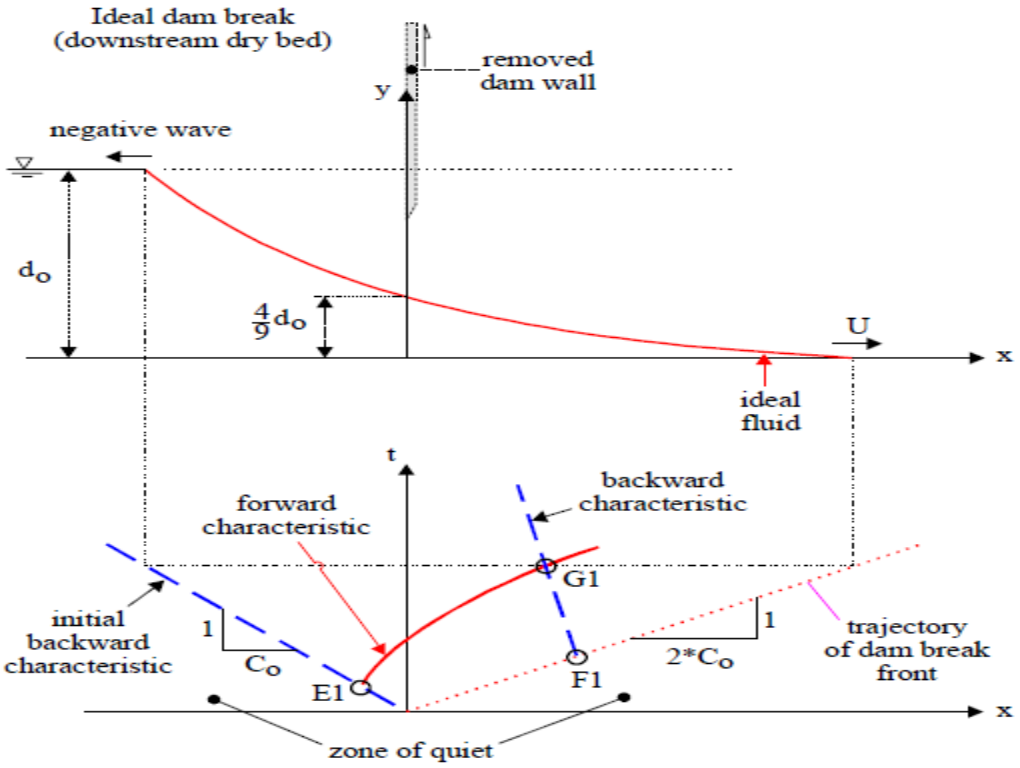

Figure 3.1: Sketch of a dam break wave in a dry horizontal channel with zero initial velocity (Adapted from Chanson, 2005).

This study uses bores formed by the fast removal of a gate with water impounded on one side, i.e. a dam break. The theory provided by Yeh et al. (1989) as well as Yeh (1991) for the bore generation system of this kind in a horizontal-bottom wave tank indicates that, just before the bore reaches the shoreline or structure, the final bore behaviour is virtually independent of the detailed initial wave condition offshore. In other words, bores created by any initial conditions behave qualitatively the same near the shoreline while the only important parameter which influences the strength of bore near-shore is the value of the terminal velocity at the shoreline, which is also a measure of the energy at the initial time (Yeh et al., 1989).

In a real fluid environment, however, dispersion effects are always present, and the bore front is not a discontinuity but has a finite length. Even if the bore generating system opens the gate almost instantaneously, the fluid must first accelerate both vertically downward and horizontally forward to form a bore. According to Yeh et al. (1989) this initial vertical acceleration generates waves of finite length which might contaminate the uniform bore with

a limited propagation distance but with a long propagation distance, those waves would disperse and separate from the bore front. Chanson (2005) also indicated that although there is considerable vertical acceleration during the initial instants of fluid motion, such acceleration is not taken into account by some methods of analytical solutions, particularly the method of characteristics while the pressure distributions are often assumed hydrostatic.

3.4 Impulse-Momentum Relationship

Wave-structure interactions are impact problems. Using Newton's second law, an impulse-momentum relation may be written as:

$$F = ma = \frac{d(mu)}{dt} \quad \ldots \; 3.26$$

Assuming the mass remains constant and can be replaced by the product of the mass density, ρ, area, *A*, and a length, *l*, and further assuming that the force, *F*, may be expressed in terms of an average pressure, *p*, acting over an area, *A*, equation 3.26 can be written as:

$$pdt = d(\rho lu) \quad \ldots \; 3.27$$

When pressures are not excessively high, the effects of the compressibility of a liquid are normally negligible. According to Kamel (1968, 1970) and Kirkgoz (1982), if there are large pressure differences, such as shock pressures, the elasticity of liquids may need to be taken into consideration.

In a compressible fluid the bulk *modulus* of elasticity, *E*, is *given* as:

$$E = \frac{\frac{dp}{dl}}{l} = \frac{\frac{dp}{d\rho}}{\rho} \quad \ldots\ldots 3.28$$

Proceeding with Equation 3.27;

$$\frac{p}{l}dt = ud\rho + du \quad \ldots\ldots 3.29$$

and substituting *dp* from Equation 3.28 into Equation 3.29 gives:

$$\frac{p}{l}dt = u\frac{\rho}{E}dp + \rho du \quad \ldots\ldots 3.30$$

The equation of motion for a steady-state flow is:

$$-dp = \rho u du \quad \ldots\ldots 3.31$$

and on substituting Equation 3.31 into Equation 3.30

$$\frac{p}{l}dt = -\frac{\rho^2}{E}u^2 du + \rho du \quad \ldots\ldots 3.32$$

Assuming all of the momentum of the mass is lost between the time the impact pressure first begins to act and the time, t_m, when the pressure reaches its peak value, p_m (Figure 3.2), then during this time interval, the velocity, u, changes from u_b, the breaking velocity, to zero.

Hence, Equation 3.32 becomes:

$$\int_0^{t_m} \frac{p}{l} dt = -\int_{u_b}^{0} \frac{\rho^2}{E} u^2 du + \int_{u_b}^{0} \rho du \quad \ldots\ldots 3.33$$

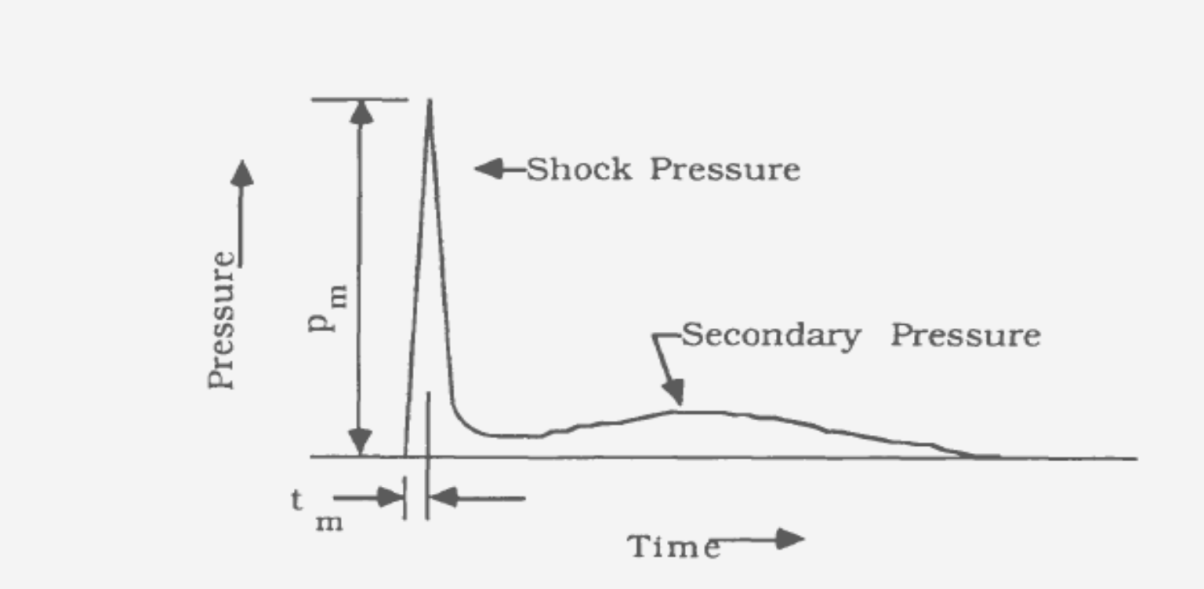

Figure 3.2: Typical Pressure-Time Curve (Adapted from Kirkgoz, 1982)

The relationship between p and t may be assumed to be linear between the time when pressure first begins to act, $t = 0$, and when pressure is maximum, $t = t_m$. Then,

$$\frac{1}{2}\left(\frac{p_m}{l}\right) t_m = \frac{\rho^2}{3E} u_b^3 - \rho u_b \quad \ldots\ldots 3.34$$

Rewriting Equation 3.34, the sign changes on the right-hand side because the interest is on the pressure exerted against the wall:

$$p_m t_m = 2l\left(\rho u_b - \frac{\rho^2}{3E} u_b\right) \ldots\ldots\ldots\ldots\ldots\ldots\ldots\ldots\ldots\ldots\ldots\ldots\ldots\ldots\ldots\ldots\ldots\ldots\ldots\ldots\ldots\ldots\ldots\ldots\ldots\ldots 3.35$$

For water wave motion, the second term inside the parentheses in Equation 3.35 is very small compared with the first term. Ignoring the elasticity term,

$$p_m t_m = 2l\rho u_b \ldots\ldots\ldots\ldots\ldots\ldots\ldots\ldots\ldots\ldots\ldots\ldots\ldots\ldots\ldots\ldots\ldots\ldots\ldots\ldots\ldots\ldots\ldots\ldots\ldots\ldots\ldots\ldots\ldots\ldots\ldots\ldots 3.36$$

The parameters on the left side of Equation 3.36 may be determined from pressure measurements, while u_b may be found from breaker measurements. The length l, may be evaluated using mass density of water, ρ.

3.5 Summary

This chapter reviewed various forms of the governing equations that relate with the phenomenon of wave-structure interaction. The governing equations which present the movement of a fluid particle are the Navier-Stokes and the continuity equations. The corresponding equations when viscous effects are ignored are known as the Euler equations. Shallow water equations are approximations of the free surface gravity flow problems, with viscosity and surface tension effects neglected. Detailed derivations, descriptions and explanations of these equations are given in this chapter.

The shallow water equations modelled waves with small ratios H/L where H denotes the wave height and L its length. There are a number of wave phenomena in nature in which the water-depth to wave length ratio is small and the vertical accelerations of the fluid particles are unimportant. Such cases are the tides in the oceans, solitary waves and breaking waves on sloping beaches, flood waves in rivers or dams and surges in open channels. Such motions are

often considered to be best represented theoretically by non-linear shallow water equations. Although the governing equations for such phenomena are the equations of Navier-Stokes, due to the complexity and difficulty of the solution of the Navier-Stokes equations, they may be reduced to Shallow-water or Saint-Venant equations by relevant assumptions. Hence, an approximation of common practice for the calculation of dam-break floods is the utilization of the shallow water equations.

Consequently, the consideration of shallow water equations and its applicability to dam-break problems were discussed in this chapter. There are three well-known analytical solutions of instantaneous dam break waves: Ritter (1892) solution for an ideal fluid flow on a horizontal channel with a semi-infinite reservoir, Whitham (1955) development for a real-fluid flow on a horizontal channel with a semi-infinite reservoir, and HUNT (1982,1984) solution for a real-fluid flow down a sloping channel. All these analytical solutions assume an instantaneous dam break, an approximation that is often reasonable for concrete dam failures. For an ideal dam break surging over a dry river bed, the method of characteristics may be applied to solve completely the wave profile as proposed by Ritter in 1892 and is presented in this chapter. Finally, the analysis of impulse-momentum relationship of the wave-structure interactions is discussed. Having reviewed various publications on the subject, an appropriate methodological approach for the present study was chosen which led to the description of the experimental rig as well as experimental programme and procedures presented in the next chapter.

CHAPTER FOUR

RESEARCH METHODOLOGY

4.1 Physical Modelling Approach

Coastal engineers rely on three complementary techniques to deal with the complex fluid flow regimes typical of many coastal projects. These techniques are field measurements and observations, laboratory measurements and observations, and mathematical or numerical techniques. Measurements of natural phenomena (Field measurement techniques) are desirable, but it is often difficult and expensive to obtain adequate data of the required degree of accuracy due to the complexity of coastal processes and wave-structure interactions. Again, with the advent of computer numerical modelling has shown steady growth and utility over the past decade (The Indian Society of Hydraulics, 2013). Numerical models are practical for cases where wave refraction, shoaling, and diffraction are the only important hydrodynamic characteristics, and considerable success has been shown in accurately simulating near-shore circulation with numerical models (Hydraulic Engineering Manual, 2002). But, though numerical modelling had recently gained an increasing utility however, numerical modelling is often run in parallel to the physical modelling for accurate and detailed simulation of the process in question. Thus, physical modelling does give a good basis for validation of numerical modelling.

Physical or scale models constructed and operated at reduced scale still offer an alternative for examining coastal phenomena that may presently be beyond our analytical and mathematical skills. Laboratory studies are generally termed physical models because often they are miniature reproductions of a physical system. The wave tank is the traditional tool of the coastal engineer for creating and generating model waves in the laboratory. It enables less expensive examination of coastal problems that can be approximated as 2-D processes (Hughes, 1993). Laboratory wave tanks and basins provide a controlled environment for the study of coastal processes and wave-structure interaction problems.

Consequently, in this study, the physical modelling technique has been considered for the investigation of the effectiveness of new seawall designs for the mitigation of floodwater waves. The study has therefore required the construction of a model wave tank. It is therefore, the intent of this chapter to describe the design and construction of the wave tank used to create

the dam-break flow geared toward testing the suitability of new seawall designs in the present investigations.

4.2 Scope

This work was carried out in the Materials and Hydraulic Laboratory of the School of the Built Environment, Liverpool John Moores University. A Low Cost Wave Tank (LCWT) was designed and constructed in the hydraulics laboratory to simulate dam failure in order to generate flood wave in a similar way to the bores or surges developed on the shoreline during tsunami events. It is as well a good approximation of the study of the terminal effect of tsunami (Yeh et al., 1989). A dam-break flow is created in the wave tank by a sudden release or impulse withdrawal of a gate separating the reservoir section and the rest of the wave tank in a vertical upward direction. The experimental tests were carried out on smooth and rough surfaced walls in vertical and sloping forms for a wide range of initial reservoir conditions. The advantage of the bores generated with this system is that the theoretical prediction of the bores can be made without difficulty from the classic dam-break theory. Furthermore, the depression wave that initially propagates offshore and is then reflected back at the end wall, does not influence the flow during the run-up process (Yeh et al., 1989).

In order to achieve objectives 5 - 8 (section 1.6) for this study, it was necessary to conduct experiments on impact wave pressures in which instrumented vertical and sloping seawall models are subjected to the floodwater waves generated in the wave tank while taking a comprehensive measurement of impact pressures on the modelled seawalls. The floodwater front velocity in the channel (objective 4) was also computed using different techniques alongside a combination of equations of motion at the initial stage of the study. The characteristics of flow or wave form in the channel (objective 3) were also analysed with digital video camera and powerful light source. The flow is photographed by an automatically triggered camera and also captured on video while registrations of visual observations are subsequently related to the digital recordings. The video footage as well as the photography shots for the flow was then transferred to a computer and analysed using suitable editing/post processing software.

4.3 Dimensional Analysis and Similitude Theory

4.3.1 *Dimensional Analysis*

The method of dimensional analysis is valid for comparison of the same phenomenon at different scales. The fact that the research tool for this study relies on scale model tests makes it essential to form a dimensional analysis for the measured parameters. Scale selection was based on the available space for the test facilities, obtainable wave generation system, and the capacities of wave probes and pressure transducers used to measure the data. The magnitude of shock pressures varies with the form of the waves as they make contact with the modelled seawall. Factors which influence the magnitude and duration of these pressures are wave dimensions, downstream slope, amount of entrained air in the water, and the pressures in air pockets trapped between the wave and the wall at contact.

Following Hudson et al. (1979), the flow over the model wall can be assumed a function of the following**:**

Depth of water in front of the wall = d_b

Modulus of elasticity of the water = E

Bulk modulus of the seawall = E_{sw}

Acceleration due to gravity = g

Wave height in front of the wall = H_b

Adiabatic constant of air = k

Pressure intensity on the wall = p

Atmospheric pressure = p_o

Mass density of the seawall = ρ_{sw}

Mass density of the water = ρ

Wave period = T

Angle of bottom slope = θ

Angle of incident wave attack = β

Wave length = L

Surface tension of the water = σ

Using the Buckingham p_i theorem, the above parameters can be put into dimensionless form following similar study carried out by Rismiller (1989). The viscous shear forces are negligible compared to gravity, inertia, pressure, and elastic forces. Also the angle of downstream bottom slope and angle of incident wave attack is considered insignificant in these experiments therefore they were dropped. According to Rismiller (1989) rearranging and combining the above terms to obtain a functional relationship for impact pressure may take the form:

$$\frac{(p-p_o)}{p_o} = f\left\{\frac{H_b}{d_b}, \quad \frac{\left[(gH_b)^{\frac{1}{2}}T\right]}{d_b}, \quad \frac{\sigma T^2}{(\rho H_b d_b^2)k}, \quad \frac{\left(E/\rho\right)^{\frac{1}{2}}T}{d_b}, \quad \frac{\left(E_{sw}/\rho_{sw}\right)^{\frac{1}{2}}T}{d_b}, \quad \frac{\rho}{\rho_{sw}}\right\} \quad 3.37$$

This functional relationship will be used to correlate the resulting test data in the form of dimensionless plots. However, the relevant terms related to the present study in the above equation are considered. It's worth mentioning here that dry-bed downstream was considered throughout this investigation when measuring impact pressures on the wall and therefore the initial depth of water in front of the wall (d_b) is taken to be one.

4.3.2 *Theory of Similitude*

A physical model may be defined as a physical system reproduced (at reduced size) so that the major dominant forces acting on the system are reproduced in the model in correct proportion to the actual physical system. To determine if a model can reproduce these dominant forces in

correct proportion requires the application of the theory of similitude. If a scale model is constructed such that all lengths in the model are in the same ratio to those in the prototype, then geometric similarity is achieved. The geometric scale is defined as the ratio of any length in the prototype (L_P) to that in the model (L_M).

Thus the length scale ratio (N_L) is defined as $N_L = L_P/L_M$. Scale ratios for area (N_A) and volume (N_V) follow directly from the length scale ratio, as area and volume are proportional to the length squared and cubed, i.e. N_L^2 and N_L^3 respectively.

Reeve et al. (2012) stated that to achieve complete similarity between model and prototype also requires similarity of motions known as kinematic similarity (velocity and acceleration) and dynamic similarity (forces or pressures). However, in fluid mechanics problems the forces acting can include gravity, viscosity, surface tension, elastic compression and pressure forces. Consequently, common forms of non-dimensional groups used in fluid mechanics are Reynolds number, Froude number, the Mach number and the Webber number. Restricting attention to typical coastal engineering situations, the principal forces acting are those due to gravity and viscosity. Hence, for perfect similitude, these force ratios must also each be equal between model and prototype.

As the predominant force in the present situation is gravity force, Froude number (Fr) is the dimensionless number that is of fundamental importance. Hence, for similitude, it is necessary that the Froude number is the same in the model and prototype i.e. $Fr_p = Fr_m$. This relationship provides the similitude criterion by which model velocities and times may be related to the prototype values.

Using Froude's law and referring by subscripts P and M to prototype and model respectively:

$$\frac{u_P}{\sqrt{gd_P}} = \frac{u_M}{\sqrt{gd_M}} \; OR \; \frac{{u_P}^2}{gd_P} = \frac{{u_M}^2}{gd_M} \quad \ldots \ldots 3.38$$

Recalling equation 2.9 (see section 2.3.3)

$$\frac{P_{max}}{\gamma} = k\frac{V_{fw}^{\ 2}}{2g} \quad \ldots\ldots\ldots\ldots\ldots\ldots\ldots\ldots\ldots\ldots (2.29\ recalled)$$

and substituting this equation into equation 3.38 gives:

$$\frac{p_P}{d_P} = \frac{p_M}{d_M}\ or\ p_P = p_M\frac{d_P}{d_M} \quad \ldots\ldots\ldots\ldots\ldots\ldots\ldots\ldots\ldots\ldots 3.39$$

$\frac{d_P}{d_M} = n$ is the length scale (where d_P and d_M are the initial water depths at the prototype and model reservoir section respectively). However, in the present study, d_P and d_M are taken as wave heights produced on impact with the wall for the prototype and model respectively.

Thus, finally equation 3.39 becomes:

$$p_P = p_M . n \quad \ldots\ldots\ldots\ldots\ldots\ldots\ldots\ldots\ldots\ldots 3.40$$

Where p_P and p_M are impact pressures on the wall for the prototype and model respectively and n is the height scale defined as $\frac{H_P}{H_M}$ (H_P and H_M are the wave heights at impact for the prototype and model respectively).

Therefore, according to equation 3.40, the non-dimensional maximum impact pressures, $\frac{p_{max}}{\rho g H_{inc}}$ (i.e. without the hydrostatic pressure) in relation to equation 3.37 (see section 4.3.1) may also be used to predict maximum pressure on a full scale structure. Consequently, a number of related field and other available experimental data are analysed and illustrated in section 5.8.2 to correlate the magnitude of the values of the maximum impact pressures in the present study.

4.4 Experimental Facilities

Within the wide range of experiments that are to be carried out in this study, many different items of equipment and instruments are to be used or developed. This section outlines the key features of the experimental facilities employed.

4.4.1 *The Low Cost Wave Tank (LCWT)*

Laboratory wave tanks and basins provide a controlled environment for the study of coastal processes and wave-structure interaction problems. A wave tank with a water release gate is constructed primarily to conduct experiments to investigate effects of flood wave on vertical and sloping seawalls. Although the wave tank was designed to model a variety of waves, the release gate was a special design to simulate sudden dam failures (water releases) for creating bores similar to the surges developed on the shoreline during tsunami events. A view of the LCWT constructed by LJMU for this study is shown in Figure 4.1.

The critical dimensions of a wave tank are the working length and cross-section (width and depth). The test section of the wave tank is 4.70 m long, 0.40m wide and 0.50m deep close in dimensions to the one used in the experiments performed by Thusyanthan and Madabhushi to determine the tsunami wave loading on coastal houses (Thusyanthan and Madabhushi, 2008). The materials used for construction are of paramount importance, not only for the durability and longevity required of such a piece of equipment, but also suitability for purpose. Also, clarity of flow visualisation is an essential feature, particularly in a situation where sophisticated photography and video footage are involved. Hence, one of the sidewalls was constructed of clear Perspex for superb optical access, both for flow visualization and quantitative imaging measurements with the entire facility supported by a steel structural frame. Wherever possible the more basic components in contact with water are made of non-corroding materials, such as plastic and treated engineered plywood. The bed slope is made to be horizontal.

Figure 4.1 : LJMU Low Cost Wave Tank

4.4.2 *Test Specimen - The Seawall Models*

Wave-action models can be divided into two general types: (1) harbour models, and (2) breakwater stability models. Harbour models usually reproduce the entire harbour area and the various shore-line structures, together with sufficient area seaward to allow proper generation of waves. This type of model is used to determine the best solution to wave- and surge-action problems involving the selection of the most efficient type, length and alignment of breakwaters, the location, alignment, shape, and width of navigation openings, the proper location and type of piers and beaches, and the effects of proposed dredging projects. Thus, the harbour model has to do with the solution of problems involving the effects of contemplated changes in static boundary conditions on wave reflection, refraction, diffraction, and attenuation.

However, breakwater or seawall stability models are useful in selecting the most efficient design of seawalls with respect to the forces imposed upon them by wave action. This type of model is used to determine the shape and magnitude of wave pressure curves on impervious, vertical and inclined walls, the stability of caissons and cribs and the proper size and density

of rock, degree of slope, crown elevation and cross-sectional shape of rubble-mound breakwaters or seawalls. Consequently, the seawall models used in the present study were fabricated using steel sections and foam plastic sheets. The steel sections are used so as to make a rigid frame and support the structure. The foam plastic sheets are fixed on the frame. The wall model was 0.40m width by 1.30m height.

The performances of four (4) different wall surfaces were investigated in this study. They included; the smoothed/plane surface wall model (wall model-A), the semi-smoothed surface wall model (wall model-B), the isotropic macro-texture surface (IMACTS) wall model (wall model-C) and the isotropic micro-texture surface (IMICTS) wall model (wall model-D). The smoothed/plane wall model (wall model-A) was initially incorporated into the downstream end of the wave tank. This wall could be easily replaced. It was designed and fixed in a way that the wall angle can be easily altered. The seawall was fixed inside the wave tank rigidly for the required angle of inclination by using supports and wedges driven between the seawall and tank wall. A total of 10 holes/cut-outs were made on the wall to fix the pressure transducers and to ensure they were flush with the wall although only six (6) of the cut-outs were used at a time.

The surface energy dissipaters of the model walls were made of geo-grid materials of various types attached to the surface of the walls. The geo-grids provided surface roughness that was quantifiable in terms of texture and/or abrasiveness. Engineers and manufacturers specify surface smoothness not only by "roughness average" or R_a which is the integral of the absolute values of the roughness profile across the surface in relation to the mean (Orvis and Grissino-Mayer, 2002), but also by the dimensions of the grits on the surface. According to Orvis and Grissino-Mayer (2002) there are some cases where specifying surface smoothness by R_a may have little or no practical meaning whereas reporting the grit sizes could be of importance.

The wall surfaces modelled in the present study were abraded with different geo-grids of various grades and grit sizes which provided various ranges of surface texture or coarseness. Grit size refers to the size of the particles of abrading materials attached to the surface. In this study, surface roughness therefore means the deviation of the wall surface from the true smooth planar surface with various characteristic dimensions of grit particles. Wall model-A had no geo-grid material attached to its surface and therefore modelled the true smooth or plane surface. Wall model-B had a wire-mesh geo-grid material attached to its entire surface area

with cavity dimensions of 30mm by 40mm hence referred to as semi-smooth surface wall. The cavity within the wire-mesh geo-grid covered about 50% of the entire surface area of the wall hence exposed nearly half of the smooth part of the surface thus given the term semi-smooth surface wall model.

Wall model-C had a hard-grit geo-grid material attached to its entire surface area (equivalent grit dimensions of 538 -1815 micro-metres). These ranges of grit dimensions were also classified as "macro-texture" (BSI 6 ISO 13473, 2002, Orvis and Grissino-Mayer, 2002) and may be obtained by suitable proportioning of the aggregate and mortar of the mix or by surface-finishing techniques. Wall model-C is therefore referred to as isotropic macro-texture surface (IMACTS) wall throughout this report. Wall model-D had a soft-grit geo-grid material attached to its entire surface area (with equivalent grit dimensions of 25.8 – 58.5 micro-metres). These ranges of grit dimensions are classified by Orvis and Grissino-Mayer (2002) as "micro-texture" thus wall model-D is referred to as isotropic micro-texture surface (IMICTS) wall. The rough surfaces (wall model-A, model-B and model-C) modelled in this investigation are shown in Figure 4.2.

The purpose of seawalls is to withstand direct wave attack. They are not necessarily designed to retain sediments or to reduce soil erosion. However, incorporating suitable materials at the wall surface may retain sediments or reduce scour at the base of the wall and also dissipate the energy of the waves significantly enhancing the performance of the defence wall. The seawall models (the test specimens) for the present study utilise the design principle, functions and material properties of groins and gabions (see section 1.3.3 in chapter 1) by investigating the behaviour of similar materials in terms of dissipation of the energy of the waves when incorporated into the surface of seawalls. Such seawall designs may not only provide rough surfaces for dissipating the energy of the flood waves but may also prevent scour at the base of the wall through retention of sediments.

Geo-grids are invaluable tools in transportation and civil construction. Geo-grids are often used as a replacement for traditional solutions (groins and gabions) in coastal defences. Geo-grids are structured polymeric materials usually made from sheets of high density polyethylene or polypropylene or by weaving or knitting and coating various high tenacity polymer yarns. The resulting geo-grid structure possesses open spaces (called apertures) ranging from 0.5 to 4.0 in. (1 to 10 cm), which enhance interaction with the soil or aggregate they are embedded within.

By adding geo-grids to soil or other geotechnical materials, the designer is able to create a composite material where one element relies on the other to provide a complete system. The expected interaction of one element with the other may be designed for an extensive range of applications (Sorensen, 2013).

Applications of geo-grids in geotechnical structures include retaining wall which is viewed as an extremely efficient and cost saving method of design application. Other applications include bridge or railway abutments, reinforced soil slopes, reinforced foundations over piles, reinforced embankments etc. all utilizing similar design principles. However, each application may have its own design method but sometimes the same design method can be modified for different applications. In all applications, the designer must analyse the interaction of the geo-grid with the geotechnical material being used to achieve the intended performance of the structure being designed.

Although geo-grids are used primarily for reinforcement, some products are designed for asphalt overlay and waterproofing or for separation and stabilization. Geo-grids also are used as gabions and sheet anchors, inserted between geotextiles and geo-membranes, or used to construct mattresses for fills or embankments over soft soils. Geo-grids improve the structural integrity of soils in roadways, walls in coastal defences and slopes by reinforcing and confining fill materials and distributing load forces. In retaining wall and slope applications, geo-grids can be combined with a wide variety of facing elements to produce the desired aesthetics for any project (Don and Low, 2006).

Semi-smooth surface (Model-B) | IMACTS surface (Model-C) | IMICTS surface (Model-D)

Figure 4.2: Photographs of the test specimen (the seawall models) showing different types of geo-grids used to model the rough surfaces

4.4.3 *The Pump*

A water tank of approximately 0.6m^3 was placed on the laboratory floor and connected to the reservoir section of the wave tank. Water is pumped into the reservoir section at the start of each experiment and drained at the end of each experiment from and into the bottom water tank through a pump rigidly fixed inside the water tank. A submersible water pump supplied by Clarke International was used. The pump was designed for use with fresh water (see Figure 4.3). The model used in this experiment was model GSE 2 with the following specifications (Clarke International – Submersible Pump GSE Range – Operational & Maintenance Instructions Manual No. 1102):

Maximum Head = 33ft/10M

Maximum Output = 110gpm/500Lpm

Volts/Phase/Hz = 240/1/50

Motor Hp/kw = 0.8/0.6

Part No. = 7230074

Serial No. = 11/L1649.15

Figure 4.3 : Clarke International Submersible Water Pump – Model GSE 2

4.4.4 *The Video Camera*

A JVC TK – 1085E high-speed digital camera was used, acquiring grey-scale images at a rate of 40 frames per second, with a resolution of 256 by 256 pixels. Video images are digitally captured onto on-board memory where they can be written to compact flash card or downloaded through Ethernet connection to PC. Custom designed software included in the package provided the ability to analyse and enhance images. The camera operated at low light level, automatically modifying the contrast of the image in real time to enhance areas of image with too little light, which maintain approximately constant picture brightness. The power consumption was low at only 3 watts and the camera operated from a 12v DC supply, resulting in a small battery drain. The camera also had a small physical size and a secure mounting point on the base, which made it easy to fix to a tripod stand positioned at a designated point away from the wave tank.

4.4.5 *The Instrumentation*

(a) Pressure Transducer

A pressure transducer is a transducer that converts pressure into an analogue electrical signal. Although there are various types of pressure transducers, one of the most common is the strain-gauge based transducer. The conversion of pressure into an electrical signal is achieved by the physical deformation of strain gauges which are bonded onto the diaphragm of the pressure transducer and wired into a Wheatstone bridge configuration. Pressure applied to the pressure transducer produces a deflection of the diaphragm which introduces strain to the gauges. The strain will produce an electrical resistance change proportional to the pressure.

The study requires the determination of the dynamic pressure profiles on the model structures under investigation. Dynamic pressure measurements under these conditions (turbulence flow) may require sensors with special capabilities such as fast response, ruggedness, high stiffness, extended ranges, and the ability to also measure quasi-static pressures.

Therefore, in order to facilitate this, Piezotronic low impedance pressure transducers were selected and used at designated elevations on the wall models. Low impedance transducers are ideally suited for applications where long or moving cables are required or in high humidity or other contaminated atmospheres. They eliminate the high impedance problems by providing a voltage signal with low impedance and a wide frequency response. A miniature electronic circuit is built into the housing of a low impedance transducer. This circuit converts the high impedance charge signal generated by the piezoelectric material into a voltage signal, with output impedance typically below 100 Ω. This allows the use of conventional, coaxial or two-wire cable between the transducer and the remotely located power supply/coupler. Both the power to and signal from the transducer are transmitted over the two wire cable. (Kistler Universal Pressure Transducer Manual).

Consequently, Kistler type 211B5 pressure transducers were selected powered by a type 5134A power supply/coupler (Figure 4.4). Model 211B5 series piezotron pressure transducers are miniature, acceleration compensated instruments, which produce a high level, low impedance signal that is the voltage analogue of dynamic pressure input. Resolution is in the order of one

part per 20,000 of full-scale range, in other words plus or minus 34.5 Pa for a 0 to 100 psi transducer. These transducers incorporate sensing elements of crystalline quartz and contain a solid-state impedance converter with sensitivity expressed in millivolts per unit of pressure. The acceleration compensation is required as the mass of the diaphragm and sensing element produces an inherent acceleration sensitivity which is eliminated by the embodiment of a quartz accelerometer whose output polarity is opposite to that of the pressure-sensing element. Thus, the accelerometer output nominally cancels or nulls what would otherwise be a component of the sensing element output attributed to the acceleration (Atherton et al., 2008).

Kistler type 211B5 pressure transducers selected for this study are powered by a type 5134A power supply/coupler (Figure 4.4). The power supply/coupler's role in the measuring system is to supply the necessary constant current excitation to the low impedance transducer and to couple the signal from the transducer to the read-out equipment. The circuit within the transducer will produce a quiescent bias voltage. The instantaneous voltage at the transducer output will, of course, vary as the transducer is exposed to stimuli. The model 5134A power supply/coupler selected for this study has a four channel signal conditioner for low impedance piezoelectric transducers. Each channel is equipped with 4mA current supply, line bias monitor, adjustable gain 1, 2, 5, 10, 20, 50 and 100x, selectable low pass filter 100Hz, 1kHz, 10kHz and 30kHz as well as internal white noise generator for system testing. These provided the choice of seven gain settings and four low pass cut-off frequencies. It is operated in a way that each channel may be set independently of the other three. A system test of the coupler may be turned on which will inject an internal generated white noise signal into the inputs of all four channels. All the unit set points are stored in non-volatile memory for immediate restoration of instrument set points upon power-up. The coupler can be configured for 230V or 115V line power as required. Calibration data of the transducers are supplied by the manufacturer.

Figure 4.4 : Pressure Transducer Power Supply/Coupler – Kistler type 5134A

(b) Wave Probes

Wave probe is a simple and robust device for measuring and recording rapidly changing water wave levels in physical modelling. It operates by measuring the electrical conductivity between two stainless steel wires that are immersed in water which is converted to an output voltage that is directly proportional to the immersed depth, or wave height. The probe is energised with a high frequency square wave voltage to avoid polarisation effects at the wire surface. The wires dip into the water and the current that flows between them is proportional to the depth of immersion. The current is sensed by an electronic circuit, which provides an output voltage proportional to the instantaneous depth of immersion, or wave height, which can be used as input to a high-speed data logger (Churchill Controls Wave Monitor Manual).

The supplied probe consists of a pair of stainless steel wires, 1.5mm in diameter and spared 12.5mm apart (Figure 4.5). However, the flexibility of the drive and sensing circuits enables a very wide variety of probe configurations to be employed. This adaptability allows the construction of probes to suit our requirements for this study.

The associated Wave Monitor Module (WMM) (Figure 4.6) carries the energisation and sensing circuits and means for compensating for the resistance of the probe connecting cable. It is powered from a separate Power Supply Module, A.C. mains operated and with sufficient capacity to power 2 Wave Monitors. When probes are used in close proximity to each other it is necessary for them to be energised at different frequencies to avoid mutual interaction. A plug and socket selector is provided on the Wave Monitor Module to enable the energisation frequency of each probe to be individually selected.

Figure 4.5: Wave Monitor Module – Churchill Controls Product

Figure 4.6: Wave Probe - Churchill Controls Product

(c) Data Logger

A data logger is an electronic device that records data over time or in relation to location either with built in instruments and sensors or through external instruments and sensors. While some data loggers interface with a personal computer and utilize software to activate it and to view and analyse the collected data, others have a local interface device and can be used as a stand-alone device.

A computer controlled National Instruments USB-6008 model (Figure 4.7) was used for data collection from the pressure transducers and the wave monitoring probes for this study.

The data logger was connected to a personal computer and controlled through the use of Labview virtual instrumentation software, which is user programmable via a graphical programming language.

Figure 4.7: National Instrument SCXI USB – 6008 Model

4.5 Experimental Arrangement

The arrangements for the present experiments are shown in Figure 4.8. A series of tests were performed in a 4.70m long, 0.40 m wide, and 0.50m deep wave tank (see Figure 4.1). The wave tank bottom bed was designed to be horizontal since this has been found to be relatively easier to construct in terms of gate release mechanism for generating bores (Ramsden, 1993). The dam itself consists of the gate made of steel plate of about 3mm thickness, which can slide freely and vertically along small plastic grooves aligned on each side of the gate frame. Tapes/Greases are used around the joints between the gate and the sides of the tank to minimize leakage. A rope was attached to the top of the gate which was drawn over a pulley positioned at about 2.5 m above the channel bed (Figure 4.9). With the gate initially in position to create a dam, an upward impulse is generated by releasing/pulling the rope through the pulley system.

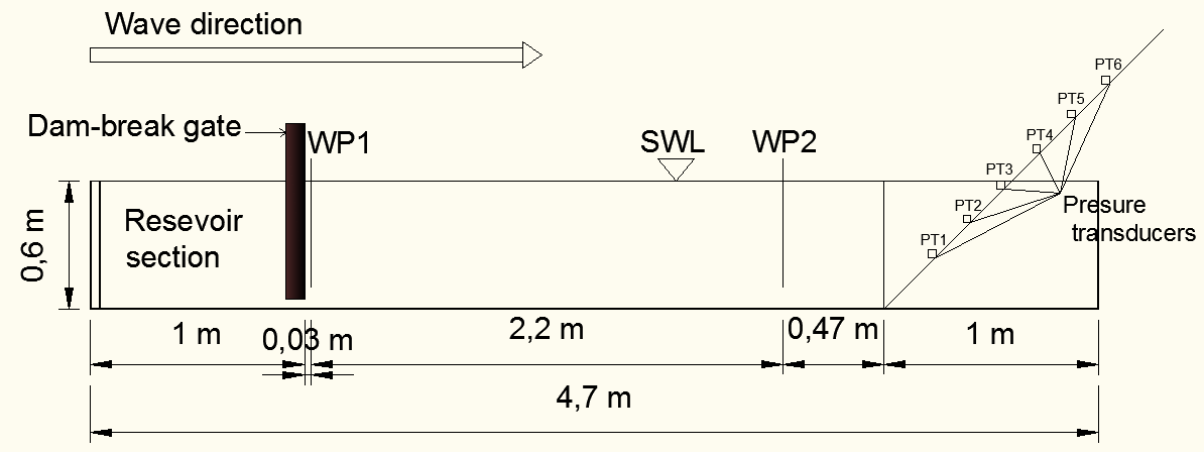

Figure 4.8: Experimental Set-up

The location of the gate which determines the proportion of reservoir length to wave propagation distance was strategically positioned using information given by Ramsden (1993) who suggested that allowing some period between the times the wave impacts the instrumented wall and the arrival of the negative wave reflected from the end of the reservoir. The reason for this distance was also to let the bores become fully developed before hitting the seawall structure on their path as suggested by Yeh et al. (1989). According to shallow-water wave theory, as long as a fully developed bore is generated offshore, the limited bore propagation distance available to the experiments should not be a significant drawback to the study of a bore near-shore and the ensuing run-up process (Yeh et al., 1989). Hence, the experimental results should be considered to be general, and not limited to this particular experimental set-up. As a result, the gate was fixed at 1.0m from the reservoir end of the wave tank to allow the wave propagation distance of at least 2.7m in order to let the bores fully develop before hitting the seawall. The tank was not too wide (0.4m width) hence the sidewall effects should be negligible for the experimental data obtained along the centreline of the tank.

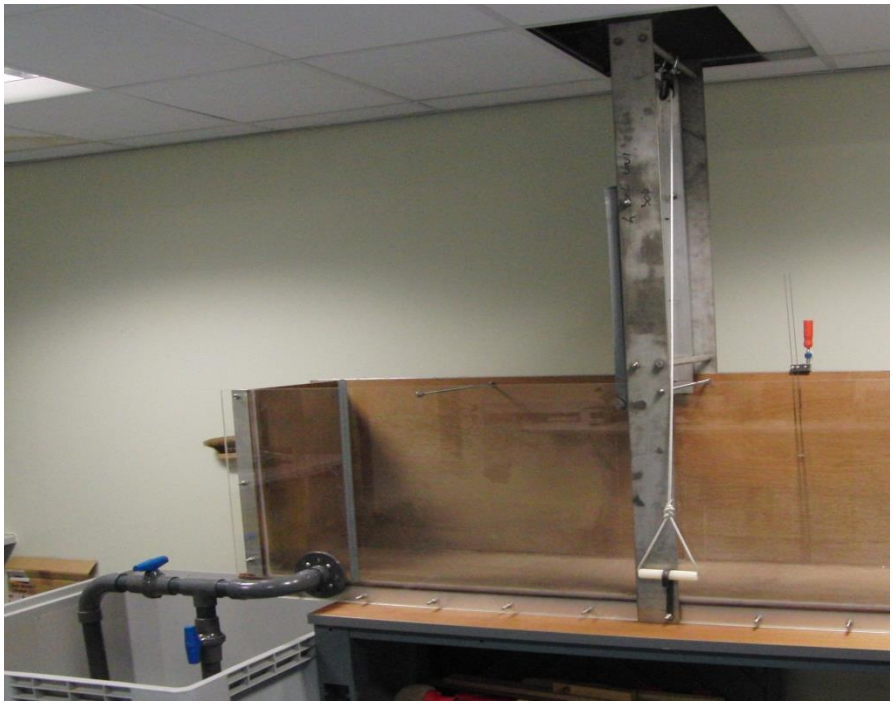

Figure 4.9: Gate release pulley mechanism showing water tank, dam section and pumping system

The wall model was fixed at 1.0m from the other end of the wave tank. The seawall was then secured inside the wave tank rigidly for the required angle of inclination. The seawall angle was adjustable, with a hinge mechanism at the lower end of the wall to allow the wall angles to be varied. Six pressure transducers were mounted on the centre line of the wall at a given interval **(**Table 4.1**)** and two wave probes were positioned in the middle line of the flume at a designated distance downstream of the channel to measure the wave heights (Table 4.3). The six transducers were fixed on the wall perpendicularly to the in-coming floodwater wave front to ensure that the horizontal impact is measured by the sensors (Figure 4.10). The first wave probe is positioned just behind the reservoir gate while the other probe is located just in front of the seawall model (Figure 4.8)). The criteria for the gauge positioning were chosen following the facts that gauges generally should be distributed across the entire flow field and that they should be installed where uniform flow is absolute.

A National Instruments USB-6008 data logger (see Figure 4.7) used for data collection from the pressure transducers and the wave monitoring probes was connected to a personal computer and controlled through the use of Labview virtual instrumentation software.

Table 4.1 : Positions of the pressure transducers (x = 0 at the base of the wall model)

Transducer Number	x (m)
1	0.02
2	0.12
3	0.22
4	0.32
5	0.42
6	0.50

Table 4.2 : Positions of the two wave probes for water level and impact pressure measurements (x = 0 at the upstream end of the reservoir)

Wave probe number	x (m)
WP1	0.03m
WP2	2.23m

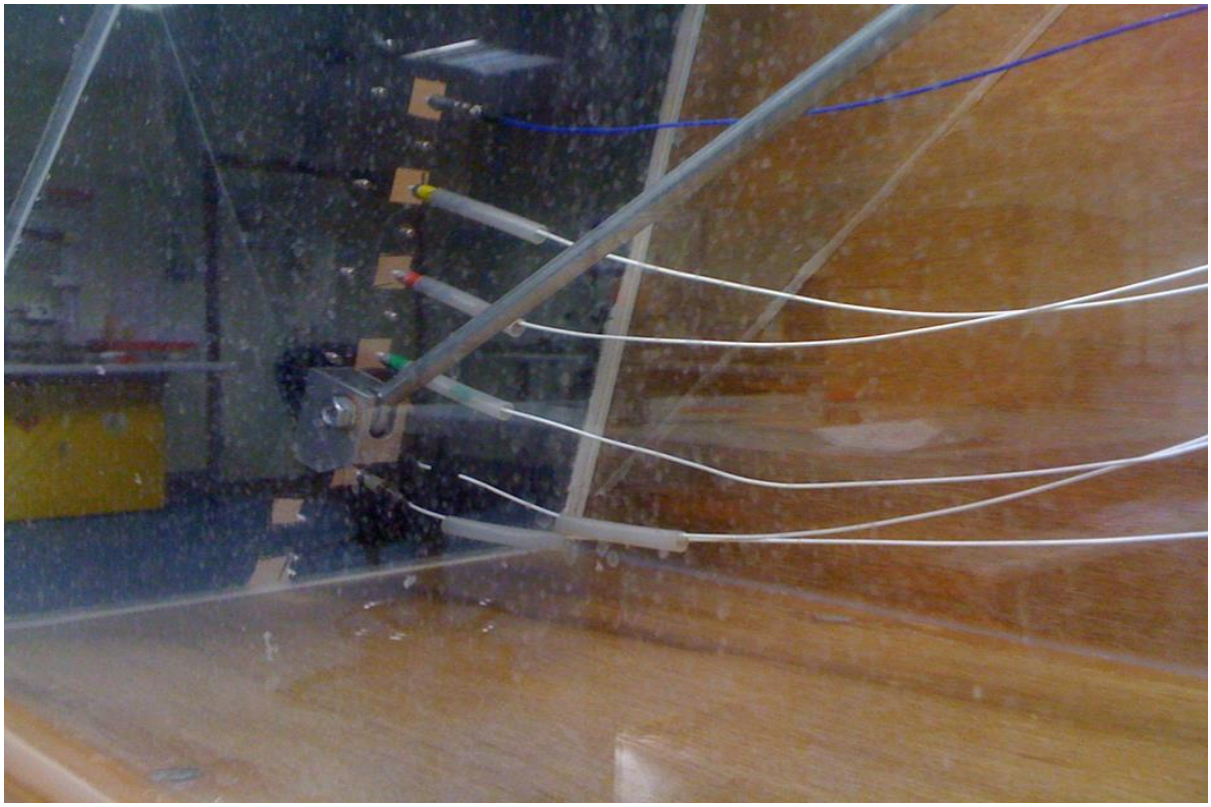

Figure 4.10: The wall model showing the six transducers attached perpendicularly to the on-coming wave front

4.6 Experimental Programme

The most important of the wave characteristics (apart from the pressure) were judged to be wave height, wave celerity and wave period, hence these were the only parameters (other than pressure) which were measured in this study except the wave period which was difficult to measure because of the turbulent nature of the floodwater wave. These parameters were chosen because they are generally featured in most equations for estimating the wave impact pressure (see chapter 2 on literature review). The only other parameter necessary is wave length which was also difficult to measure in the present study. Hence, emphasis had been made in the measuring of the wave height within the channel, impact pressure on the wall as well as the computation of floodwater propagation velocity.

The experimental tests were carried out on four types of wall surface models namely; smooth surface wall model, IMACTS wall model, IMICTS wall model and semi-smooth surface wall model. Each of the wall models was varied at different wall orientations ranging from vertical

to 75^o to 60^o and 45^o backward-inclined. A wide range of initial reservoir depths were used for each of the models at each of the wall angles as initial input conditions. The initial level of the water body within the reservoir can be chosen up to 0.6 m however the water level was set at various heights from the bottom of the channel ($0.15\ m \leq d_o \leq 0.55\ m$) so as to create varying wave heights within the channel. Five different wave heights were created within the channel by varying the initial reservoir depths from 0.15m to 0.55m with increment of 0.1m. Tests on the performance of the wall surfaces and slopes were only carried out for the dry-bed downstream while tests for the computation of the floodwater propagation velocity were extended to various downstream water depths of 0m (dry-bed), 0.05m, 0.10m and 0.15m to explore the effect of wet-bed conditions downstream. The experimental matrix of all the tests conducted is shown in Table 4.3.

Table 4.3: Experimental Test Matrix

Experiment	Initial reservoir depth (m)	Wall angle (degree)	No of repeatability for each initial reservoir depth	No of test for each wall angle	Total no of test for each wall model	Measured/Computed parameters
Smooth surface wall (wall model-A)	0.55, 0.45, 0.35, 0.25, 0.15	90°, 75°, 60°, 45°	5	25	100	Wave heights (WP1&WP2), Impact pressures (Transducers 1,2,3,4,5 & 6)
IMICTS wall (wall model-B)	0.55, 0.45, 0.35, 0.25, 0.15	90°, 75°, 60°, 45°	5	25	100	Wave heights (WP1&WP2), Impact pressures (Transducers 1,2,3,4,5 & 6)
IMACTS wall (wall model-C)	0.55, 0.45, 0.35, 0.25, 0.15	90°, 75°, 60°, 45°	5	25	100	Wave heights (WP1&WP2), Impact pressures (Transducers 1,2,3,4,5 & 6)
Semi-smooth surface wall (wall model-D)	0.55, 0.45, 0.35, 0.25, 0.15	90°, 75°, 60°, 45°	5	25	100	Wave heights (WP1&WP2), Impact pressures (Transducers 1,2,3,4,5 & 6)
Preliminary experiments for the computation of floodwater propagation speed						
Smooth-surface wall (dry-bed)	0.55, 0.45, 0.35, 0.25, 0.15	90°	5	25	25	Time taken, Velocity
Smooth-surface wall (0.10m wet-bed)	0.55, 0.45, 0.35, 0.25, 0.15	90°	5	25	25	Time taken, Velocity
Smooth-surface wall (0.15m wet-bed)	0.55, 0.45, 0.35, 0.25, 0.15	90°	5	25	25	Time taken, Velocity
Total Number of Experiments Conducted					**475**	

4.7 Experimental Procedure

With the dam gate initially closed, water was pumped into the reservoir section of the wave tank to a required level in order to create an upstream reservoir. The gate was then lifted manually by a quick-lift mechanism. The gate release was possible through a pulley mechanism incorporated into the system. However, effort is still on-going to improve the gate release mechanism to a pneumatic system so as to maintain constant power for future studies on the rig. Meanwhile, this was corrected for to a reasonable extent during the present experiment by repeating each test five times to check that the bores are generated by almost instantaneous openings of the gate in a repeatable manner. Although the repeatability was good, the average value of the five trials in each experimental set was again considered.

Floodwater waves are then generated with the lifting of the gate which initially separates the quiescent water on the reservoir section of the tank from the rest of the wave tank. The time required to lift the gate was less than 0.1sec which, being small compared with wave propagation time, seemed likely to simulate full and instantaneous collapse of a dam. The wave heights were measured at two positions of interest with one probe located just behind the gate downstream and the other positioned just in front of the wall model (see Table 4.2) while the impact pressures were measured at six different locations on the wall model (see Table 4.1).

4.8 Data Acquisition and Analysis

Trial experiments were conducted to select appropriate 'Gain', 'Filter' and 'Bias' on the transducer coupler. After several runs optimum settings of the coupler's Gain, Filter and Bias were obtained. Coupler's Gain was set at 50Hz, the Filter at 100 and the Bias at 1. The trial runs also enabled the fixing of optimum time interval for capturing the flow in the channel and the impact on the wall model which was programmed into the computer software. It was found that the longer the time selected, the smaller the value of the peak wave pressure due to low sampling data. When time, t, selected is low (<0.001s), the data contain much noise, hence we agreed to select capturing time, t, = 20ms (0.002s) as the optimum.

To use all the measurements together it was important to be able to know what is going on at specific times for each measurement device. A trigger system was set up so that when the gate

was released, a precise clock started in view of video for the visual data. The trigger also sends an indication of the gate release to the data gathering systems.

The measured outputs encompassed the surge heights obtained from the two probes installed at the designated positions in the channel as well as the impact pressure obtained from the fitted pressure transducers. The propagation time for the floodwater from the start of the gate release to the location of the wall model was also obtained which was used to compute the propagation velocity. Wave heights are determined from the changes in conductance of the resistance type wire of the wave probe as the water height increases. As the wave impacted the structure, the six transducers measured the impact pressure simultaneously at different locations. The impact pressure histories and data as well as the wave height data and histories were then stored and post processed by a personal computer. Figure 4.11 showed the schematic procedure of data acquisition system.

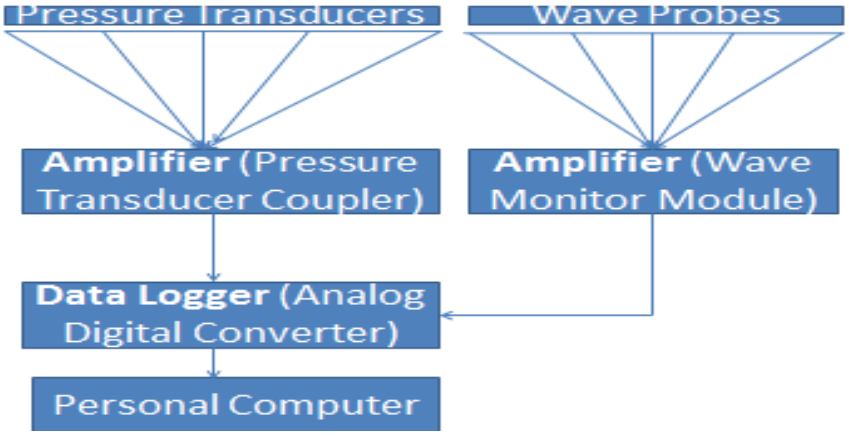

Figure 4.11: A schematic diagram of the data acquisition system

4.8.1 Floodwater Front Velocity Measurements

Digital Particle Image Velocimetry (DPIV) techniques are commonly used for measurements of velocities of this nature because it can measure the flow velocity in two-dimensional plane. Another velocity measuring device that can be used is a non-instructive two-component back-scattering Laser Droppler Velocimeter (LDV) system which can offer more frequent measurements than the DPIV, but can only measure velocity at one point at a time though it could also measure two-dimensional velocity components in a plane perpendicular to the laser beam. These techniques however, require the water to be seeded with reflective particles for the laser light to reflect off and be visible on the video (Bellos et al., 1992, Chegini et al., 2004). These techniques are slightly modified in this study though the same principle and approach was adopted.

The present study assumed the case by which the leading edge of floodwater is captured rather than seeding method. Two different approaches were then used for the capturing. The first approach is by using the video system comparable to Digital Particle Image Velocimetry method hence referred to as Imaging System (IS). The second approach involved signal capturing of the leading edge of floodwater by suitably positioning two wave probes (sensors) in the channel hence termed Sensor Signal Capture (SSC) technique. For the SSC technique the two wave probes were placed at two different distances apart (0.41m and 2.2m apart) to compare the results with that of the Imaging System. Table 4.4 showed the detailed arrangement of the wave probes for the preliminary experiments which focussed on the computation of the propagation velocity of the floodwater.

Table 4.4: Positions of the two wave probes for the preliminary experiments for the computation of the propagation velocity

Wave probe number	x = 0 at the upstream end of the reservoir	
	0.41m apart	2.2m apart
WP 1	1.82m	0.03m
WP 2	2.23m	2.23m

The wave front propagation velocity was therefore estimated from the arrival times of the leading edge of the floodwater wave using combination of appropriate equations. An example of the computation of the propagation velocity is given in data analysis section (section 5.3.1).

4.8.2 Water Level Measurements

In this study, the time evolution of the water level was measured using SSC technique. Resistive gauges were used to record the water level at two different locations. Wave probe 1 (WP 1) was placed 0.03m from the reservoir gate and wave probe 2 (WP 2) at 2.23m from the reservoir gate (Figure 4.8). The resistive gauges used to measure the flow consist of two rigid wires placed within the flow regime. The water depth was deduced from the measurement of the voltage measured by the gauges. The exact coordinate of the gauges is indicated in Table 4.2.

4.8.3 Impact Pressure Measurements

The dynamic pressure, along with the static pressure and the pressure due to elevation of the flood waves formed the total pressure exerted on the wall being a closed system. The transducers give a measure of the products of floodwater velocity and the density (analogous to equations 2.17 and 5.10) and measured the difference between the total pressure and the static pressure which is basically the dynamic pressure in isolation. The six transducers were located at the faces of the wall vertically but each transducer is positioned perpendicularly to the incoming flood waves allowing the transducers to essentially measure the pressure in the direction of flow hence measured mainly the dynamic pressures. Hence, the impact pressure referring to throughout this thesis indicates the measure of the dynamic pressure in isolation.

Impact pressures can only occur over the height of the breaking wave so as the SWL rises and falls, so too will the location of the impact pressure on the seawall. Therefore impact pressures can only be measured when the pressure transducers are within the region of the breaking wave. During this investigation impact pressures have been measured simultaneously on six pressure transducers covering an area of 0.5m by 0.7m. The channel was 0.6m high but the seawall model was 1.0m high to prevent overtopping. Thus, for the dry-bed downstream experiments the largest potential floodwater height (depth limited) which can reach the wall would not be more than 0.6m. With this in mind the pressure transducers were located vertically between 0.02m and 0.5m of the wall height. The lowest transducer was located at exactly 0.02m from the base of the wall. The exact coordinates of the transducers are indicated in Table 4.1.

Previous studies have revealed that the durations of maximum impact pressures are typically less than 0.01seconds (Wood, 1997). Therefore, to acquire a record of the pressure response, an adequate sampling rate was necessary. It was determined that a 100-Hz sampling rate was satisfactory. Again, to obtain adequate data for secondary pressures (longer durations) on the wall model the optimum capturing period was set at 20ms.

The effects of four different wall surfaces (smooth surface wall, IMICTS wall, IMACTS wall and semi-smooth surface wall) when varying initial reservoir depth on the wave heights at impact and on the impact pressure on the walls were analysed using appropriate statistical analysis. The effects of varying the slope (90^o, 75^o, 60^o, 45^o) for each of the wall surfaces, as initial reservoir depth is varied, on the impact pressure, were also analysed. The results of the

analyses are anticipated to give a clear understanding of the present problem and identify the importance and influences of all these parameters.

4.9 Preliminary Experiments

The preliminary experiments were conducted with a focus on the estimation of floodwater front velocity as well as the characterisation of the flow in the channel. The flow velocity of floodwater in the channel is of paramount importance since it is closely related to the impact pressure on the wall (see Chapter 2). The estimation or computation of propagation velocity was therefore a target in this study. Due to the limited space available and also the concern over the obstruction to the flow of the floodwater, a velocimeter could not be used to measure floodwater velocity directly.

The length of the reservoir was 1.0 m while the propagating distance of the floodwater wave was 2.7 m. One side of the channel as well as its bottom was made of plywood while the other side of the channel was made of clear Perspex which enabled optical measuring video footage of the whole process. RCD protected lights were used in the process to improve visual observation and the quality of video footage. The flow was imaged by a strategically positioned camera through the side of the channel made of clear Perspex. A JVC TK – 1085E high-speed digital camera was used, acquiring grey-scale images at a rate of 40 frames per second, with a resolution of 256 by 256 pixels.

Tests were conducted with the downstream channel completely dry prior to experimentation, essentially modelling the dry beach common at urban waterfronts. Experiments were also conducted with wet-bed downstream at various ratios of upstream-downstream depths (H_{ds}/H_{us}). Positive dam-break waves downstream were exclusively considered throughout the study. The initial levels of the water body within the reservoir were varied between $0.15\ m \leq d_o \leq 0.55\ m$. An initial water depth of 0.15 m was chosen because it was found during the experiment that the minimum reservoir depth of which effects of viscosity on the front propagation characteristics could be neglected within the downstream channel length considered was at least 0.1 m.

However, for wet-bed downstream experiments, downstream depths (H_{ds}) of 0.05m, 0.10m and 0.15m could only be investigated to show the effect of wet-bed downstream due to the fact that the minimum initial reservoir depth has been set as 0.15m. Within the available experimental facilities any downstream depth higher than 0.15m did not give appreciable outcomes. Only the smooth surface wall (wall model-A) in vertical angle was chosen for the trial experiments

and each run of initial reservoir depth was repeated five times to analyse the spread of data in terms of the time taken for the wave front to hit the wall from the point of release.

Flow patterns of floodwater in the channel were visualized and video recorded. The camera was strategically positioned to cover the entire flow area of interest. The flow period between the two locations of interest (point of gate release and position of the seawall) within the channel was obtained from the digitized image analysis. The movement of front water within this field of view (immediately the gate was opened through to when it hits the wall) was then analysed.

The propagation velocity was estimated using two methods described in detail in chapter 5 (data analysis and results). The first method was through the analysis of the water movement with appropriate video editing software to deduce the time taken for the front water to reach the dead end (location of the wall model) and the computation of the velocity using appropriate equations of motion. The other method was from the translation of the records of the two wave probes in the channel (see chapter 5 for detail).

4.10 **Verification of Rig Performance**

A series of experiments were carried out to verify repeatability of the instrumentation and the performance of the entire set-up. A configuration of 0.35m initial reservoir depth was chosen for the validation. Twenty (20) experimental runs were carried out repeatedly in similar conditions while measurements on both the wave probes and the transducers were taken. The data obtained were then statistically analysed for repeatability.

4.11 **Summary**

Coastal engineers rely on three complementary techniques to deal with the complex fluid flow regimes typical of many coastal projects. These techniques are field measurements and observations, laboratory measurements and observations, and mathematical or numerical techniques. Laboratory measurements or physical/scale models constructed and operated at reduced scale still offer an alternative for examining coastal phenomena that may presently be beyond our analytical and mathematical skills.

Physical modelling technique has been considered in the present study for the investigation of the effectiveness of new seawall designs for the mitigation of floodwater waves. The study has therefore required the construction of a model wave tank. Thus, this chapter described the design and construction of the wave tank used to create the dam-break flow geared toward testing the suitability of the new seawall designs.

Within the wide range of experiments that are to be carried out in the study, many different items of equipment and instruments are to be used or developed. This chapter also outlines the key features of the experimental facilities employed. Such facilities and equipment include the test specimen (the seawall models), the pump, the video camera as well as pressure transducers, wave probes and data logger for the acquisition and analysis of data. The fact that the research tool for this study relies on scale model tests makes it essential to form a dimensional analysis for the measured parameters and it is covered in this chapter. The modelling technique for this study was according to Froude's scaling law. A functional relationship given in equation 3.37 was obtained and used later in chapter 5 to correlate the resulting test data in the form of dimensionless plots.

Also in this chapter, detailed descriptions of experimental arrangement (Figure 4.8), experimental programme as well as experimental procedures are covered. The techniques of measuring the wave characteristics that are of great interest to this study were described. Such wave characteristics include floodwater wave elevation in the channel, wave celerity or floodwater wave propagation velocity as well as impact pressure on the wall models. An adapted Digital Particle Image Velocimetry (DPIV) technique was used for measurements of velocities because it can measure the flow velocity in a two-dimensional plane as appropriate for the nature of the flow in the present study. The time evolution of the water level was also measured using Sensor Signal Capture (SSC) technique. Consequently, the impact pressures

have been measured simultaneously on six pressure transducers covering an area of 0.5m by 0.7m.The acquisition of interested data described in this chapter then leads to the next chapter which provides the analysis of the data obtained during the experiments.

CHAPTER FIVE

DATA ANALYSIS AND RESULTS

5.1 Wave Tank Construction: Cost Analysis

In this study, a physical model technique has been considered for the investigation of the effectiveness of new seawall designs for the mitigation of floodwater waves. The study has required the construction of a model wave tank. An Instrumented Low Cost Wave Tank (ILCWT) was successfully constructed to create dam-break flow geared toward testing the effectiveness of various wall designs. This section intends to give cost analysis and report some cost effective solutions to the development of these simple systems.

This instrumented wave-structure tank was designed and built on a limited budget hence the cost of construction has been conscientiously estimated. In the course of development, concerted efforts have been made to source for quality but affordable materials of construction by the senior technical staff in the research team which helped to bring down the total direct costs actually expended to build and equip the wave tank. Some of the equipment used to build the whole system has either been designated for disposal (DfD) or previously used (PU) for various research some years back, they are specified as estimated replacement costs in Table 5.1. An estimated labour cost based on 230 hours of labour at an average rate of £30/hour, is also included in Table 5.1. However, all labour was performed by the research student and by the technical staff of the LJMU School of the Environment and so was not a direct cost.

Table 5.1 lists all direct and indirect costs actually expended on the wave tank. It can be seen from the table that though the grand total cost of constructing the wave tank including all the measuring instruments attached to it is £30,570.00 the actual total direct expenses is £3, 270 which is only 10.70% of the grand total cost.

Table 5.1**:** Actual and Estimated Costs for the Instrumented Low Cost Wave Tank (ILCWT)

Item	Description	Cost Status	Cost value (Pounds)
Perspex	3000mm x 1500mm x 12mm	Actual	700.00
Plywood	Treated engineered type	Actual	120.00
Aluminium frame	50mm x 6mm	Actual	200.00
Pump	1/15-hp, 3,400-rpm	Actual	400.00
Analog-to-Digital Converter	National Instrument SCXI USB - 6008 Model	Actual	200.00
Miscellaneous hardware	Bench, Vacuum, Fixings, Assorted materials and Sealants	Actual	1500.00
PVC Pipes	25-mm diameter	Actual	150.00
Total actually expended			**3,270.00**
Wave gauge	Churchill Wave Monitor Module	Estimated replacement cost (PU)	10,000.00
Pressure transducer	Kistler type 211B5 Model	Estimated replacement cost (PU)	10,000.00
Desk top computer	Pentium III	Obtained at no cost (DfD)	400.00
Labour	Mechanical/Instrumentation	Estimate (not a direct cost)	6,900.00
Total value of indirect costs			**27,300.00**
Grand total costs (actual and estimate)			**30,570.00**

5.2 Performance Analysis of the Set-up

The efficiency of the whole set-up has been assessed. With the gate initially in position to create a dam, an upward impulse is generated by releasing/pulling the rope through the pulley system to generate floodwater waves. Data collection begins simultaneously with the gate release. Impact pressures on the model seawall were measured by the pressure transducers while the floodwater wave heights were measured by the wave monitoring probes. All data were collected through the National Instrument USB-6008 data logger which is again connected to a personal computer and controlled through the use of Labview Virtual Instrumentation Software.

The performance analysis is being carried out on the whole system. A repeatability experiment was carried out to assess the performance of the whole set-up. Twenty trial experiments were carried out with the same initial reservoir depth and under the same experimental conditions. Table 5.2 showed the summary of the results obtained for the twenty trials. The mean value, the standard deviation and the repeatability indices for all the twenty trials for each of the sensors were indicated in Table 5.2. It can be seen from the table that the standard deviations obtained for all the sensors are relatively low. For instance, for the transducers the standard deviations are between 0.10287kPa and 0.15508kPa while those of the wave probes are also between 0.13523m and 0.22452m. The low values of standard deviation obtained relative to the mean values for all the sensors in the repeatability experiments (20 runs) as indicated in Table 5.2 is a clear indication of the consistency of the system which invariably suggests the efficiency of the whole set-up.

The repeatability indices for all the sensors have been found to be between 7.81% and 13.25% (Table 5.2). The repeatability indices are computed as the ratio of standard deviation to the mean value expressed as a percentage and are measures of the performance of the equipment. Consequently, the low values obtained for this parameter apparently suggest how effectively the whole system performed. The indication of this high level of repeatability of the sensors lends credibility to measurements taken in the study.

Again, Figure 5.1 shows an example of the pressure-time curve obtained from pressure transducers 1 to 4 during the experiments. Interestingly, they are found to follow a typical pressure-time curve for wave-structure interaction (see Figure 3.2 in section 3.4) suggesting that the whole set-up is suitable for the study. Also, Figure 5.2 shows Pressure-time histories

for the transducer at the base of the wall model (transducer 1) for three trials to indicate the consistency of the sensor. It can be seen from the figure that the repeatability of the sensor is good.

Table 5.2: Repeatability indices of selected test measurements for the pressure transducers (PTs) and the wave probes (WPs)

Sensor	Mean value	Standard deviation	Repeatability indices
PT1	1.83828kPa	0.14358kPa	7.81%
PT2	1.72584kPa	0.14234kPa	8.25%
PT3	1.49162kPa	0.15508kPa	10.40%
PT4	1.13682kPa	0.12290kPa	10.81%
PT5	0.77614kPa	0.10287kPa	13.25%
WP1	1.41834m	0.13523m	9.53%
WP2	2.24521m	0.22452m	10.00%

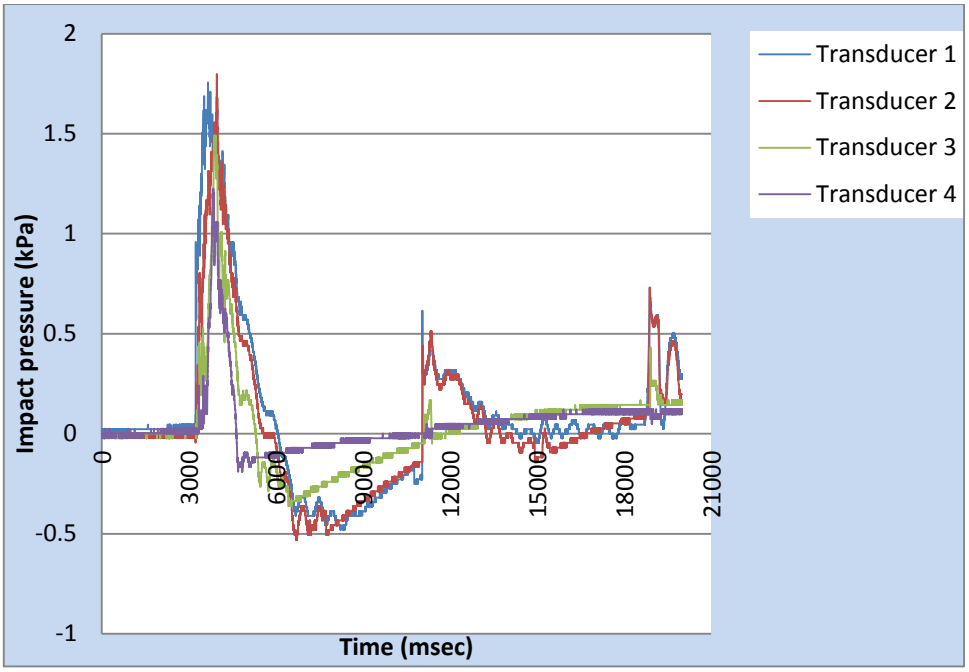

Figure 5.1: Pressure time histories of selected pressure transducers (r-depth = 0.35m, vertical smooth-surface wall)

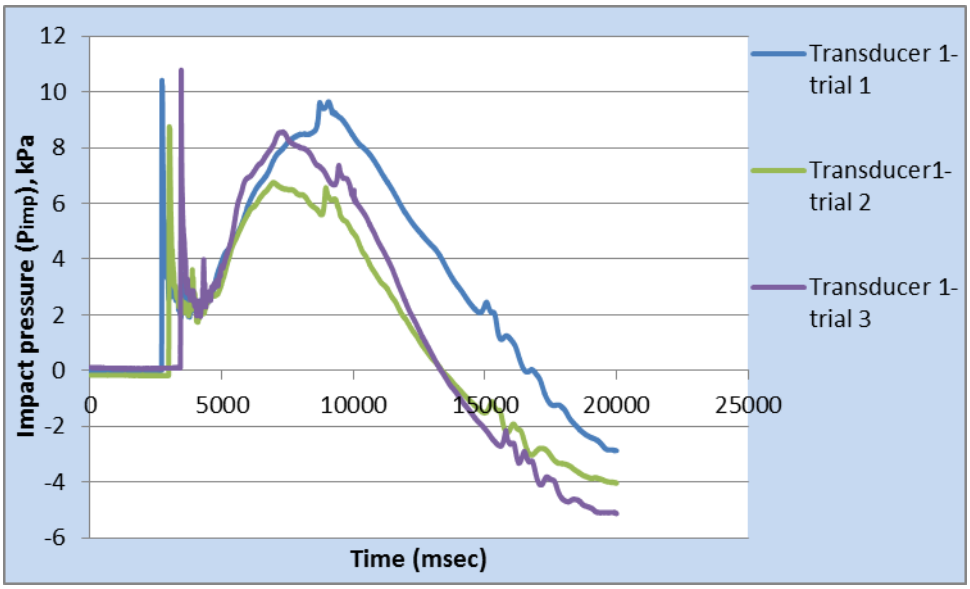

Figure 5.2: Pressure-time histories for the transducer at the base of the wall (transducer 1) for three trials showing the repeatability of the sensor (r-depth = 0.55m)

5.3 **Qualitative Analysis of the Flow Structure in the Channel**

Prior to the gate's removal, inflow created a reservoir upstream. The initial levels of the water body within the reservoir were chosen from 0.15m to 0.55m for this study given the minimum initial water head against the gate as d_o = 0.15m and the maximum water head against the gate as d_o = 0.55m. As soon as the dam collapsed, the dam-burst wave moved downstream until it was reflected by the downstream dead end (Seawall model). It was apparent from the analysis of the video recordings that the gate is often completely removed in about three and a half frames which makes the gate removal time computed to be 0.0875s, much less than the propagation time (1.21s to 2.08s in Table 5.3) thereby likely to indicate instantaneous removal. Although, in practice the release of water will be more gradual than this idealization and may depend on concrete fracture at the beach as in the case of an embankment dam however, an instantaneous release may be expected and represent the worst case scenario.

The gate opens with a manually operated pulley system at estimated time of 0.0875s in the present experiment. This opening time is compared to the criterion established by Vischer and Hager (1998) as well as Hager and Blaser (1998) stating that a dam break can be considered as instantaneous if the gate opening time t_{op} satisfies the following relationship;

$$t_{op} \leq 1.25\sqrt{\frac{d_o}{g}} \quad \ldots\ldots 5.1$$

For minimum reservoir depth d_o = 0.15m, t_{op} = 0.155s while for maximum reservoir depth of 0.55m, t_{op} = 0.296s (Hager and Blaser, 1998, Vischer and Hager, 1998). The obtained value of t_{op} = 0.0875s in the present study is less than t_{op} values obtained from Lauber and Hager expression for both upper and lower limits of the initial reservoir depths. Thus, the criterion of Vischer and Hager is satisfied within the range of the initial reservoir depths in the present study (0.15m ≤ t_{op} ≤ 0.55m).

Another criterion was developed by Lauber and Hager (1998a) , stating that;

$$t_{op} = \sqrt{\frac{2d_o}{g}} \quad \ldots\ldots 5.2$$

Again, with minimum d_o of 0.15m, t_{op} = 0.175s while with maximum d_o of 0.55m, t_{op} = 0.335s. The obtained value of t_{op} of 0.0875s in the present study also satisfies Lauber and Hager criterion. These suggest that the gate release system for the present experiment is a good approximation of instantaneous dam-break problem.

The floodwater propagation time obtained was between 1.2s to 2.1s (Table 5.3). It means it took about 1.2s for the front floodwater with initial reservoir depth, d_o = 0.55m to reach the dead end where the model seawall is situated. Analysis of experimental data in terms of the time taken for the wave front to hit the wall for various reservoir depths (Table 5.3) indicated decrease with increasing reservoir depth which is in agreement with shallow water theory**.** For the reservoir depth of 0.15 m, the average propagation time for the wave front to hit the wall is 2.08sec and in all cases the bore formed by reflection against the wall travelled back in the upstream direction creating more turbulent flow in the channel. The two wave probes which were situated downstream of the channel showed records of constant fluctuation which is an indication that the flood wave propagation is a turbulent and complex phenomenon.

The photographs in Figure 5.3 through Figure 5.5 showed the snapshots of the flow moments after the opening of the gate to when the flow hit the wall model. Figure 5.3 to Figure 5.5 highlighted the chaotic nature of the wave front, with strong spray and further splashing and wavelets. A detailed analysis of the video recordings indicated that the flow though turbulent, may be considered to be a smooth regime which was essentially the result of a smoothed downstream bed condition. Careful visual and video observations of the flow showed that the surge front propagated as a succession of free-falling nappes or jets and horizontal run-off. The observations also emphasised that the wave front was highly aerated, in particular for the flow with higher reservoir depth (Figure 5.4). As can be seen from the figures, there could have been a pocket of air under the crest of the wave just before the wave impacts the wall. The shape formed just before the impact in front of the wall (Figure 5.5) confirms that air is entrapped between the wave and the wall. The figure also shows that the degree of reflection and spray at the wall affects the next incoming wave and at times, the impact of the next breaking wave was considerably less than the first.

Figure 5.3: Snap shot photograph of the floodwater at the instant of gate release for wet-bed downstream experiment

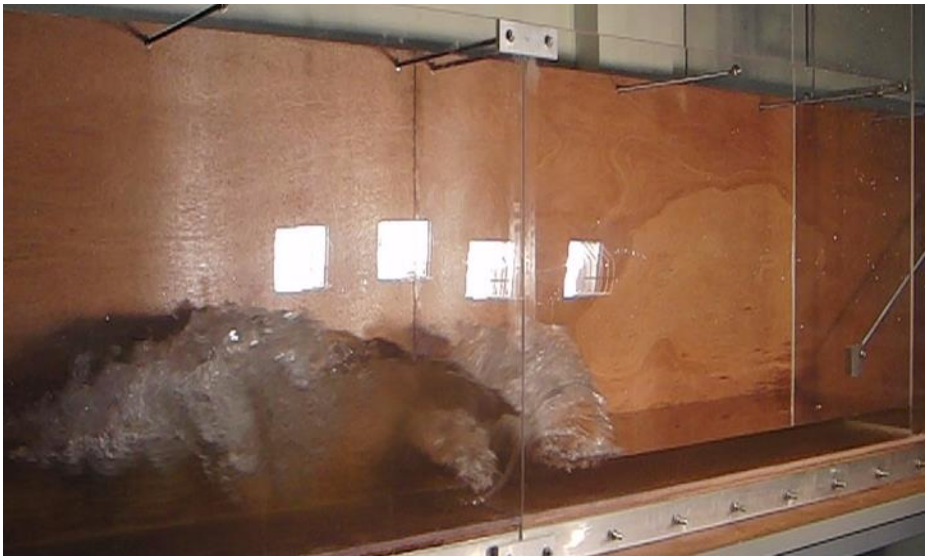

Figure 5.4: Snap shot photograph of the floodwater wave within the channel for wet-bed downstream experiment

Figure 5.5: Snap shot photograph of the floodwater wave at the moment of impinging the wall model for dry-bed downstream experiment

5.4 Characteristics of the Measured Flow Parameters

5.4.1 *Floodwater Front Velocity*

The two techniques (Imaging System, IS and Sensor Signal Capture, SSC) described earlier (see section 4.8.1) had been used for the measurement of front water propagation velocity within the channel. The front water propagation velocities were estimated from the arrival times of the leading edge of the floodwater wave coupled with the use of a combination of appropriate equations. For example, when the reservoir water depth d_o = 0.15 m, propagation time t = 2.08s (Table 5.3). The propagation distance is a constant value and is given as, S = 2.7 m (Figure 4.7). Rate of acceleration of wave front, a is computed from;

$$S = ut + \frac{1}{2}at^2 \quad \ldots\ldots 5.3$$

Where S is the propagation distance, u is the initial velocity of the floodwater, a is the rate of acceleration and t is the propagation time.

The average wave front velocity is then calculated from;

$$v = \sqrt{2aS} \dots\dots\dots\dots\dots\dots\dots\dots\dots\dots\dots\dots\dots\dots\dots\dots\dots\dots 5.4$$

Thus, when d_o = 0.15 m, the average floodwater front velocity is obtained as 2.5962m/s (Table 5.3).

Table 5.3: Computed floodwater front velocity at varying reservoir water depths (dry-bed downstream)

Depth of water in the reservoir, d_o (m)	Average Time taken, t (s)	Front water velocity, v (m/s)
0.15	2.08	2.5962
0.25	1.60	3.3751
0.35	1.50	3.6000
0.45	1.31	4.1222
0.55	1.21	4.4628

Using this approach interesting results were obtained in terms of the wave front velocity for dry-bed and wet-bed downstream conditions at varying reservoir depths. Figure 5.6 depicts the variation of the obtained floodwater front velocity against reservoir depth using imaging system (IS). The figure shows that the front velocity of the floodwater increases with increased reservoir depth. The correlation coefficient (R^2) is 0.9811 indicating a strong relationship exists between the velocity and the initial depth of water in the reservoir section. This linear variation is expected from the analytical solution of one-dimensional frictionless and horizontal dam-break flow problem developed by Ritter in 1892 (Chanson, 2005) .

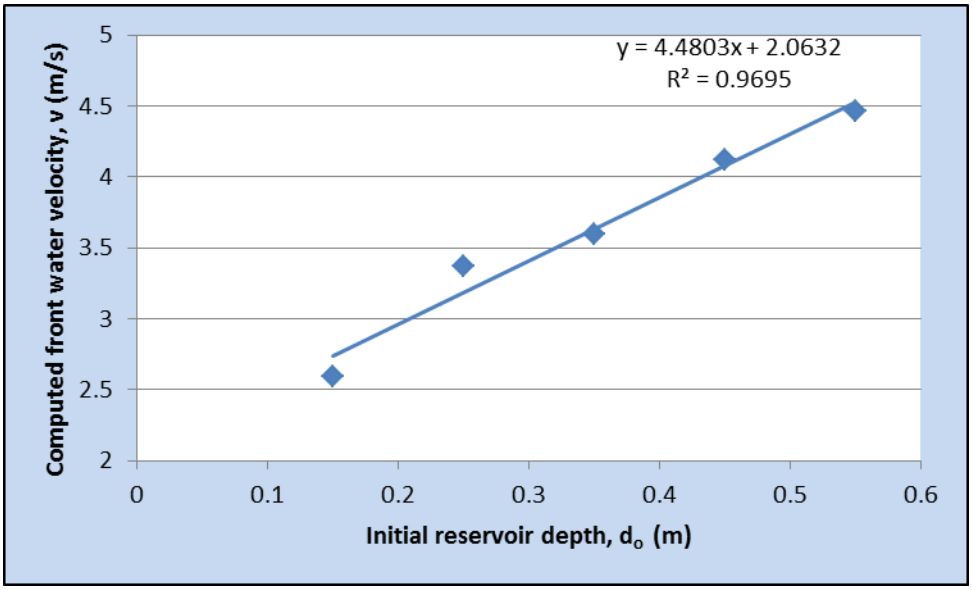

Figure 5.6: Variation of front water velocity with varying initial reservoir depths for dry-bed downstream

The results of the front velocity with wet-bed downstream conditions are shown in Table 5.4. Initial downstream water depths of 0.05m, 0.10m and 0.15m were investigated with varying initial reservoir depths and compared (Table 5.4). Figure 5.6 emphasizes that the velocity decreases as the downstream initial water depth increases. Dry-bed downstream gave some unexpected results in this case which is a rare occasion. Figure 5.7 as well as visual and video analysis also showed that higher values and complexity of most flow characteristics were obtained for the lower downstream water depth case than for the case with higher downstream water depths. Figure 5.7 also shows that the initial slope of the velocity variation decreases as the downstream initial water depth increases. For all depth ratios, the velocity profiles would eventually became quite stable after the bore develops downstream which is considered to be satisfactory for the downstream subcritical flow region.

Table 5.4: Computed front water velocity for dry bed and wet-bed downstream at varying reservoir depths

Depth of water in the reservoir, d_o (m)	Velocity, v (dry-bed) (m/s)	Velocity, v (H_{ds}=0.05m) (m/s)	Velocity, v (H_{ds}=0.1 m) (m/s)	Velocity, v (H_{ds}=0.15 m) (m/s)
0.15	2.5962	2.70	2.17	2.06
0.25	3.3751	3.53	1.56	1.70
0.35	3.6000	4.50	1.23	1.47
0.45	4.1222	4.50	1.23	1.29
0.55	4.4628	5.19	1.07	1.23

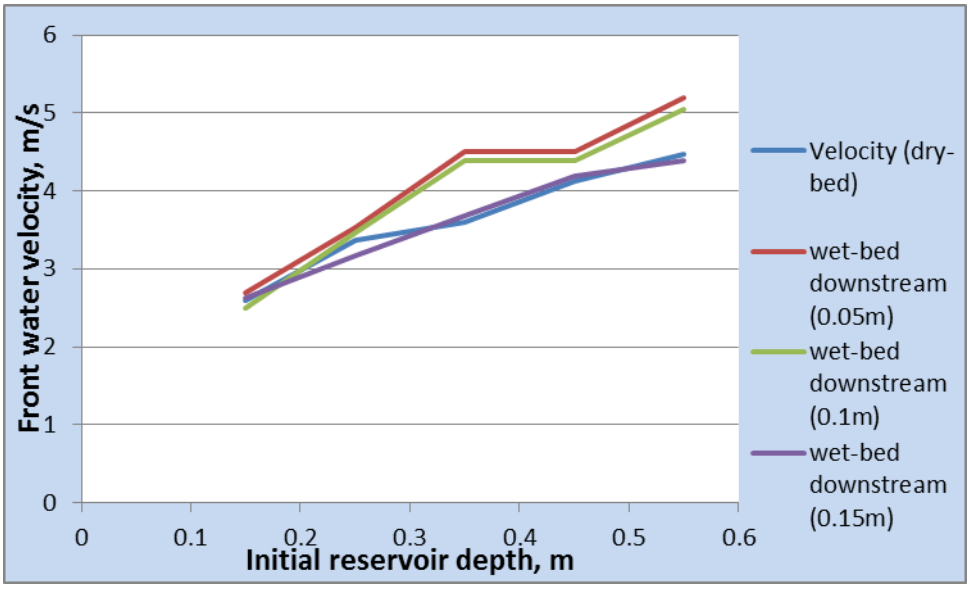

Figure 5.7: Comparison of the front water velocities for dry- bed and wet-bed at various initial water depths downstream

The accuracy of the flow velocity relies on several factors. In the present experiment the flow velocity is mainly associated with the precision of the time interval between image pairs and the exactness of the displacement measurement. Thus, floodwater front velocity was again computed using data obtained from the two wave probes installed downstream of the channel, a technique referred to in this study as sensor signal capture (SSC) to validate the reliability and accuracy of the measured velocity with the imaging system (IS). The time at which each wave probe received signal of the leading flow was deduced. Knowing the distance between the two wave probes, average front water flow velocity was again calculated using an appropriate combination of equations following the example discussed earlier.

For comparison, the two wave probes were positioned in two different distances apart (0.41m and 2.2m apart) and the flow velocity was calculated for the time obtained in each case at varying reservoir depths. Figure 5.8 compares the results of front water velocity obtained by the two methods with the results obtained by imaging system (IS).

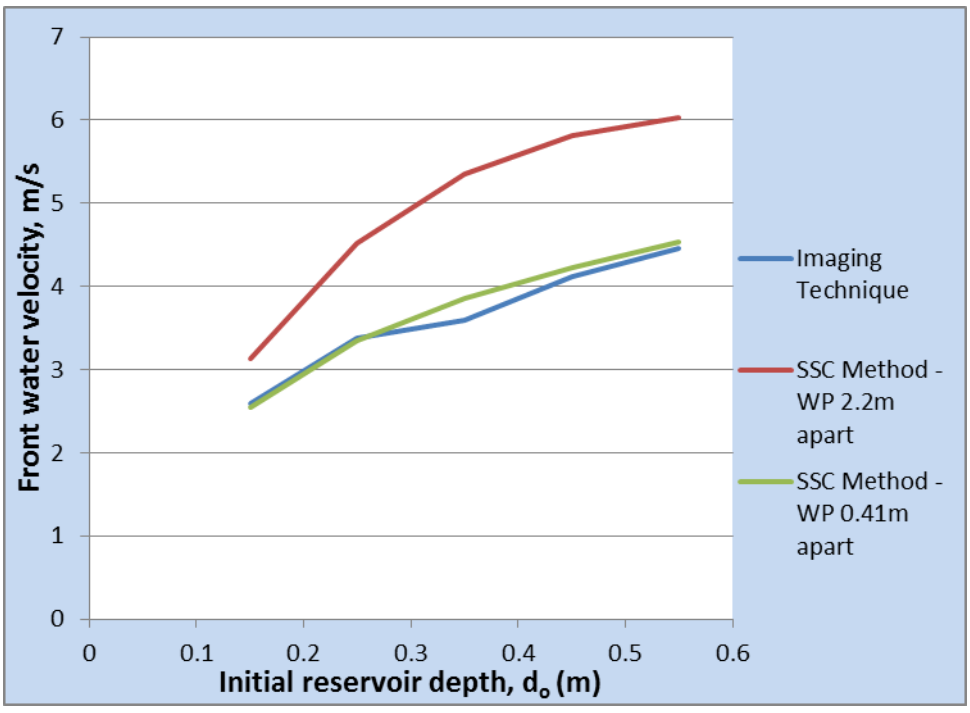

Figure 5.8: Comparison of the computed front water velocity using various methods for dry bed downstream condition

Comparisons were also made between analytical and theoretical solutions of various researchers with the experimental data set for this study under dry-bed flow conditions. In a similar experiment by Liem and Kongeter (1999) wave front velocity, v_F was estimated for time average of $t = 0.057$ s. According to the report, the derived wave front velocity at this time was expected to be between 2.43 m/s and 2.67 m/s but found to fluctuate between 2.0 m/s and 2.5 m/s which are much lower than the Ritter v_F prediction of 3.43m/s. Comparable wave front velocity to Liem and Kongeter (1999) prediction was computed for the present study. This velocity was found to be 3.6 m/s when the initial reservoir depth was 0.35 m (Table 5.4). An equivalent wave front velocity following Ritter's theory is computed at 0.3m initial reservoir depth as 3.09 m/s. Figure 5.8 shows the comparison of the results of Liem and Kongeter (1999) and other previous studies with the present results. The deviation from the Ritter prediction may be because Ritter assumed steady conditions within the dam break wave (Chanson, 2005) or may be due to the simplified assumptions for the present approach.

Furthermore, Lauber and Hager (1998b) identified two positive wave forms close to the beach section named as initial waves and dynamic waves. It was found in the study that these two wave forms propagate at different velocities, v_I *and* v_D respectively. The Shallow Water Equations (SWE) are said not to be applicable for the initial propagation velocity because the initial wave results essentially from orifice flow and is strongly affected by streamline curvature. However, as time progresses the initial wave is overtaken by the faster dynamic wave. The time origin of the dynamic wave is taken as the time of free fall of the surface point at the gate section until reaching the channel bottom ($T = \sqrt{((g/d_o)t}$). The study used Saint-Venant equations;

$$d\frac{\left(v+2\sqrt{(gd_o)}\right)}{d_x} = g\left(S_o - S_f\right) \quad \ldots\ldots 5.5$$

for modelling the positive wave characteristics, where x is the downstream coordinate with the origin at the gate position, S_o the bottom slope and S_f the friction slope. The computed wave front velocity for this study was found to be close in agreement with dynamic wave velocity suggested by Lauber and Hager (1998b) (see Figure 5.9). This is expected as qualitative analysis and characteristics of the flow obtained in the present study are comparable with the flow depicted by these investigators Lauber and Hager (1998b).

Some previous investigators interchanged wave celerity with front water flow velocity hence it is important to clarify this concept in the present study as well. An approximation of wave celerity was obtained from the shallow water relationship taken as;

$$C = \sqrt{gd_o} \quad (as\ a\ first\ order\ approximation) \ldots\ldots\ldots\ldots\ldots\ldots\ldots\ldots\ldots\ldots\ldots\ldots\ldots\ldots\ldots\ldots\ldots\ldots 5.6$$

Where C = wave celerity, g = gravity acceleration and d = initial reservoir water depth.

The solitary wave theory gives celerity for the steep waves as;

$$C = \left(gd\left(1 + \frac{H}{d}\right)\right)^{\frac{1}{2}} \ldots\ldots\ldots\ldots\ldots\ldots\ldots\ldots\ldots\ldots\ldots\ldots\ldots\ldots\ldots\ldots\ldots\ldots\ldots\ldots\ldots\ldots\ldots\ldots\ldots\ldots\ldots\ldots\ldots\ldots 5.7$$

which could give better results. (where H = water depth in the channel and d = water surface elevation from SWL).

Estimating the wave celerity using this method relies heavily on an accurate evaluation of the water surface elevation, d. However, in this study an estimate of water surface elevation could not be easily made because of the nature of the flow although the use of measuring staff suitably positioned enabled an approximate estimate of this parameter but not very reliable.

Recalling equation 2.18 (see section 2.5.3) and considering dry-bed downstream condition, the equation is simplified to the form of shallow water relationship, hence enabling the computation of floodwater wave celerity using equation 5.6. Also, equations 2.14 through 2.16 (see section 2.5.2) allowed the computation of front water velocities using the theories proposed by various previous investigators.

Figure 5.9 compares the wave celerity of the present study using equation 5.6 with the front water velocity of previous researchers. It can be seen from the figure that the flow celerity of the present study is in close agreement with the front water velocity of Lauber and Hager while other investigators appeared to overestimate the front water velocity in relation to celerity of the flow.

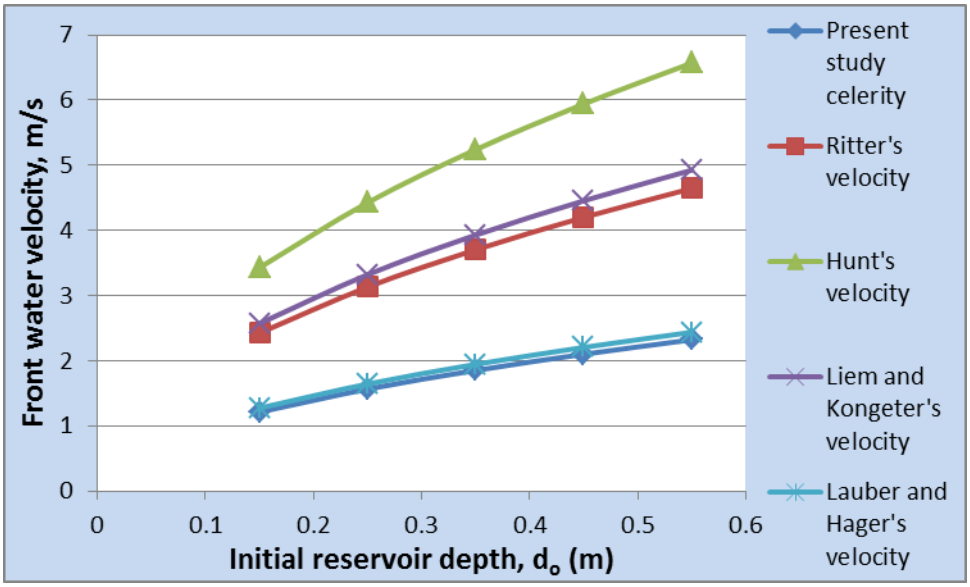

Figure 5.9: Comparison of floodwater front velocity of existing theories with the flow celerity of the present study

Besides, Figure 5.10 compares the front water flow velocity of previous investigators with the floodwater front velocity obtained in the present study. It can again be seen from the figure that the front water velocity computed using SSC method with wave probes 0.41m apart and that of imaging system (IS) in the present study appeared to be in close agreement with Liem and Kongeter's theory as well as Ritter's predictions. Hunt's theory has fair agreement with front water velocity computed using SSC method but with wave probes of 2.2m apart. It should be noted that a comparison with Hunt's theory may be incorrect at the upstream end of the channel since Hunt's equation is said to be valid only once the wave front has travelled a distance of more than 4 times the reservoir length (see section 2.5.2).

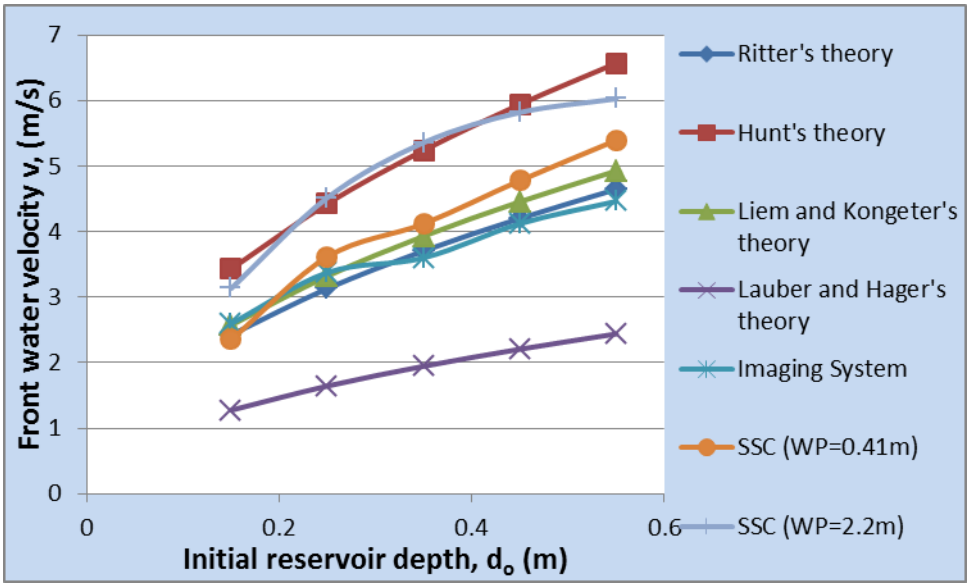

Figure 5.10: Comparison of the computed front water velocities for this study with various existing theories.

5.4.2 *Water Level Measurements*

Wave probe 1 (WP1) was located 0.03m away from the reservoir gate hence records the incident floodwater level (H_{inc}) just after the gate is released while wave probe 2 (WP2) was located 0.47m away in front of the seawall model thereby records the floodwater elevation just before impact (H_{imp}). WP2 was located as close as possible to the seawall model, so the value obtained for the floodwater elevation at the wall can be assumed to be actually occurring at the moment of impact. The exact location at which this parameter is measured was a compromise between being close to the wall and being out of the region of disturbance caused by the wall reflection so that individual wave heights could still be picked out.

The repeatability of the wave probes is assessed. Figure 5.11 indicated the results of the water elevation-time histories of measurements at WP2 for three different runs at the same experimental conditions (for initial reservoir depth, d_o = 0.35m). The good agreement between the experimental series allows combining several measurement campaigns to enhance the data set. This was particularly useful for both visual and video observations. Visual estimates of water level at the two locations were also made by sighting against a graduated levelling staff suitably positioned. However, though measurements from the wave probes seem to be more accurate, fairly good agreement was obtained between the two methods. The first peak for wave

probe 2 in Figure 5.11 is considered as maximum water level elevation as succeeding peaks were caused by reflection of the bore after the impact with the wall structure.

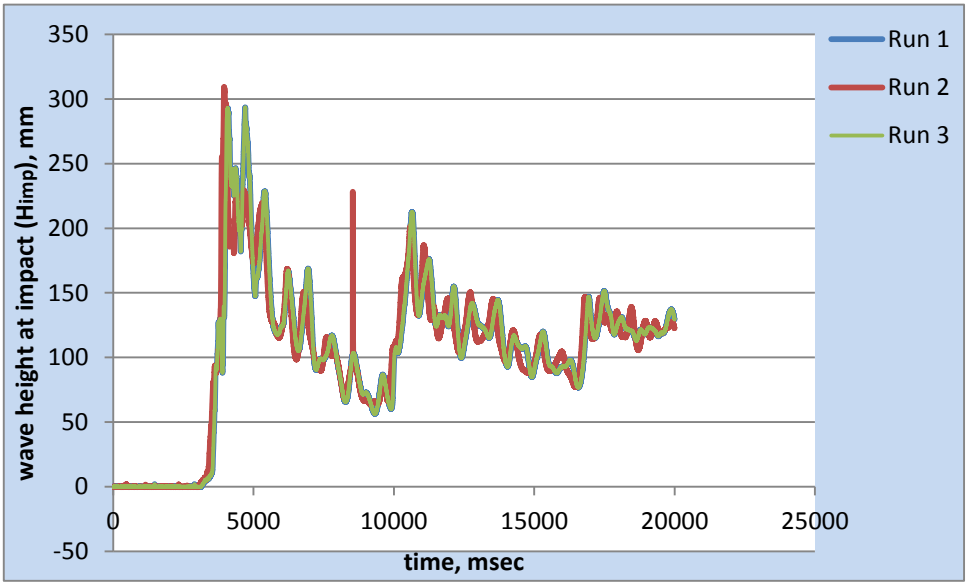

Figure 5.11**:** Water elevation time history at wave probe 2 for reservoir depth, d_o = 0.35m (3 trials at the same experimental condition)

Tests were conducted for five different initial reservoir depths. In each case, floodwater level at both probe locations was considered and measured. The results obtained for smooth-surface seawall model in vertical position is summarized in Table 5.5.

Table 5.5: Water level measurements at WP1 and WP2 for smooth-surface wall model (dry-bed downstream)

Initial reservoir water depth, d_o (m)	Maximum water level at WP 1, H_{inc} (m)	Maximum water level WP 2, H_{imp} (m)	% difference $(H_{imp} - H_{inc})\%$
0.55	0.20097	0.44018	54.34%
0.45	0.19065	0.31582	40.0%
0.35	0.11065	0.21083	47.5%
0.25	0.07461	0.16587	55.01%
0.15	0.06680	0.09725	31.3%

Figure 5.12 showed the elevation-time histories of water level records with WP1 and WP2 when the initial reservoir depth is 0.35m for dry-bed downstream with smooth-surfaced vertical wall model. For this dry-bed downstream condition, the percentage difference between the maximum floodwater heights of the two probes for various reservoir depths lay between 40% and 55% (Table 5.5) except for the lowest reservoir depth which gives a lower value of 31.3%. In most cases, the maximum elevation of floodwater is always present around the region of the impact with the structure (H_{inc} is always higher than H_{imp}). The highest water level recorded by the probe close to the dam-site (H_{inc}) indicated approximately half of the highest height obtained by the probe close to the model structure (H_{imp}). This is obtained in most cases for all other reservoir depths except for lowest initial reservoir depth (d_o = 0.15) which is relatively lower than 50%. This relationship is in agreement with analytical solution for a one dimensional frictionless and horizontal dam-break flow problem explained in chapter 2.

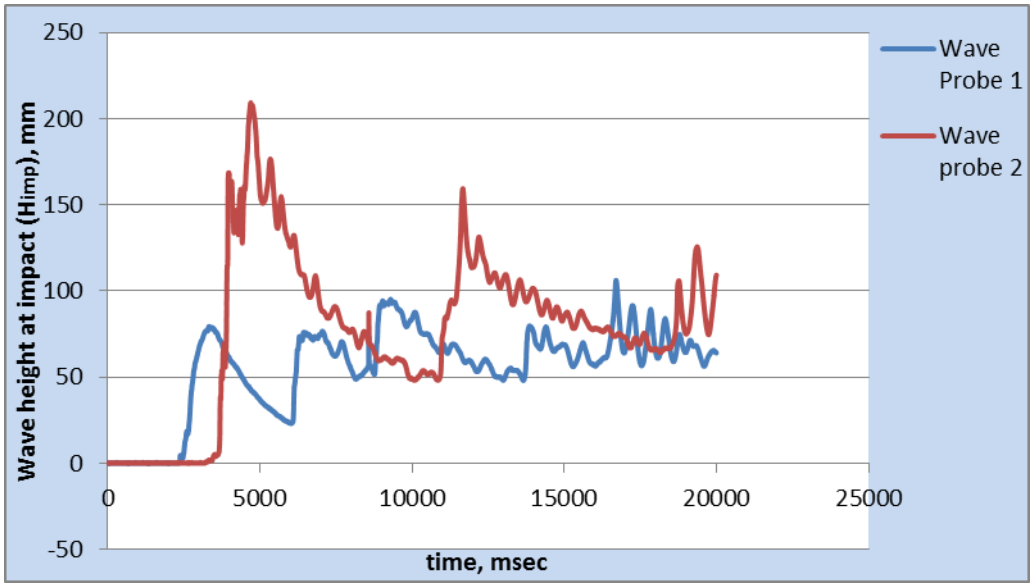

Figure 5.12**:** Water elevation-time history for dry-bed downstream smooth-surface wall model (reservoir depth, d_o = 0.35m, wave probe 2.2m apart)

The experiments were repeated with the same range of initial reservoir depths ($0.15m \leq d_o \leq 0.55m$) but with wet-bed of various initial water depths downstream. Figure 5.13 shows the plot of the maximum water elevations obtained with WP1 (H_{inc}) against various initial reservoir depths (d_o) to deduce the effect of wet-bed conditions and also to compare it with Ritter's theory. The floodwater heights for WP1 (H_{inc}) have a tendency to reach an approximate constant height $(4/9)d_o$ suggested by Ritter (Chanson, 2005) better in dry-bed case than in wet-bed cases (Figure 5.13). A critical observation of variation of water surface elevation with time along the channel with the initial downstream wet-bed flow conditions (H_{ds} = 0.05m and H_{ds} 0.1m) shows a gradual increase with increasing initial downstream water depth but fewer oscillations at each probe position with increasing initial water depth downstream (Figure 5.13).

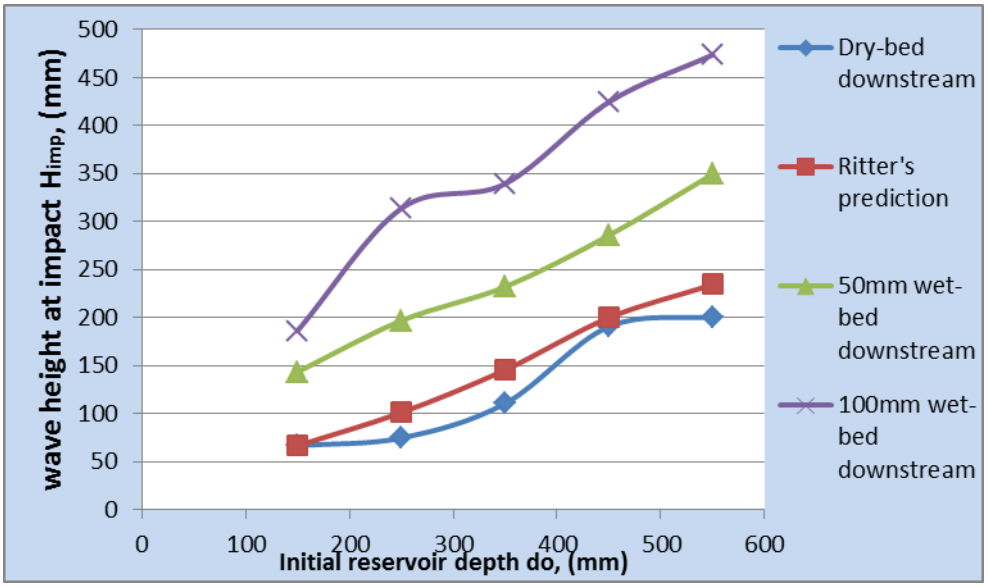

Figure 5.13: Comparison of floodwater incident wave height (H_{inc}) obtained at various initial reservoir depths for dry-bed and wet-bed conditions with Ritter's theory.

The influence of downstream water depth on the floodwater height at impact (H_{imp}) was also investigated using a different approach. To achieve this, wave height at impact (H_{imp}) was plotted against the initial reservoir depth (d_o). But, to compare the heights all throughout the entire experiments both the reservoir depth and bore height (H_{imp}) were normalized by accounting for downstream water levels (Figure 5.14). In general, the higher the initial downstream water level (DSWL) the lower the actual water level elevation from SWL though the floodwater height at impact (H_{imp}) or in the channel may appear higher for higher DSWL than lower DSWL. An approximate linear relationship between initial reservoir depth (d_o) and bore height (H_{imp}) is obtained for the dry bed downstream condition (Figure 5.14). However further experimentation with larger initial water depths and shallower downstream water depth may be needed to determine the precise relationships at the upper right region for the wet-bed downstream conditions.

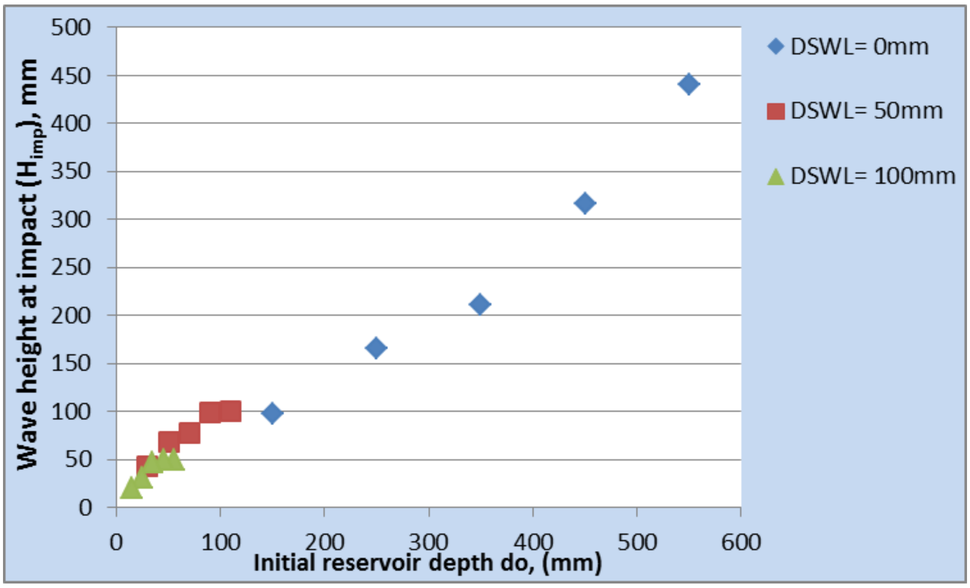

Figure 5.14: Variation of initial reservoir depth with the bore height to explore the influence of various initial water depths downstream of the channel (wet-bed conditions)

Again, the water level obtained with WP2 (H_{imp}) was compared with analytical expression of (Homma and Horikawa, 1965). Homma and Horikawa (1965) reported an analytical expression of a first order approximation of;

$$H = 0.78d_o \quad \text{...} \quad 5.8$$

where H is the wave height at the front of the structure and d_o is the water depth at the dam site.

The data obtained from WP2 (H_{imp}) are then compared with equation 5.8. The agreement with Homma and Horikawa's prediction is better for dry-bed downstream condition than the wet-bed downstream conditions (Figure 5.15).

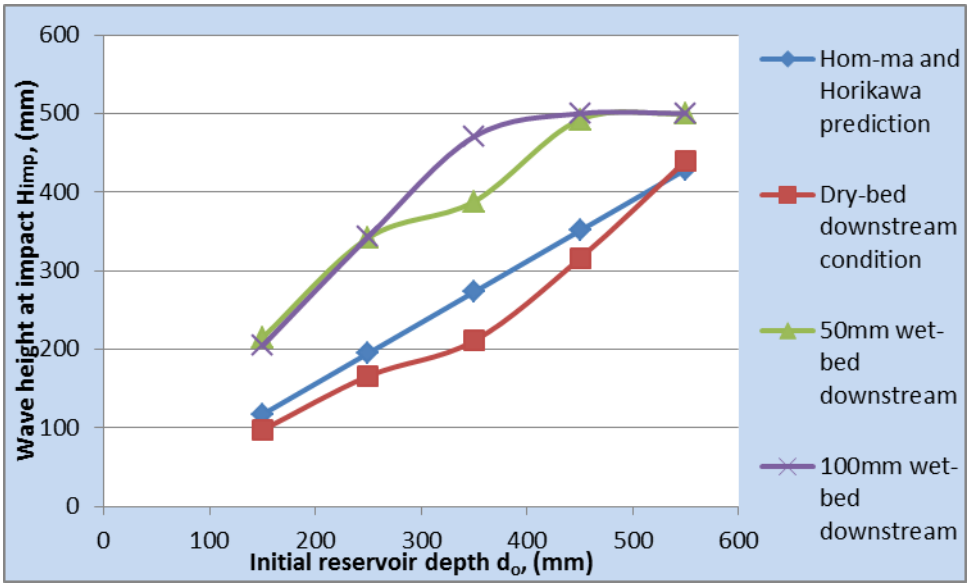

Figure 5.15**:** Comparison of floodwater elevation at impact (H_{imp}) for dry-bed and various initial water depths downstream of the channel (wet-bed conditions) with equation 5.8

5.4.3 *Characteristics of Measured Impact Pressures*

During this investigation impact pressures have been measured simultaneously on six pressure transducers fixed at designated positions on the wall model. The transducers were located at the face of the wall model vertically between 0.02m and 0.5m of the wall height. The lowest transducer was located at exactly 0.02m from the base of the wall. The measured pressures are mainly dynamic pressures (see section 4.8.3). Hence, the impact pressure referred to throughout this thesis indicates the measure of the dynamic pressure in isolation.

Figure 5.16 and Figure 5.17 show pressure-time plots of impact pressures for transducers 1 to 6 for initial reservoir depth d_o = 0.25m and d_o = 0.55m respectively for vertically positioned smooth surface wall. As seen in the figures there is an initial impact pressure experienced at different locations on the wall. The extent to which each of these locations experienced these initial impacts differs. In both Figure 5.16 and 5.17, the initial impact pressures at the base of the wall (transducer 1 position) showed a distinct feature of high peak as compared to the upper section of the wall (transducers 2 to 6). This could mean that the maximum impact pressure occurred at the base of the wall structure in this instance. However, for the case of do = 0.55m there are distinct indications of false signals overshooting the initial or actual maximum

pressure (Figure 5.17 a). This is the result of overtopping and output from the accelerometer compensation due to water impacting the sensor body. Hence, Figure 5.17 (b) showed the drawn-out of the actual signals with overshooting false signals truncated.

The subsequent impacts after the initial impact and wall reflection for the upper section of the wall (transducers 2 to 6) appeared similar in shape and relatively with lower peaks particularly for initial reservoir depth of 0.25m (Figure 5.16). This is not the case for initial reservoir depth of 0.55m clearly shown in Figure 5.17 (b), for some transducers though the curves looked similar but the peaks were relatively very high. This could be the results of the higher wave height (for the case of d_o = 0.55m) which may generate greater propagation speed and magnitude, whereas for the case of d_o = 0.25m the wall reflection and the distance between the wall and the reservoir gate may considerably reduce the propagation speed thereby significantly negate the impact effects.

Moreover, in the case of initial reservoir depth = 0.25m only the transducer at the base of the wall (transducer 1) experienced wave impact after the reflection by the wall as a result of reduced wave height at impact. This may also contribute to the negative impact pressures showed for the case of initial reservoir depth of 0.25m. In the case of d_o = 0.55m in Figure 5.17 (a) where in some locations the secondary pressures (impact after wall reflection) tend towards negative values may probably be due to entrapped air. As shown in Figure 5.16 (for the case of d_o = 0.25m) there are a reduced number of peaks for the transducers located at the upper section of the wall model which makes the impact pressure histories obtained with the transducer located at the base of the wall a good representative and depiction of the wave – structure interaction discussed in section 3.4. However, for the case of do = 0.55m (Figure 5.17) all the transducers experienced the impact of the flood wave.

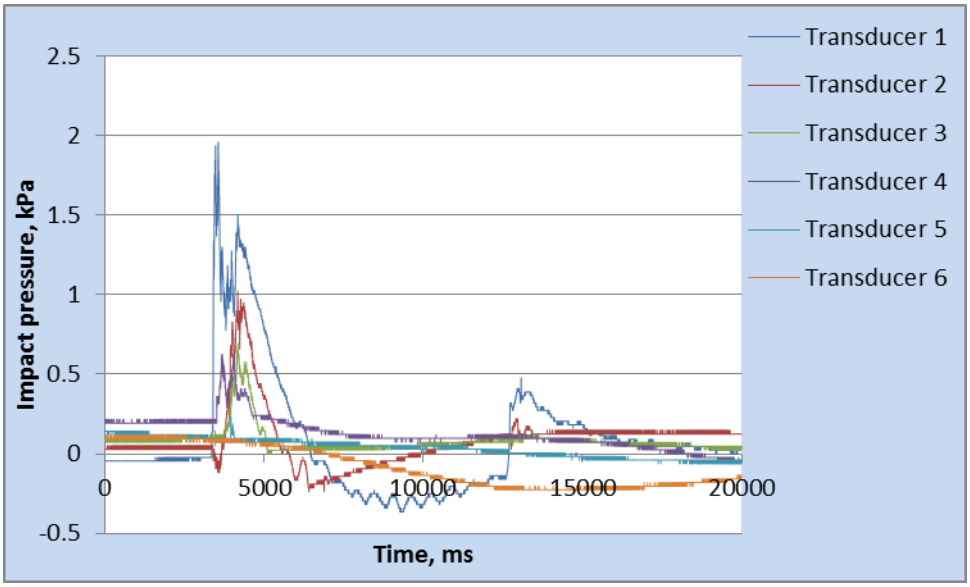

Figure 5.16: Pressure-time plot for transducer 1 to 6 for initial reservoir depth, d_o=0.25m for the smooth surface wall in vertical position

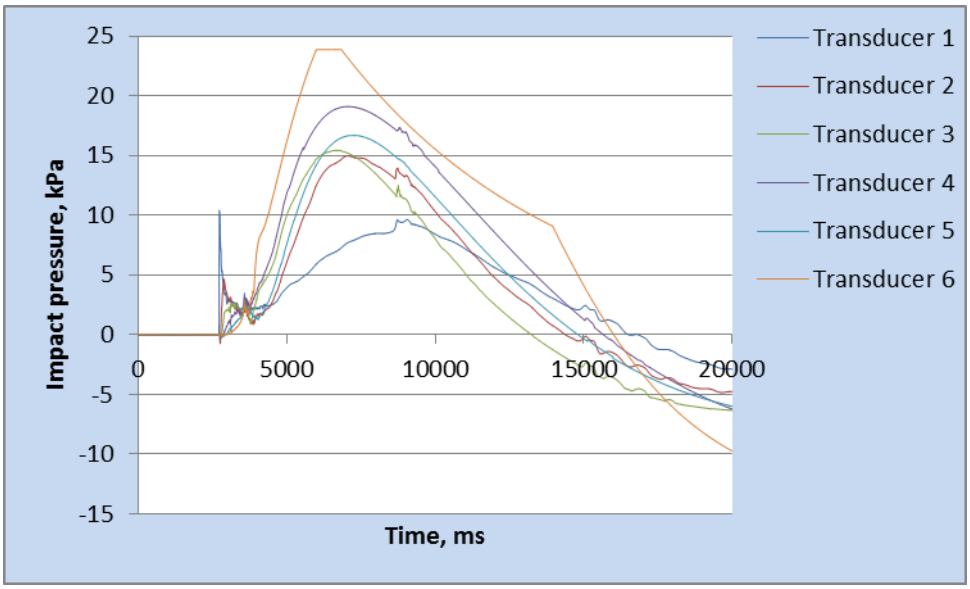

Figure 5.17 (a)

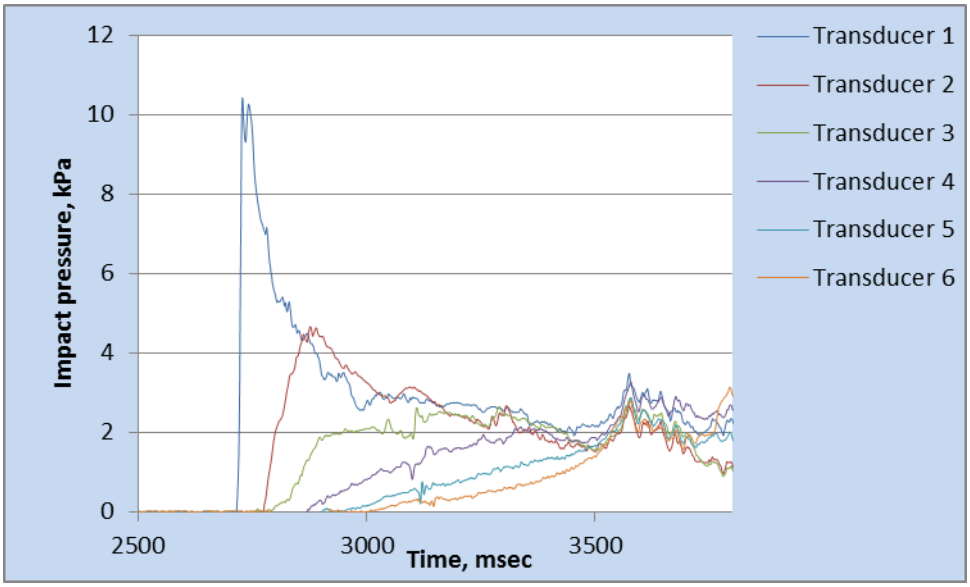

Figure 5.17 (b)

Figure 5.17: Pressure-time plot for transducer 1 to 6 for initial reservoir depth, d_o=0.55 for the smooth surface wall in vertical position (a) with false signal (b) without false signal

5.5 Impact Pressures on Smooth-Surface Vertical Seawall Model

The experimental investigation on the smooth-surface vertical seawall model was in the first instance carried out and analysed. The results obtained for the smooth-surface vertical model wall are then validated with previous results and again its performance is compared with that of sloped and rough-surfaced wall models. Thus, this section aimed to present some of the results obtained for smooth-surface vertical wall model.

5.5.1 *The Magnitude and the Variation of the Maximum Impact Pressure*

The maximum value of the impact pressures, p_{max}, has been reported not to be described deterministically but only probabilistically taking the form of a log-normal distribution (Fuhrgohter, 1986). In this study, the maximum dynamic pressures obtained for each transducer varied with initial reservoir depth. Table 5.6 shows the maximum dynamic pressures obtained with the smooth-surface wall model at vertical position. Table 5.6 indicates that the highest dynamic pressure values arose from the transducer located at the base of the wall for all the

initial reservoir depths investigated (i.e. from transducer 1). For instance, for reservoir depth of 0.55m the lowest and highest maximum impact pressure for the six transducers are 2.523792 and 9.522115 kPa respectively. The peak being obtained with transducer located at the base of the wall (transducer 1) and the lowest impact was obtained from transducer 6 located at the upper section of the wall (see Table 5.6).

Figure 5.18 shows the variation of maximum impact pressure with respect to the initial reservoir depth for each of the transducers. The highest impact was experienced at the base of the smooth-surfaced wall when in vertical form as indicated in Figure 5.18. The upper part of the wall model experienced closely similar impact as may be seen from the figure. The agreement is reasonably good in most parts of the pressure data range and may suggest that the probability distribution of the maximum impact pressures of breaking waves on a smooth-surfaced vertical wall can be described by the log-normal distribution as suggested by Fuhrgohter (1986) .

Table 5.6: Magnitude of maximum impact pressure obtained for each of the transducers at varying initial reservoir depths (for smooth surface wall in vertical form)

r-depth d_o, m	Trans.1 kPa	Trans.2 kPa	Trans.3 kPa	Trans.4 kPa	Trans.5 kPa	Trans.6 kPa
0.55	*9.522115	4.097406	3.437317	3.021514	2.842908	2.523792
0.45	*6.892416	2.841872	2.37013	2.344086	1.819794	1.606881
0.35	*3.959378	2.01698	1.567337	1.019212	1.072398	0.89169
0.25	*1.993376	1.012553	0.543414	0.495983	0.156381	0.075638
0.15	*1.103886	0.197366	0.043471	0.083159	0.047006	0.10773

*Highest Dynamic Pressure Values

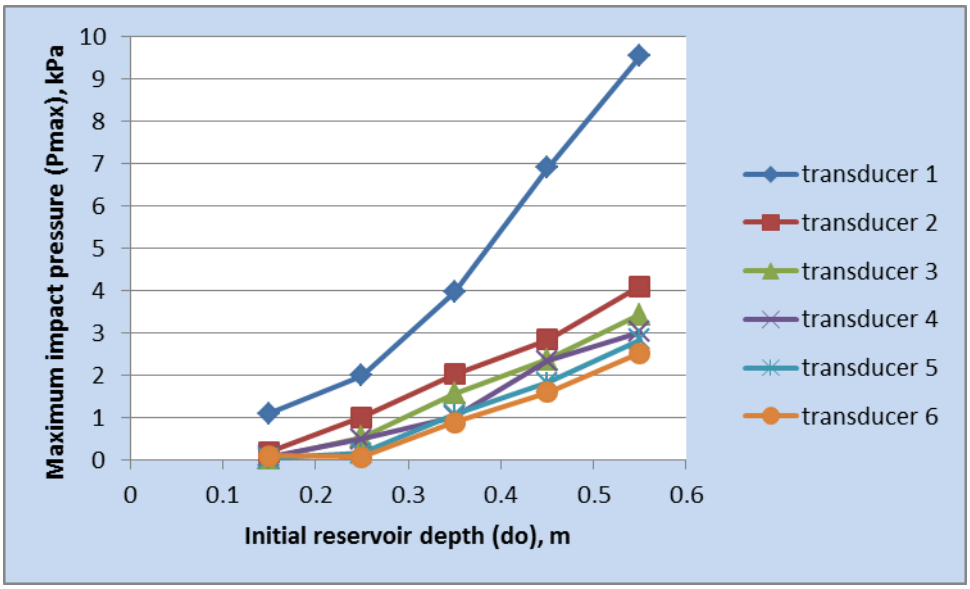

Figure 5.18: Variation of maximum impact pressure with respect to initial reservoir depth for smooth surface wall model in vertical form.

5.5.2 *Duration/Rising time of Maximum Impact Pressure*

According to Blackmore (1982), the pressure-time history of a standing wave or non-breaking wave can be identified by its slow rise time and relatively low intensity. However, the pressure-time history of a braking wave was said to be characterised by a fast rise time and often a high intensity transient pressure followed by a longer duration pressure of the order of the standing wave pressure. Figure 5.19 showed example of pressure-time history obtained for reservoir depth, d_o = 0.45m for the smooth-surfaced vertical wall (wall model-A). The triangular spike is characterised by the maximum reached by the signal during loading (P_{max}), the time taken to get to P_{max} from 0 (rise time, t_r) and back (duration time, t_d). This is followed by a slowly varying (pulsating) pressure of lower magnitude but longer duration. The area covered by the triangular spike in Figure 5.19 represents momentum transfer to the structure during the impact (the impulse) in which a substantial amount of the wave momentum is destroyed. As the impulse represents a fixed area, the implication is that more violent impacts will correspond to shorter rise times and vice versa.

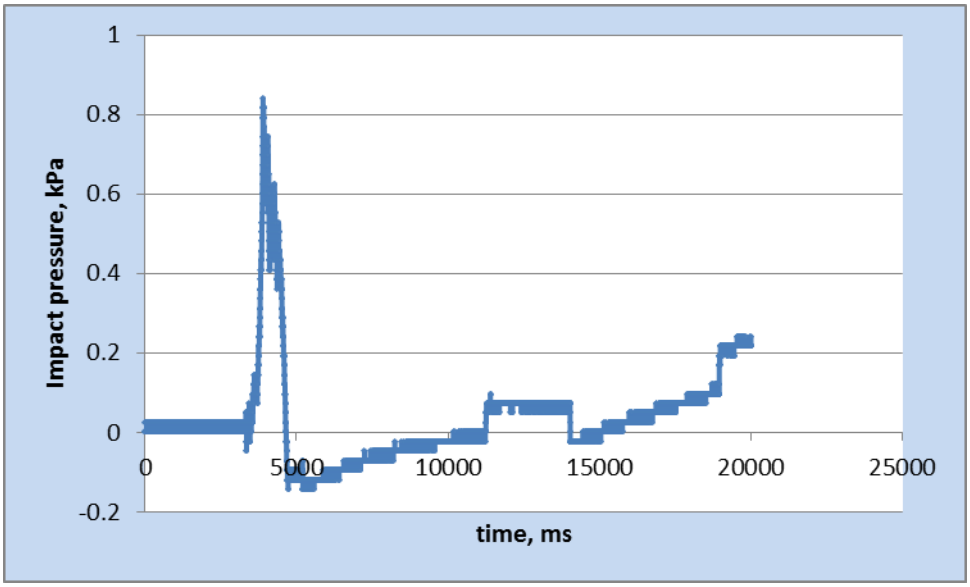

Figure 5.19**:** Pressure-time history obtained at the base of the wall model (with transducer 1) for smooth-surfaced vertical wall (for initial reservoir depth, d_o = 0.45m).

Consequently, Figure 5.20 shows the results of duration of the maximum impact pressure with respect to the wave height at impact (H_{imp}) for each of the transducers. It can be seen from the figure that the duration of the maximum impact pressure is very short as reported by previous investigators and is in the range of 1ms and 5ms for the present experiments. Therefore, the combined effect of the surge on the defence structure should be considered in terms of both the duration and magnitude of maximum pressure on the wall in order to determine the extent of the destructiveness of the surge on the wall structure although the peak pressure of the surge could appear to be the most important factor.

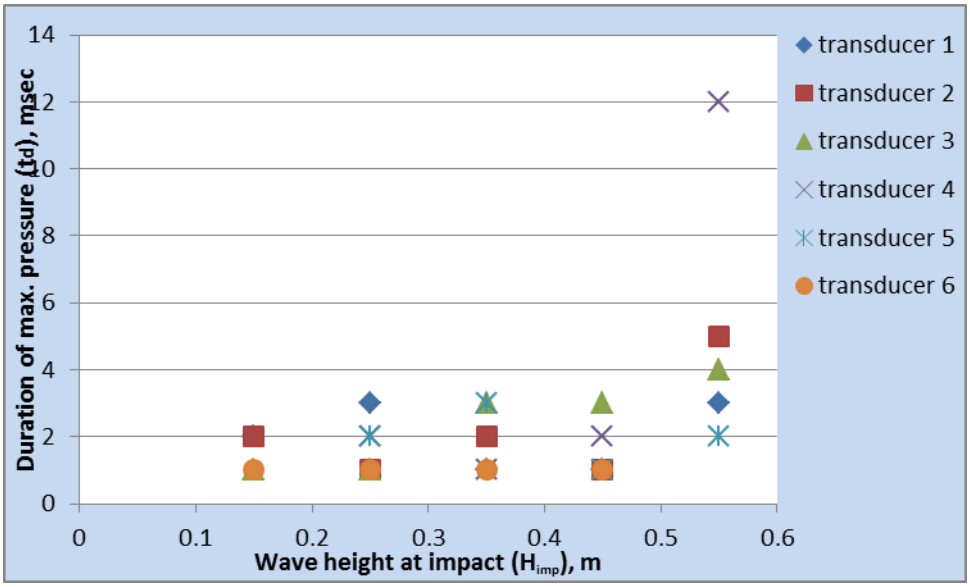

Figure 5.20: Duration of maximum impact pressure against wave heights at impact produced with varying initial reservoir depths (for the smooth-surface vertical wall model).

5.5.3 *Vertical Impact Pressure Distributions*

There had been a considerable amount of disagreement as to the extent of the wave impact pressure over the face of the wall, as well as to the location of the maximum impact pressure (see chapter 2). In this experiment, the location of the maximum impact pressure has been investigated for both vertically positioned and sloping seawall.

Figure 5.21 showed the vertical distribution of maximum impact pressure for the smooth-surface wall model for the present study. The results of vertical pressure distribution for the sloping walls are presented in section 5.5.5. In the figure the maximum impact pressure is plotted against the percentage wall height of the position of transducer (that is the % height of the transducer to the height of wall model). This is presented for each of the initial reservoir depths.

It can be seen from Figure 5.21 that the most frequent location of P_{max} lies within the toe of the seawall (the experiment was conducted for dry-bed downstream condition), hence with the present results, it seems reasonable to suggest that the still water level (SWL) is the most likely location for P_{max}. There was a similar trend for the semi-smoothed surface wall (wall model-B), isotropic macro-texture surface (IMACTS) wall (wall model-C) and isotropic micro-texture

surface (IMICTS) wall (wall model-D) depicted in Figure 5.22, Figure 5.23 and Figure 5.24 respectively. It showed that the maximum impact pressures do occur, although less frequent, above the toe of the seawall as well for vertically positioned seawall irrespective of the wall surface.

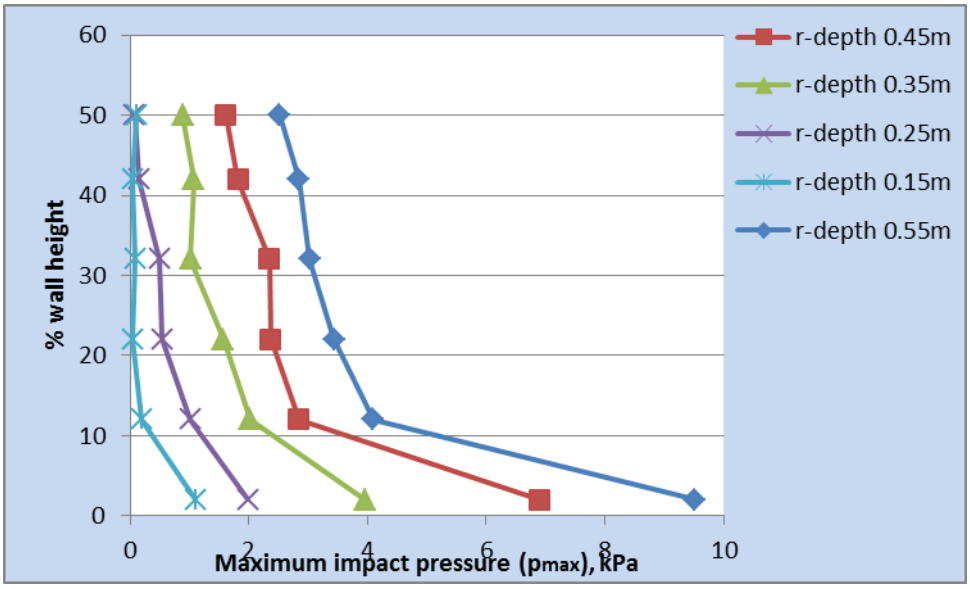

Figure 5.21: Vertical maximum impact pressure distribution for the smooth-surfaced wall model (wall model-A) in vertical form

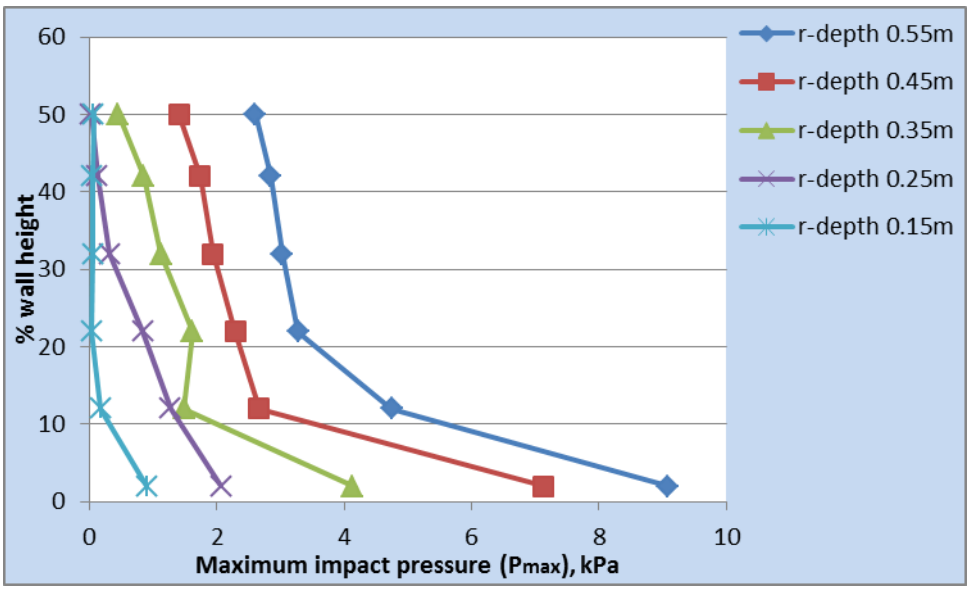

Figure 5.22: Vertical maximum impact pressure distribution for the semi-smoothed surface wall (wall model-B) in vertical form

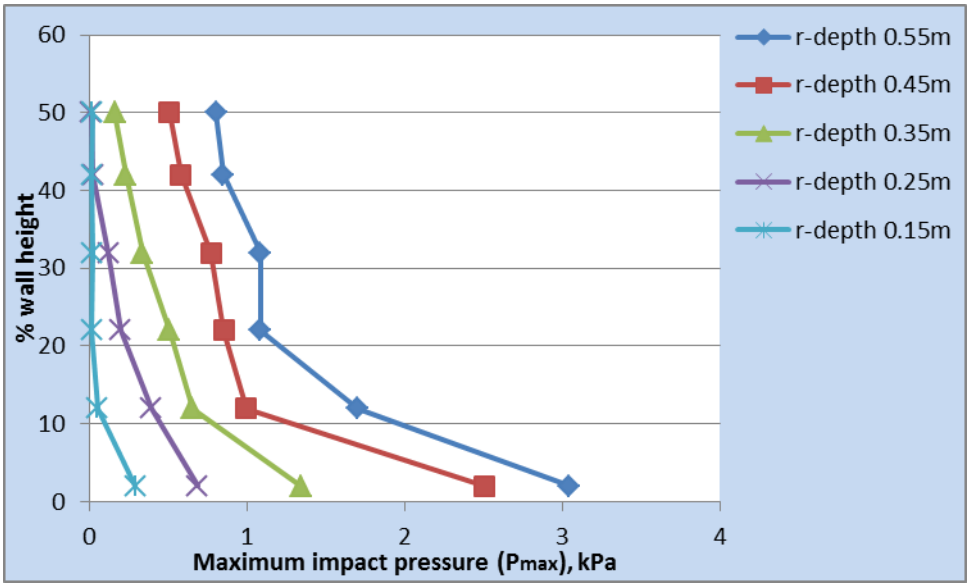

Figure 5.23: Vertical maximum impact pressure distribution for the isotropic macro-texture surface (IMACTS) wall (wall model-C) in vertical form

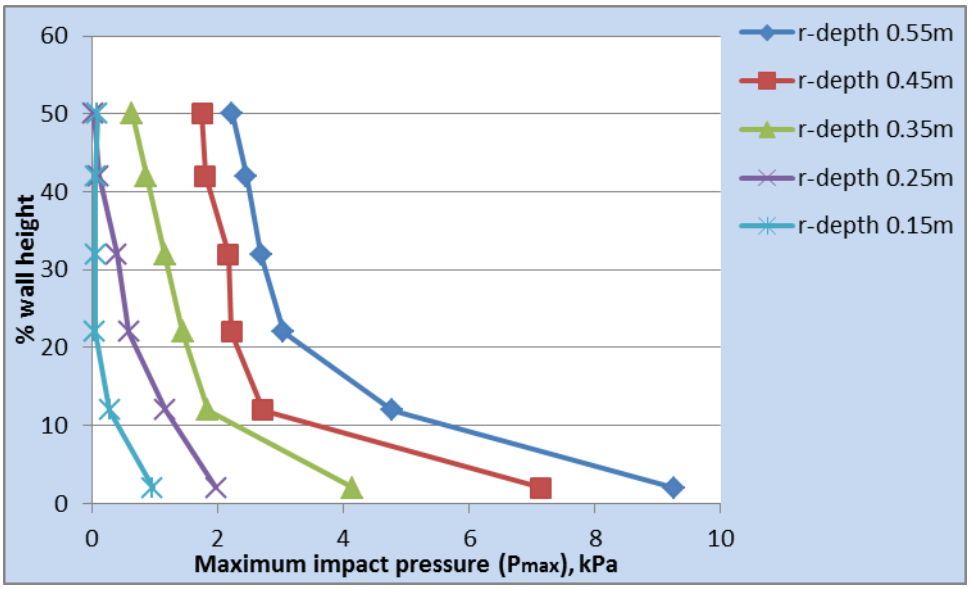

Figure 5.24: Vertical maximum impact pressure distribution for the isotropic micro-texture surface (IMICTS) wall (wall model-D) in vertical form

5.5.4 ***Hydrostatic and Dynamic Impact Pressures***

The pressure exerted on a seawall by breaking waves can be grouped into two distinct types; (1) a slowly varying pressure of relatively long duration with a magnitude of the order of the standing wave pressure i.e hydrostatic and (2) a short duration transient pressure lasting from only a few milli-seconds in the laboratory experiments, but with a maximum generally much greater than the hydrostatic pressure (Blackmore and Hewson, 1984). This short duration impact pressure only occurs for certain conditions of wave breaking, whilst the hydrostatic wave pressure occurs for every wave that impinges on a seawall whether it breaks or not. The magnitude of the hydrostatic pressure is easily and accurately calculated from theory, whereas the magnitude of the impact pressure cannot yet be estimated entirely by theoretical analysis due to the high complex mechanism of wave breaking. These two pressure types identified by Blackmore and Hewson (1984) have been estimated in the present study. The impact pressures from which the transient pressure (maximum impact pressure) are deduced are measured with transducers suitably installed at the centreline of the surface of the model seawall while the corresponding hydrostatic pressures were computed from various theoretical equations given by previous researchers.

Minikin (1963) further gives an adaptation of his previous work which enables the pressures due to breaking waves to be calculated on nearly vertical wall. Minikin, however assumed that the hydrostatic pressure may be calculated from:

$$P_{hydrostatic} = \rho g \left(d_w + \frac{H_b}{2}\right) \dots \dots \dots \dots \dots 5.9$$

Where ρ is the density of the water, g is the gravitational acceleration, d_w is the initial water depth in the channel (d_w is taken to be 0 in the present study for dry-bed downstream condition) and H_b is the wave height at impact.

Besides, Fukui et al. (1963) termed the hydrostatic pressure as the 'continuous' pressure at the wall after the wall reflection and assumed that the average of the impact pressures obtained to be the hydrostatic pressure. In addition, Nakamura and Tsuchiya (1973) also study the shock

pressure of a tsunami bore on a composite structure. Large pressure heads of relatively short duration just after the impact were measured and reported to be followed by a nearly constant hydrostatic pressure from the height of the reflected bore (see chapter 2). The impact pressure-time histories obtained in the present study also shown at least two peaks (see Figure 5.1), the first peak was considered to be the initial impact of the wave front before the reflection by the wall model having magnitude dependent upon the wave celerity, period, percentage of entrained air, etc. The second or subsequent peaks which sometimes appeared constant may then probably be the hydrostatic pressures exerted by the following body of waves after the reflection by the wall according to previous suggestions (Blackmore and Hewson, 1984, Nakamura and Tsuchiya, 1973, Fukui et al., 1963) .

Following the definition of hydrostatic pressure by both Fukui et al. (1963) and Nakamura and Tsuchiya (1973) the present study has also assumed that the continuous and relatively constant pressure obtained during the experiment is secondary or hydrostatic pressure. This has allowed considering the average of the impact pressure obtained from each of the transducers in the present experiment as hydrostatic pressure while Minikin hydrostatic pressures were computed from equation 5.9. The results obtained for the hydrostatic pressure for all the wall models investigated in the present study using Fukui et al and Minikin's theories are given in Tables 5.7 and Table 5.8 respectively.

Table 5.7: Fukui et al. hydrostatic pressures (F_{hp}) for all the seawall models in vertical position (Fukui et al. theory)

r-depth, d_o, m	Wall model-A		Wall model-B		Wall model-C		Wall model-D	
	wave height at impact, H_{imp}, m	Fukui et al. hydrostatic pressure, F_{hp}, Pa	wave height at impact, H_{imp}, m	Fukui et al. hydrostatic pressure, F_{hp}, Pa	wave height at impact, H_{imp}, m	Fukui et al. hydrostatic pressure, F_{hp}, Pa	wave height at impact, H_{imp}, m	Fukui et al. hydstatic pressure, F_{hp}, Pa
0.55	0.416779	1571.4390	0.457996	968.3548	0.459293	581.4498	0.416779	2008.251
0.45	0.317132	335.5344	0.314962	129.9685	0.314400	8.8942	0.317132	946.321
0.35	0.246658	186.0402	0.238049	113.4001	0.217375	93.5568	0.246658	229.792
0.25	0.167694	190.9484	0.164646	93.1194	0.16931	54.6311	0.167694	148.222
0.15	0.095816	141.4414	0.100939	70.6328	0.096131	66.5942	0.095816	118.148

Table 5.8: Minikin hydrostatic pressures (M_{hp}) for all the seawall models in vertical position (Minikin's theory)

r-depth, d_o, m	Wall model-A		Wall model-B		Wall model-C		Wall model-D	
	wave height at impact, H_{imp}, m	Minikin hydrostatic pressure, M_{hp}, Pa	wave height at impact, H_{imp}, m	Minikin hydrostatic pressure, M_{hp} , Pa	wave height at impact, H_{imp}, m	Minikin hydrostatic pressure, M_{hp} , Pa	wave height at impact, H_{imp}, m	Minikin hydrostatic pressure, M_{hp} , Pa
0.55	0.41677	2044.30	0.45799	2246.47	0.45929	2252.83	0.41677	2044.30
0.45	0.31713	1555.53	0.31496	1544.89	0.31440	1542.13	0.31713	1555.53
0.35	0.24665	1209.86	0.23804	1167.63	0.21737	1066.22	0.24665	1209.86
0.25	0.16769	822.54	0.16464	807.59	0.16931	830.47	0.16769	822.54
0.15	0.09581	469.98	0.10093	495.11	0.09613	4715.20	0.09581	4699.78

5.5.5 *Influence of wave height on the maximum impact pressure for the vertical walls*

This section is mainly concerned with the floodwater level in the region at which the flow impinges the structure. The data obtained from the experiment were analysed to explore the relationship between the maximum impact pressure and the wave height at impact, $H_{imp.}$

Figure 5.25 showed the variation of simultaneous maximum impact on each of the transducers with respect to the wave height produced at impact for the smooth-surfaced vertical wall model. It can be seen that generally the impact pressure increases with increased wave height for each of the transducers (Figure 5.25). It may also be seen from Figures 5.25 that the impact pressure reaches its maximum at certain wave height conditions such as the water depth at the foot of the structure, amount of air entrapped by the wave etc. Beyond this wave height, the impact pressure seems to approach gradually to a certain value .Only transducer 1 showed an exceptional variation probably being at the base of the wall.

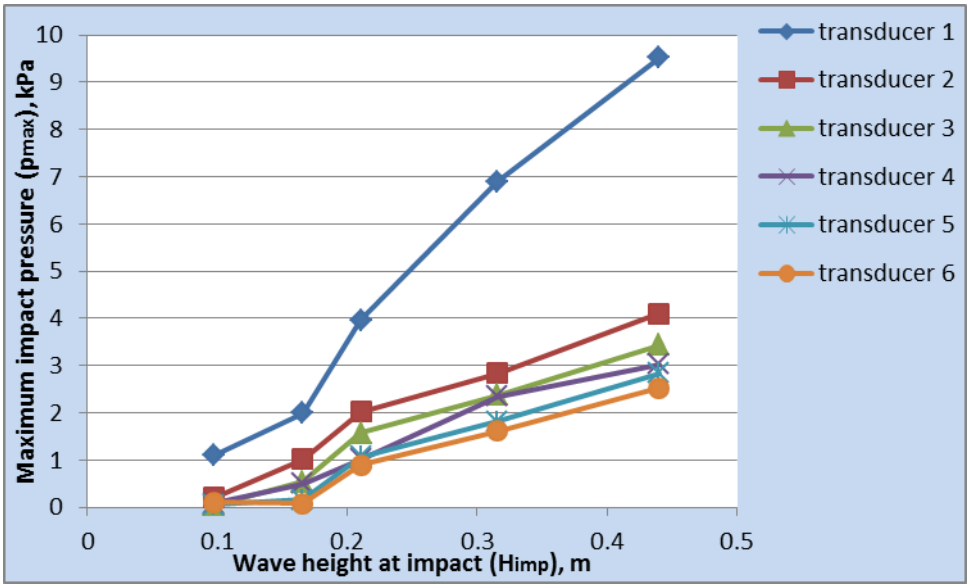

Figure 5.25: Variation of the maximum impact pressure with wave height at impact for all the transducers (for smooth-surfaced vertical wall model)

Similar relationship was obtained for each of the wall models in vertical form (see section 5.7.2) in which maximum pressures of all the six transducers are considered. Thus, the variation of maximum impact pressure with either initial reservoir depth (see Figure 5.43 in section 5.7.2) or wave height at impact (Figure 5.25) on the wall was generally found to be linear for the vertical walls. This is illustrated for the smooth-surface vertical wall model (wall model-A) in Figure 5.26. Figure 5.27 showed the pressure-time history as well as the time history for the wave height at impact plotted together for further illustration.

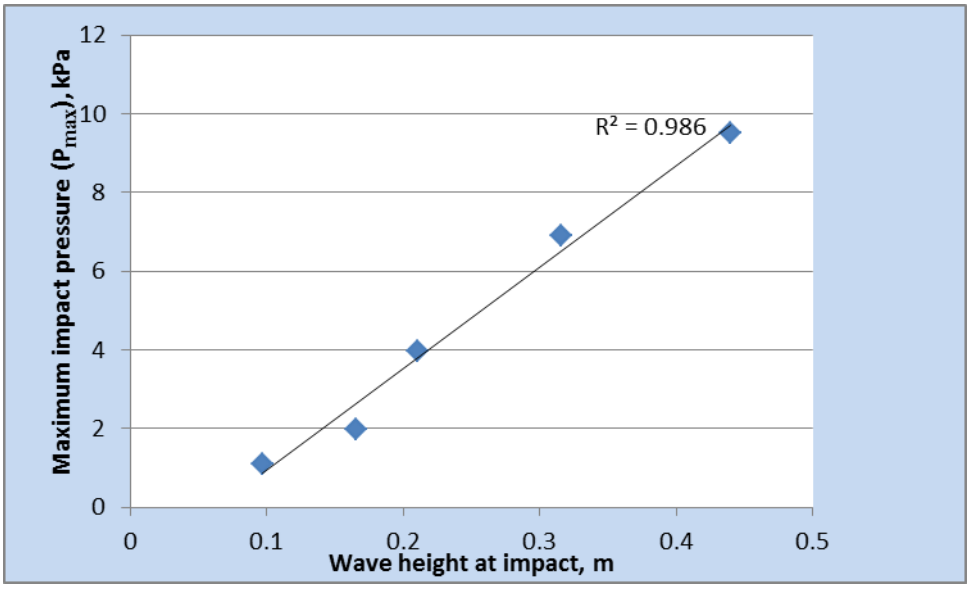

Figure 5.26: An example of linear variation of maximum impact pressure with respect to wave height at impact for the smooth-surface wall (wall model-A)

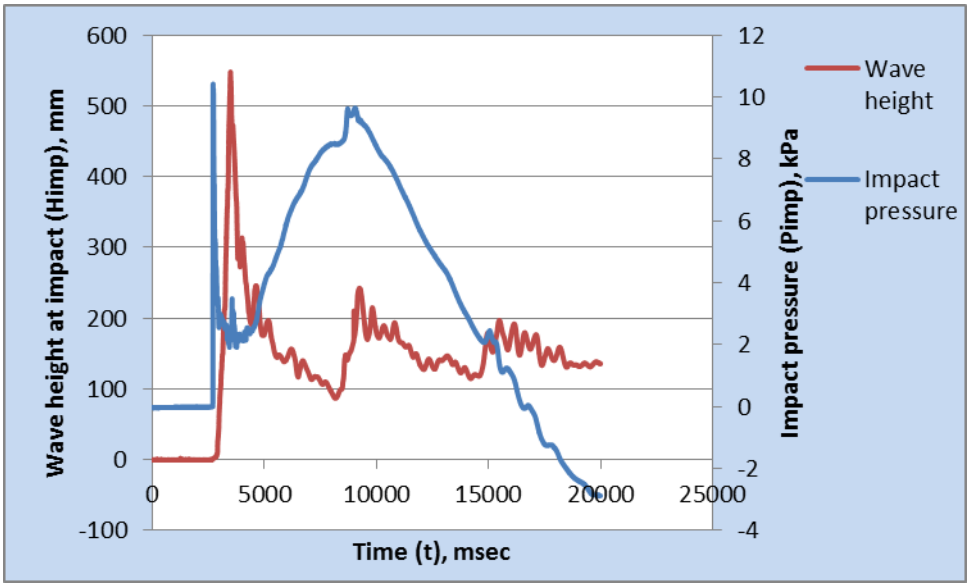

Figure 5.27: Pressure- and wave height- time histories for transducer 1 (r-depth = 0.55m)

5.6 Influence of Wall Orientations on the Impact Pressures

Reported test results are contradictory concerning the effect of wall inclination on wave impact pressures. To clarify this situation, model tests on wave impact pressures on inclined walls were conducted to establish the relationship between the angle of the wall and the arising impact pressures. Wave heights at impact on the wall were varied by varying the initial reservoir depths from 0.15m to 0.55m. Impact pressures were measured at six locations on the face of the wall at vertical (90^o), 75^o, 60^o and 45^o backwards inclined. This entire section is designated for the analysis of data and results obtained in the present study to elucidate the effect of wall slope on the impact pressures.

5.6.1 *Pressure-time histories of sloping walls as compared with vertical wall*

The present study is particularly concerned with a type of impact where the wave breaks, by plunging directly on the wall. When this happens the resulting impact pressure history contains a peak value denoted by P_{max} which is generated shortly after the wave front makes contact with the wall. Similarly, for sloping walls as with vertical wall there are at least two peaks, the first peak represents the initial impact of the floodwater wave with the wall immediately after

the gate was released while the second and subsequent peaks indicate the impact made with the wall after the reflection at the wall.

Figure 5.28 through 5.31 shows the pressure-time histories for each of the wall models at different orientations. Figure 5.28 compares the pressure-time history for the smooth-surfaced wall when placed at various slopes to when positioned vertically. Similarly, Figure 5.29, 5.30 and 5.31 also compared the pressure-time histories for the semi-smoothed surface wall (wall model-B), IMACTS wall (wall model-C) and IMICTS wall (wall model-D) respectively when placed at various slopes to the verticals. The time t is measured from the removal of the gate.

In Figure 5.28 (a), for the case of wall angle 45 degree, certain impacts after wall reflection appeared so high compared with the initial impacts. This is due to the results of further flattening of the wall which consequently caused unusual overtopping leading to false signals indicated by the sensors. However, Figure 5.28 (b) again shows the drawn-out of the actual signals with overshooting false signals truncated. Similar pattern was seen with IMACTS wall shown in Figure 5.30 (a) but in this case at angle 90^{o}. However, since this pattern was not indicated by other wall models at this angle it may possibly be a false signal due to some experimental inaccuracies. The drawn-out of the actual signals with overshooting false signals truncated is therefore indicated in Figure 5.30 (b). However, it could be seen that usually the vertical wall has the highest initial impacts for most of the wall models apart from the few exceptions mentioned. Again, it can be seen that generally, subsequent impacts after wall reflection are repeatedly lower than the initial load for most of the wall models at every orientation (Figure 5.28 through 5.31). This is expected as a result of energy lost due to impulse as well as wall reflection.

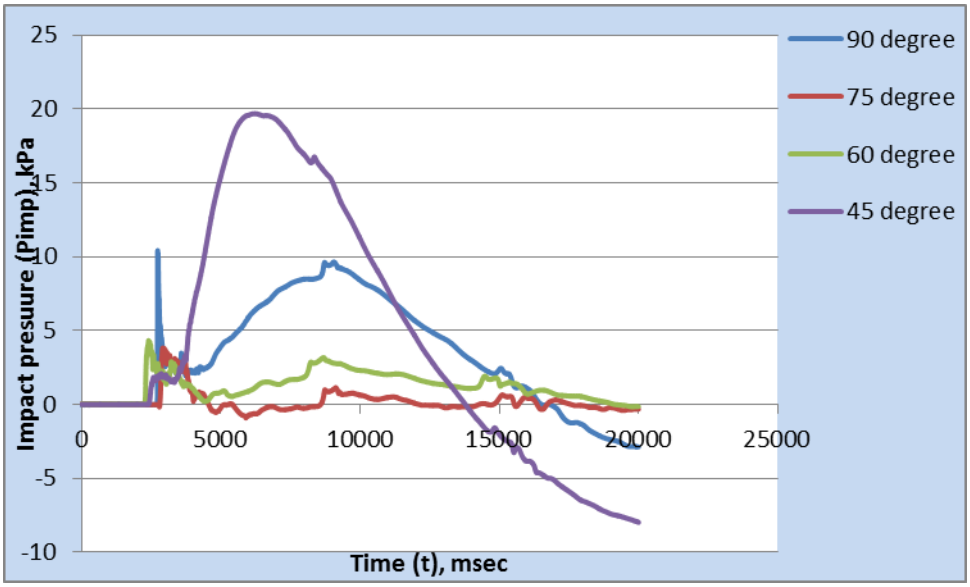

Figure 5.28 (a)

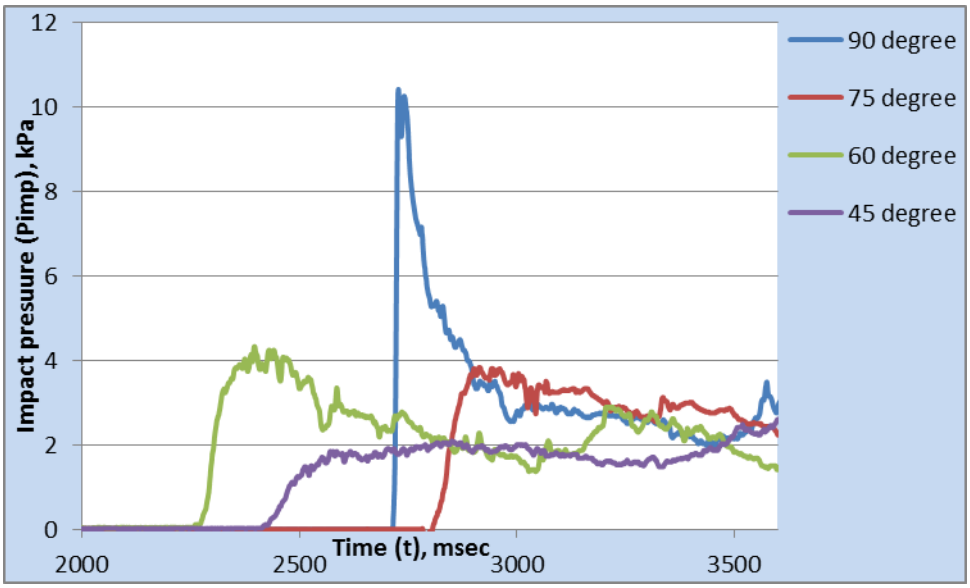

Figure 5.28 (b)

Figure 5.28: Comparison of the pressure-time histories for the smooth-surfaced wall (wall model-A) at different orientations, r-depth = 0.55m; (a) with false signal (b) without false signal

The implication of Figure 5.28 and Figure 5.30 is that the smooth surface wall (Figure 5.28) and the IMACTS wall (Figure 5.30) could cause a significant change in the general pattern of impact pressure-time history with a change to certain wall orientations. For the present study, these wall models displayed these unusual performances at 45^{o} slope. It can also be seen in Figure 5.28 that as time passes, the pressure region following each peak lasts longer before another peak. One obvious consequence of this would be an increase in the likelihood of the simultaneous actions of impact pressures which would result in a greater and longer lasting impact force on the structure.

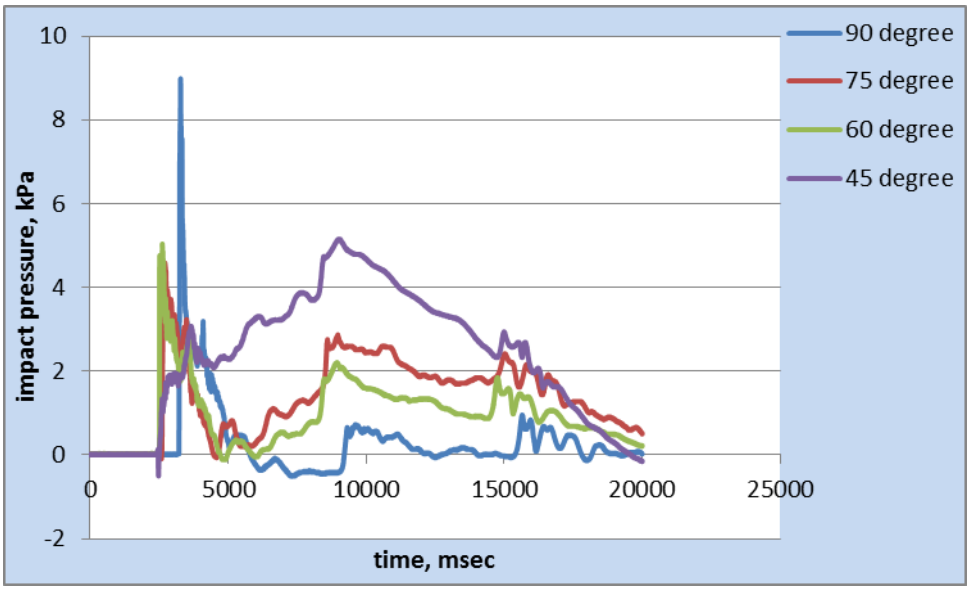

Figure 5.29: Comparison of pressure-time histories for the semi-smoothed surface wall (wall model-B) at different orientations (r-depth = 0.55m)

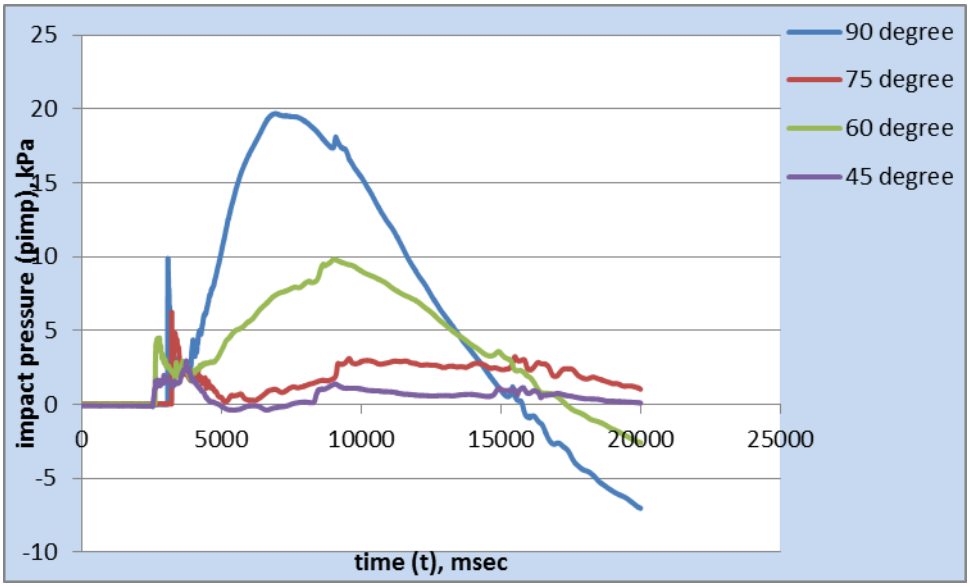

Figure 5.30 (a)

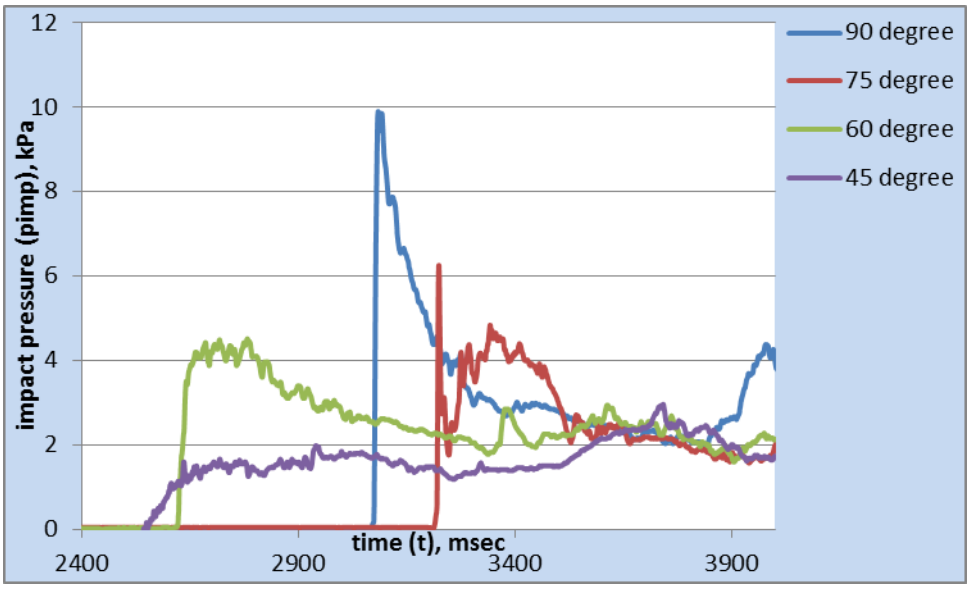

Figure 5.30 (b)

Figure 5.30: Comparison of pressure-time histories for IMACTS wall (wall model-C) at different orientations, r-depth = 0.55m; (a) with false signal (b) without false signal

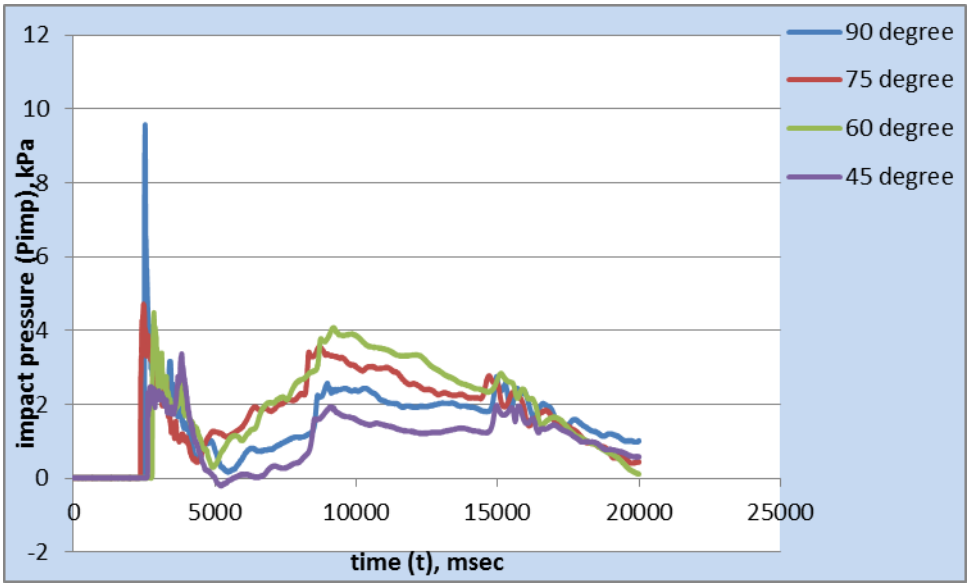

Figure 5.31: Comparison of pressure-time histories for IMICTS wall (wall model-D) at different orientations (r-depth = 0.55m)

5.6.2 *Wall Sloping Effect on the Maximum Impact Pressure with varying Initial Reservoir Depths*

Table 5.9 gives the results of the magnitude of the maximum impact pressures obtained for different wall angles at various initial reservoir depths for all the wall models. Figure 5.32 through 5.35 depicted the variation of maximum impact pressure with initial reservoir depth for four different wall slopes (90^o, 75^o, 60^o and 45^o). Figure 5.32 showed this variation for the smooth-surfaced wall while Figure 5.33, 5.34 and 5.35 showed the variation for the semi-smoothed surface wall, the IMACTS wall and the IMICTS wall respectively.

As shown in Table 5.9 and Figures 5.32 through 5.35, for most of the wall models the impact pressures obtained for the vertical wall are the highest amongst other orientations except for IMACTS wall (Figure 5.34). For the cases of smooth surface wall, semi-smooth surface wall and IMICTS wall (Figure 5.32, Figure 5.33 and Figure 5.35 respectively) the maximum impact pressure generally reduces as the wall angle becomes flattened. However, in those cases the reduction was evident between angle 90^o and other angles investigated (75^o, 60^o and 45^o) but marginal within these other angles (75^o, 60^o and 45^o). The only exception was the IMACTS wall which causes an increase in the maximum impact as the wall is varied from 90^o to any of the angle investigated (75^o, 60^o and 45^o).

Again, in general, for all the wall models, reduction in the initial reservoir depth causes a decrease in the maximum impact pressure on the walls (Figure 5.32 through Figure 5.35). The few exceptional cases (though still the same trend) were the unusual upsurge indicated by the smooth surface wall at angle 45^o when the initial reservoir depth was 0.55m (Figure 5.32) and the case of IMACTS wall which causes similar upsurge at the same wall angle (angle 45^o) when the initial reservoir depth is 0.55m. This may probably be the results of the prompt splash due to high level of initial reservoir depth (d_o = 0.55m) as compared with the depth of the channel or may be due to the flattening of the wall angle.

Table 5.9: Magnitude of maximum impact pressure for all the seawall models at different wall angles with varying initial reservoir depths

r-depth (d_o), m	Wall model-A (kPa)				Wall model-B (kPa)			
	90 degree	75 degree	60 degree	45 degree	90 degree	75 degree	60 degree	45 degree
0.55	9.5221150	4.0734154	4.1828912	9.2466180	9.0864927	4.3516663	4.5158799	3.5575547
0.45	6.8924161	2.5225089	2.7095300	2.6164774	7.1296136	2.6183002	2.9475854	2.5772467
0.35	3.9593782	1.9065720	1.8839003	1.9509635	4.1372763	2.1396152	1.8952682	2.0481139
0.25	1.9933761	1.3300724	1.3958209	1.3720576	2.0709214	1.1905538	1.3137141	1.3866979
0.15	1.1038855	0.4242236	0.6568595	0.6467712	0.9031800	0.4242236	0.6473934	0.5245763

r-depth (d_o), m	Wall mode-C (kPa)				Wall mode-D (kPa)			
	90 degree	75 degree	60 degree	45 degree	90 degree	75 degree	60 degree	45 degree
0.55	3.0461767	4.0819954	4.4442401	9.3061229	9.2541275	4.5199408	4.4292116	3.2481008
0.45	2.5050457	2.8346550	2.8646206	2.4925062	7.1432981	2.5681238	3.0698876	2.6235184
0.35	1.3428355	1.7433521	1.9384666	1.8868669	4.1418378	1.7744245	1.9651491	1.9979375
0.25	0.6840030	1.1905538	1.1640429	1.3045911	1.9751301	1.2863451	1.2489952	1.2544147
0.15	0.2916646	0.3056248	0.5747527	0.4515925	0.9624794	0.4379080	0.5656297	0.5200148

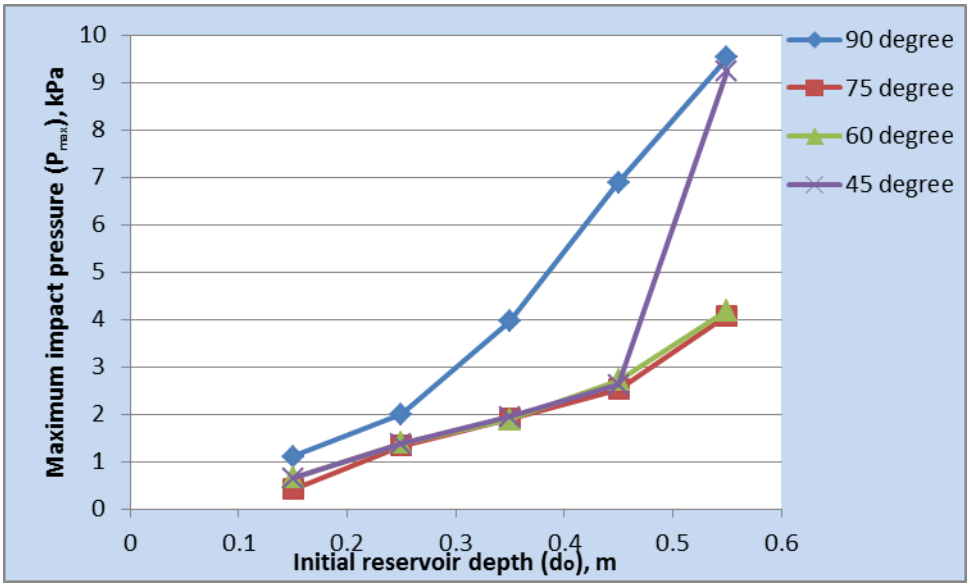

Figure 5.32: Effect of initial reservoir depth and seawall slope on the measured maximum impact pressure for the smooth surface wall (wall model-A)

Therefore, it can largely imply that the variation of the maximum impact pressure with the initial reservoir depth is linear for most wall models at angles 90º, 75º and 60º but non-linear at wall angle 45º. It can therefore be suggested that in general, maximum impact pressure reduces with decreasing wall slope and at a given wall slope the maximum impact pressure on the wall at dead end during dam-break increases with increasing initial reservoir depth.

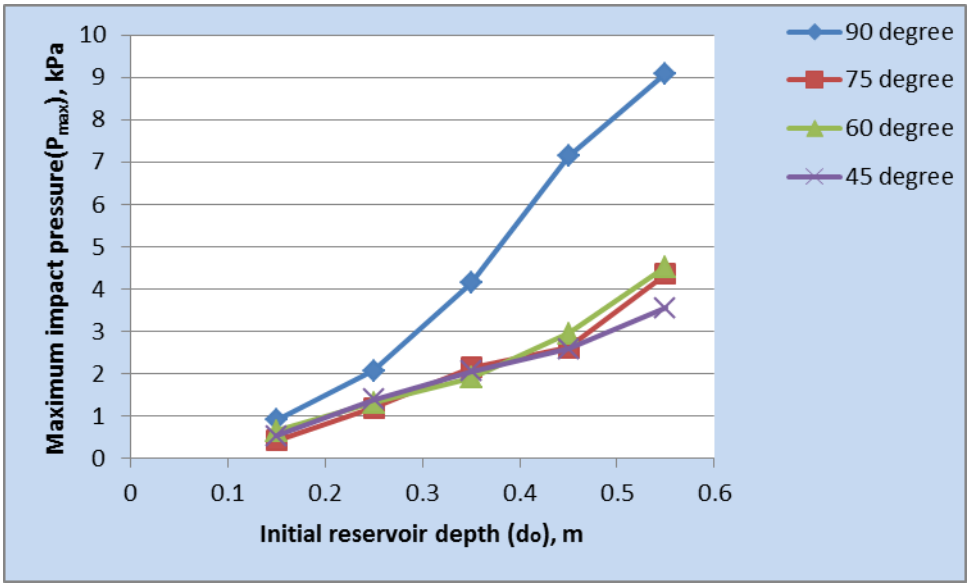

Figure 5.33: Effect of initial reservoir depth and seawall slope on the measured maximum impact pressure for the semi-smoothed surface wall (wall model-B)

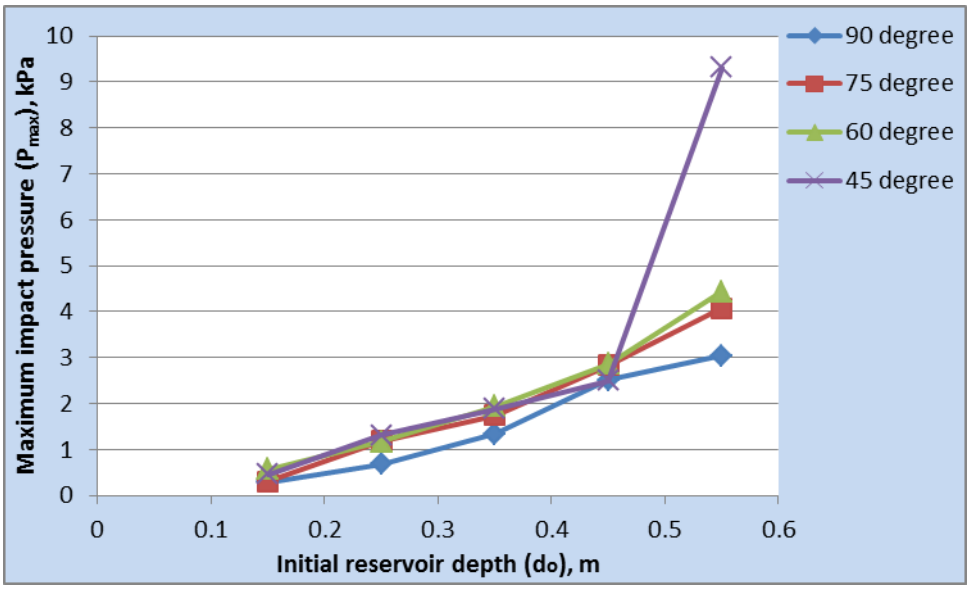

Figure 5.34: Effect of initial reservoir depth and seawall slope on the measured maximum impact pressure for the IMACTS wall (wall model-C)

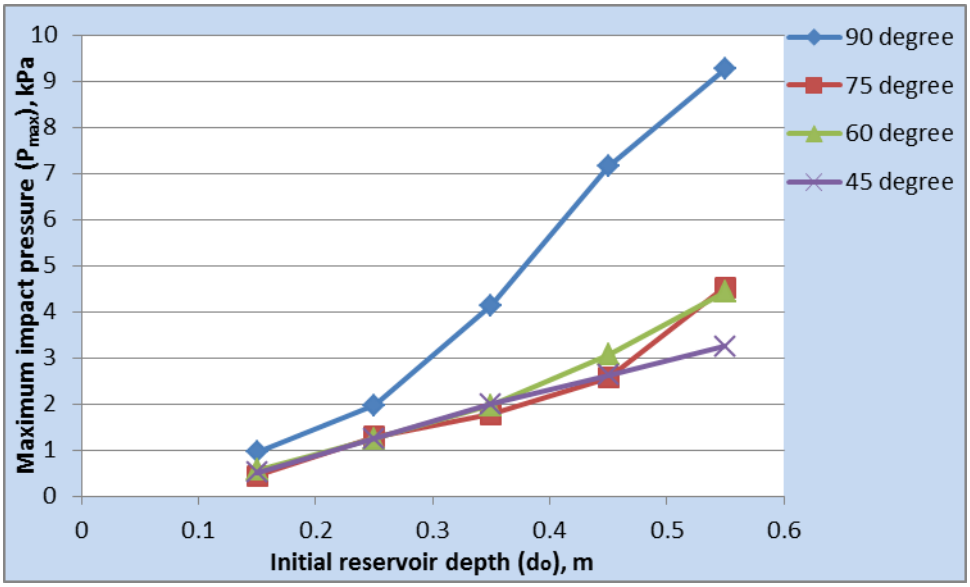

Figure 5.35: Effect of initial reservoir depth and seawall slope on the measured maximum impact pressure for the IMICTS wall (wall model-D)

5.6.3 *Load Reduction by the Sloping Walls*

This section is mainly concern with the analysis of the quantifiable level of reduction of the wall slopes by various wall models investigated. The ratio of the maximum impact pressure on the inclined wall to maximum impact pressure on the vertical wall (reduction factor) as well as percentage reduction of the sloping wall relative to the vertical was found for all the wall models and angles for each of the initial reservoir depths.

Table 5.10 to Table 5.13 showed reduction factors and percentage reductions of the wall inclination relative to vertical for each of the wall models at various initial reservoir depths. Table 5.10 presented the reduction factor and percentage reduction for the smooth-surfaced wall (wall model-A) at various inclinations relative to its vertical while Table 5.11, Table 5.12 and Table 5.13 presented similar data for the semi-smoothed surface wall (wall model-B), IMACTS wall (wall model-C) and IMICTS wall (wall model-D) respectively. The reduction factor was calculated from $P_{max(slope)}/P_{max(vertical)}$ and computed for each of the slope 75^o, 60^o and 45^o. Percentage reduction relative to the vertical wall was also computed using the following expression: $((P_{max(vertical)} - P_{max(slope)})/P_{max_{(vertical)}})*100\%$.

The percentage reduction for the smooth-surfaced wall (wall model-A) at 75^{o} to its vertical was found to be 53.46% while it was 49.70% and 46.34% when the smooth-surface wall was placed at angle 60^{o} and 45^{o} respectively (Table 5.10). Similarly, for the semi-smoothed surface wall (wall model-B) the percentage reduction at 75^{o} slope relative to its vertical was 51.84% (Table 5.11). However, the percentage reductions when the wall was placed at angle 60^{o} and 45^{o} were 45.61% and 50.03% respectively (Table 5.11).

For the IMACTS wall (wall model-C) (Table 5.12), it is evident that IMACTS wall did not reduce the wave load when placed at different angles to its vertical but rather increased the wave load. This has been discussed earlier and again herein the values obtained for the percentage reduction are negative values for all the wall angles. For example, when the initial reservoir depth was 0.55m the percentage reduction obtained when the wall was positioned at angles 75^{o}, 60^{o} and 45^{o} are -30.69%, -45.9% and -205.5% respectively. Similarly, for the initial reservoir depth of 0.15m the percentage reduction obtained when the wall was placed at angles 75^{o}, 60^{o} and 45^{o} are -4.79%, -97.06% and -54.83 respectively. Similar trend was obtained with this wall model for nearly all the wave heights investigated (Table 5.12).

A critical consideration of Table 5.13 indicated that IMICTS wall (wall model-D) produced the highest wave energy dissipation amongst the other wall models particularly when placed at both angles 75^{o} and 45^{o}. For example, the average percentage reductions of IMICTS wall when placed at angle 75^{o} and 45^{o} are 52.35% and 52.48% respectively while the average percentage reduction of this wall when placed at angle 60^{o} is 47.94%.

The ratio of the maximum pressure for the inclined wall to the maximum pressure for that of the vertical wall was computed and presented as reduction factor. This parameter (reduction factor) was computed for all the wall models as shown in Table 5.10 through Table 5.13. For the smooth-surfaced wall (wall model-A), the average reduction factor at 75^{o} wall angle to its vertical is 0.47 while it was found to be 0.52 and 0.62 when the wall was placed at angle 60^{o} and 45^{o} respectively (Table 5.10).

Similarly, for the semi-smoothed surface wall (wall model-B) the average reduction factor at 75^{o} wall angle is 0.48, but found to be 0.54 and 0.50 when the wall was placed at angle 60^{o} and 45^{o} respectively (Table 5.11). The IMACTS wall (wall model-C) as explained earlier did not dissipate wave energy when placed at any other angles from its vertical hence produced negative reduction factors (Table 5.12). This implies that there was little or no wave energy

dissipation when this particular wall model was varied from it vertical to any of the angles investigated in the present study. The IMICTS wall (wall model-D) produced a reduction factor of 0.48 to its vertical when inclined at angle 75^{o} and reduction factors of 0.52 and 0.46 when placed at angles 60^{o} and 45^{o} respectively (Table 5.13).

Table 5.10: Reduction factor and percentage reduction of the wall inclination relative to the vertical for the smooth surface wall (wall model-A)

Wall angle, degree	r-depth = 0.55m		r-depth = 0.45m		r-depth = 0.35m		r-depth = 0.25m		r-depth = 0.15m		Average % reduction	Average reduction factor
	% reduction	reduction factor	% reduction	reduction factor	% reduction	reduction factor	% reduction	reduction factor	% reduction	reduction factor		
90	0	1	0	1	0	1	0	1	0	1	0	1
75	57.22	0.43	63.40	0.37	51.85	0.48	33.28	0.67	61.57	0.38	53.46	0.47
60	56.07	0.44	60.69	0.39	52.42	0.48	29.98	0.70	49.35	0.60	49.70	0.52
45	2.89*	0.97	62.04	0.38	50.73	0.49	31.17	0.69	41.41	0.59	46.34	0.62

*****unreliable – not used to compute average

Table 5.11: Reduction factor and percentage reduction of the wall inclinations relative to the vertical for the semi-smooth surface wall (wall model-B)

Wall angle, degree	r-depth = 0.55m		r-depth = 0.45m		r-depth = 0.35m		r-depth = 0.25m		r-depth = 0.15m		Average % reduction	Average reduction factor
	% reduction	reduction factor	% reduction	reduction factor	% reduction	reduction factor	% reduction	reduction factor	% reduction	reduction factor		
90	0	1	0	1	0	1	0	1	0	1	0	1
75	52.11	0.48	63.28	0.37	48.28	0.52	42.51	0.57	53.03	0.47	51.84	0.48
60	50.30	0.50	58.66	0.41	54.19	0.46	36.56	0.63	28.32	0.71	45.61	0.54
45	60.85	0.39	63.85	0.36	50.50	0.50	33.04	0.67	41.92	0.58	50.03	0.50

Table 5.12**:** Reduction factor and percentage reduction of the wall inclinations relative to the vertical for the IMACTS wall (wall model-C)

Wall angle, degree	r-depth = 0.55m		r-depth = 0.45m		r-depth = 0.35m		r-depth = 0.25m		r-depth = 0.15m		Average % reduction	Average reduction factor
	% reduction	reduction factor	% reduction	reduction factor	% reduction	reduction factor	% reduction	reduction factor	% reduction	reduction factor		
90	0	1	0	1	0	1	0	1	0	1	0	1
75	-32.69	1.54	-13.16	1.13	-29.83	1.30	-75.06	1.74	-4.79	1.05	-30.91	1.35
60	-45.90	1.46	-14.35	1.14	-44.36	1.44	-70.18	1.70	-97.06	1.97	-54.37	1.54
45	-205.5	3.06	0.50	0.99	-40.51	1.41	-90.73	1.91	-54.83	1.55	-78.21	1.78

Table 5.13: Reduction factor and percentage reduction of the wall inclinations relative to the vertical for the IMICTS wall (wall model-D)

Wall angle, degree	r-depth = 0.55m		r-depth = 0.45m		r-depth = 0.35m		r-depth = 0.25m		r-depth = 0.15m		Average % reduction	Average reduction factor
	% reduction	reduction factor	% reduction	reduction factor	% reduction	reduction factor	% reduction	reduction factor	% reduction	reduction factor		
90	0	1	0	1	0	1	0	1	0	1	0	1
75	51.16	0.49	64.05	0.36	57.19	0.43	34.87	0.65	54.5	0.46	52.35	0.48
60	52.14	0.49	57.02	0.43	52.55	0.47	36.76	0.63	41.23	0.59	47.94	0.52
45	64.9	0.35	63.27	0.38	51.76	0.48	36.49	0.63	45.97	0.54	52.48	0.46

5.6.4 *Duration (rising time) of Maximum Impact Pressure for the Sloping Walls*

In section 5.4.2 the pressure-time histories of impact pressure for the smooth-surface wall (wall model-A) when placed vertically was briefly discussed. Section 5.5.2 was also designated for the results of the duration of the maximum impact pressure with respect to wave height for each of the six transducers for the same wall model. This section analyses the duration of the maximum pressure with respect to wave height for the same wall (wall model-A) when placed at various orientations from its vertical. This is to reveal the effect of wall orientation on the duration of the maximum impact pressure on the wall. Table 5.14 showed the rising time (duration) of maximum impact pressure for this wall (wall model-A) at various wall angles investigated. Table 5.14 indicated that the maximum impact pressure duration was between 1ms and 3ms for the wall angles when the initial reservoir depths were 0.45m and 0.35m. The durations of the maximum impact pressure when the initial reservoir depths are 0.15m and 0.25m were also between 2ms and 3ms for all the wall angles. However, for the initial reservoir depth of 0.55m the duration of the maximum impact pressure ranged between 2ms and 5ms.

Table 5.14: Rising time (duration) of the maximum impact pressure for wall model-A at different wall angles

r-depth (d_o), m	90 degree		75 degree		60 degree		45 degree	
	Max impact pressure, kPa	Duration of max pressure, msec	Max impact pressure, kPa	Duration of max pressure, msec	Max impact pressure, kPa	Duration of max pressure, msec	Max impact pressure, kPa	Duration of max pressure, msec
0.55	9.522115	5	4.073415	4	4.182891	3	9.246618	2
0.45	6.892416	3	2.522509	1	2.70953	1	2.616477	2
0.35	3.959378	3	1.906572	1	1.8839	1	1.950963	2
0.25	1.993376	3	1.330072	2	1.395821	2	1.372058	3
0.15	1.103886	2	0.424224	2	0.65686	3	0.646771	2

5.6.5 *Location of the maximum impact pressure on the sloping walls as compared with the vertical wall*

The vertical distribution of maximum impact pressure on vertical wall for the smooth surface wall model had been presented earlier (see section 5.4.3). But, only a few studies have reported the vertical distribution of maximum impact pressure on sloping walls (1982, Kirkgoz, 1978) . However, in the present study the location of the maximum impact pressure for wall angles 90^o, 75^o, 60^o and 45^o have been investigated against various floodwater wave heights.

Figure 5.36 and Figure 5.37 showed the vertical distributions of maximum impact pressures obtained for the smooth–surface wall and the semi-smooth surface wall at various wall angles. Figure 5.36 presented the vertical distribution of the maximum impact pressure for the smooth-surfaced wall (wall model-A) at various wall orientations for the initial reservoir depth of 0.45m while Figure 5.37 depicted the vertical distributions of the maximum impact pressure for the semi-smoothed surface wall (wall model-B) at various wall orientations for the reservoir depth of 0.55m.

It can be deduced from the two figures that the most frequent location of maximum impact pressure is around the toe of the wall (at transducer 1 position which is located at about 2% of the wall height) for most of the wall angles. A critical examination of Figure 5.36 and Figure 5.37 revealed that for vertical wall (wall angle 90^o), in general the occurrence of maximum pressure was evident at the toe of the wall. However for the sloping walls particularly for wall angles 75^o and 60^o the location of the maximum pressure though occurred at the toe of the wall but not as evident as when the wall was vertical. This is because the highest pressure occasionally occurred at the upper part of the wall for the sloping walls. Moreover, the differences in the magnitude of the pressure obtained at the base of the wall and the upper part of the wall for the sloping walls are not as significant as for the vertical wall (Figure 5.36 and Figure 5.37). Placing the smooth surface wall at angle 45^o (Figure 5.36) showed trend that is slightly similar to the vertical wall but different from the results obtained for the other wall slopes. However, for the semi-smooth surface wall (Figure 5.37) the location of maximum impact pressure for the sloping walls (75^o, 60^o and 45^o) also followed the trend obtained for the sloping forms for the smooth-surface wall.

Figure 5.36 and Figure 5.37 indicates that wall orientation influenced the location of the highest dynamic pressure very slightly and that significant parts of the wall surface experienced relatively high dynamic pressure when in sloping form. As stated earlier in section 5.5.1, the highest dynamic pressure for each of the initial reservoir depth was obtained from the transducer with the highest reading regardless of it position. For the smooth-surface wall (wall model-A) it has been indicated that for all the initial reservoir depths, the highest dynamic pressure arose from the transducer at the base of the wall (transducer 1 – see Table 5.6). However, for the same wall model at sloping forms (75^o, 60^o and 45^o) the highest dynamic pressures were still obtained from transducer 1 except on few occasions where the highest readings were obtained from the upper transducers. Details of the transducer number (or position) that recorded the highest dynamic pressure values for each of the initial reservoir depths for all the wall models investigated are given in appendix 4.

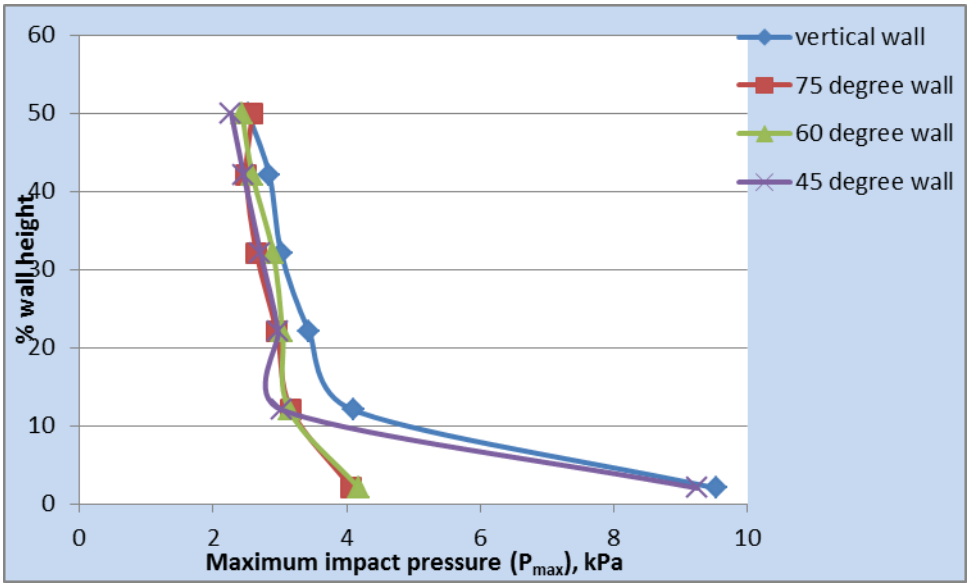

Figure 5.36: Vertical distribution of maximum impact pressure for the smoothed surface wall (wall model-A) at various wall angles (for r-depth = 0.45m)

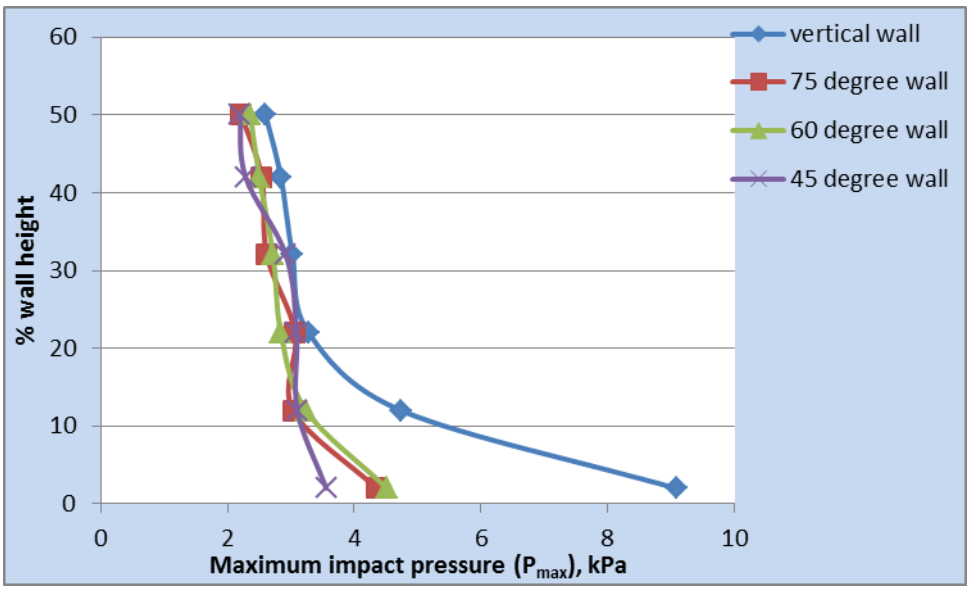

Figure 5.37: Vertical distribution of maximum impact pressure for the semi-smooth surface wall (wall model-B) at various wall angles (for r-depth = 0.55m)

5.7 The Effects of Wall Surfaces on the Impact Pressure

Various investigators have studied the effect of seawall surface on the dissipation of the energy of the wave. Some studied these effects only on the plane or smooth wall surface while others investigated the effect on different types or models of rough surfaces (see section 2). Neelamani et al. (1999) and Neelamani and Sandhya (2005) used wall surface roughness designs termed serrated and dentated surfaces and compared these designs with the plane or smooth surface. The general result reported by Neelamani and Sandhya (2005) was that serrated surface seawall was found to be about 20-40% better than plane seawall in reducing wave impact. A number of previous investigators are in agreement with this view (see chapter 2).

The present study has investigated the effect of various surfaces on the dissipation of energy of the flood wave. Thus, this section meant to analyse the data obtained in terms of impact pressures for various surfaces investigated to elucidate the effect of these particular surfaces on the dissipation of the energy of the floodwater wave which may further broaden our understanding on this subject matter.

5.7.1 *Pressure-time histories of the rough surface walls as compared with the smooth-surface wall*

Figure 5.38 through Figure 5.41 shows the histories of impact pressure for all the wall models at various orientations. Figure 5.38 presented the case for all the wall surfaces when vertically placed while Figure 5.39, Figure 5.40 and Figure 5.41 displayed the pressure-time histories of all the wall surfaces when placed at 75^o, 60^o and 45^o respectively.

A critical examination of Figure 5.38 through 5.41 showed that the initial impact on the smooth-surface wall was marginally higher than the rest of the wall models. This is particularly evident for most of the wall orientations. In Figure 5.38 through Figure 5.41, generally the second and subsequent peaks which are the impact after the waves have been reflected by the wall were lower than the first peak. However, certain impacts showed some unusual peaks for the IMACTS wall (wall model-C) both at vertical indicated in Figure 5.38(a) and at angle 60^o shown in Figure 5.40(a), also for the smooth surface wall at angle 45^o shown in Figure 5.41(a). The reason for the overshoot of the actual impacts therein is due to the issues explained earlier.

However, for each case the drawn-out of the actual signals with overshooting false signals truncated are indicated in the respective Figure 5.38(b), Figure 5.40(b) and Figure 5.41(b).

For the semi-smoothed surface wall (wall model-B) and the IMICTS wall (wall model-D) in vertical form (Figure 5.38) there was a significant reduction in the heights of the second and subsequent peaks compared to the first peak and rapidly tends towards a constant value. This indicates that the semi-smoothed surface and IMICTS walls though dissipated a certain amount of the energy of the flood waves but caused a substantial wave reflection which may be partly due to the present of planar/smoothed part in wall model-B and the softness (low coasive) of the geo-grid material used for wall model-D surface. The wall models performed in different manners in terms of wave reflection when in sloping forms (Figure 5.49 through Figure 5.41).

Besides, it can be seen in Figure 5.38 through Figure 5.41 that IMACTS wall (wall model-C) behaved almost in the same manner at angles 90^o, 75^o and 60^o (Figure 5.38, Figure 5.39 and Figure 5.40 respectively) except at angle 45^o (Figure 5.41). Again, it can be seen that the smooth surface wall also performed virtually in similar way when placed at angles 90^o, 75^o and 60^o (Figure 5.38, Figure 5.39 and Figure 5.40 respectively) except at angle 45^o (Figure 5.41). This could imply that placing the defence wall against floodwater wave at angle 45^o may not be so practical in the real world as the behaviour of all the surfaces investigated in the present study at this particular wall orientaion was very unusual and unexpected. This result was in agreement with what was obtained earlier in the analysis of the influence of slope on the wave impact pressure. More importantly, the IMACTS wall dissipated a greater amount of floodwave energy very rapidly than the other wall models in vertical form.

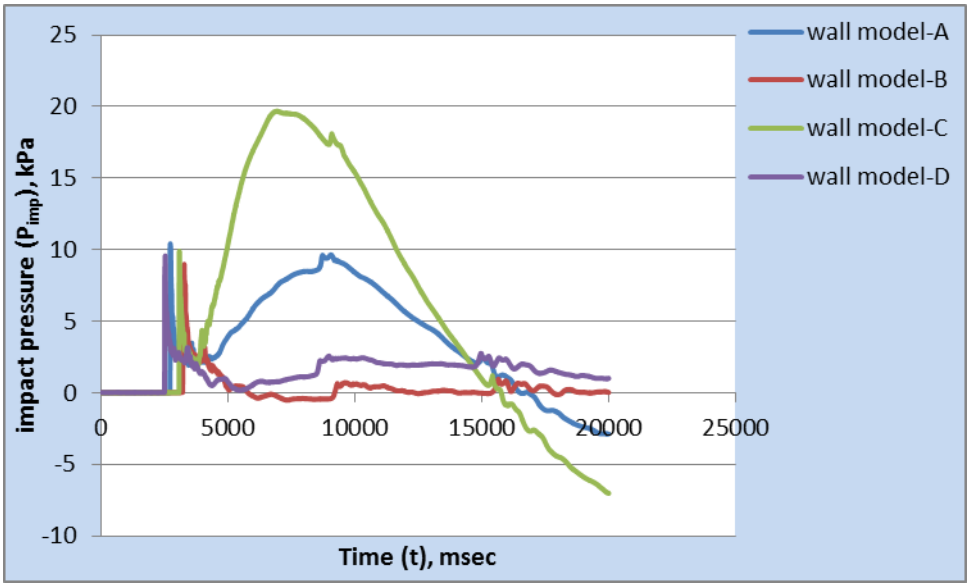

Figure 5.38 (a)

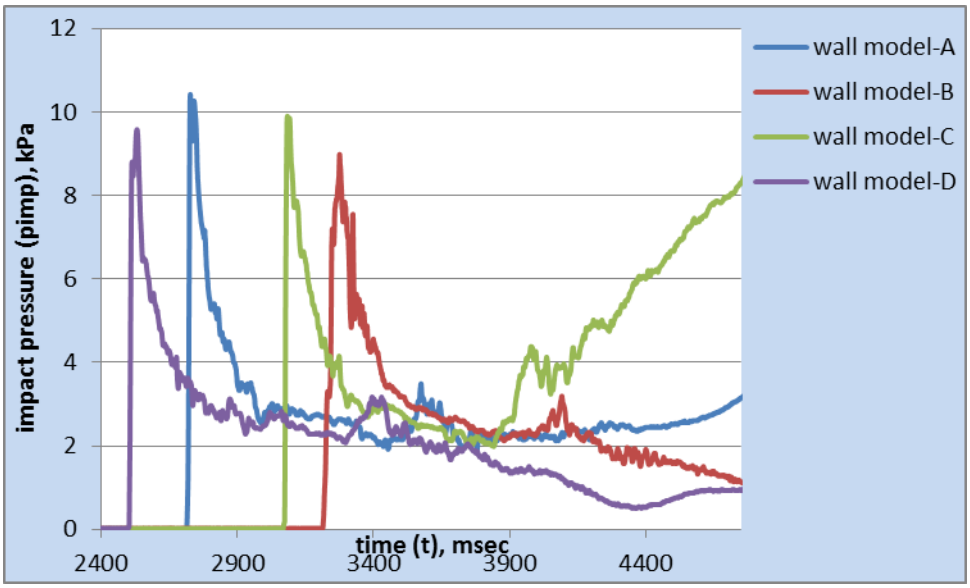

Figure 5.38 (b)

Figure 5.38: Comparison of pressure-time histories of various wall surfaces in vertical orientation, r-depth = 0.55m; (a) with false signal (b) without false signal

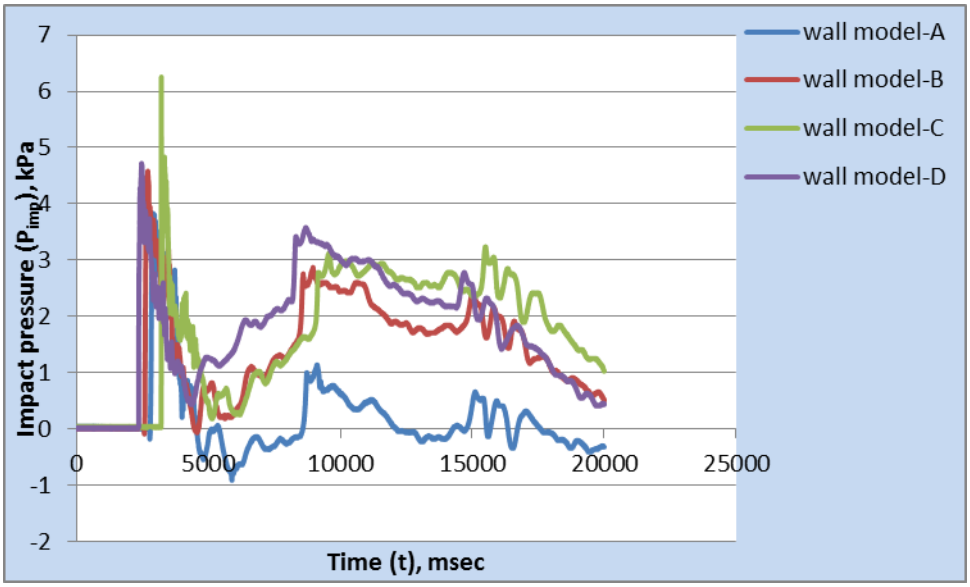

Figure 5.39: Comparison of pressure-time histories of various wall surfaces at 75 degree slope (r-depth=0.55m)

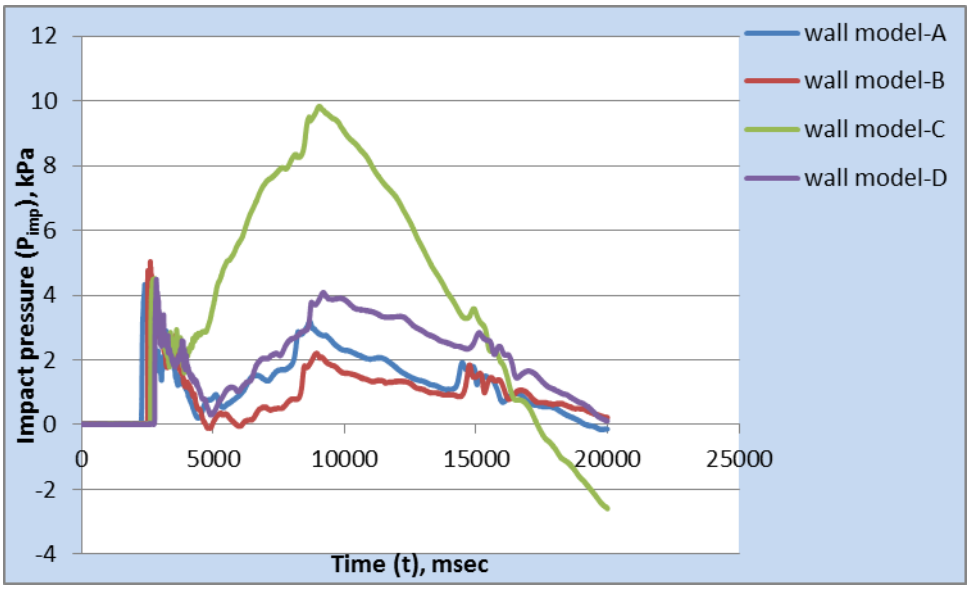

Figure 5.40 (a)

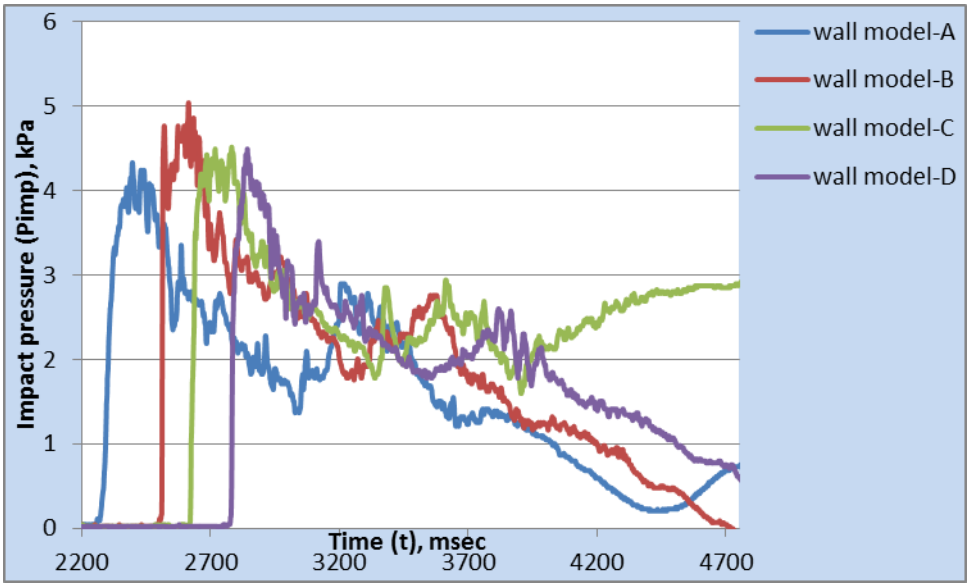

Figure 5.40 (b)

Figure 5.40: Comparison of pressure-time histories of various wall surfaces at 60 degree slope, r-depth=0.55m; (a) with false signal (b) without false signal

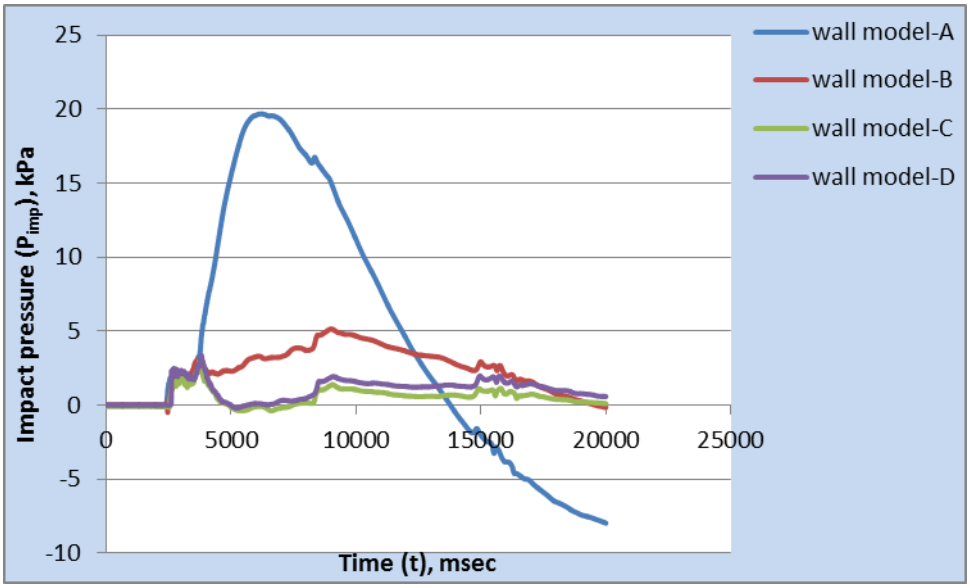

Figure 5.41 (a)

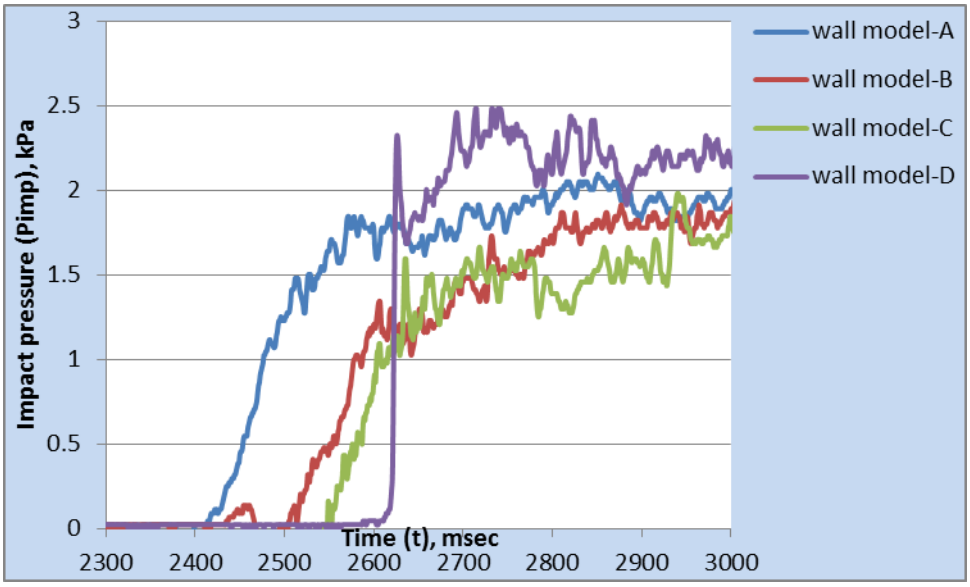

Figure 5.41 (b)

Figure 5.41: Comparison of pressure-time histories of various wall surfaces at 45 degree slope, r-depth=0.55m; (a) with false signal (b) without false signal

5.7.2 *Influence of Rough Surface on the Maximum Impact Pressure for varying Initial Reservoir Depths*

Table 5.15 is a summary of the results of the maximum impact pressures for all the wall surfaces investigated in the present study. Table 5.15 allows direct evaluation and assessment of the wall surfaces effect when other variables such as the wave height as well as the wall angle vary. Table 5.15 was again used in section 5.7.4 for prompt computation of percentage load reduction as well as reduction factor for each of the rough-surfaced wall models relative to the smooth-surfaced wall. Thus, the performance of the rough surfaces in terms of the magnitude of impact pressure when the initial reservoir depth as well as wall orientation were varied is analysed and represented in Figures 5.42 through Figure 5.45.

Table 5.15: Summary results of the maximum impact pressures for all the wall models at various initial reservoir depths and wall orientations

	Vertical wall (90 degree)				Wall angle 75 degree			
r-depth d_o, m	max impact pressure (model-A), kPa	max impact pressure (model-B), kPa	max impact pressure (model-C), kPa	max impact pressure (model-D), kPa	max impact pressure (model-A), kPa	max impact pressure (model-B), kPa	max impact pressure (model-C), kPa	max impact pressure (model-D), kPa
0.55	9.522115	9.086493	3.046177	9.254127	4.073415	4.351666	4.081995	4.519941
0.45	6.892416	7.129614	2.505046	7.143298	2.522509	2.618300	2.834655	2.568124
0.35	3.959378	4.137276	1.342836	4.141838	1.906572	2.139615	1.743352	1.774425
0.25	1.993376	2.070921	0.684003	1.975130	1.330072	1.190554	1.190554	1.286345
0.15	1.103886	0.903180	0.291665	0.962479	0.424224	0.424224	0.305625	0.437908

Wall angle 60 degree				Wall angle 45 degree			
max impact pressure (model-A), kPa	max impact pressure (model-B), kPa	max impact pressure (model-C), kPa	max impact pressure (model-D), kPa	max impact pressure (model-A), kPa	max impact pressure (model-B), kPa	max impact pressure (model-C), kPa	max impact pressure (model-D), kPa
4.182891	4.515880	4.444240	4.429212	9.246618	3.557555	9.306123	3.248101
2.709530	2.947585	2.864621	3.069888	2.616477	2.577247	2.492506	2.623518
1.883900	1.895268	1.938467	1.965149	1.950963	2.048114	1.886867	1.997938
1.395821	1.313714	1.164043	1.248995	1.372058	1.386698	1.304591	1.254415
0.656860	0.647393	0.574753	0.565630	0.646771	0.524576	0.451592	0.520015

Figure 5.42 through Figure 5.45 showed the variation of maximum impact pressure with initial reservoir depth for the four wall models at various orientations. Figure 5.42 presented these variations when each of the walls was vertically positioned while Figure 5.43, Figure 5.44 and Figure 5.45 depicted the variations when each of the walls was placed at angles 75^o, 60^o and 45^o respectively.

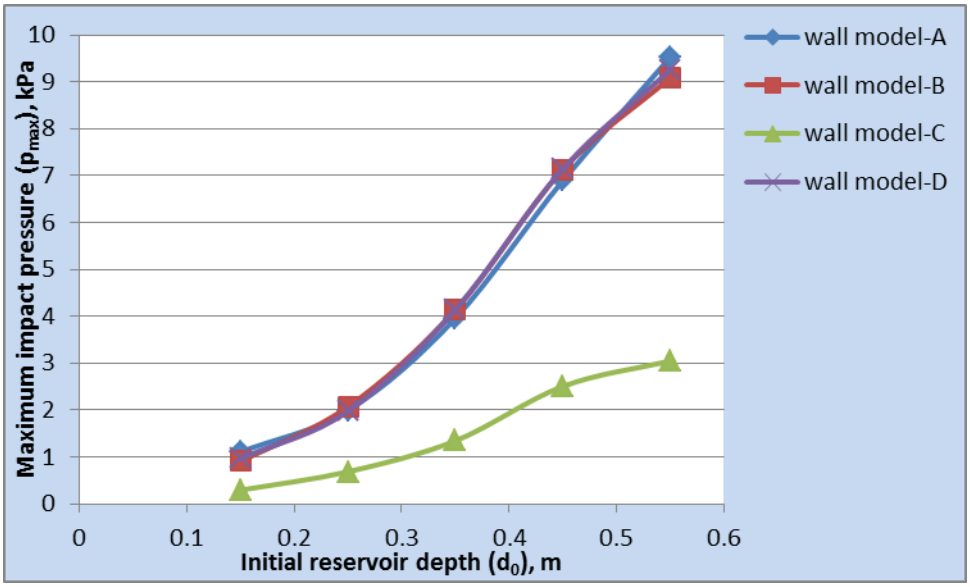

Figure 5.42: Variation of maximum impact pressure with initial reservoir depth showing the effect of the wall surfaces (wall angle 90^o)

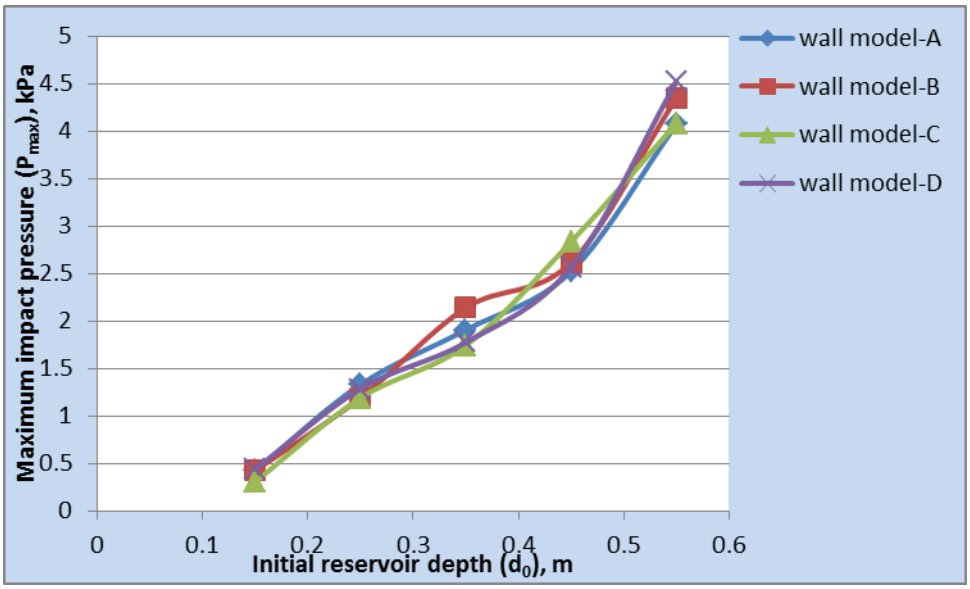

Figure 5.43: Variation of maximum impact pressure with initial reservoir depth showing the effect of the wall surfaces (wall angle 75^o)

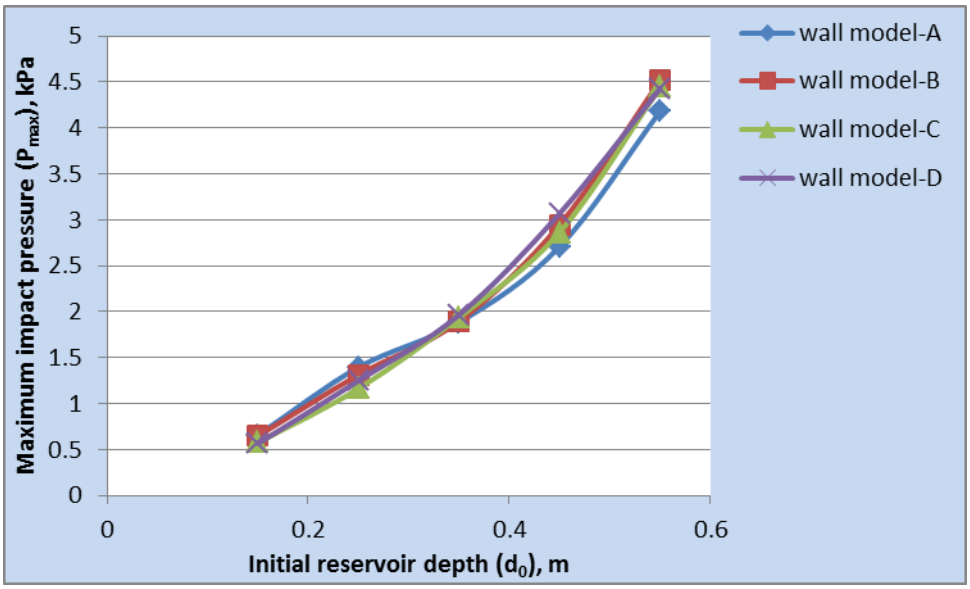

Figure 5.44: Variation of maximum impact pressure with initial reservoir depth showing the effect of wall surfaces (wall angle 60^o)

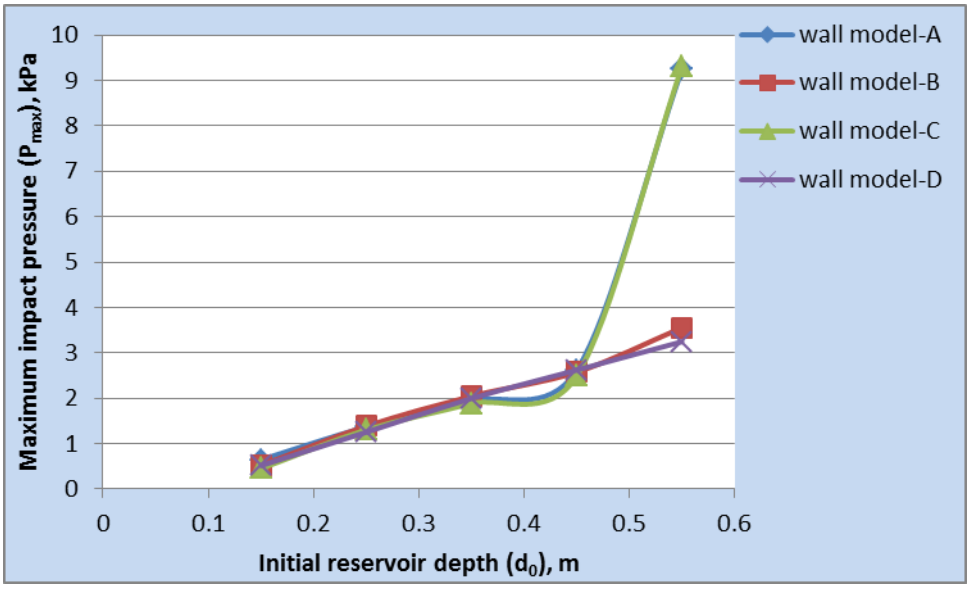

Figure 5.45: Variation of maximum impact pressure with initial reservoir depth showing the effect of seawall surfaces (wall angle 45^o)

Irrespective of the wall angle (Figure 5.42 through Figure 5.45) all the wall surfaces showed similar patterns in terms of variation of the magnitude of maximum impact pressure with respect to changes in the initial reservoir depth. In general for all the wall models investigated in the present study, increase in the initial reservoir depth causes an increase in the impact pressure on the walls. However, for the vertically inclined walls (Figure 5.42) IMACTS wall showed a remarkably lower magnitude of maximum impact compared with other wall models whereas for the sloping walls the reduction in the magnitude of the maximum impact pressure amongst all the wall models is marginal. This is anticipated, because for a constant wave period and higher degree of wall surface roughness, when the incident wave height increases, then the wave becomes spilling type (Neelamani et al., 1999) which results in an increase of energy dissipation thereby reducing the impact load on the wall. The wave energy dissipation increases due to significant spilling of waves. The harder the coarseness or abrasiveness of a surface the higher the roughness as IMACTS wall appeared to be the hardest of all the surfaces.

5.7.3 *Wall Surface Effect on Wave Height at Impact for varying Initial Reservoir Depth*

Table 5.16 showed the data obtained for the wave heights at impact (H_{imp}) at various initial reservoir depths (d_o) for all the wall surfaces at various orientations. Figure 5.46 presented the effects of each of the wall surface models on the wave height at impact as the initial reservoir depth varied for vertically inclined walls while Figures 5.47 through 5.49 showed these effects when the walls were placed at angle 75^o, 60^o and 45^o. In general, from Figure 5.46 through Figure 5.49 it could be seen that an increase in the initial reservoir depth causes an increase in the elevation of the flood wave produced on impacting the wall. However, the wall models showed little or no difference in terms of the wave height generated on impact irrespective of the wall angle (Figure 5.46 through Figure 5.49).

Table 5.16: Variations of wave height produced at impact with initial reservoir depth for all the wall models

	Wave height at impact , H_{imp} (90 degree wall)				Wave height at impact, H_{imp} (75 degree wall)			
r-depth do, m	model-A, m	model-B, m	model-C, m	model-D, m	model-A, m	model-B, m	model-C, m	model-D, m
0.55	0.440181	0.457996	0.459293	0.416779	0.389476	0.404570	0.398880	0.415628
0.45	0.315818	0.314962	0.314400	0.317132	0.274099	0.311012	0.292796	0.287402
0.35	0.210825	0.238049	0.217375	0.246658	0.216694	0.212079	0.223615	0.219391
0.25	0.165875	0.164646	0.169310	0.167694	0.177433	0.177586	0.178265	0.154777
0.15	0.097248	0.100939	0.096131	0.095816	0.096085	0.097608	0.099164	0.103010

	Wave height at impact, H_{imp} (60 degree wall)				Wave height at impact , H_{imp}(45 degree wall)			
r-depth do, m	model-A, m	model-B, m	model-C, m	model-D, m	model-A, m	model-B, m	model-C, m	model-D, m
0.55	0.339130	0.388906	0.368497	0.349830	0.365908	0.396223	0.361845	0.306700
0.45	0.235644	0.308479	0.303999	0.260393	0.294930	0.339731	0.301685	0.271587
0.35	0.202529	0.223823	0.303999	0.203555	0.213399	0.237041	0.232596	0.190111
0.25	0.158851	0.199701	0.170150	0.160718	0.183808	0.192451	0.162806	0.162162
0.15	0.094995	0.103660	0.101138	0.098034	0.104397	0.107032	0.104759	0.092069

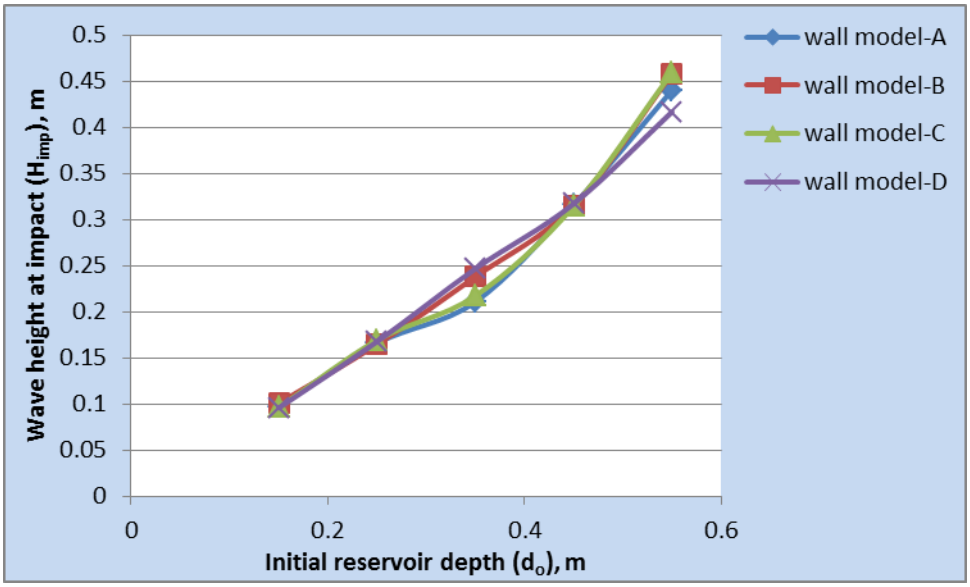

Figure 5.46**:** Effect of change in initial reservoir depth on wave height produced at impact showing the influence of the wall surfaces at vertical orientation

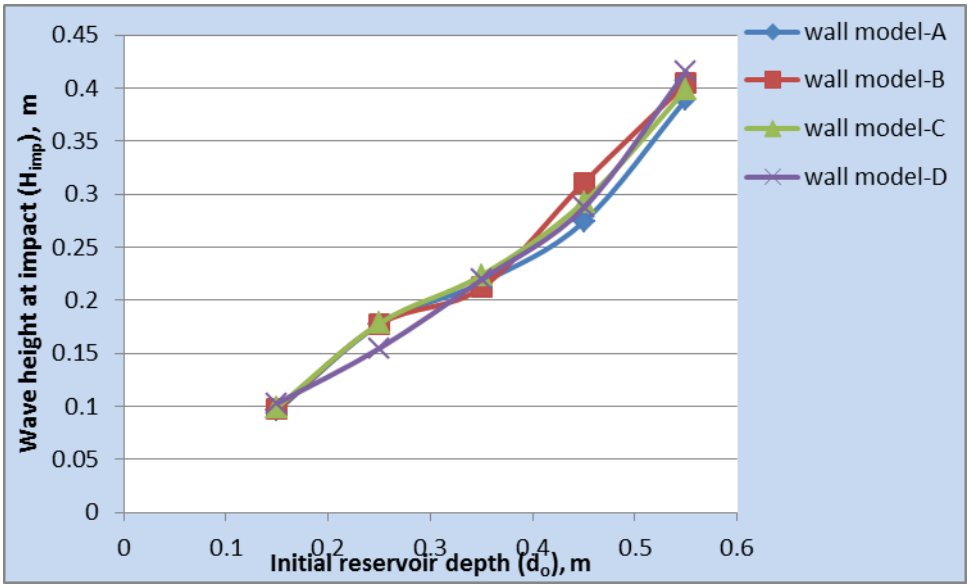

Figure 5.47: Effect of change in initial reservoir depth on wave height produced at impact showing the influence of the wall surfaces placed at angle 75^o

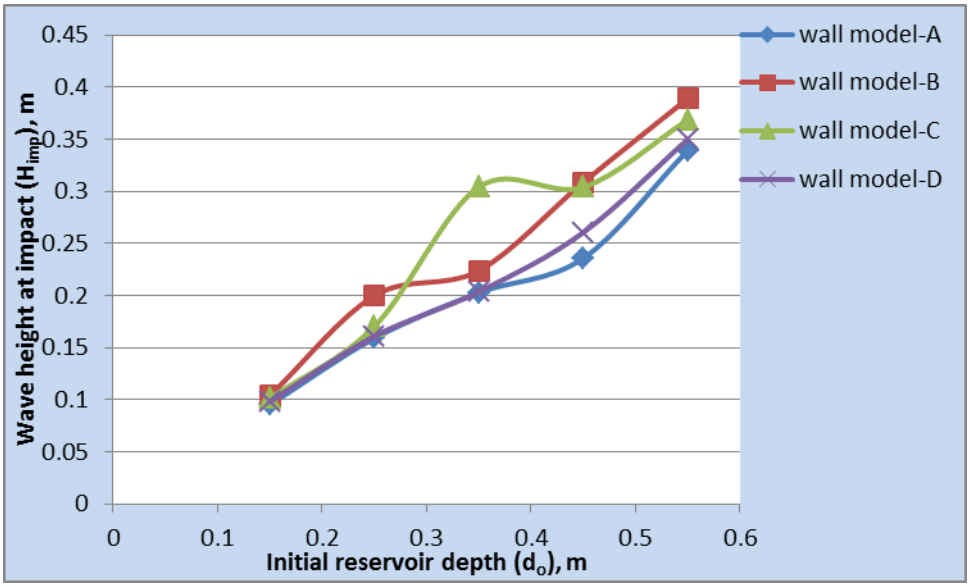

Figure 5.48: Effect of change in initial reservoir depth on wave height produced at impact showing the influence of the wall surfaces placed at angle 60^o

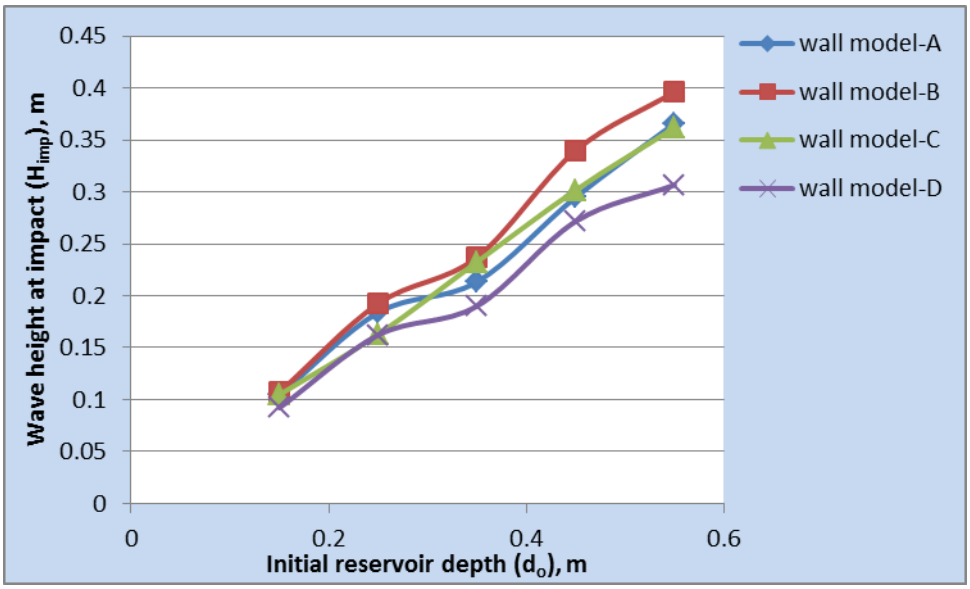

Figure 5.49: Effect of change in initial reservoir depth on wave height produced at impact showing the influence of the wall surfaces placed at angle 45^o

5.7.4 *Wave Energy Dissipating Ability of the Wall Surfaces*

Table 5.15 (discussed earlier in section 5.7.2) presented the magnitude of maximum impact pressure for all the wall surfaces at various initial reservoir depths for each wall angles. Table 5.15 however, allows prompt computation of percentage reduction and reduction factor for each of the rough surfaces relative to the smooth-surface wall for each wall angle. Percentage reduction was calculated from $(P_{max(smooth\text{-}surface)} - P_{max(rough\text{-}surface)})/P_{max_{(smooth\text{-}surface)}}*100\%$ while the reduction factor was calculated from $P_{max(rough\text{-}surface)}/P_{max(smooth\text{-}surface)}$. These parameters were computed for each of the initial reservoir depths and presented in Table 5.17 through Table 5.20.

The average percentage reduction for the semi-smoothed surface wall (wall model-B) relative to the smooth-surface wall (wall model-A) when placed vertically is 2.18% (Table 5.17) while that of the IMACTS wall (wall model-C) and IMICTS wall (wall model-D) relative to the smooth-surface wall are 67.4% and 1.66% respectively. When the seawalls are placed at angle 75^o, the average percentage reductions of the semi-smoothed surface wall, IMACTS wall and IMICTS wall to that of the smooth-surface wall are -2.47%, 6.89% and -1.16% respectively (Table 5.18). For the wall models at 60^o, the average percentage reduction for the semi-smoothed surface (wall model-B) to its vertical is -2.00% while that of IMACTS (wall model-C) and IMICTS (wall model-D) surfaces are 2.85% and 0.18% respectively (Table 5.19). When the wall models were placed at angle 45^o, the average percentage reduction for the semi-smoothed surface (wall model-B) to its vertical is 3.58% while IMACTS (wall model-C) and IMICTS (wall model-D) produced percentage reductions of 8.5% and 6.37% respectively (Table 5.20).

Table 5.17: Load reduction factor and % reduction for the rough-surfaced wall models relative to the smooth-surfaced wall in vertical form

	r-depth=0.55m		r-depth=0.45m		r-depth=0.35m		r-depth=0.25m		r-depth=0.15m			
Wall model	% reduction	Reduction factor	% reduction	Reduction factor	% reduction	Reduction factor	% reduction	Reduction factor	% reduction	Reduction factor	Average % reduction	Average reduction factor
model-A	0	1	0	1	0	1	0	1	0	1	0	1
model-B	4.57	0.95	-3.44	1.03	-4.49	1.04	-3.89	1.03	18.18	0.82	2.18	0.97
model-C	68.01	0.32	63.65	0.36	66.08	0.34	65.69	0.34	73.58	0.26	67.4	0.32
model-D	2.81	0.97	-3.64	1.04	-4.61	1.05	0.92	0.99	12.81	0.87	1.66	0.98

Table 5.18: Load reduction factor and % reduction for the rough-surfaced wall models relative to the smooth-surfaced wall at angle 75^{o}

	r-depth=0.55m		r-depth=0.45m		r-depth=0.35m		r-depth=0.25m		r-depth=0.15m			
Wall model	% reduction	Reduction factor	% reduction	Reduction factor	% reduction	Reduction factor	% reduction	Reduction factor	% reduction	Reduction factor	Average % reduction	Average reduction factor
model-A	0	1	0	1	0	1	0	1	0	1	0	1
model-B	-6.83	1.07	-3.80	1.04	-12.22	1.12	10.49	0.9	0.00	1.00	-2.47	1.03
model-C	-0.21	1.00	-12.37	1.12	8.56	0.89	10.49	0.9	27.96	0.72	6.89	0.93
model-D	-10.94	1.11	-1.81	1.02	6.93	0.93	3.29	0.97	-3.23	1.03	-1.16	1.01

Table 5.19: Load reduction factor and % reduction for the rough-surfaced wall models relative to the smooth-surfaced wall at angle 60^{o}

	r-depth=0.55m		r-depth=0.45m		r-depth=0.35m		r-depth=0.25m		r-depth=0.15m			
Wall model	% reduction	Reduction factor	% reduction	Reduction factor	% reduction	Reduction factor	% reduction	Reduction factor	% reduction	Reduction factor	Average % reduction	Average reduction factor
model-A	0	1	0	1	0	1	0	1	0	1	0	1
model-B	-7.96	1.08	-8.79	1.09	-0.60	1.00	5.88	0.94	1.44	0.99	-2.00	1.02
model-C	-6.25	1.06	-5.72	1.06	-2.90	1.03	16.61	0.83	12.50	0.88	2.85	0.97
model-D	-5.89	1.06	-13.30	1.13	-4.31	1.04	10.52	0.89	13.89	0.86	0.18	1.00

Table 5.20: Load reduction factor and percentage reduction for the rough-surfaced wall models relative to the smooth-surfaced wall at angle 45^{o}

	r-depth=0.55m		r-depth=0.45m		r-depth=0.35m		r-depth=0.25m		r-depth=0.15m			
Wall model	% reduction	Reduction factor	% reduction	Reduction factor	% reduction	Reduction factor	% reduction	Reduction factor	% reduction	Reduction factor	Average % reduction	Average reduction factor
model-A	0	1	0	1	0	1	0	1	0	1	0	1
model-B	61.53	0.39	1.50	0.99	-4.97	1.05	-1.07	1.01	18.89	0.81	3.58	0.97
model-C	-0.64	1.00	4.74	0.95	3.29	0.98	4.92	0.95	30.18	0.70	8.50	0.92
model-D	64.87	0.35	-0.27	1.00	-2.41	1.02	8.57	0.91	19.60	0.80	6.37	0.93

5.8 Dimensionless representation of maximum impact pressure and application of similitude criterion

The following sections apply the theory of similitude to compare the model teat results obtained in this investigation with the work of other using various scales.

5.8.1 *Dimensionless representation of maximum impact pressure*

The results of the maximum impact pressure on the wall, P_{max}, produced with change in initial reservoir depth, d_o are presented non-dimensionally in Figure 5.50. The dimensionless variables are $\frac{P_{max}-P_o}{P_o}$ and d_o/H_{inc} (see section 4.3), where d_o is the initial reservoir depth and H_{inc} is the water level immediately after gate release (WP1), P_{max} is the measured maximum pressure and P_o is computed from $\rho g H_o$ (H_o is taken as H_{inc} in the study), ρ is the density of the water and g is the gravitational acceleration. However, it was found in this study that the wave height at impact (H_{imp}) was affected considerably by the presence of the wall. In particular the run-up height at the wall tends to decrease considerably with increasing wall angle. Therefore, instead of using breaker height (H_{imp}) to normalise the maximum impact pressure at the wall, the wave height measured just immediately the gate was released with wave probe 1 (WP1), referred to in the study as incident wave height (H_{inc}), was used to non-dimensionalise the maximum impact pressures.

Hence, the dimensionless maximum pressure was then obtained from $\frac{P_{max}-\rho g H_{inc}}{\rho g H_{inc}}$ while the initial reservoir depth d_o, was consequently normalised by the incident wave height, H_{inc}. These parameters were obtained for each of the wall surfaces for various initial reservoir depths, d_o. Thus, Figure 5.50 presented the dimensionless representation of the results for each of the wall surfaces. From Figure 5.50 it is apparent that two parameters influence the maximum impact pressure on the wall, P_{max}, as well as the wave height just before the impact on the wall, H_{imp}. These two parameters are the initial reservoir depth, d_o, and the wall surface. Following the previous results however, it is interesting to point out in Figure 5.50 that the IMACTS wall indicated clearly the most load reduction as compared with other surfaces. Also, the load reduction between other wall surfaces which was earlier found to be marginal was again maintained in this circumstance. Thus, the dimensionless representation of the maximum impact pressure used in the present study is appropriate and may be good for practical purposes.

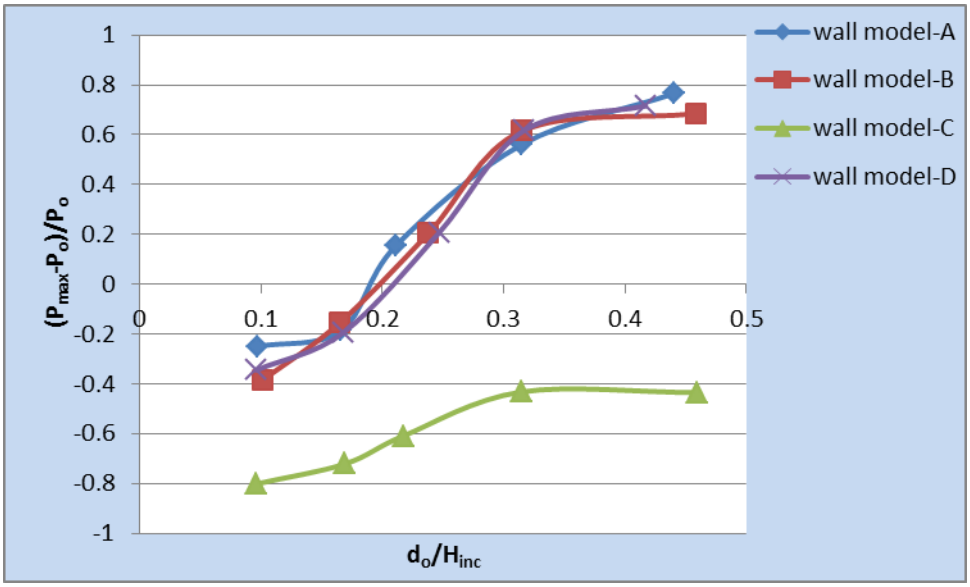

Figure 5.50: Dimensionless maximum impact pressure variations against dimensionless initial reservoir depth for various wall surfaces in vertical form

5.8.2 *Application of Similitude Criterion*

Traditionally, scaled physical models have been used extensively in the design of major hydraulic engineering works, notably river engineering schemes, estuary schemes, hydraulic structures, coastal engineering schemes and port and harbour developments. Many physical models used in coastal engineering require investigation of wind and swell waves (e.g. short waves) and associate effects. Short-wave hydrodynamic model experiments can be conducted in either a wave flume or a wave tank. In a wave flume or a wave tank, two-dimensional effects can be studied including stability of breakwater amour units, overtopping rates at coastal structures, wave reflection and transmission, wave forces on coastal structures and wave energy extraction devices.

The material and the scale of the model test rig used in the present investigation were chosen to allow the effects of friction to be ignored due to the smooth surfaces, thus leaving the gravitational forces to be correctly modelled. The fact that the predominant force in the present situation is gravity force, the Froude number (Fr) is the dimensionless parameter that is of fundamental importance. Hence, a Froudian scaled model is used. According to Hughes (1993), although the similitude arguments (discussed in section 4.3.2) may be used to justify the use of a model to prototype application, it can however, also be shown that the use of a Froudian scaled model satisfies all terms in the Navier-Stokes equations. Hence, this enables the

modelling of refraction, shoaling, diffraction and reflection, surf zone processes including turbulent energy dissipation, wave-induced currents and tidal currents.

For comparison, the results of the present investigation in terms of maximum impact pressures were scaled up to full size field and experimental data available. In most of the full scale and many of the experimental investigations reviewed, the main objective has been the measurement of wave impact pressures. However, it is vital to note that in many cases the equally important wave characteristics (height, celerity, period and length) have been neglected. It is therefore makes it difficult to relate these wave pressures between models as well as to the sea state which produced them. Another major problem apparent in most investigations is that authors do not clearly define how or where the wave parameters were measured, so it is often not clear whether the wave heights and celerities were measured in deep or shoaling water. For these reasons it is difficult to be sure, when comparing data from different investigations, that like is being compared with like. However, efforts are being made to carefully relate those that are comparable and hence a number of representative illustrations are therefore given below:

(a) Comparison with Neelamani and Sandhya (2005) Experimental Data

By using the equation and the data provided by Neelamani and Sandhya (2005) as follow:

$$\frac{P_{max}}{\rho g H_s} = 1.03 \ldots\ldots\ldots\ldots\ldots\ldots\ldots\ldots\ldots\ldots\ldots\ldots\ldots\ldots\ldots\ldots\ldots\ldots\ldots\ldots\ldots\ldots\ldots\ldots\ldots\ldots\ldots\ldots\ldots\ldots 5.10$$

Where P_{max} is the maximum impact pressure, ρ = density of the water, g = acceleration due to gravity and H_s = significant wave height. H_s is given as $\frac{H_s}{d}$ = 0.14 and d is the initial water depth in the channel = 0.07m

Using equation 5.10:

$$P_{max} = 1.03 \times 1000 \times 9.81 \times 0.0098$$

$$= \mathbf{99.02\ Pa}$$

Using experimental test data for wall model-A in vertical form, the following data could be deduced: P_{max} = 9522.11 Pa for the wave height of 0.55m

By scaling-up using equation 3.40 gives:

$$p_P = 9522.11 \times \left(\frac{0.0098}{0.55}\right)$$

= **169.66 Pa**

(b) Comparison with Kato et al. (2004) Experimental Data

From Kato et al (2004), the following experimental data were deduced:

For the seawall placed at the toe of the seaward slope, maximum pressure for the wave height of 1.1 m above the toe of the seawall is given as **39.20 kPa**

Similarly, using experimental test data for wall model-A in vertical form, P_{max} = 9522.11 Pa for the wave height of 0.55m

By scaling-up using equation 3.40 gives:

$$p_P = 9522.11 \times \left(\frac{1.1}{0.55}\right)$$

= 19044.22 Pa

= **19.04 kPa**

(c) Comparison with Neelamani et al. (1999) Experimental Data

By using the equation and the data provided by Neelamani et al. (1999) as follow:

$$\frac{P_{maxswl}}{\rho g H_i} = 1 \ldots\ldots\ldots\ldots\ldots\ldots\ldots\ldots\ldots\ldots\ldots\ldots\ldots\ldots\ldots\ldots\ldots\ldots\ldots\ldots\ldots\ldots\ldots\ldots\ldots\ldots\ldots\ldots..5.11$$

Where P_{maxswl} is the maximum impact pressure at still water level, ρ = density of the water, g = acceleration due to gravity and H_i = incident wave height. An average of incident wave height used was given as 0.24m

Using equation 5.10:

$$P_{maxswl} = 1.00 \times 1000 \times 9.81 \times 0.24$$

= **2354.40 Pa**

Similarly, using experimental test data for wall model-A in vertical form, P_{max} = 9522.11 Pa for the wave height of 0.55m

By scaling-up using equation 3.40 gives:

$$p_P = 9522.11 \times \left(\frac{0.24}{0.55}\right)$$

= **4155.10 Pa**

(d) **Comparison with field investigation carried out by Kuribayashi et al. (1959) – data provided by Blackmore (1982)**

From Blackmore (1982), the following full size data were deduced:

For vertical seawall, maximum pressure for the wave height of 4.5 m was obtained as **150.00 kPa**

Similarly, using experimental test data for wall model-A in vertical form, P_{max} = 9522.11 Pa for the wave height of 0.55m

By scaling-up using equation 3.40 gives:

$$p_P = 9522.11 \times \left(\frac{4.5}{0.55}\right)$$

= 77908.17 Pa

= **77.907 kPa**

(e) **Comparison with field investigation carried out by Rouville et al. (1937) – data provided by Blackmore (1982)**

From Blackmore (1982), the following full size data were deduced:

For vertical seawall, maximum pressure for the wave height of 2.5 m was obtained as **689.7 kPa**

Similarly, using experimental test data for wall model-A in vertical form, P_{max} = 9522.11 Pa for the wave height of 0.55m

By scaling-up using equation 3.40 gives:

$$p_P = 9522.11 \times \left(\frac{2.5}{0.55}\right)$$

$$= 43281.81 \text{ Pa}$$

$$= \mathbf{43.281\ kPa}$$

(a) **Comparison with field investigation carried out by Miller et al. (1974) – data provided by Blackmore (1982)**

From Blackmore (1982), the following full size data were deduced:

For vertical seawall, maximum pressure for the wave height of 1.25 m was obtained as **41.4 kPa**

Similarly, using experimental test data for wall model-A in vertical form, P_{max} = 9522.11 Pa for the wave height of 0.55m

By scaling-up using equation 3.40 gives:

$$p_P = 9522.11 \times \left(\frac{1.25}{0.55}\right)$$

$$= 21640.91 \text{ Pa}$$

$$= \mathbf{21.64\ kPa}$$

For the cases of Neelamani and Sandhya (2005) and that of Neelamani et al. (1999) which are experimental data, the present experimental scenario over-estimates the magnitude of the maximum impact pressures for the smooth surface vertical wall. The differences are 71.33% and 76.48% based on the experimental data given by Neelamani and Sandhya (2005) and Neelamani et al. (1999) respectively. The only exception is the case of Kato et al. (2004) where the present experimental setup under-estimates the magnitude of the maximum impact pressure with a difference of -51.43% expressed in terms of the Kato et al. (2004) model data.

However, for the cases of field data, the present experimental set-up appears to under-estimate the magnitude of the maximum impact pressures almost by halve for the smooth surface vertical wall. For instance, the differences based on the field studies by Kuribayashi et al. (1959) and Miller et al. (1974) are -48.06% and -47.74% respectively. For the case of Rouville et al. (1937) this reduces to almost 100% and may be the result of the primitive apparatus used for the measurement by these researchers.

Generally, the values obtained from both available field and experimental data illustrated above compared well with the measured values obtained in the present investigation. Nevertheless, there are differences and the reason to account for such differences may vary and therefore discussed in detail in section 6.9.

5.9 Wave Impact Pressure Equations

Before a seawall can be designed the magnitude of maximum wave impact pressure and vertical pressure distribution must be obtained, these are usually found, for coastal structures, by calculating a maximum (design) wave for a given return period (Shore Protection Manual (SPM), 1984). The total or maximum pressure for this design wave is then calculated from one of the many available empirical equations (see section 2.4). As presented in section 2.4, there are numerous formulae to estimate the magnitude of the maximum impact pressure particularly on vertical wall. The choice depends on the judgemental decision of the researcher on the assumptions made in the study. With the assumptions specified earlier on for this present experiment, the maximum wave impact pressures obtained are compared with some available empirical equations for estimating maximum wave impact pressures.

The empirical equations for estimating maximum impact pressure by various researchers have been discussed in chapter 2. Previous studies which have comparable experimental conditions with the present data-set are therefore validated herein. The Shore Protection Manual (SPM) (1984) gives an adaptation of the impact pressure equations which enables maximum pressures due to breaking waves to be calculated on nearly vertical wall as:

$$P_{\max impact} = \frac{1}{2}\rho C_b^2 \quad \ldots\ldots 5.10$$

where ρ is the density of the water and C_b is the wave celerity.

Fukui et al. (1963) arrived at an empirical equation given as:

$$P_{\max dynamic} = 0.12\frac{\rho C^4}{gH} \quad \ldots\ldots 5.11$$

Where ρ is the water density, C is the wave celerity, g is the gravitational acceleration and H is the wave height.

Table 5.21 and Figure 5.51 showed the comparison of the maximum impact pressure obtained from the present study with the values obtained using Fukui et al theory as well as the adapted form of SPM model.

Table 5.21: Comparison of the magnitude of maximum impact pressure of previous studies at various wave heights at impact with the present data-set for smooth-surfaced vertical wall

Wave height at impact (H_{imp}), m	Maximum impact pressure		
	Present study, Pa	SPM model, Pa	Fukui et al model, Pa
0.440181	9522.115	39833.17	11023.28
0.315818	6892.416	33985.07	11183.86
0.210825	3959.378	25920.00	9745.41
0.165875	1993.376	22782.60	9569.25
0.097248	1103.886	13480.00	5714.58

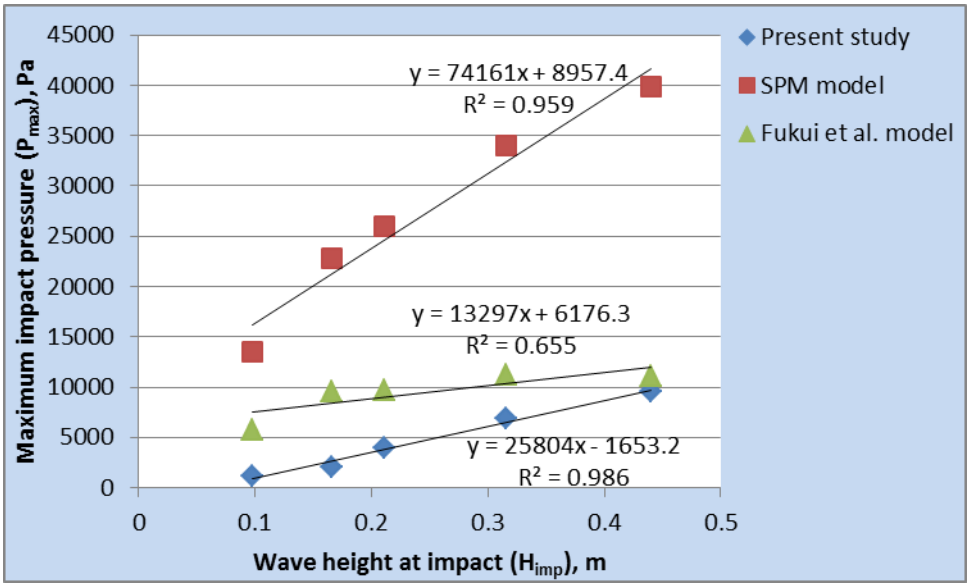

Figure 5.51**:** Comparison of maximum impact pressure of previous studies with the present data-set.

5.10 Prediction of Wave Impact Pressure Using Multivariable Regression Analysis (MRA)

Multivariable regression analysis (MRA) was employed to develop a model for the prediction of maximum wave impact pressure when the initial reservoir depth and the wall angle were varied. The purpose of MRA is to simultaneously identify two or more independent variables that determine variations in the dependent variable. The general MRA equation is given below, with the dependent variable being a linear function of more than one independent variable but may take different forms when the dependent variable is a non-linear function of independent variables.

$$Y = b_0 + b_1X_1 + b_2X_2 \dots\dots\dots\dots b_kX_k = \pm e \dots\dots\dots\dots\dots\dots\dots\dots\dots\dots\dots\dots\dots\dots\dots\dots\dots\dots 5.11$$

Where Y is the dependent variable; b_0 is the Y-intercept; b_1, b_2, and b_k are the slopes associated with X_1, X_2 and X_k respectively. X_1, X_2 and X_k are the values of independent variables and e represents the error.

For the prediction of the maximum impact pressure in this study, P_{max} is considered as a dependent variable, while the initial reservoir depth (RDEPTH) and wall slope (WSL) are independent variables (Table 5.22). Model-A equation was developed to predict the maximum impact pressure with varied initial reservoir depth and wall angle for the smooth-surface wall (wall model-A) while model-B, model-C and model-D equations were developed to predict the maximum impact pressure for the semi-smooth surface wall (wall model-B), the IMACTS wall (wall model-C) and the IMICTS wall (wall model-D) respectively (Table 5.22). The data used for the MRA modelling for instance, for the smooth-surface wall were the maximum impact pressures obtained for the smooth-surface wall when placed at angle 90^o, 75^o, 60^o and 45^o using five different initial reservoir depths (0.55m, 0.45m, 0.35m, 0.25m and 0.15m) for each of the angles. In each case the initial reservoir depth and the wall angle are the independent variables. Neelamani and Sandhya (2003) indicated the effect of seawall slope on reflection coefficient of plane, dentated and serrated seawalls as $\cot\theta$ and also used $\cot\theta$ in the predictive equations for the reflection coefficient instead of direct angles measured. The reason for using $\cot\theta$ instead of direct measured angles was not clearly stated however, in this study it was found that $\cot\theta$ provides the best fit (acceptable value of R^2) for the measured values of maximum impact pressures rather than using the direct angle measured. The inputted data into the SPSS for model-A, model-B, model-C and model-D equations are indicated in appendix 1.1, 1.2, 1.3 and 1.4 respectively (Appendix 1).

Statistical Package for Social Science (SPSS) was used to develop the regression models. MRA employs a procedure for selecting variables in which all the variables in a block are entered in a single step. When the experimental data were inputted on the SPSS for each of the wall types and analysed both for linearity and non-linearity, the relationship was best fitted as non-linear, as the values of determination coefficients (R^2) obtained for non-linear analysis are better than that of linear in each case, hence non-linear MRA was chosen for the modelling. However, the ANOVA results of linearity for each model (see appendix 2) allow the determination of the deviation from linearity and non-linearity (see discussion in section 6.11). A number of statistical parameters are associated with the MRA. Some of the most important parameters for non-linear MRA include the determination coefficient (R^2), sum of squares – regression (the regression coefficient), sum of squares - residual (the residual coefficient), the significant level, standard error, model error, etc. Detail explanation of these parameters can be found in most statistical literature, for examples Pallant (2010) and Field (2013).

As a summary of the regression models, Table 5.22 lists the statistical parameters calculated at the 95% confidence level, as this level is commonly used in analysis of statistical data. The MRA ANOVA outputs (non-linear) for each of the models are given in Table 5.23 through Table 5.26. Predictive model equations of maximum impact pressure as derived by MRA are given in equations 5.12 through 5.15. However, it should be noted that RDEPTH and WSL in Table 5.22 are d_o and cot θ respectively in the following equations. Thus, the model equations are given as follows:

For model-A;

$$P_{max} = b_0 + b_1 \cot\theta + b_2 d_o + b_3 d_o \cot\theta + b_4 (\cot\theta)^{b_5} + b_6 (d_o)^{b_7} \quad \ldots\ldots\ldots\ldots\ldots\ldots\ldots\ldots 5.12$$

For model-B;

$$P_{max} = b_o + b_1 \cot\theta + b_2 d_o + b_3 (\cot\theta)^{b_4} (d_o)^{b_5} \quad \ldots\ldots\ldots\ldots\ldots\ldots\ldots\ldots\ldots\ldots\ldots\ldots\ldots\ldots\ldots 5.13$$

For model-C;

$$P_{max} = b_0 + b_1 \cot\theta + b_2 d_o + b_3 d_o \cot\theta + b_4 (\cot\theta)^{b_5} + b_6 (d_o)^{b_7} \quad \ldots\ldots\ldots\ldots\ldots\ldots\ldots\ldots 5.14$$

For model-D;

$$P_{max} = b_o + b_1 \cot\theta + b_2 d_o + b_3 \cot\theta \, d_o + b_4 (\cot\theta)^{d_o} + b_5 (d_o)^{\cot\theta} \quad \ldots\ldots\ldots\ldots\ldots 5.15$$

Where P_{max} is the maximum impact pressure (kPa), θ is the wall angle (degree) and d_o is the initial reservoir depth (m). The values of coefficients b_0, b_1, b_2, b_3, b_4, b_5, b_6 and b_7 for model-A, model-B, model-C and model-D are given in the coefficient tables of the MRA outputs in appendix 3.1, appendix 3.2, appendix 3.3 and appendix 3.4 respectively (Appendix 3).

The validity of the models was assessed by considering the behaviour of the following statistical parameters: determination coefficient (R^2), sum of squares for regression (regression coefficient), sum of squares for residual (residual coefficient) as well as the plot of predicted values against the measured values. The statistical results for all models investigated which indicated the values obtained for all the aforementioned parameters are summarised in Table 5.22.

Table 5.22: Summary statistics of MRA for the four models at the 95% confidence level

Model	Wall surface type	Dependent variable	Independent variable	Regression determination coefficient (R^2)	Sum of squares (Regression)	Sum of squares (Residuals)
1	Type-A surface wall	Pmax	Constant RDEPTH WSL	0.870	149.075	8.685
2	Type-B surface wall	Pmax	Constant RDEPTH WSL	0.955	91.408	1.070
3	Type-C surface wall	Pmax	Constant RDEPTH WSL	0.873	151.841	9.090
4	Type-D surface wall	Pmax	Constant RDEPTH WSL	0.948	88.832	1.241

NB: RDEPTH = d_o and WSL = cot θ

Table 5.23: ANOVA Output for Model-A (Smooth-surface wall)

ANOVA[a]

Source	Sum of Squares	df	Mean Squares
Regression	149.075	10	14.907
Residual	8.685	10	.868
Uncorrected Total	157.760	20	
Corrected Total	66.894	19	

Dependent variable: PMAX

a. R squared = 1 - (Residual Sum of Squares) / (Corrected Sum of Squares) = .870.

Table 5.24: ANOVA Output for Model-B (Semi-smooth surface wall)

ANOVA[a]

Source	Sum of Squares	df	Mean Squares
Regression	91.408	6	15.235
Residual	1.070	14	.076
Uncorrected Total	92.478	20	
Corrected Total	23.619	19	

Dependent variable: PMAX

a. R squared = 1 - (Residual Sum of Squares) / (Corrected Sum of Squares) = .955.

Table 5.25: ANOVA Output for Model-C (IMACTS wall)

ANOVA[a]

Source	Sum of Squares	df	Mean Squares
Regression	151.841	10	15.184
Residual	9.090	10	.909
Uncorrected Total	160.931	20	
Corrected Total	71.705	19	

Dependent variable: PMAX

a. R squared = 1 - (Residual Sum of Squares) / (Corrected Sum of Squares) = .873.

Table 5.26: ANOVA Output for model-D (IMICTS wall)

ANOVA[a]

Source	Sum of Squares	df	Mean Squares
Regression	241.576	6	40.263
Residual	7.145	14	.510
Uncorrected Total	248.721	20	
Corrected Total	97.545	19	

Dependent variable: PMAX

a. R squared = 1 - (Residual Sum of Squares) / (Corrected Sum of Squares) = .927.

Again, the plots of predicted values of maximum impact pressure against the measured values in the laboratory tests were shown in the normal Probability Plots (P-P) in Figures 5.52 through Figure 5.55. Figure 5.52 compared the predicted values of maximum impact pressure with that of measured values in the laboratory for model-A (Smooth surface wall). Figure 5.53, Figure 5.54 and Figure 5.55 compared the predicted values with the measured valued for model-B (Semi-smooth surface wall), model-C (IMACTS wall) and model-D (IMICTS wall) respectively.

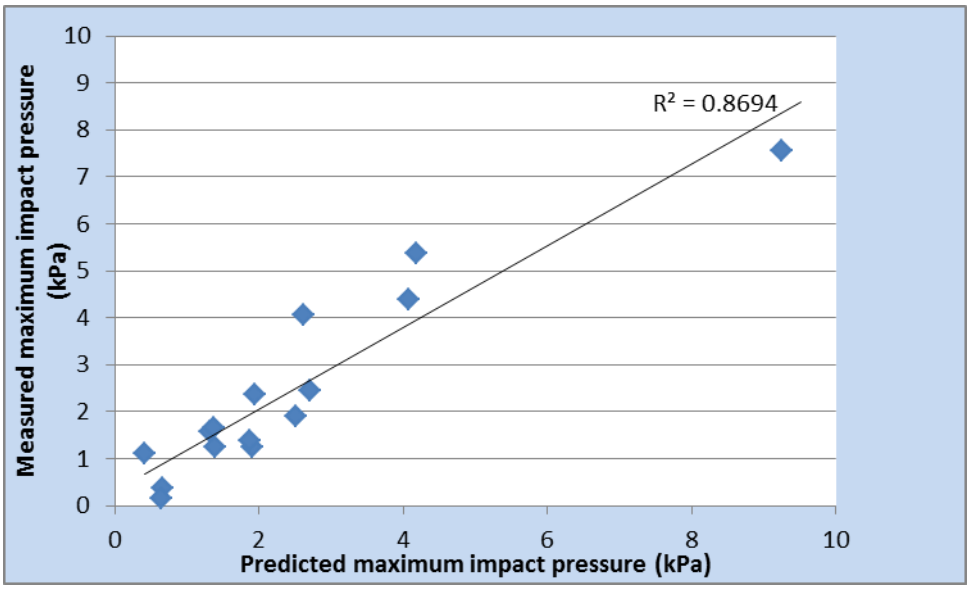

Figure 5.52: Comparison of predicted and measured maximum impact pressure for model-A (Smooth surface wall)

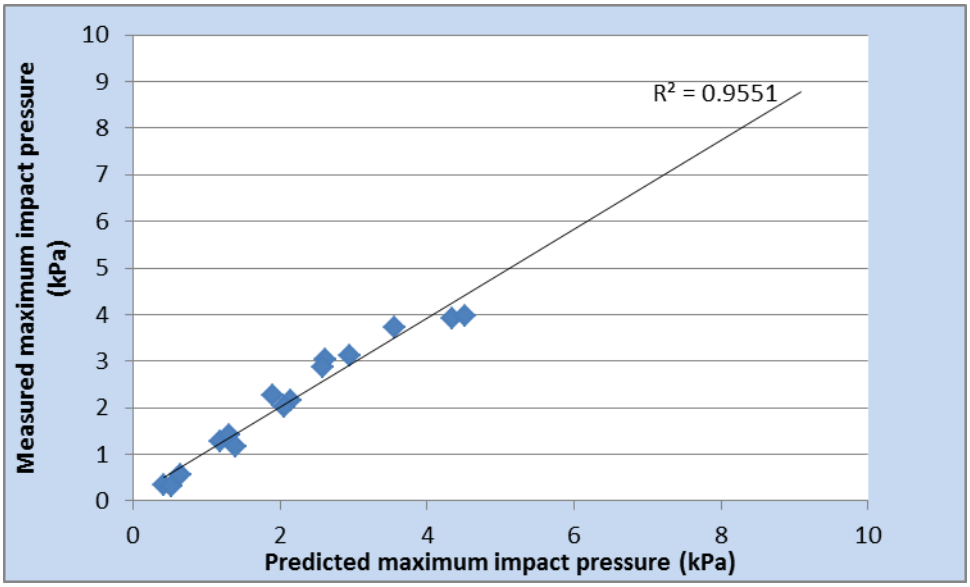

Figure 5.53: Comparison of predicted and measured maximum impact pressure for model-B (Semi-smooth surface wall)

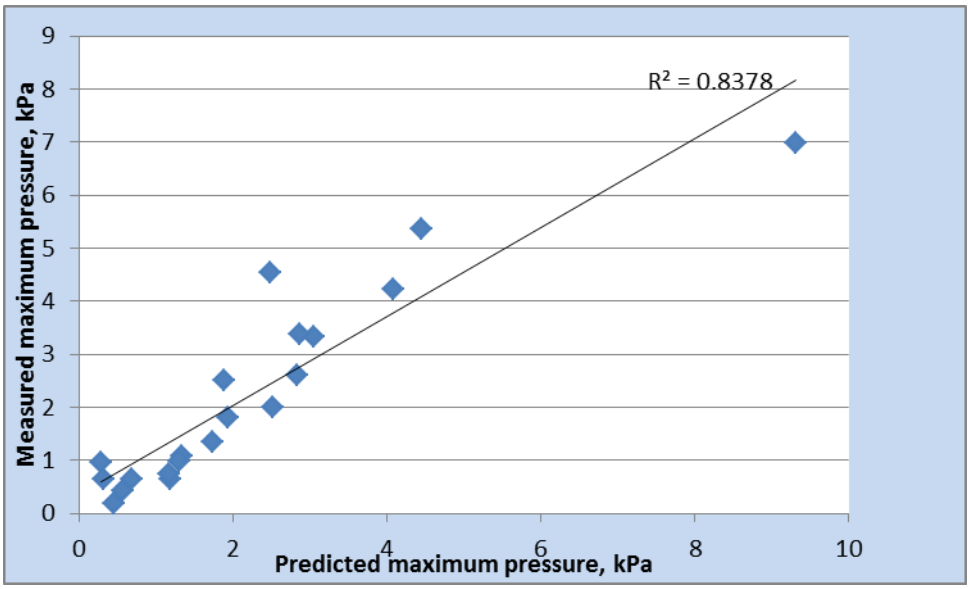

Figure 5.54: Comparison of predicted and measured maximum impact pressure for model-C (IMACTS wall)

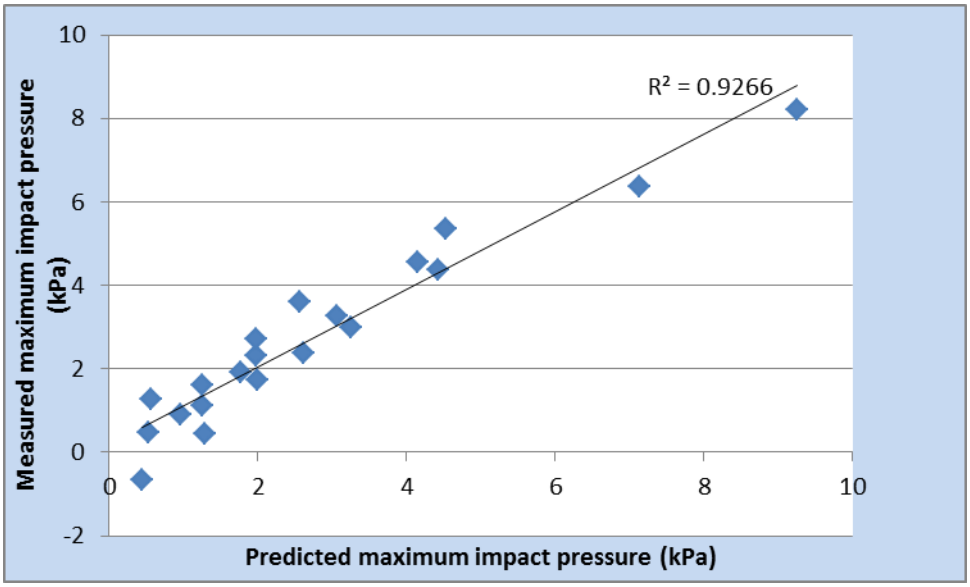

Figure 5.55: Comparison of predicted and measured maximum impact pressure for model-D (IMICTS wall)

5.11 Validation of the model equations

The main aim of this investigation was to quantify the magnitude of the highest dynamic pressures exerted on the wall models to allow the determination of the extent to which each of the model walls dissipates the energy of the floodwater waves. From the vast amount of data collected, model equations were developed using multivariable regression analysis (MRA) for the prediction of maximum wave impact pressures when the initial reservoir depth and the wall angle were varied.

The performance of these model equations have been evaluated initially against the measured values from which they were derived (see section 5.10). However, in an attempt to further validate this work various related equations suggested by other researchers and the relative results are presented in this section. The following pieces of work were chosen from the literature reviewed due to the nature of their various methodologies and the fact that the studies are to a reasonable extent, suitable for comparison with the results produced from this investigation. Wall model-D was considered to be suitable for comparison with those pieces of work selected. However, there are certain limitations to the scope of the works in any one case. In some cases, the work described may not be directly associated with the measurements of

dynamic pressure in isolation, yet it may be possible to make certain assumptions in order to compare the findings.

The related works originally identified in the literature review include the theoretical equation given for impact pressure as a function of stagnation pressure, the modified forms of this equation as given by Hayashi and Hattori (1958) as well as maximum impact pressure equation as a function of wave height given by Hiroi (1920). All of these therefore form the basis for comparison for the orders of magnitude for the highest dynamic pressures observed.

(a) Comparison with stagnation pressure theory:

Using equation 2.16, for example for vertical wall with initial reservoir depth of 0.55m, the floodwater flow velocity is computed as 4.4628 (see Table 5.3) hence;

According to Blackmore (1982), the maximum resulting impact pressure may then be calculated from:

$$P_{max} = \frac{1}{2}\rho v^2 \ldots\ldots\ldots\ldots\ldots\ldots\ldots\ldots\ldots\ldots\ldots\ldots\ldots\ldots\ldots\ldots\ldots\ldots\ldots\ldots\ldots\ldots\ldots\ldots\ldots\ldots\ldots 2.16\ recalled$$

as;
$$P_{max} = \frac{1}{2} \times 1000 \times 4.4628^2$$

$$= 9958.29 \text{ Pa}$$

Now using equation 5.15 for wall model-D in vertical form as an example;

$$P_{max} = b_o + b_1 \cot\theta + b_2 d_o + b_3 \cot\theta\, d_o + b_4(\cot\theta)^{d_o} + b_5(d_o)^{\cot\theta} \ldots\ldots\ldots\ldots\ldots 5.15$$

With initial reservoir depth do = 0.55m, wall angle θ = 90^o and constants b_1 to b_5 as defined in Appendix 3.4, the measured maximum impact pressure is 9254.12 Pa (Table 5.9) while the predicted maximum impact pressure is computed as 8214.46 (data in appendix 1.4). The measured and predicted maximum impact pressures obtained are similar in magnitude and therefore compared well with the theoretical equation of stagnation pressure for the vertical wall model-D. However, the situation is different for the inclined walls.

(b) Comparison with Hayashi and Hattori (1958) empirical equation:

Hayashi and Hattori (1958) investigated equation 2.17 experimentally with model seawalls and found coefficient f to be 4.

$$\frac{P_{max}}{\rho g} = \frac{f v^2}{2} \dots\dots\dots\dots\dots\dots\dots\dots\dots\dots\dots\dots\dots\dots\dots\dots\dots\dots\dots\dots\dots\dots\dots\dots\dots\dots\dots\dots 2.17\ recalled$$

Similarly, using equation 2.17, for example for vertical wall with initial reservoir depth of 0.55m and the floodwater flow velocity of 4.4628 (deduced from Table 5.3);

The maximum resulting impact pressure may therefore be calculated as:

$$P_{max} = \frac{f \rho g v^2}{2}$$

$$= \frac{4 \times 1000 \times 9.81 \times 4.4628^2}{2}$$

$$= 390763.37 \text{ Pa}$$

Also with initial reservoir depth of 0.55m for wall model-D in vertical form, the measured maximum impact pressure is 9254.12 Pa (Table 5.9) while the predicted maximum impact pressure is computed as 8214.46 (data in appendix 1.4). The model equation results appeared to under-estimate the maximum dynamic pressure in this case as the magnitude of the maximum dynamic pressure obtained with Hayashi and Hattori (1958) equation is much higher. However, Hayashi and Hattori did not state the range of applicability of this equation in terms of incident wave height, hence the wave height used for the computation may affect the result and account for the difference obtained.

(c) Comparison with model equations given as a function of wave height:

Hiroi (1920) proposed a linear relationship between impact pressure and the wave height. Hiroi suggested an experimental coefficient F as 1.5 for equation 2.21 for estimating the maximum impact pressure as:

$$p_{imax} = F\rho g H \dots\dots\dots\dots\dots\dots\dots\dots\dots\dots\dots\dots\dots\dots\dots\dots\dots\dots\dots\dots\dots\dots\dots\dots\dots..2.21\ recalled$$

Again, using equation 2.21, for example for vertical wall with initial reservoir depth of 0.55m and the floodwater flow velocity of 4.4628m/s;

The maximum impact pressure on the wall may be computed as:

$$p_{imax} = F\rho g H$$

$$= 1.5 \times 1000 \times 9.81 \times 0.55$$

$$= 8093.25\ Pa$$

Also with an initial reservoir depth of 0.55m for wall model-D in vertical form, the measured maximum impact pressure is 9254.12 Pa (Table 5.9) while the predicted maximum impact pressure is computed as 8214.46 (data in appendix 1.4). This value again compared well with measured and predicted values of the magnitude of the maximum dynamic pressure obtained from the model results. It worth mentioning here that most of the available related previous studies in terms of maximum impact pressures are for vertical walls, hence the data obtained for the inclined walls in terms of maximum impact pressures in this investigation may therefore require further verification in the future.

5.12 **Summary**

A number of previous researchers have attempted to address some of the problems highlighted in chapter 1 using a range of different approaches described in chapter 2 including dam-break analogies, channel releases, CFD techniques and many others. In each case it has been difficult to make exact comparisons between the results due to the different ranges in the parameters used in each of the investigations. For the purposes of validation of the results from this research, the analyses presented in this chapter provide sufficient information on the following: cost analysis and cost effective solutions to the development of the simple systems used in the present study; assessment of the performance of the experimental tool employed; the characteristics of the measured flow parameters such as floodwater wave elevation, floodwater wave propagation velocity as well as the impact pressures on the model walls; the comparisons of the results reported by previous researchers particularly for the smooth-surface vertical wall with the present results mainly in terms of the magnitude of impact pressures, duration of the maximum impact pressures, vertical impact pressures distributions as well as hydrostatic and dynamic pressures.

Consequently, reported test results are contradictory concerning the effect of wall inclination on wave impact pressures. Thus, also in this chapter the relationship between the angle of the wall and the arising impact pressures for the present investigation is established. Various investigators have studied the effect of seawall surface on the dissipation of the energy of the wave thus the analysis of the data obtained in terms of impact pressures for various surfaces investigated in the present study is again presented in this chapter. Various empirical formulae for the estimation of maximum impact pressures given by previous researchers were also evaluated and validated and thus presented in this chapter. This is possible, as over the range of work considered there are a number of suitable cases that are relatively similar dimensionally to those investigated.

As a result of contradictory information due to the different ranges in the parameters used by each investigator, multivariable regression analysis (MRA) was employed to develop a model for the prediction of maximum wave impact pressure when the initial reservoir depth and the wall angle were varied in the present study. Model equations were established to predict the maximum impact pressure with varied initial reservoir depth and wall angle for all the wall models investigated. Statistical Package for Social Sciences (SPSS) was used to develop the

regression models and the summary of the model equations obtained for each of the wall model is presented in this chapter.

The summary of the results presented in this chapter aims to confirm the extent of the problem of the seawall in dissipating the energy of the flood wave as well as the ability of various seawall surfaces in vertical and sloping forms in dissipating the energy of the flood wave. However, it is worth pointing out here that the results are presented in both table and chart format, making use of non-dimensional parameters to illustrate the magnitudes of impact pressures. The outcomes/findings of each of the analyses made in this chapter were therefore fully discussed in the next chapter.

CHAPTER SIX

DISCUSSION OF RESULTS

6.1 High Performance Instrumented Low Cost Wave Tank (ILCWT)

Many flow conditions and problems in coastal engineering are however not amenable to mathematical analysis because of the nonlinear character of the governing equations of motion, lack of information on wave breaking, turbulence or bottom friction, or numerous connected water channels. In these cases it is often necessary to resort to physical models for predicting prototype behaviour or observing results not readily examined in nature. Physical or scale models constructed and operated at reduced scale still offer an alternative for examining coastal phenomena that may presently be beyond our analytical skills. Physical modelling technique has been considered for this investigation and an instrumented wave tank has been constructed locally to generate the flood waves. Measurements of the interested flood wave parameters have been taken simultaneously during the experiments.

The approach however, used for both the direct and the labour costs during the construction has resulted in a relatively less expensive but high performing wave tank. The cost analysis of the construction of the wave tank discussed in section 5.1 has shown that the actual cost of construction was only 10.70% of the total cost of building the entire instrumented wave tank. A comparable small wave-sediment tank was built in the soil mechanics laboratory of the department of Civil Engineering at Johns Hopkins University using a similar approach, however the actual costs expended on the construction was reported to be about $10,000.00 which is about 30% of the total costs (Hudson et al., 1979). This was reported to be very economical at the time of construction and that the ratio of the actual cost to the total cost was said to be reasonable (Hudson et al., 1979). Table 5.1 (see section 5.1) showed the actual costs expended on the constructed LJMU ILCWT as £3,270.00 hence putting inflation and the present exchange rate into consideration, this LJMU laboratory tool may also be considered to be cost-effective and that the proportion of the actual cost to that of the total cost is also enormous and reasonable.

6.2 Performance of the Experimental Equipment

The performance analysis carried out on the whole system shows that the wave tank, gate release mechanism and the sensors performed absolutely well though any study executes with the wave tank may again be refined and eventually expanded to more complex experiments in large wave tanks or flumes. The small values of standard deviation obtained relative to the mean values for all the sensors in the repeatability experiments (20 runs) as indicated in Table 5.2 (see section 5.2) is a clear indication of the consistency of the system which invariably suggest the efficiency of the whole set-up.

Besides, past studies have shown that the appearance of the pressure-time curve depends on the performance of the pressure measuring equipment (Kirkgoz, 1978, Kirkgoz and Mamak, 2004). In the past the most commonly used pressure measuring device was the spring dynamometer which was incapable of responding to high frequency variations in pressure. Later, when more realistic impact pressure measurement instruments were available it became clear that the response of the measuring and recording equipment could have an enormous influence on the pressure–time curve, magnitude of the pressure, duration of the shock pressure and on other parameters.

The most recent instruments which have been used by many investigators for measuring impact pressure are transducers (see chapter 2) and many of them have reported various forms of pressure-time curves obtained during their experiments. However, most of these curves reported in terms of impact pressure using transducers followed a similar pattern (Kirkgoz and Mamak, 2004). Consequently, the pressure-time histories obtained in the present study with the use of pressure transducers followed typical pressure-time histories for wave-structure interaction (see Figure 5.1 in section 5.1) which was also similar to the curve obtained with the experiment conducted by (Kirkgoz and Mamak, 2004).

This newly constructed LJMU laboratory tool has been successfully used for the present investigations. Although, the wave tank is primarily designed for a specific study and built with a limited budget, it has resulted in a robust and versatile experimental tool. Hence, though small compared to most wave tanks and basins it is cost effective and well-suited to educational and basic research studies. The system can be used for studies ranging from undergraduate projects up to research projects. At the moment, about 2 or 3 final year students of the BEng Civil Engineering have already used the rig for their research projects. The performance of the whole

facility confirms the suitability of the rig for further studies on wave–structure problems. This shows that, overall it is possible to build our own wave tank, get useful results and still achieve significant savings. Further work is expected to be done on these systems to modify and improve them in order to allow the development of new models for different aspect of wave-structure problems.

6.3 Idealization of Instantaneous Dam-break

In the performed series of experiments differences in the gate elevation time was considered to be insignificant thus the construction of automatic gate elevation mechanism was not found to be necessary for the present study. As mentioned in section 5.3, the average gate opening time obtained throughout the experiment was 0.0875s which satisfied the criteria set by Vischer and Hager (1998) as well as the one set by Lauber and Hager (1998a) for instantaneous dam-break. Thus, the gate release system for the present experiment is a good approximation of instantaneous dam-break problem.

In theory, initially after the failure, the movement of water particles from the top is accelerated by gravity. The vertical downward velocity then increases with time until the water particle has reached the bottom. Negative flood wave is then generated in the upstream section of the dam site though not considered in this study. In the present study, only the positive flood wave created downstream is explicitly investigated. At the instant of the gate completely opened, a horizontal jet is formed which is clearly visible and plunges forward into the downstream section generating a further upward motion or splash (see Figure 5.3 to Figure 5.5 in section 5.3). The rise of this water may result in overtopping which, in certain circumstances, could have serious consequences.

The upward motion or splash generated up the vertical face of the wall is in the manner of a plunging breaker in a coastal engineering context. Visually the surge leading edge had a similar appearance to that observed and described by Kim and Lynett (2011). Prior to the reflection of the floodwater, conditions could be described as representing the usual dam-break situation while the situation at the dead-end may represent the behaviour of floodwater on the defence structure.

6.4 Floodwater Propagation Velocity

It is generally accepted that the higher the flow velocity of the floodwater, the greater the probability and extent of structural damage (Soetanto and Proverbs, 2004). Nicholas and Proverbs (2002) stated that velocity is a major factor that contributes to structural damage. High velocities limit the time available for emergency measures and evacuation when dam fails. Water depth and wave front velocity are hence needed to be considered as the hydraulic parameters which determine the flow profile in varying time step. For instance, Smith (1994) and McBean et al. (1988) showed some more critical combinations of water depth and flow velocities for building failure, indicating for instance that a velocity of 3m/s acting over a 1m depth will produce a force sufficient to exceed the design capacity of a typical residential wall.

Consequently, as flow velocity is generally presumed to influence the extent of flood damage hence its quantification is paramount when it comes to dam break problems. This is because dam engineers are interested in how long it takes the resulting flood to reach the nearest settlement and the maximum level of the flood at the settlement in the case of dam failure. Although the energy head has been suggested as a suitable flood impact parameter for reliable forecasting of structural damage to residential buildings however, forecasts of structural damage to road infrastructure and defence structures along the path of floodwater have been reported to be primarily grounded on flow velocity (Kreibich et al., 2009). Hence, the contribution of propagation velocity in floodwater damage to defence structures, particularly in dam break flow is of great concern. The strong focus on inundation depth as the main determinant for flood damage might be due to limited information about other parameters characterising the flood, for example flow velocity.

In the present study, propagation velocities of floodwater flow have been computed in an idealized dam break problem using various approaches. The Imaging System (IS) and the Sensor Signal Capture (SSC) method described in section 4.8.1 and section 5.4.1 have been adopted. The results obtained using the two techniques showed a good agreement with the dam break wave theory however; it was observed that the obtained velocities using SSC method with wave probes at shorter distance away from each other (0.41m apart) appeared to be closer in agreement to that obtained by using imaging system (IS) (see Figure 5.8 in section 5.4.1). In addition, Figure 5.10 (see section 5.4.1) also showed that the propagation velocity obtained using SSC method with wave probes 0.41m apart and that of Imaging System (IS) appeared to

be in close agreement with Liem and Kongeter's theory and Ritter's theory (Liem and Kongeter, 1999). This result follows Chegini (1997) concept that has earlier used a similar approach and concluded that this distance needs to be small enough to maintain a degree of correlation and accuracy in the measurements of floodwater propagation velocity. Figure 5.9 (see section 5.4.1) also revealed that most previous investigators over- estimate front water velocity by interchanging it for the wave celerity. Only the front velocity of Lauber and Hager is close to the celerity obtained in the present study. Furthermore, the results of comparison of front velocity with various downstream water levels (DSWL) (see Figure 5.7 in section 5.4.1) revealed that higher DSWL reduces the speed of the bore, which indicates that the water in front of the travelling bore reduces the speed of the flood wave.

6.5 Water Level Measurements

Flood hazard encompasses two aspects; (1) it is characterised by its impact parameters such as water depth and its associated probability. (2) the vulnerability, often due to exposure and susceptibility of affected elements (Messner and Meyer, 2006, Van der Veen and Logtmeijer, 2005). This section is meant to discuss the benchmark data for water level measurements at two different locations of interest downstream of the dam-site due to quick lifting of the dam-gate.

In recent years, there has been an increasing interest in the use of gauges/probes for measuring water levels. Resistive gauges have been used in the present experiment to measure water levels within the channel. The water level is deduced from the measurement of the voltage measured with the gauges. Such gauges allow following very rapid variations of the water level, but they have disadvantage of disturbing the flow locally by the presence of the wire. However, the time histories of water level recorded by the probes shown in Figure 5.11 (see section 5.4.2) indicated that this perturbation does not affect significantly the accuracy of the measurements. Leakage and the immersed length of the probe rods in the downstream initial water level for the wet-bed downstream condition did not appear to cause an appreciable problem.

For dry-bed downstream condition, the percentage difference between the maximum floodwater heights of the two probes for various reservoir depths lay between 40% and 55% (Table 5.5) except for the lowest reservoir depth which gives a lower value of 31.3%. In most

cases, the maximum elevation of floodwater is present around the region of the impact with the structure. This is probably due to the high acceleration, jumping like jet at impact (Figure 5.11). The highest water level elevation recorded by the probe close to the dam-site indicated approximately half of the highest height obtained by the probe close to the model structure (see Figure 5.12). This is obtained in most cases for all other reservoir depths except for few anomalies which may be due to some experimental inaccuracies. This relationship is in agreement with analytical solution for a one dimensional frictionless and horizontal dam-break flow problem explained in chapter 2.

As it is generally established that preventing structural failure will help prevent loss of life and minimize the cost of repairs to the structures, therefore, it is imperative to understand the loading of floodwater bores for the preservation of the integrity of the defence structures. However, the fluid dynamics must be understood before defining a relationship between bore characteristics and the resulting impact load. Bore heights within the channel therefore become one of the main parameters to be given due consideration. In the present study, as expected an increase in initial reservoir depths resulted in larger bore heights and the relationship appeared to be almost linear. Further studies examining greater initial reservoir depths and deeper downstream water depths may be necessary to assist in verifying this linear relationship.

6.6 Vertically Inclined Smooth-Surface Wall Model

Studies on smooth-surface vertical seawall had already been extensively carried out by many investigators and the results have been established (see chapter 2). This section aims to compare the results obtained mainly for vertically inclined smooth-surface wall in the present investigation with the previous results.

6.6.1 *Pressure-Time Curve*

Some early researchers, such as Gaillard (1905) and Molitor (1935) have reported breaking wave pressures lasting significantly longer than initial impacts, however, they were unable to measure the pressure characteristics because they lacked the necessary sensitive measuring and recording equipment. Following the first proper recording of pressure histories by Rouville Besson and Petry in 1938 (Kirkgoz, 1978) it became clear that the pressure variations consisted of two distinct parts:

(1) A high shock pressure of very short duration (the first peak);
(2) A low pressure of longer duration (the second peak)

In recent time, most experimental work has been directed to investigation of the first peak as being the probable cause of structural damage although some engineers have held the view that pressures with short durations, regardless of their magnitudes, are unlikely to be important in structural design (Ross, 1955, Carr, 1954). The maximum shock rising time recorded in the present experiments was around 0.0006s (6ms). Similar values were also measured by Bagnold (1939) and Weggel and Maxwell (1970). However, it is desirable therefore, to combine the effect of both the duration and magnitude of the maximum impact on the wall to determine the extent of the destructiveness caused by the surge.

The pressure-time histories obtained for transducers 1 to 6 for smooth-surfaced vertical wall model is shown in Figure 5.16. Figure 5.16 revealed that different peaks in wave pressure acted on the structure. The first peak could be described as dynamic wave pressure that appears when the incident wave first impinges the wall while the subsequent peaks could be referred to as hydrostatic which correspond to the impingement after the wave reflection by the wall and these last longer than the first peak. The second part of the pressure history, in general, shows

two types of variation, smooth and oscillatory. Some investigators recorded the smooth type (Nagai, 1960, Mitsuyasi, 1966) whereas some recorded the oscillatory type (Bagnold, 1939, Hayashi and Hattori, 1958, Lundgren, 1969, Richert, 1968).

In the present set of tests the low pressure variations (subsequent peaks after the first peak) generally consist of both smooth and oscillatory types. There was always more of the smooth type than the oscillatory type for higher level of initial reservoir depth, for instance when initial reservoir depth is 0.55m (Figure 5.15) while the oscillatory type appeared more than the smooth type for lower level of initial reservoir depth, for example, when the initial reservoir depth is 0.25m (Figure 5.16). This may be due to fast movement of the flood water (higher front water velocity) with higher initial reservoir depth coupled with the smoothed downstream bed while the lower initial reservoir depth propagates very slowly.

It is generally known that impact pressure of this nature often varies slightly even between runs of the same experimental conditions (Blackmore, 1982). This variation is very common due to the irregularity of the impact phenomena. Impact pressure on the wall usually depends on the percentage of air entrained by the wave and it is unlikely that the entrained air will be evenly distributed throughout the height of the floodwater in every case. The results obtained for impact pressure in this experiment indicated that impact pressures at each transducer showed these slight variations occasionally. However, in most cases similar wave impact curves are obtained for every trial with the same experimental conditions (see Figure 5.2 in section 5.2).

Furthermore, missing impact pressure values (zero values) also shown in Figures 5.16 do not again necessarily mean there was no impact pressure on the transducer at that time but the impact pressure might be so small probably on the order of the noise reading and therefore not discernible from the noise. The suction formed as a result of air entrapment of the flow along the face of the wall surface could again probably cause the transducer diaphragm to experience a zero or negative impact pressure (Figure 5.16).

6.6.2 *Vertical Impact Pressure Distributions*

There has been much speculation as to the vertical pressure distribution of a breaking wave, the Shore Protection Manual (SPM) (1984) recommended that the maximum pressure be taken at SWL, decreasing parabolically above and below this level. Miller et al. (1974) suggested that the location of the maximum pressure is dependent on the type of breaking wave, with a plunging breaker exerting its maximum pressure above SWL and a bore exerting its maximum pressure below SWL.

Some investigators measured the maximum impact pressure at still water level (SWL) (Hiroi, 1920, Gaillard, 1905, Luiggi, 1922). This has led to the well-known vertical impact distribution of Minikin (1963) with its maximum at SWL, reducing parabolically to zero at both the wave crest and trough. Other investigators measured the maximum impact pressure near the wave crest (Hunt et al., 2002) or near the wave trough (Rundgren, 1958). Thus there seems to be a considerable amount of disagreement as to the extent of the wave impact pressure over the face of the wall, as well as to the location of the maximum impact pressure.

The location of the maximum impact pressure has been investigated for vertically positioned wall models with various surfaces in the present experiment (see section 5.5.3). The proportion of the maximum impact pressure measured at the toe of the wall model for smoothed-surfaced vertical wall in this experiment was approximately 90%. The few (approximately 10%) which were measured near the wave crest at the upper section of the wall structure were randomly distributed. Hence, the vertical impact pressure distributions of Luiggi (1922) and Minikin (1963) which have a maximum value at SWL with a triangular type distribution above and below this level do not generally represent the worst case of loading. Although this type of vertical impact pressure distribution was again reported by Risk Management Solutions (2008) however, the worst case could probably occur for a maximum pressure at or near the wave crest. In the light of the current data it suggests that maximum pressure can also occur above the still water level (see section 5.5.3) thus it may be indisputable to propose that vertical impact pressure distribution would seem to be a uniform distribution over the height of the breaking wave. As a result, it is then possible to choose the location of maximum impact pressure somewhat above the still water level (SWL) as suggested for instance by Kirkgoz (1982).

6.6.3 *Hydrostatic and Dynamic Impact Pressures*

The hydrostatic pressures are produced by every wave impinging on the wall, whilst the short duration transient pressures are produced by only about 2% of the waves striking the wall (Blackmore and Hewson, 1984). Generally, the occurrence of transient pressures depends upon the orientation of wave front at the moment of impact, for instance, a vertical wave front will produce impact pressures but a non-vertical front may not. The magnitude of the hydrostatic pressure is dependent upon the wave height and water depth above it (see Minikin equation in chapter 2). The magnitude of the transient pressures are much more difficult to determine, being dependent upon wave steepness, volume of air entrained in the wave, wave celerity, period, etc.

Dynamic impact pressures are caused by the leading edge of the bore impinging on a structure while hydrostatic pressures are pressures of the reflected surges (Blackmore, 1982). In a field measurement of wave impact pressure by Blackmore (1982), it was found that the impact pressure was about twice the hydrostatic pressure in one site and as much as seven times at another site. Nakamura and Tsuchiya (1973) also found the maximum impact pressure to be about 50% of the following hydrostatic pressure. Blackmore (1982) also reported that the mechanism by which these two types of impacts are formed is different and suggested that an increase in hydrostatic pressure may not necessarily imply an increase in dynamic impact pressure and vice versa though some relationship might be expected.

Consequently, by comparing the maximum impact pressures obtained in the present study for the smooth surface wall (wall model-A) in vertical position (Table 5.6) with Fukui et al hydrostatic (Table 5.7) and Minikin hydrostatic (Table 5.8) for the same wall (wall model-A) in vertical position, it can be seen that the maximum impact pressure for the smooth-surfaced wall (wall model-A) in vertical form was found to be between 1.4 and 4.5 times hydrostatic pressure using Fukui et al.'s theory (From Table 5.6 and Table 5.7). However, with the theory proposed by Minikin (1963) the maximum impact pressure for wall model-A was found to vary between 10 and 40 times hydrostatic pressure (From Table 5.6 and Table 5.8). Previous studies have found maximum impact pressure to be as much as 1 to 100 times hydrostatic pressure depending on the prevailing conditions and judgement of individual assumptions (Blackmore and Hewson, 1984). Hence, the obtained results in the present investigation can be considered to be within an acceptable range.

6.7 Influence of Wall Orientation on Impact Pressure

The effect of inclined walls on breaking wave pressures is unclear in quality and quantity. Most of the previous researchers have reported that the steeper the slope the greater the amount of energy that may be dissipated. However, some few studies reported contradictory results to this view (see chapter 2). The present study intended to elucidate further on this subject matter. Thus, model tests on wave impact pressures on inclined walls were conducted to establish the probable relationship between the angle of the wall and the arising impact pressures. The results obtained were analysed and presented in terms of quality and quantity. Both the qualitative and the quantitative features of the influence of slope on the impact loading are discussed in this section.

6.7.1 *Variation of the Impact Pressure with Initial Reservoir Depth for the Sloping Wall*

As may be noted in Table 5.9 and Figures 5.32 through 5.35 the maximum impact pressure in the present study are influenced considerably by the wall angle. It is apparent from Figure 5.32 that the maximum impact pressure tends to increase with the increase in the initial reservoir water depth for each of the wall angles. This trend was obtained for all the wall orientations investigated and may be the result of an increase in the propagation speed as the incident wave height increases. Nevertheless, for the smooth surface wall, semi-smooth surface wall and the IMICTS wall, there was a significant reduction in the maximum impact pressure when the walls are flattened as compared to the vertical. Although, the reduction in the maximum pressure within the sloping forms of the wall is marginal however, the results as presented in Figure 5.32 through Figure 5.35 indicated that generally the maximum wave impact pressure decreases with increasing backward inclination of the wall.

Previous studies have revealed that when the wall slope is flattened for a given incident wave height the waves on the slope become spilling type rather than surging (Neelamani et al., 1999). The spilling of the waves on the slope may then result in wave energy dissipation which may be the reason for the significant reduction in the wave impact experienced by most of the sloping walls to the vertical. However, this concept may not be absolutely accurate for all wall

surfaces because in the present experiment the IMACTS wall (wall model-C) did not show positive response to load reduction in sloping forms as compared to other wall models.

6.7.2 *Quantifiable Load Reduction by the Sloping Walls*

Table 5.10 indicated that the smooth-surface wall (wall model-A) produced the highest percentage reduction (53.46%) when positioned at 75^{o} to its vertical form as compared with other angles. The implication is that the optimal position of the smooth-surfaced wall to dissipate a considerable amount of energy of the flood wave is 75^{o} relative to its vertical. It can also be seen from Table 5.11 that the semi-smoothed surface wall (wall model-B) also performed best in terms of dissipating the energy of the flood wave when placed at angle 75^{o}. This is because the load reduction was appreciably good (51.84%) at this particular wall angle amongst other orientations.

The IMACTS wall (wall model-C) increases the load instead when placed in varying orientations to its vertical (Table 5.12). However, detailed analysis of the obtained results in Table 5.12 indicated that the load increment when the wall was placed at angle 75^{o} relative to its vertical position was the smallest compared to when the wall was placed at angles 60^{o} and 45^{o}, for nearly all the initial reservoir depths investigated. This implies that the optimal position for the IMACTS wall (wall model-C) to dissipate a significant amount of the energy of the wave may be considered to be in vertical form. However, the lowest load increment was obtained when this wall model was positioned at 75^{o} as compared to other angles investigated. This implies that the IMACTS wall (wall model-C) best position in sloping form is still at angle 75^{o} relative to the other angles investigated.

A critical consideration of Table 5.13 indicated that IMICTS wall (wall model-D) dissipated the highest wave energy when placed at both angle 75^{o} and 45^{o}. This is because the difference in the percentage reductions produced by the wall at these angles is marginal (52.35% at 75^{o} and 52.48% at 45^{o}). Consequently, it can be concluded that amongst the wall angles investigated in the present study, placing a seawall defence at angle 75^{o} may dissipate a

significant amount of energy of the flood wave relative to the vertical form. Ultimately, the highest pressure load is expected for the vertical wall.

The effects of wall inclination is also elucidated in terms of reduction factor (which is the ratio of the maximum pressure on inclined wall to the maximum pressure on vertical wall) and are presented for all the wall models in Table 5.10 through Table 5.13. The results from Richert (1968) and Whillock (1987) in terms of reduction factor shown in Table 2.2 (see section 2) appeared to be in accordance with the present study. According to these investigators wave impact pressure generally decreases with increasing wall inclination. The experiments reported by Kirkgoz (1990) yielded quite contrary trends, with a marked increase of pressures for backwards inclined walls up to a slope of 30^o as can be seen from Table 2.2. Kirkgoz (1990) initially stated that no ready explanation is given for this contradiction but the latter concluded that the inconsistency might be due to the particles in the wave accelerating further after the vertical front face is established (1995, Kirkgoz, 1991). But, no theoretical explanation for these results could be found.

For the present data set, there was also no further load reduction with some wall models (wall model-B and wall model-D) beyond angle 75^o (i.e. for 60^o and 45^o) and that wall model-C caused load increments instead. Previous reports have generally concluded that the steeper the slope the greater the amount of wave energy that is being dissipated. However, this may not be a general representative as each wall model in the present study presented an optimal orientation at which the highest amount of energy is being dissipated.

6.7.3 *Duration of Maximum Impact Pressure for the Sloping Walls*

Table 5.14 showed that the rising times of maximum pressures are relatively very short; the longest impact pressure duration being around 5ms (0.005s) for the reservoir depth of 0.55m when the smooth surface wall was vertically positioned. The duration of the maximum impact appears to be higher for all the initial reservoir depths investigated when the wall is vertically positioned as compared to other angles. This could suggest that the wall sloping probably tends to reduce the duration of the maximum impact on the wall.

The duration of maximum impact pressure on the vertical wall had been found by previous investigators to be very short and in the range of 0.001s to 0.01s (Kirkgoz, 1978, Wood, 1997). However, following the results obtained in the present study it implies that duration of these intensive pressures is in agreement with previous predictions also for the floodwater wave. In essence, it can be concluded wall orientation as well as wave type could have influence on the duration of these intensive pressures.

6.7.4 *Location of the Maximum Impact Pressure on the Sloping Walls*

In the past, widely varying positions have been suggested for the point of the maximum impact pressure on a vertical wall, ranging from the whole depth from the toe of the wall (Nagai, 1960) to the top of the impinging wave crest (Kirkgoz and Mamak, 2004) (see section 5.4.3). However, it is now generally acknowledged that the greatest impact pressures on a vertical wall take place in the vicinity of the still water level. Not many studies have been carried out to verify this concept particularly on sloping walls. Nevertheless, a few available studies (Kirkgoz, 1982) found that the location of maximum impact pressure for regular waves breaking directly on vertical walls changes with foreshore slope. Kirkgoz (1982) also found that backward wall slopes had little or no influence on the location of the maximum impact pressure.

In the present study, in the example shown in Figure 5.40 and Figure 5.41 the maximum impact pressures were seen to occur over the heights of the wall particularly for the wall angles 75^o, 60^o and 45^o compared to the vertical. Hence, for practical purposes however, it seems reasonable to suggest the still water level, SWL (for wet-bed condition) or somewhere around the toe of the wall (for dry-bed condition) to be the most likely location for P_{max} particularly for the vertical wall but not generally the case for the sloping walls. Kirkgoz (1982) found that maximum impact pressures do occur above still water level as well but less frequently. The results obtained in the present study are therefore in agreement with these findings as the locations of maximum pressure for the sloping walls investigated are interchangeable between the toe of the wall and the wave crest (somewhere at the upper part of the wall depending on the height of the wave).

6.8 **Effects of the Wall Surfaces on the Impact Pressure**

6.8.1 ***Influence of Rough Surface on the Maximum Impact Pressure***

The magnitude of the maximum impact pressures for all the wall models at various wall angles are presented in Table 5.15. Similarly, Figure 5.46 through Figure 5.49 showed the variation of maximum impact pressure with initial reservoir depth for the four wall models at various orientations. In general, for each wall model the maximum impact pressure increases with increasing initial reservoir depths. However, it can be deduced from Figure 5.46 that the smooth-surface wall (wall model-A), semi-smoothed surface wall (wall model-B) and IMICTS wall (wall model-D) appeared to present similar trend in terms of change in the magnitude of the maximum impact as the initial reservoir depth varied. The changes produced by the semi smooth surface wall and the IMICTS wall relative to the smooth surface wall are marginal. However, the figure also revealed that the IMACTS wall (wall model-C) produced a significant reduction of pressure impact as compared to the smooth-surface wall, semi-smooth surface wall and IMICTS wall in the vertical form. This suggests that IMACTS wall model appeared to dissipate the greatest wave energy as compared to the other surfaces when each of the walls was vertically inclined.

Quite different results were obtained for the behaviour of the surfaces when the walls were in sloping forms. All the four wall surfaces appeared to present similar performance at angles 75^{o} and 60^{o} (Figure 5.47 and Figure 5.48) indicating a marginal difference in magnitude. Also, similar trend was observed for all the four wall surfaces at angle 45^{o} except for the upsurge of impact produced by both IMACTS wall and smooth surface wall with initial reservoir depth of 0.55m (Figure 4.49). The unusual presentation of the wave form at this wall angle (45^{o}) may be due to the complex interaction of the flood wave with the flattened wall coupled with a relatively high initial reservoir depth (r-depth = 0.55m). However, a critical examination of Figures 5.46 through Figure 5.49 showed that load reduction due to the wall models investigated in the present study is marginal when the walls are in sloping forms compared to when vertically positioned.

6.8.2 *Wall Surface Effects on the Maximum Wave Height at Impact*

From Figure 5.50, it can be seen that generally the wave height produced at impact (H_{imp}) increases with an increase in the initial reservoir depth for all the wall surfaces when vertically inclined. Likewise, when the walls were placed at angles 75^o, 60^o and 45^o (Figure 5.51, Figure 5.52 and Figure 5.53) the wall surfaces appeared to behave almost in a similar manner in terms of wave height produced at impact. The implication is that there was no significant difference in the way the wall surfaces perform in respect to the wave height each of the walls produced at the moment of wave impingement with the wall. This may suggest that the wall surfaces investigated in the present study have little or no effect on the maximum wave height generated in front of the wall just before impact.

6.8.3 *Wave Energy Dissipating Ability of the Wall Models*

From Table 5.17 through Table 5.20 together with the previous discussion, it could be deduced that IMACTS wall (wall model-C) produced the greatest load reduction relative to the smooth surface wall (wall model-A) when all the walls are vertically inclined as compared with semi-smoothed surface wall (wall model-B) and IMICTS wall (wall model-D). When the wall models were placed at angle 75^o IMACTS wall (wall model-C) retained the greatest load reduction relative to the smooth surface wall amongst other wall models investigated though in a minimal extent as compared to when the walls are in vertical form.

Thus, it implies that a significant load reduction was achieved with IMACTS wall (wall model-C) in vertical form compared with when inclined at angle 75^o. Similar trend was observed for the IMACTS wall at angle 60^o and at angle 45^o compared with other wall models. Consequently, it implies that the IMACTS wall dissipates energy of the floodwater wave relative to the smooth-surface wall at any wall angle and that its ability to dissipate the energy of the flood wave was most evident and significant when vertically positioned. However, for the semi-smoothed surface wall and the IMICTS wall, the dissipation ability was less obvious compared to the smooth surface at both vertical and inclined positions.

As discussed earlier (see section 5.6.3), wall model-C gives some unusual behaviour in terms of pressure reduction in sloping form compared with other wall models (causes increment

rather than reduction relative to its vertical position). It was again observed in Table 5.17 that wall-C in vertical form indicated a relatively high reduction in pressure (67.4%) relative to the smooth surface wall (wall model-A) compared with wall model-B (2.18%) and wall model-D (1.66%) in the same form. This has led to further interrogation of wall model-C data so as to justify the experimental procedures by establishing the nature of the pressure profiles. This was achieved by verifying and substantiating the obtained data through the extraction of the maximum impact pressures recorded by each of the six transducers fixed to wall model-C (data presented in Appendix 5) and the plots of the vertical distribution of the maximum impact pressures on the wall model (Figures also presented in Appendix 5).

The figures depicted in Appendix 5 indicated some level of consistency in terms of the vertical distribution of the maximum impact pressures. For instance, when the wall is in vertical form, for most of the initial reservoir depths the results indicated that the maximum impact pressure reduces from transducer 1 located at the base of the wall to transducer 6 fixed at the upper part of the wall (see Appendix 5.2). This was similar to what was obtained for other wall models represented in terms of percentage wall height shown in Figure 5.21 to Figure 5.24. Additionally, some level of consistency was noticed in the figures when the wall is in sloping forms (75^o, 60^o and 45^o) for most of the reservoir depths (see Appendix 5.3 to 5.5). This indicates that, even if the position of the transducers are varied, the vertical distribution of the maximum pressures will follow this pattern and that the wall would still experience the maximum impact around the location of the transducer which initially recorded the maximum pressure.

6.9 Comparison of the experimental results with the available data

Modern wave generators are capable of simulating regular or random wave sequences with a pre-defined wave energy spectrum. Active absorption of reflected waves can also be incorporated to ensure that the generated incident waves are not contaminated by re-reflected waves from the generators (see section 2.4.2). However, such models are not still free of scale effects. According to Reeve et al. (2012), in essence, scale effects will generally be present and may include those associated with reflection and transmission (which may be increased or decreased compared to the prototype), viscous and frictional effects (which will generally be increased compared to the prototype), and wave impact and shock forces (which may not be properly represented due to the effects of air entrainment). More importantly, laboratory effects may also need to be considered. In two dimensional models as in the present investigation, laboratory effects are mainly related to the effects of the side walls referred to as boundary layer effect as well as end conditions and non-linear effects spuriously generated by the mechanical wave generation system. All these may contribute to the differences between the measured pressures and that of full scale and other experimental data.

To account for the difference between the full-scale pressures in particular and the model data in this investigation the fact that, in the laboratory studies the fresh water waves tended to be smooth and regular and therefore not provide a true representation of real sea waves needs to be considered. This conclusion is also borne out by Denny (1951) who found pressure was heavily dependent upon the smoothness of the wave front. Denny states that, "when the waves carried ripples even with only four percent of the wave height, the shock pressures was nearly halved". Denny later found from his model studies that although the shock pressures were variable for similar waves, the highest recorded pressure for a given wave seemed to be substantially proportional to the wave height and the maximum pressure exerted by a wave was dependent upon the smoothness of both the seawall and the front face of the wave. In addition, the density of sea water will vary with levels of salinity and will be greater than the density of the fresh water used in this study.

Kirkgoz (1991) also revealed that the dimensionless impact pressures obtained by various researchers are different from each other. According to Kirkgoz (1991), the differences which exist among the results of various investigations even in dimensionless form may be attributed to various factors. These include the fact that some used wave height at breaking point to normalise the maximum impact pressure while some used water depth at the toe of the wall.

Other reasons may include (a) the number of waves tested (b) the type and slope of the beach in front of the wall (c) the wall inclination about the vertical (d) the type of wave, such as solitary or oscillatory used in the experiment (e) the type and size of the pressure measuring device (f) the positioning of the pressure sensors with respect to the breaking wave as well as to each other (g) the wave steepness (h) the type of recording equipment and (i) scale effect, which are supposedly biased towards reducing the impact pressure magnitude in larger models.

Kirkgoz (1991) concluded in his study that the types of pressure measuring device and the recording equipment are probably the most important factors that affect the precision of the results of any particular wave impact experiment. These contradicting results as presented by various researchers (Kirkgoz, 1990, Richert, 1968, Whillock, 1987) make the results presented in this present study appear conservative. However, the most important thing is that each investigator may need to state clearly the specific parameter used to normalise the impact pressure as well as specifying other experimental conditions or assumptions peculiar to their studies.

Consequently, in the case of the present study, the reason for these differences may be primarily due to the scale effect along with some simplified assumptions made. Such assumptions include: (i) breaking wave impact pressures are similar to those produced by a jet of water striking a vertical wall defence structure (ii) breaking wave impact pressures are influenced by entrapped air just before impact (iii) breaking wave impact pressures are proportional to the wave height. However, in the present study every attempt was made to keep each run identical for the same wave condition though very slight differences in the pressure measurements could not be avoided. The reasons for this are, firstly, that in a closed channel the production of identical oscillatory waves is virtually impossible due to reflection and secondly, that the insertion of the wall into the water always caused some disturbances. Despite these problems, however, the data does not appear to be unreasonable when compared with measurements made by other investigators.

6.10 **Estimating Wave Impact Pressure**

The various formulae which are purely theoretical in origin are not easy to apply in design, nor are they always reliable for the reasons discussed earlier. For instance, in both Bagnold's adiabatic air compression model (Bagnold, 1939) and Mitsuyasu's air leakage model (Mitsuyasi, 1966), the results are very dependent on the assumed dimensions of the initial air cushion. Unfortunately, these dimensions are difficult to specify. In contrast, the elastic-wave models, containing variables which are more easily specified, give results which are greater than the measured pressures. Blackmore (1982) and Crawford (1999) both predicted values which are about 100 times greater than laboratory scale measurements and 10 times greater than the full-scale values. Kamel's formula also gives results which are about eight times greater than measurements taken in the laboratory (Kamel, 1970). As a result, various semi-empirical formulae have most frequently been used in design to predict breaking wave pressures.

According to Kirkgoz (1978), among the early empirical formulae, those of Gaillard and Hiroi considerably underestimate impact pressures and, therefore, are not suitable for extensive use. Minikin's formular (Eq. 2.17), which was modified from Bagnold's expression also gives values which are low compared with the experimental results for breaking waves. Nagai (1960) compared his results with Minikin's formula and also found that the formula considerably underestimated impact pressures. However, Nagai (1960) confirmed that his formulae gave better results for composite-type breakwaters with a near-shore steeper slope than either Hiroi's or Minikin's expressions.

Consequently, it can be seen from Table 5.22 that the Shore Protection Manual overestimates the maximum impact pressures as compared to the present data-set. Blackmore and Hewson (1984) obtained similar results and reported that the overestimation of the maximum impact pressure by the SPM model is expected because the equation used is based on Bagnold's model-scale experiments which dependent on the amount of initial air entrapped. Conversely, it can be seen in Table 5.22 that Fukui et al. (1963) model came very close to the data-set of the present study though on the high side. Figure 5.53 revealed that though the Fukui et al. (1963) model appeared so close in agreement with the present study however, the correlation coefficient, R^2 (R^2=0.655) only shows a moderately strong linear relationship compared to the present study.

Thus, it seems that the SPM and Fukui et al. models shown in Figure 5.53 do not adequately fit the model-scale wave impact pressure data for the present study. However, for every steep and very mild wall slope it appears possible to choose an expression, such as those of Gaillard (1905), Minikin (1963), and Nagai (1960) which gives reasonable results for steep and very mild beach slopes.

It has been reported that impact pressure estimations have shown some extremely unpredictable values both between different investigations and within each investigation (Blackmore and Hewson, 1984). As a result, it appeared that there is no single formula available for estimating wave impact pressures on defence structure such as seawalls. In particular, the impact pressures on model walls investigated in the present study are not adequately predicted by the existing formulae. Hence, a more fundamental approach which is related to easily measurable parameters based on the specific assumptions for the present investigations is necessary. For these reasons, model equations for maximum impact pressure incorporating independent variables applicable to this particular study have been developed using Multiple Regression Analysis (MRA). As a result, equations 5.19 – 5.22 are proposed for the present study.

6.11 **Predictive Equations for Maximum Impact Pressure Using MRA**

Multivariable regression analysis (MRA) was employed to develop model equations for the prediction of maximum wave impact pressure at varying initial reservoir depths and wall angles. Predictive model equations for maximum impact pressure as derived by MRA are referred to as model-A, model-B, model-C and model-D equations and are given as equations 5.12, 5.13, 5.14 and 5.15 (see section 5.10) for wall model-A, wall model-B, wall model-C and wall model-D respectively.

The behaviour of the statistical parameters such as determination coefficient (R^2), sum of squares for regression (regression coefficient), sum of squares for residual (residual coefficient) as well as the plot of predicted values against the measured value have been used to test the validity of the obtained model equations.

The determination coefficient (R^2) for model-A (smooth surface wall/wall model-A) lied in an acceptable range (R^2=0.87). This implies that expressing this value as a percentage means that the model which includes the initial reservoir depth (RDEPTH) and wall slope (WSL) explains 87% of the variance in the maximum impact pressure. The values of the multivariable regression determination coefficient (R^2) for model-B (semi-smooth surface wall/wall model-B), model-C (IMACTS wall/wall model-C) and model-D (IMICTS wall/wall model-D) are also appreciable and again lay in an acceptable range R^2 = 0.96, R^2 = 0.87 and R^2 = 0.93 respectively (Table 5.23 through Table 5.26).

Furthermore, Atici (2011) reported that a high value of the regression determination coefficient (R^2) does not necessarily indicate the superiority of the model. The value of R^2 does not establish the validity of a model unless the results of other MRA parameters indicate consistency between the model and the experimental results. Consequently, MRA was coupled with an analysis of variance (ANOVA) for linearity. The linearity ANOVA results (Appendix 2) were used to determine the significance of the deviation from linearity and non-linearity for the established regression line. The linearity ANOVA determines whether the regression line was the most suitable curve in representing the relationship between the sample data sets of two correlated variables. The linearity ANOVA produced two values for each model: an F-value, which indicates the degree to which the regression equation fits the data, and a second value that indicates the statistical significance of the F-value. In the case that the statistical significance of the F-value was less than 0.05 at the 95% confidence level meaning that the

relationship between P_{max} and the target independent variable could be expressed as a linear or non-linear equation at the 95% confidence level (Field, 2013, Pallant, 2010). Otherwise, it was assumed that the relationship could not be represented as a regression model. However, the significance of F-values was less than 0.05 for all the models **(**see Appendix 2**)** hence the models are considered to be valid with respect to this particular parameter.

The validity of the models was also assessed by considering the sum of squares of regression (regression coefficient) and the sum of squares of residual (residual coefficient) from the outputs of ANOVA analysis - nonlinear (Table 5.23 through Table 5.26). In general the residual coefficient must be smaller than the regression coefficient for validity of the regression determination coefficient (R^2) (Field, 2013, Pallant, 2010). It can be seen from Table 5.23 for model-A that the residual coefficient is 8.685 and the regression coefficient is 149.075. These values are in agreement with the above assumption suggesting that model-A is good for practical purposes based on this standard. Similarly, the ANOVA analysis (non-linear) results for model-B, model-C and model-D shown in Table 5.24, Table 5.25 and Table 5.26 respectively agreed with these assumptions therefore validating the R^2 values for each of the models suggesting that these models are good for practical purposes based on those assumptions.

In the Normal Probability Plots (P-P) shown in Figures 5.56 through Figure 5.59, the values of maximum impact pressure predicted by model-A, model-B, model-C and model-D equations are compared with the measured values in the laboratory tests. In all cases, the distributions of the data point about R = 1 line are good implying that no major deviations from normality occurred. This suggests that the model equations are reasonable and reliable for practical applications. From the figures, it can again be seen that the regressions also showed strong correlations between the calculated and predicted values with R^2 of 0.8694, 0.9551, 0.8378 and 0.9266 for model-A, model-B, model-C and model-D respectively. This implies for instance, that using model-A equation it is possible to predict the maximum impact pressure that will be generated when floodwater waves of a specified initial reservoir depth impinge a smooth-surfaced wall (wall model-A) inclined at a specified angle. Consequently, with the use of model-B, model-C and model-D equations it is possible to predict the maximum impact pressure for the semi-smooth surface wall (wall model-B), IMACTS wall (wall model-C) and

the IMICTS wall (wall model-D) respectively at varying initial reservoir depths and wall orientations.

6.12 **Summary**

The findings from each of the selected results presented in chapter five were discussed in this chapter. The cost analysis of the construction of the wave tank presented in section 5.1 has shown that the actual cost of construction was only 10.70% of the total cost of building the entire instrumented wave tank. The performance analysis carried out on the whole system shows that the wave tank, gate release mechanism and the sensors performed absolutely well though any study executed with the wave tank may again be refined and eventually expanded to more complex experiments in large wave tanks or flumes. The average gate opening time in the experiments satisfied the criteria set by Vischer and Hager (1998) as well as the one set by Lauber and Hager (1998a) for modelling instantaneous dam-break. Thus, the gate release system for the present experiment is a good approximation of instantaneous dam-break problem.

Water depth and flow velocity are generally presumed to influence the extent of flood damage hence the quantification of these parameters in relation to dam-break problems were elucidated and discussed in this chapter. In the present study, as expected an increase in initial reservoir depths resulted in larger bore heights and the relationship appeared to be almost linear. It is also generally accepted that the higher the flow velocity of the floodwater, the greater the probability and extent of structural damage. Thus, Imaging System (IS) and the Sensor Signal Capture (SSC) method employed in the present study for the computation of the propagation velocity have shown good agreement with the dam break wave theory.

Also in this chapter, the outcomes of the comparisons of the results obtained for vertically inclined smooth-surface wall in the present investigation with the previous results were discussed. The pressure-time history obtained for this wall model followed the typical pressure-time history obtained by most previous investigators. In the light of the current data it is possible to choose the location of maximum impact pressure at still water level (SWL) or/and above the still water level (SWL) as suggested by various previous researchers.

The effect of inclined walls on breaking wave pressures is still not absolutely certain therefore the findings about this effect in the present study are again discussed in this chapter. Previous studies have revealed that when the wall slope is flattened for a given incident wave height the waves on the slope become spilling type rather than surging (Neelamani et al., 1999). The spilling of the waves on the slope may then result to wave energy dissipation. However, this concept may not be absolutely accurate for all wall surfaces because in the present experiment the IMACTS wall (wall model-C) did not show positive response to load reduction in sloping forms as compared to other wall models.

Various formulae which are purely theoretical in origin are not easy to apply in design, nor are they always reliable for the reasons discussed in section 6.10 of this chapter. However, this chapter has also presented model equations for the prediction of maximum wave impact pressure at varying initial reservoir depths and wall angles, and the equations were found to be suitable for practical purposes though caution may be required when using them as some of the results obtained are conservative.

Having considered the aims and objectives of this study and adequately reviewed various methods employed by previous researchers in the subject, the physical modelling technique was considered most suitable to achieve these aims. Hence, a suitable test facility was constructed. The methodology adopted including the experimental arrangements, test procedures as well as means of generating and analysing data (the use of suitable sensors and data logger) has established repeatable and reliable results presented in chapter 5. This has allowed an accurate quantification of the extent of dissipation of the energy of the flood waves discussed in this chapter for the wide range of wall surfaces and wall slopes investigated. Thus, the ultimate goal of the present study which is to predict the energy dissipation ability of various seawall designs against the floodwater waves generated by dam-break events was made possible through the chosen methodology. This has also allowed other significant findings and salient deductions that were presented in the next chapter. However, there are still room for improvements on this approach as larger wave tanks or flumes and pressure transducers of a wider range and better resolution than the one used in the present study are expected to produce better results.

CHAPTER SEVEN

CONCLUSIONS AND SUGGESTIONS FOR FURTHER RESEARCH

7.1 Conclusions

The present work used the mechanism of the dam-break to generate floodwater wave, measured the flow characteristics (surface elevation and propagation velocity) and examined the effectiveness of defence structures such as seawalls against flood hazards.

Most hydraulic laboratories generate dam-break flows using a gate plate and in most cases measure the dam-break flow hydrograms as dam engineers are interested in the time the flood will reach the nearest or nearby settlements. However, in this study, the flow is generated by sudden removal of the gate plate mechanically (see chapter 4) while the focus is on the terminal effect of floodwater waves on exclusively new seawall designs. An Instrumented Low Cost Wave Tank (ILCWT) was primarily designed and constructed in the hydraulics laboratory of the School of Built Environment, LJMU for this purpose.

Flow propagation along the channel includes friction dissipation and energy loss due to wave breaking at the dead end. When modelling dam-break flow motions with a free surface in a laboratory, the modelling forces are gravity, friction and surface tension. The friction forces are ignored in this study because they are much smaller than the gravity forces and the materials used for the construction of the wave tank (marine ply and Perspex) have low friction coefficient coupled with the fact that the downstream bed slope is also smooth and horizontal. Surface tension forces were also neglected in the present study when considered the size of the wave tank and for the fact that the flow was measured approximately in the centre of the channel. Hence, Froude number was shown to be the dominant modelling parameter.

The wall models are new designs which incorporated surface energy dissipaters using geo-grid materials of various textures and grit sizes with the aim of determining the effect of these surfaces and structures on the flood wave heights and the impact pressures. When the initial downstream condition was dry the flows clearly indicated the jet formation with a strong turbulence region of moving fluid in the channel and around the dead end. The complex phenomenon was caused by flow interaction due to the accelerated flow immediately downstream of the dam-site as was well illustrated by the video results.

In general, the floodwater height in the channel was found to increase with increasing initial downstream depth (for wet-bed downstream conditions). This resulted in the complex flow phenomena system though becoming less vigorous for increasing initial downstream depths. This process of transition, from complex phenomenon with jet and mushroom formation to oscillation form could be achieved by a varying flow regime from supercritical to subcritical. The flow phenomena obtained for this study both around the dam-site and the defence wall appeared qualitatively similar to the other researchers' work. Floodwater surface elevations were measured using wave probes located at suitable positions downstream of the channel. The probes were located at two stations along the channel to measure the resistance of the floodwater. The majority of the results for the variations of the floodwater surface elevation with time along the channel were reasonable. However, the results obtained using wave probes appeared good and comparable with other techniques such as visual and video analysis methods.

To measure the instantaneous propagation velocity, a digital system has been employed. The system is based on the established technique of PIV. This technique is useful with a relatively small area for measuring velocity and is being slightly adapted in the present study. The accuracy of the imaging system (IS) used in the present study was assessed by comparison with wave probe measurements termed sensor signal capture (SSC) technique. In general, the accuracy of the system was reasonable, although errors were initially detected with the wave probe close to the dam gate being shifted by the force of the floodwater. Overall, the results presented herein are reasonably consistent with other results obtained from tests employing similar techniques particularly the commonly used PIV method. The size of the test section is limited by the channel size and possibly the illumination area for the digital system. However, the use of a camera with sufficient resolution allows larger areas to be analysed. From the results, it is clear that the system has some limitations, particularly with regard to its response to high flow speed, however, as long as these limitations are minimised and corrected for (which was done in the present experiments), this adapted SSC technique is a useful laboratory scheme for analysing hydrodynamics model studies.

Furthermore, very little information is available for assessing wave loads when designing seawalls subject to breaking waves due to floodwater. In the present study, new impact pressure measurements due to breaking waves generated by the flow of floodwater were compared with predictions from a range of existing methods. New prediction formulae have been proposed for the evaluation of maximum wave impact pressures on seawalls. When comparing the predicted

outputs from these equations with the measurements taken from the physical model tests, the agreement between measurements and predictions is very good. Hence, for the range of variables investigated, empirical equations have been proposed for predicting maximum impact pressures for the purposes of assessment of seawalls and mitigation against flood hazards.

The focus of the study is mainly on the data obtained for the maximum impact of the dynamic pressures. Therefore, on the basis of the experimental results the following main conclusions could be summarily made:

- The pressure reduction obtained for the smooth surface wall (53.46%) and for the semi-smooth surface wall (51.84%) are highest at 75^o relative to their respective vertical form indicating that these wall models performed best at angle 75^o.
- The IMACTS wall (wall model-C) increases the load instead on inclination but again produces the lowest increment at angle 75^o suggesting that angle 75^o as well remain the most efficient angle if sloping is required for this wall.
- The IMICTS wall (wall model-D) also produces an appreciable reduction (52.35%) at angle 75^o relative to its vertical which also implies that angle 75^o is the most efficient orientation for the wall.
- Load reduction in respect to the wall surfaces in sloping forms is marginal suggesting that the performance of the surfaces compared to each other in sloping forms is not appreciable.
- IMACTS wall is about 65% better than the semi-smooth surface and IMICTS walls relative to the smooth surface wall in dissipating the energy of the floodwater wave in the vertical position.
- In general, IMACTS wall is superior to the semi-smooth surface and the IMICTS walls relative to the smooth surface in all positions or orientations
- The reduction factors for IMACTS wall at angles 75^o, 60^o and 45^o relative to its vertical are negative values suggesting that no energy of the floodwater wave is dissipated when inclined compared to its vertical position.
- The magnitude of the shock pressures for the sloping walls are often less than those experienced for the corresponding vertical wall except for the IMACTS wall

- The predictive equation for the maximum impact pressure for the smooth surface wall (wall model-A) is $P_{max} = b_0 + b_1 \cot\theta + b_2 d_o + b_3 d_o \cot\theta + b_4(\cot\theta)^{b_5} + b_6(d_o)^{b_7}$ with $R^2 = 0.87$ for the range of initial reservoir depth $0.15\text{m} \leq d_o \leq 0.55\text{m}$ and wall slopes $30^o \leq \theta \leq 90^o$. The values of all the constant variables are as stated in appendix 2.1 (Appendix 2).
- The predictive equation for the maximum impact pressure for the semi-smooth surface wall (wall model-B) is $P_{max} = b_0 + b_1 \cot\theta + b_2 d_o + b_3(\cot\theta)^{b_4}(d_o)^{b_5}$ with $R^2 = 0.93$ for the range of initial reservoir depth of $0.15\text{m} \leq d_o \leq 0.55\text{m}$ and wall slopes $30^o \leq \theta \leq 90^o$. The values of all the constant variables are as stated in appendix 2.2 (Appendix 2).
- The predictive equation for the maximum impact pressure for the IMACTS wall (wall model-C) is $P_{max} = b_0 + b_1 \cot\theta + b_2 d_o + b_3 d_o \cot\theta + b_4(\cot\theta)^{b_5} + b_6(d_o)^{b_7}$ with $R^2 = 0.93$ for the range of initial reservoir depth of $0.15\text{m} \leq d_o \leq 0.55\text{m}$ and wall slopes $30^o \leq \theta \leq 90^o$. The values of all the constant variables are as stated in appendix 2.3 (Appendix 2).
- The predictive equation for the maximum impact pressure for the IMICTS wall (wall model-D) is $P_{max} = b_0 + b_1 \cot\theta + b_2 d_o + b_3 \cot\theta\, d_o + b_4(\cot\theta)^{d_o} + b_5(d_o)^{\cot\theta}$ with $R^2 = 0.93$ for the range of initial reservoir depth of $0.15\text{m} \leq d_o \leq 0.55\text{m}$ and wall slopes $30^o \leq \theta \leq 90^o$. The values of all the constant variables are as stated in appendix 2.4 (Appendix 2).

Understanding the loading of floodwater waves is essential for preserving the integrity of defence structure in the event of dam-break or coastal flooding. Preventing structural failure will help prevent loss of life and minimize the cost of repairs to structures. Thus, the main findings of the present study stated above would enhance our understanding on the effectiveness of small-scale seawalls in reducing the energy of the floodwater waves. Above all, the implication of this is that coastal engineers and other seawall proponents would be able to make an informed decision when faced with the quest of selecting the most suitable seawall surface and slope particularly among the wide range of surfaces and slopes presented in the present investigation.

Furthermore, a number of previous researchers have attempted to address some of the problems related to wave-structure interaction using a range of different approaches. In each case it has

been difficult to neither make exact comparisons between results nor make precise conclusions due to the different ranges in the parameters used in each of the investigations. However, the information provided by each investigator enhances our understanding on the subject and eases the decision making process for all seawall proponents. Therefore, in addition to the main findings stated above, there are still some other outcomes which are either unique to the present study or meant to clarify some of the contradictory results and suggestions of previous researchers on the subject in question. Thus, on the basis of the theoretical and experimental considerations, the following deductions, clarifications or/and conclusions could again be made:

- The approach used for the construction of the instrumented wave tank discussed in section 5.1 causes a significant reduction of the actual expenditure on the rig compared to the total cost (only 10.70% of the total cost), hence considers being cost effective.
- This newly constructed laboratory tool has been successfully used for the present investigations. The performance of the rig confirms its suitability for further studies on wave–structure problems and the whole facility is well-suited for educational and basic research studies.
- In some cases, pressure-time histories for the range of wave heights tested do not show sharp peaks, indicating that the seawall may effectively reduce the impulsive wave pressure
- The results obtained for the computation of the floodwater propagation velocity using the imaging system (IS) and the sensor signal capture (SSC) techniques show good agreement. However, the SSC method with wave probes at shorter distance (0.41m apart) appears better and accurate in line with the results obtained by previous investigators.
- The floodwater propagation velocity is an important parameter governing the magnitude of the impact pressures. Direct replacement of wave celerity for water-particle front velocity as suggested by some previous researchers could lead to under-estimation of the magnitude of the impact pressures.
- Measurement using wave probes is widely used but has the disadvantage of disturbing the flow locally by the presence of the wires whereas the digital imaging technique is non-intrusive; however both techniques show appreciable and reasonable results. The applicability of imaging system is conditioned by the fact that the flow can be viewed

through the side walls of the channel thus only one-dimensional flows can be handled by such a technique.

- The location of the maximum impact pressure has been investigated for vertically positioned wall models with various surfaces in the present experiment. In the light of the current data it suggests that maximum pressure may occur more frequently below the still water level than above the wave crest for the vertical walls as suggested by some previous investigators.
- The location of the maximum impact pressure, P_{max}, has also been reported to occur above still-water-level (SWL) by some previous researchers. However, the present study confirms that the location of maximum pressure can also be well above SWL under certain conditions.
- The second and subsequent peaks in the pressure-time curve are of the order of hydrostatic pressure
- Hydrostatic pressure of reflected surge on the wall is generally an important factor as well as the peak shock pressure of the surge on the wall. The low impact pressures which last longer produce greater wall deflections and, consequently should be taken into consideration in the design of the vertical walls.
- For all tests in the present study, the maximum impact pressure was found to be between 1.4 and 40 times the hydrostatic pressure using Minikin and Fukui et al theories and is considered to be within an acceptable range.
- The magnitude of the shock and secondary pressures are very dependent on the wave characteristics and include the initial reservoir depth, the breaking wave height and the propagation velocity
- As the initial reservoir depth and the breaking wave height increase, the magnitude of the shock and secondary pressure increases
- Maximum shock pressures as high as $9.522 kN/m^2$ were recorded
- The shock pressures measured for apparently identical waves were only slightly variable
- The location of maximum shock pressures for the sloping walls occurs not as frequently as that of vertical walls at SWL.
- The maximum impact pressure measurements on the smooth surface vertical wall (Model wall-A) were used to evaluate the existing prediction formulas. Fukui et al

model for shock pressures came close in agreement to the measured shock pressures though for design purposes the model should be used with caution as it appeared to overestimate the shock pressures.

- The shock pressures produced on impact are sometimes irregular. This may be due to the wave form and the amount of air entrapped between the wave and the wall at impact.
- Results of the impact pressures obtained for the smooth-surface wall in vertical form (Table 5.6) indicate that a small change of 0.10m initial reservoir depth causes a decrease in average maximum impact pressure of approximately 41.10% at the base of the wall (transducer 1) while the decrease caused at the upper part of the wall model (above wave crest – transducer 6) reduces to an average of 32.48%
- The non-dimensional impact pressures (i.e $\frac{p_{max}}{\rho g H_{inc}}$) determined in the laboratory in the present experiment (see section 5.8) may be used directly to predict maximum pressures on any prototype structure.
- None of the existing wave-impact formulae is applicable to the entire range of beach slopes and wave steepness in practice. Each formula has its own limitations hence assumptions made in the course of study should be clearly specified.
- Froude's similarity law could be used in modelling the impact pressure of waves therefore the non-dimensional results presented in this study may be applied to any size of prototype by scaling-up.

7.2 Suggestions for further work

In the present study the gate opens with a manually operated pulley system however, the design of automated gate opening may be considered necessary for future studies on the rig.

Tapes/Greases were used around the joints between the gate and the sides of the tank to minimize leakages but stronger sealants may be considered in the future. This is because with these sealants there were still slight leakages which made the downstream channel not to be completely dry just before the start of another experiment but instead produced a thin film of water downstream.

The working model could in future be considered to include a bed slope, wide reservoir and general dam-site configurations so as to produce 2D or 3D effects in subcritical and super

critical flow to further enhance our understanding of their limitations and predictions for simulating dam-break problems.

The pressure distribution can be better described using miniature transducers with a wider range for better resolution and the number of transducers increased to cover more of the upper part of the test wall face.

In this study, the frictional and surface tension effects were neglected when considering energy dissipation in the breaker zone. It is expected that better results could be obtained if the turbulent losses due to friction and surface tension could be taken into consideration. Consequently, it is recommended that a comprehensive study which would take into consideration various mechanisms by which the flood waves shed their energy be conducted.

In the present study the beach/bed slope in front of the seawall is horizontal. It seems desirable to expand this range to at least include the rather gentler beach slopes more commonly encounter in nature.

The primary concern of this study is to describe the impact loading on seawall model structures from breaking waves and the effectiveness of these structures in dissipating the energy of the flood waves. However, it does not consider the importance of a number of other variables which may affect the performance of these structures which may include the dynamic response characteristics of both the structure itself and the soil foundation as well as riprap effect on the structure. Also, the reflection characteristics of the wall surface as well as the run-up and overtopping were not considered. Therefore, future research aimed at establishing the dynamic behaviour of these structures to verify some of these aforementioned variables might be worthwhile.

All the present tests employed flood waves generated through the dam-break phenomenon against the newly designed wall models. Whilst the test results are essential in order to gain a fundamental understanding of the wave impact phenomenon of the flood wave on these designs however, it is also necessary to carry out tests on these structures using other wave forms such as random, oscillatory and solitary waves. These tests should aim at establishing amongst other things the effects of the highly-complicated interactions which take place between the incident waves and the structure.

A complete method of estimating the maximum shock pressure of flood waves or surges on a wall should be established for practice, referring to more experimental results and theoretical considerations.

REFERENCES

ADEYEMO, M. D. Velocity Fields in the Wave Breaker Zone. Proceedings of 12th Conference on Coastal Engineering, ASCE, , 1970.

ADRIAN, R. Engineering Application of Particle Image Velocimeters. Proceedings of ICALOE, Laser Institute of America 1989. 56-71.

AHRENS, J. P. 1989. Stability of reef breakwaters. *Journal of Waterways, Port, Coastal and Ocean Engineering,* 115**,** 221-234.

AHRENS, J. P., SEELIG, W. N., WARD, D. L. & ALLSOP, W. Wave run-up on and wave reflection from coastal structures. Conference Proceedings of ASCE on Waves, 1993. 489–502.

ALLSOP, N. W. H. 1986. Sea Wall: A Literature Review. Hydraulic Research and CIRIA, Report No. EX1490.

ALLSOP, N. W. H. & HETTIARACHCHI, S. S. L. 1988. Reflections from coastal structures. *Coastal Engineering in Japan,* 1988**,** 782-794.

ALLSOP, W., BRUCE, T., PEARSON, J. & BESLEY, P. Wave overtopping at vertical and steep seawalls. Proceedings of the Institute of Civil Engineers- Maritime Engineering, 2005. 103-114.

ANDERSON, J. D. 1995. *Computational Fluid Dynamics*, McGraw-Hill.

ARNASON, H. 2005. *Interactions between an Incident Bore and Free-Standing Coastal Structure.* Ph.D., Civil Engineering, University of Washington, USA.

ATHERTON, W., ASH, J. W. & AL KHADDAR, R. M. The modelling of spills resulting from the catastrophic failure of above ground storage tanks and the development of mitigation. International Oil Spill Conference, 2008. 949-955.

ATICI, U. 2011. Prediction of the strength of mineral admixture concrete using multivariable regression analysis and artificial neutral network. *Expert Systems with Applications,* 38 (2011)**,** 9609-9618.

BAGNOLD, R. A. 1939. Interim Report on Wave-Pressure Research. *Journal of the Institute of Civil Engineers,* 12**,** 201-226.

BALLINGER R. AND SMITH H. 1994. The Management of the Coastal Zone of Europe. *Ocean and Coastal Management,* 22 45-85.

BALLINGER, R. C. & SMITH, H. D. 1994. The Management of the Coastal Zone of Europe. *Ocean and Coastal Management,* 22**,** 45-85.

BELLOS, C. V. & SAKKAS, J. G. 1987. 1-D dam-break flood-wave propagation on dry bed. *Journal of Hydraulic Engineering, ASCE,* 113 (12)**,** 1511-1525.

BELLOS, C. V., SOULIS, J. V. & SAKKAS, J. G. 1992. Experimental investigation of two-dimensional dam-break induced flows. *Journal of Hydrology Research,* 30 (1).

BERZ, G. Flood Disasters: Lessons from the Past: Worries for the Future. Proceedings of International Symposium on River Flood Defence, in: F. Toensmann and M. Koch, Kassel (eds.), Reports on Hydraulic Engineering No. 9/2000, 2000 Kassel, Germany.

BIESEL, F. & SUQUET, F. 1951. Laboratory Wave-generating Apparatus. *La Hoville Blanche,* 6**,** 147-165.

BISCARINI, C., DI FRANCESCO, S. & MANCIOLA, P. 2010. CFD modelling approach for dam break flow studies. *Hydrology and Earth System Sciences,* 14**,** 705-718.

BLACKMORE, P. A. 1982. *The Evaluation of Wave Forces on Seawalls.* Ph.D., Plymouth, University of Plymouth.

BLACKMORE, P. A. & HEWSON, P. J. 1984. Experiments on Full Scale Wave Impact Pressures. *Coastal Engineering in Japan,* 8**,** 331-346.

BS 6349 1991. British Standard Code of Practice for Maritime Structures, Part 7 Guide to the Design and construction of Breakwaters. *British Standards Institute (BSI).* London, UK.

BSI 6 ISO 13473 2002. Characterization of pavement texture by use of surface profiles – Part 2: Terminology and basic requirements related to pavement texture profile analysis. *Publication of British Standard Institute, ISBN 0 580 40674 1.*

BURCHARTH, H. F. & HUGHES, S. A. 2003. Types and Functions of Coastal Structures.

CAPART, H., YOUNG, D. L. & ZECH, Y. 2002. Voronoi imaging methods for the measurements of regular flows. *Experimental Fluids,* 32**,** 121-135.

CARR, J. H. 1954. Breaking Wave Forces on Plane Barriers. Hydrology Laboratory, Califonia Institute of Technology.

CHADWICK, A., MORFETT, J. & BORTHWICK, M. 2004. *Hydraulics in Civil and Environmental Engineering,* Spon Press, London, ISBN 10: 0-415-30609-4.

CHANSON, H. 2004. *Environmental Hydraulics of Open Channel Flows*, Elsevier Butterworth-Heinemann, Oxford, UK, ISBN 0 7506 5978 5.

CHANSON, H. 2005. Applications of the Saint-Venant Equations and method of Characteristics to the Dam Break Wave Problem. *Hydraulic Model Reports of Department of Civil Engineering, University of Queensland, Report No. CH55/05, ISBN 1864997966.*

CHANSON, H. 2008. A simple Solution of the Laminar Dam Break Wave. *Journal of Applied Fluid Mechanics,* 1**,** 1-10.

CHANSON, H. 2009. Application of the method of characteristics to the dam break wave problem. *Journal of Hydraulic Research,* 47**,** 41-49.

CHEGINI, A. 1997. *Fundamental Investigations of Dam-break Flows.* Ph.D., Civil Engineering, University of Manchester.

CHEGINI, A. H. N., PENDER, G., SLAOUTI, A. & TAIT, S. J. Velocity measurement in dam-break flow using imaging system. 2nd International Conference on Fluvial Hydraulics 2 June 2004 Naples, Italy. IAHR/AIRH, 858-867.

CHOWDHURY, J. Bangladesh, A State at Permanent Flood Risk. Proceedings of International Symposium on River Flood Defence, in: F. Toensmann and M. Koch (eds.), Kassel Reports on Hydraulic Engineering No. 9/2000, 2000 Kassel, Germany.

CIRIA 1996. Beach Management Manual. Construction Industry Research and Information Association, Report No. 125.

CRAWFORD, R. A. 1999. *Measurement and Analysis of Wave Loading on a Full Scale Coastal Structure.* Ph.D., Civil Engineering, University of Plymouth

CRESCENT CITY PLANNING DEPARTMENT 2010. Hazard Mitigation Plan Volume 1: Planning-Area-Wide Elements. *Report of Crescent City Planning Department.* Canada.

CROSS, R. H. 1967. Tsunami surge forces. *Journal of Waterways and Harbor Division ASCE,* 93**,** 201–231.

CRUZ, J. 2008. *Ocean wave energy*, Springer, Berlin.

CUMBERBATCH, E. 1960. The impact of a water wedge on a wall. *Journal of Fluid Mechanics,* 7 (3)**,** 353-373.

DEAN, R. G. & DALRYMPLE, P. A. 1991. Water Waves Mechanics for Engineers and Scientists. *Advanced Series on Ocean Engineering.* Singapore: World Scientific.

DEAN, R. G. & DALRYMPLE, P. A. 1994. Water waves mechanics for engineers and scientists. *Publication of Cornell University, USA.*

DENNY, D. F. Further experiments on wave pressures. Proceedings I.C.E, Feb., 1951. 330-345.

DEPARTMENT OF ENVIRONMENT CLIMATE CHANGE AND WATER (DECCW) 2010. Draft guidelines for assessing the impacts of seawalls. *Publication of the Government of the Hong Kong special administrative region.* Hong Kong.

DON & LOW 2006. A Geotextiles Design Guide. LOTRAK Publications, www.lotrak.com.

DOUXCHAMPS, D., SPINEWINE, B., CAPART, H., ZECH, Y. & MACQ, B. Particle-Based Imaging Methods for the Characterisation of Complex Fluid Flows. Conference Proceedings of the IEEE on Oceans, 2004.

DRESSLER, R. F. 1952. Hydraulic resistance effect upon the dam-break functions. *Journal of Research of the National Bureau of Standards,* 49 (3)**,** 217–225.

DRESSLER, R. F. 1954. Comparison of theories and experiments for the hydraulic dam-break Wave. *Hydrology* 38 (3)**,** 319-328.

ENVIRONMENTAL JUSTICE FOUNDATION 2004. Mangrove: Nature's defense against Tsunamis. *A report of Environmental Justice Foundation, on the impact of mangrove loss and shrimp farm development on coastal defenses.*

EUROPEAN UNION 2002. Choices for a greener future. *European Union and the Environment.*

FALNES, J. 2002. *Ocean waves and oscillating systems*, Cambridge University Press.

FAO 2007. An overview of the impact of the tsunami on selected coastal fisheries resources in Sri Lanka and Indonesia. *RAP Publication.*

FEMA 2008. Guidelines for Design of structures for vertical evacuation from tsunami. Federal Emergency management Agency.

FIELD, A. 2013. *Discovering Statistics Using IBM SPSS Statistics*, SAGE Publications Inc.

FREAD, D. L. The development and testing of a dam-break flood forecasting model. Proceedings of Dam-break flood modelling workshop, 1977 Washington, D. C. U. S. Water Resources Council, 164-197.

FUHRGOHTER, A. 1986. Model and prototype tests for wave impact and run-up on a uniform 1:4 slope. *Coastal Engineering,* 10**,** 49-84.

FUKUI, Y., NAKAMURA, M., SHIRAISHI, H. & SASAKI, Y. 1963. Hydraulic study on tsunami. *Coastal Engineering in Japan,* 6**,** 67–82.

GAILLARD, D. D. 1905. Wave Action in Relation to Engineering Structures. *US Army Corps of Engineers Report.* Reprinted 1935 ed.

GARATWA, W. & BOLLIN, C. 2002. Disaster risk management. *Deutsche Gesellschaft fur – Technische Zusammenarbeit (GTZ) GmbH, Division 4300.* Eschborn: Health, Education, Nutrition and Emergency Aid.

GODA, Y. 1972. Experiments on the Transition from Non-breaking to Post-breaking Wave Pressures. *Coastal Engineering in Japan,* 15**,** 81-90.

GODA, Y. New wave pressure formulae for composite breakwaters. Proceedings of Coastal Engineering Conference, 1974. 1702-1720.

GODA, Y. 1985. Random seas and design of maritime structures. *Publication of University of Tokyo.* Tokyo.

GODA, Y. & SUZUKI, Y. Estimation of incident and reflected waves in random wave experiments. Proceedings of 15th Coastal Engineering Conference, ASCE, 1976. 628-645.

GUO-LIN, Y., ZHE-ZHE, L., GUI-LIN, X. & XIANG-JING, H. 2010. Protection Technology and Applications of Gabion. *In: Advances in Environmental Geo-technics.* Springer.

HAGER, W. H. & BLASER, F. 1998. Drawdown curve and incipient aeration for chute flow. *Canadian Journal of Civil Engineers,* 25**,** 291-307.

HAMZAH, M. A., MASE, H. & TAKAYAMA, T. 2000. Simulation and experiment of hydrodynamic pressure on a tsunami barrier. *Coastal Engineering* 1501-1507.

HATTORI, M., ARAMI, A. & YUI, T. 1994. Wave impact pressure on vertical walls under breaking waves of various types. *Coastal Engineering* 22**,** 79-114.

HAYASHI, T. & HATTORI, M. 1958. Pressure of the breaker against a vertical wall. *Coastal Engineering in Japan,* 25**,** 3-7.

HEALTH AND SAFETY EXECUTIVE (HSE) 2005. An experimental investigation of bund wall overtopping and dynamic pressures on the bund wall following catastrophic failure of a storage vessel. *Research report of the Health and Safety Executive.* UK.

HERRINGTON, T. Coastal Hazard Mitigation. Proceedings of 23rd Annual Submerged Land Management Conference, 2004 Halifax. NJDEP Coastal Management Program.

HIROI, I. 1920. The Force and Power of Waves. *The Engineer***,** 184-185.

HOMMA, M. & HORIKAWA, K. 1965. Experimental study on total wave force against seawall. *Coastal Engineering in Japan,* 8(1965)**,** 119-129.

HORIKAWA, K. & KUO, C. T. A study on Wave Transformation Inside Surf Zone. Proceedings of 10th Conference on Coastal Engineering, ASCE Vol 1, Chapter 15, 1966.

HUDSON, R. Y., HERMANN, F. A., JR., SAGER, R. A., WHALIN, R. W., KEULEGAN, G. H., CHATHAM, C. E., JR. & HALES, L. Z. 1979. Coastal Hydraulic Models. *Special Report No. 5 of the U.S. Army Waterways Experiment Station.* Coastal Engineering Research Centre, Vicksburg, Miss.

HUGHES, S. A. 1993. *Physical Models and Laboratory Techniques in Coastal Engineering*, World Scientific Publishing Co. Pte Ltd., USA, ISBN 981-02-1540-1.

HUGHES, W. F. 1979. *An introduction to viscous flow*, Hemisphere Publishing Corporation, Kingsport Press, USA.

HUNT, M. L., ZENIT, R., CAMPBELL, C. S. & BRENNEN, C. E. 2002. Revisiting the 1954 Suspension Experiments of R. A. Bagmold. *Journal of Fluid Mechanics,* 452(2002)**,** 1-24.

HYDRAULIC ENGINEERING MANUAL 2002. Tidal Hydrology, Hydraulic, and Scour at Bridges. *Hydraulic Engineering Circular (HEC) 25.* USA: US Department of Transportation, Federal Highway Administration.

HYDRAULIC RESEARCH 1987. Design, Construction and Maintenance of Seawalls. *Summary of seminars held at Hydraulic Research, Wallingford.* UK: Construction Industry Research and Information Association (CIRIA).

IIZUKA, H. & MATSUTIMI, H. 2000. Estimation of Damage Caused by Tsunami Flow. *Proceedings of Coastal Engineering, JSCE,* 47**,** 381-385.

IPCC 2001. Climate Change 2001. *In:* WATSON, R., T., AND THE CORE WRITING TEAM, (ed.) *IPCC Synthesis Report, A Contribution of Working Groups I, II, and III to the Third Assessment Report of the Intergovernmental Panel on Climate Change.* Cambridge, United Kingdom: Cambridge University Press.

IPPEN, A. T. & KULIN, F. The Shoaling and Breaking of the Solitary Wave. Proceedings of 5th Conference on Coastal Engineering, ASCE, 1954. Chapter 4.

IRIBARREN, C. R. & NOGALES, C. Protection of Ports. 17th International Navigation Congress, 1949 Lisbon. Section II, Com. 4, 31-80.

ISAACSON, M. 1991. Measurement of regular wave reflection. *Journal of Waterway, Port, Coastal and Ocean Engineering, ASCE,* 117 (6)**,** 553-569.

IVERSEN, H. W. Waves and Breakers in Shoaling Water. Proceedings of 3rd Conference on Coastal Engineering, 1952. Chapter 1.

IWAGAKI, Y., SAKAI, T., KAINUMA, J. & KAWASHIMA, T. (1971. Experiments on Horizontal Water Particle Velocity at Water surface of Near Breaking Waves. *Coastal Engineering in Japan,* 14**,** 15-21.

KAJIMA, R. 1969. Estimation of incident wave spectrum in the sea area influenced by reflection. *Coastal Engineering in Japan,* 12 (J.S.C.E 1969)**,** 9-16.

KAMEL, A. 1968. Water Wave Pressures on Seawalls and Breakwaters. *Research Report No. 2-10, U.S. Army Engineer Waterways Experiment Station.* Vicksburg, USA.

KAMEL, A. M. 1970. Shock pressure on coastal structures. *Journal of Water Way, Harbour Coastal Engineering Division, ASCE,* 96**,** 689-699.

KATO, F., INAGAKI, S. & FUKUHAMA, M. 2004. Wave Forces on Coastal Dike due to Tsunami. *Journal of Disaster Research,* 4 (6).

KATOPODES, N. & STRELKOFF, T. 1978. Computing two-dimensional dam-break flood waves. *Journal of Hydraulic Division, ASCE,,* 104 (9) 1269-1287.

KIM, D. & LYNETT, P. J. 2011. Dispersive and Non-hydrostatic Pressure Effects at the Front of Surges. *Journal of Hydraulic Engineering, ASCE,* 2011(July).

KING, D. A. 2004. Climate change science: Adapt, mitigate, or ignore? *Science,* 303**,** 176-177.

KIRKGOZ, M., S. & MAMAK, M. 2004. Impulsive modelling of wave impact pressures on vertical wall. *Ocean Engineering,* 31**,** 343-352.

KIRKGOZ, M. S. 1978. *Breaking waves: their actions on slopes and impact on vertical seawalls.* Ph.D., Civil Engineering, University of Liverpool, Liverpool, UK.

KIRKGOZ, M. S. 1982. Shock Pressure of Breaking Waves on Vertical Walls. *Journal of the Waterway, Port, Coastal, and Ocean Division, ASCE,* 108 (WW1)**,** 81-95.

KIRKGOZ, M. S. 1990. An Experimental Investigation of a vertical Wall Response To Breaking Wave Impact. *Ocean Engineering,* 17**,** 379-391.

KIRKGOZ, M. S. 1991. Impact pressure of breaking waves on vertical and sloping walls. *Ocean Engineering,* 18 (1/2)**,** 45-59.

KIRKGOZ, M. S. 1995. Breaking wave impact on vertical and sloping coastal structures. *Ocean Engineering,* 22 (1)**,** 35-48.

KOSHIMURA, S. 2002. Multiple Reflection of Tsunamis Incident on a Continental Slope. *Journal of Hydraulic, Coastal and Environmental Engineering, JSCE,* 705/II-59**,** 151-160.

KREIBICH, H., THIEKEN, A. H., GRUNENBERG, H., ULLRICH, K. & SOMMER, T. 2009. Extent, perception and mitigation of damage due to high groundwater levels in the city of Dresden, Germany. *Natural Hazards Earth Syst. Sci.,* 9 (2009)**,** 1247–1258 http://www.nat-hazards-earth-syst-sci.net/9/1247/2009.

KUNDZEWICZ, Z. W. & TAKEUCHI, K. 1999. Flood Protection and Management: Quo Vadimus? *Hydrologic Sciences Journal,* 44**,** 417- 432.

KURIBAYASHI, T., MURAKI, Y. & UDAI, G. 1959. Field investigation of wave forces on breakwaters. *Coastal Eng. in Japan***,** 17-27.

LANGFORD, P. S., ROGER, I. N. & WALTERS, R. A. 2006. Experimental Modelling of Tsunami Generated by Underwater Landslides. *Science of Tsunami Hazards,,* 24**,** 267.

LAUBER, G. & HAGER, W. H. 1998a. Experiments to dam-break waves: Horizontal channel. *Journal of Hydraulic Research* 36(3)**,** 291-307.

LAUBER, G. & HAGER, W. H. 1998b. Experiments to Dam-Break Wave: Sloping Channel. *Journal of Hyraulic Research,* 36(5)**,** 761-773.

LI, Y. & RAICHLEN, F. 2002. Non-breaking and breaking solitary wave run-up. *Journal of Fluid Mechanics* 456 (2002)**,** 295 – 318.

LIEM, R. & KONGETER, J. Application of High-Speed Digital Image Processing to Experiments on Dam Break Waves. Proceedings of Concerted Action on Dam-Break Modelling (CADAM) Conference, 1999 European Community Workgroup, Zaragossa, Spain. 399-411.

LIGGET, J. A. 1994. *Fluid mechanics*, McGraw-Hill, New York, USA.

LINHAM, M. M. & NICHOLLS, R. J. 2010. Technologies for Climate Change Adaptation-Coastal Erosion and Flooding. *A report for UNEP.*

LIU, H., WU, W. & LU, Y. J. 2008. Hydrodynamic loads on seawalls induced by wave overtopping in regular waves. Shanghai, China: Shanghai Jiao Tong University.

LIU, P., LYNETT, P. & WU, T. 2002. Modelling wave run-up with depth integrated equations. *Journal of Waterways, Port, Coastal and Ocean Engineering ASCE,* 46**,** 89-107.

LIU, P. L. F. & AL-BANAA, K. 2004. Solitary wave runup and force on a vertical barrier. *Journal of Fluid Mechanics,* 505**,** 225-233.

LUIGGI, L. Correspondence on improvement of the Port of Va'lparaiso. Proc. I.C.E., 1922. 214 40-45.

LUNDGREN, H. Wave Shock Forces: An Analysis of Deformation and Forces in the Wave and in the Foundation. Proceedings of Symposium on Research on Wave Action, 1969 Delft Hydraulic Laboratory, Delft, The Netherlands.

MAGUIRE, A. E. 2011. *Hydrodynamics, control and numerical modelling of absorbing wave-makers.* PhD, The University of Edinburgh.

MALLAYACHARI, V. & SUNDAR, V. 1994. Reflection characteristics of permeable seawalls. *Coastal Engineering,* 23 (1-2)**,** 135-150.

MARTINELLI, L., ZANUTTIGH, B. & CORBAU, C. 2010. Assessment of coastal flooding hazard along the Emilia Romagna littoral, IT. *Coastal Engineering in Japan,* 57**,** 1042-1058.

MCBEAN, E. A., GORRIE, J., FORTIN, M., DING, J. & MOULTON, R. 1988. Adjustment Factors for flood damage curves. *Journal of Water Resources Research, ASCE,* 114(6)**,** 635–646.

MCCONNELL, K. 1998. Revetment Systems Against Wave Attack - A Design Manual. Thomas Telford, London.

MCCOWAN, J. 1894. On the Highest Wave of Permanent Tupe. *Philosophical Magazine.* Vol. 38, series 5 ed.

MCMAHON, J. J. 2008. *Piston-type Laboratory Wave Generator.* PhD, University of NSW, Canberra, AS.

MELITO, I. & MELBY, J. A. 2002. Wave run-up, transmission and reflection for structures armourd with CORE-LOC. *Coastal Engineering,* 45 (1)**,** 33-52.

MESSNER, F. & MEYER, V. 2006. Flood Damage, Vulnerability and Risk Perception – Challenges for Flood Damage Research. *In:* SCHANZE, J., ET AL., (ed.) *Flood Risk Management: Hazards, Vulnerability and Mitigation Measures.* Springer.

MILLER, R. L., LEVERETTE, S., O'SULLIVAN, J., TOCHKO, J. & THERIAULT, J. Field Measurements of Impact Pressures in Surf. 14th Conference Proceedings of Coastal Engineering, 1974. 1761-1777.

MIMURA, N. & NUM, P. D. 1998. Trends of Beach Erosion and Shoreline Protection in Rural Fiji. *Journal of Coastal Research,* 14 (1).

MINIKIN, R. R. 1963. *Winds, Waves and Maritime Structures,* London, UK, Charles Griffen.

MITSUYASI, H. 1966. Experimental study on wave force against a wall. *Coastal Engineering in Japan,* 5 (1962)**,** 23 - 47.

MOLITOR, D. A. 1935. Wave Pressures on Sea-Walls and Breakwaters. *ASCE Transactions,* IQQ (1913)**,** 984-1002.

MORISON, J. R. 1951. The Effect of Wave Steepness on Wave Velocity. *Transactions, American Geophysical Union,* 32 (2)**,** 201-206.

MORISON, J. R. & CROOKE, R. C. 1953. The Mechanics of Deep Water, Shallow Water, and Breaking Waves. *Beach Erosion Board, Technical Manual No. 40.*

MURAKI, Y. Field observations of wave pressure, wave run-up, and oscillation of breakwaters. Proceedings of 10th ICCE Conference, ASCE, 1966 New York. 4302-4321.

MYLONAS, E. & VORDONIS, A. Flexible floating structures providing for both coastal protection and wave energy exploitation and their integration in coastal management systems. Conference Proceedings on Energy Ocean, June 28-29 2004 2004 Florida, USA.

MYLONAS, E. M. An integral methodology for sustainable coastal zone management & development, via exploitation of multipurpose wave/wind energy capture & conversion platforms. Proceedings Cairo 10th International Conference on Energy and Environment, March 11-15, 2007 2007 Luxor, Egypt.

NAGAI, S. 1960. Shock pressures exerted by breaking waves on breakwaters. *Journal of Water Ways Harbour Division, America Society of Civil Engineers,* 86**,** 1-38.

NAKAMURA, S. & TSUCHIYA, Y. 1973. On shock pressure of surge on a wall. *Bulletin of the Disaster Prevention Research Institute,* 23(12)**,** 47–58.

NEELAMANI, S. & SANDHYA, N. 2003. Wave reflection characteristics of plane, dentate and serrated seawalls. *Ocean Engineering,* 30.

NEELAMANI, S. & SANDHYA, N. 2005. Surface roughness effect of vertical and sloped seawalls in incident random wave fields. *Ocean Engineering,* 32.

NEELAMANI, S., SCHUTTRUMPF, H., MUTTRAY, M. & OUMERACI, H. 1999. Prediction of wave pressures on smooth impermeable seawlls. *Ocean engineering,* 26 (1999)**,** 739-765.

NICHOLAS, J. & PROVERBS, D. G. 2002. Assessing flood damage to domestic dwellings: the present and future state of knowledge. *Construction Information Quarterly,* 4 (1)**,** 1-3.

OLESON, J. P., BRANDON, C., CRAMER, S. M., CUCITORE, R., GOTTI, E. & HOHLFELDER, R. L. 2004. The ROMACONS Project: a Contribution to the Historical and Engineering Analysis of Hydraulic Concrete in Roman Maritime Structures. *The International Journal of Nautical Archaeology,* 33**,** 199-229.

ORVIS, K. H. & GRISSINO-MAYER, D. H. 2002. Standardizing the Reporting of Abrasive Papers used to surface Tree-Ring Samples. *Tree-Ring Research,* 58 (1/2)**,** 47-50.

PALLANT, J. 2010. *SPSS Survival Manual – A step by step guide to data analysis using SPSS,* Open University Press, England, Mc Graw Hill, ISBN – 13: 978-0-33-524239-9.

PILARCZYK, K. W. 1998. Dikes and Revetments Design, Maintenance and Safety Assessment. *In:* A.BALKEMA, A. (ed.). Netherlands.

PLATE, E. J. Flood management as part of sustainable development. Proceedings International Symposium on River Flood Defence in: F. Toensmann and M. Koch, Kassel Reports on Hydraulic Engineering No 9/2000, 2000 Kassel, Germany.

RAFFEL, M., WILLERT, C. E. & KOMPENHAUS, J. 1998. *Particle Image Velocimetry – A Practical Guide,* New York, Springer Berlin Heidelberg, ISBN 3-540-63683-8.

RAMSDEN, J. D. 1993. *Tsunami: Forces On A Vertical Wall Caused By Long Waves, Bores, and Surges On A Dry Bed.* Ph.D., Civil Engineering, California Institute of Technology, USA.

RAMSDEN, J. D. 1996. Forces on a vertical wall due to long waves, bores, and dry-bed surges. *Journal of Waterway, Port, Coastal, and Ocean Engineering*.

REEVE, D., CHADWICK, A. & FLEMING, C. 2012. *Coastal Engineering Processes, theory and Design Practice*, Spon Press.

RICHERT, G. Model law for shock pressures against breakwaters. Proceedings of Coastal Engineering Conference, , 1968 London, UK.

RISK MANAGEMENT SOLUTIONS 2008. The 1908 Messina Earthquake: 100-Year Retrospective. *In:* RISK MANAGEMENT SOLUTIONS INC. SPECIAL REPORT (ed.). www.support.rms.com/publications/1908_Messina_Earthquake.

RISMILLER, G. R. 1989. *Dynamic Water Wave Pressures on a Re-curved Model Seawall.* MSc. Dissertation, Department of Ocean Engineering, Texas A & M University, USA.

RITTER, A. 1892. The propagation of water waves. *VDI Zeitschrift, Berlin,,* 36 (33) part 2**,** 947-954.

ROSS, C. W. 1955. Laboratory Study of Shock Pressures of Breaking Waves. *Beach Erosion Board, Technical Manual No. 59.*

RUNDGREN, L. 1958. Water Wave Forces. *Trans. of the Royal Institute of Technology, Bulletin No. 54.* Stockolm, Sweden.

SAKKAS, J. G. & STRELKOFF, T. 1973. Dam-break flood in a prismatic dry channel. *Journal of Hydraulic Division, ASCE,,* 99 (Hy12)**,** 2195-2216.

SAWARAGI, T. & IWATA, K. On Wave Deformation After Breaking. Proceedings of 14th Conference on Coastal engineering, ASCE, Vol. 1, Chapter 27, 1974.

SEFTON COUNCIL 2007. Report on Hard Sea Defences on the Sefton Coast. *Publication of Coastal Defence Unit, Sefton Council.* UK.

SHANKAR, N. J. & JAYARATNE, M. P. R. 2003. Wave run-up and Overtopping on smooth and Rough Slopes of Coastal Structures. *Ocean Engineering* 30 (2003)**,** 221-238.

SHORE PROTECTION MANUAL (SPM) 1984. Shore Protection Manual. *U.S. Army Coastal Engineering Research Centre.* U.S. Government Printing Office, Washington, D.C, Vol. II.

SHUTO, N. Standing waves in front of a sloping dike. Proceedings of the 13th Coastal Engineering Conference, 1982 Vancouver, BC, Canada. 1629-1647.

SHUTO, N. Tsunami Research – Its past, Present and Near Future. Proceedings of the 6th International Workshop on Coastal Disaster Prevention, December 1-2, 2009 Bangkok, Thailand.

SMITH, D. I. 1994. Flood damage estimation – A review of urban stage damage curves and loss functions. *Water SA,* 20 (3)**,** 231–238.

SOETANTO, R. & PROVERBS, D. G. 2004. Impact of flood characteristics on damage caused to UK domestic properties: the perceptions of building surveyors. *Structural Survey,* 22 (2)**,** 95 – 104.

SORENSEN, M. 2013. Critical functions and design criteria for geo-grids used in reinforced aggregate raft foundations for the Christchurch rebuild programme. Cirtex Industries Ltd, www.cirtex.co.nz.

SRIVASTAVA, A. & SIVAKUMAR BABU, G. L. 2009. Analysis and Design of Reinforced earth Wall for Shore Protection System against Tsunami. *Science of Tsunami Hazards,* 28 (3)**,** 186.

STEVENSON, T. 1874. *The Design and Construction of Harbours,* Edinburgh, UK, 2nd Edition.

STOKER, J. J. 1957. *Water Waves*, Interscience Publishers, New York.

SU, S. T. & BARNES, A. H. 1970. Geometric and frictional effects on sudden release. *Journal of Hydraulic Division, ASCE,,* 96 (11)**,** 2185-2200.

SUTHERLAND, J. & GOULDBY, B. Vulnerability of coastal defences to climate change. Proceedings of ICE, Water Management, 2003. 137-145.

SYNOLAKIS, C. E. 1987. The run-up of solitary waves. *Journal of Fluid Mechanics,* 185**,** 523-545.

TANIZAWA, K. The state of the art on numerical wave tank. 4th Osaka colloquium on sea-keeping, 2000 Osaka.

THE INDIAN SOCIETY OF HYDRAULICS 2013. Report on the National Conference on Hydraulics, Water Resources, Coastal and Environmental Engineering. *HYDRO 2012 – ISH NEWS, ISSN- 0971-5002.*

THOMAS, R. S. & HALL, B. 1992. *Seawall Design*, Butterworth Heinemann, ISBN 0 7506 1053 0.

THORNTON, E. B. & CALHOUN, R. J. Spectral resolution of breakwater reflected waves. Proceedings of A.S.C.E, 1972. 443-460.

THUSYANTHAN, N. I. & MADABHUSHI, S. P. G. Tsunami wave loading on coastal houses: A model approach. Proceedings of the Institution of Civil Engineers, Civil Engineering, 2008. ISSN 0965-089X, 77-86.

TWU, S. W., LIU, C. C. & HSU, W. H. 2000. Wave damping characteristics of deeply submerged breakwaters. *Journal of Waterways, Port, Coastal and Ocean Engineering,* 127 (2000)**,** 97-104.

UNITED NATIONS EDUCATIONAL SCIENTIFIC AND CULTURAL ORGANIZATION (UNESCO) 2009. UNESCO-IOC International Tsunami Interim Field Survey. *Report of UNESCO, Australian Tsunami Research Centre.*

UNITED STATES ARMY CORPS OF ENGINEERS (USACE) 2003. Coastal Engineering Manual. USACE, Part I-V.

USACE-CETN-III-8 1981. Seawalls – Their Applications and Limitations. *Coastal Engineering Technical Note (CETN).*

USACE 1995. Design of Revetments, Seawalls and Bulkheads. *EM 1110 – 2 -1614.*

VALLINGA, P. & KLEIN, R. J. J. 1993. Climate Change, Sea Level Rise and Integrated Coastal Zone Management: An IPCC Approach. *Ocean and Coastal Management,* 21**,** 245-268.

VAN DER MEER, J. W. 1997. Wave run-up and wave overtopping at dikes. *Report H2458/H3051.* Delft Hydraulics, Delft, The Netherland.

VAN DER MEER, J. W. & JANSSEN, J. P. F. M. Wave run-up and wave overtopping at dikes. *In:* KOBAYASHI, N., AND DEMIRBILEK, Z. , ed. Conference Proceedings of ASCE on Wave Forces on Inclined and Vertical Wall Structures, 1995 New York. 1-26.

VAN DER VEEN, A. & LOGTMEIJER, C. 2005. Economic hotspots: Visualizing vulnerability to flooding. *Natural Hazards,* 36 (1–2)**,** 65–80.

VAN DYKE, M. 1982. *An Album of Fluid Motion*, Parabolic Press.

VISCHER, D. L. & HAGER, W. H. 1998. *Dam Hydraulics,* Chichester, UK, Wiley.

WEGGEL, J. R. & MAXWELL, W. H. C. Experimental Study of Breaking Wave Pressures. Off-shore Technology Conference, Paper No OTC 1244, 1970 Texas.

WHILLOCK, A. F. 1987. Measurements of forces resulting from normal and oblique wave approaches to small-scale sea walls. *Coastal Engineering,* 11**,** 297-308.

WHITHAM, G. B. The effects of hydraulic resistance in the dam-break problem. Proceedings of Royal Society of London, Series A (227), 1955 London, UK. 399-407.

WHO. Floods: Climate Change and Adaptation Strategies for Human Health. Report on a WHO Meeting, June 30 to July 2, 2002, 2002 London, United Kingdom. WHO Regional Office for Europe, Copenhagen, Denmark.

WOOD, D. J. 1997. *Pressure-impulse Impact Problems and Plunging Wave Jet Impact.* Ph.D. Thesis, University of Bristol.

YEH, H. 2007. Design Tsunami Forces for On Shore Structure. *Journal of Disaster Research,* 2**,** 531-536.

YEH, H. H. 1991. Tsuanmi Bore Run-up. *Natural Hazards,* 4**,** 209-220.

YEH, H. H., GHAZALI, A. & MARTON, I. 1989. Experimental study of bore run-up. *Journal of Fluid Mechanics* 206**,** 563-578.

YIP, T. L., ZHANG, D. & CHWANG, A. T. Environmental and Safety Considerations for Design of a Perforated Seawall. Proceedings of the 12th International Offshore and Polar Engineering Conference,, May 26-31 2002 Japan.

ZHANG, Y. Improvement of flood risk management in Chin. Proceedings of the Second International Symposium on River Flood Defence, 10th – 13th September 2002 2002 New York, USA. Science Press New York Ltd, 438-450.

ZIMMERMANN, M., GLOMBITZA, K. & ROTHENBERGER, B. 2010. Disaster risk reduction programme for Bangladesh. *Swiss Agency for Development and Co-operative (SDC).* CH-3003, Bern: Directorate of Humanitarian Aid and SHA

APPENDICES

APPENDIX 1: The input data into the SPSS for model-A, model-B, model-C and model-D equations

Appendix 1.1: The input data into the SPSS for model-A

Trial	RDEPTH (m)	WSL (Cotθ)	Pmax (Measured) kPa	Pmax (Predicted) kPa
1	0.55	0.00	9.52	-
2	0.55	0.27	4.07	4.38
3	0.55	0.58	4.18	5.38
4	0.55	1.00	9.25	7.57
5	0.45	0.00	6.89	-
6	0.45	0.27	2.52	1.90
7	0.45	0.58	2.71	2.46
8	0.45	1.00	2.62	4.06
9	0.35	0.00	3.96	-
10	0.35	0.27	1.91	1.25
11	0.35	0.58	1.88	1.37
12	0.35	1.00	1.95	2.37
13	0.25	0.00	1.99	-
14	0.25	0.27	1.33	1.58
15	0.25	0.58	1.40	1.25
16	0.25	1.00	1.37	1.66
17	0.15	0.00	1.10	-
18	0.15	0.27	0.42	1.12
19	0.15	0.58	0.66	0.36
20	0.15	1.00	0.65	0.16

Appendix 1.2: The input data into the SPSS for model-B

Trial	RDEPTH (m)	WSL (Cotθ)	Pmax (Measured) kPa	Pmax (Predicted) kPa
1	0.55	0.00	9.09	-
2	0.55	0.27	4.35	3.91
3	0.55	0.58	4.52	3.97
4	0.55	1.00	3.56	3.71
5	0.45	0.00	7.13	-
6	0.45	0.27	2.62	3.04
7	0.45	0.58	2.95	3.12
8	0.45	1.00	2.58	2.86
9	0.35	0.00	4.14	-
10	0.35	0.27	2.14	2.16
11	0.35	0.58	1.90	2.27
12	0.35	1.00	2.05	2.02
13	0.25	0.00	2.07	-
14	0.25	0.27	1.19	1.27
15	0.25	0.58	1.31	1.42
16	0.25	1.00	1.39	1.17
17	0.15	0.00	0.90	-
18	0.15	0.27	0.42	0.34
19	0.15	0.58	0.65	0.56
20	0.15	1.00	0.52	0.32

Appendix 1.3: The input data into the SPSS for model-C

Trial	RDEPTH (m)	WSL (Cotθ)	Pmax (Measured) kPa	Pmax (Predicted) kPa
1	0.55	0.00	3.05	3.34
2	0.55	0.27	4.08	4.23
3	0.55	0.58	4.44	5.36
4	0.55	1.00	9.31	6.98
5	0.45	0.00	2.51	2.01
6	0.45	0.27	2.83	2.60
7	0.45	0.58	2.86	3.39
8	0.45	1.00	2.49	4.54
9	0.35	0.00	1.34	1.08
10	0.35	0.27	1.74	1.36
11	0.35	0.58	1.94	1.82
12	0.35	1.00	1.89	2.50
13	0.25	0.00	0.68	0.65
14	0.25	0.27	1.19	0.64
15	0.25	0.58	1.16	0.75
16	0.25	1.00	1.30	0.98
17	0.15	0.00	0.29	0.96
18	0.15	0.27	0.31	0.65
19	0.15	0.58	0.57	0.42
20	0.15	1.00	0.45	0.19

Appendix 1.4: The input data into the SPSS for model-D

Trial	RDEPTH (m)	WSL (Cotθ)	Pmax (Measured) kPa	Pmax (Predicted) kPa
1	0.55	0.00	9.25	8.21
2	0.55	0.27	4.52	5.35
3	0.55	0.58	4.43	4.36
4	0.55	1.00	3.25	3.00
5	0.45	0.00	7.14	6.38
6	0.45	0.27	2.57	3.60
7	0.45	0.58	3.07	3.27
8	0.45	1.00	2.62	2.37
9	0.35	0.00	4.14	4.56
10	0.35	0.27	1.77	1.93
11	0.35	0.58	1.97	2.33
12	0.35	1.00	2.00	1.74
13	0.25	0.00	1.98	2.73
14	0.25	0.27	1.29	0.43
15	0.25	0.58	1.25	1.61
16	0.25	1.00	1.25	1.12
17	0.15	0.00	0.96	0.90
18	0.15	0.27	0.44	0.67
19	0.15	0.58	0.57	1.27
20	0.15	1.00	0.52	0.49

APPENDIX 2: Linear ANOVA Outputs for model-A, model-B, model-C and model-D

Appendix 2.1: Linear ANOVA Output for Model -A

ANOVA[b]

Model		Sum of Squares	df	Mean Square	F	Sig.
1	Regression	84.682	2	42.341	14.461	.000[a]
	Residual	49.776	17	2.928		
	Total	134.458	19			

a. Predictors: (Constant), Hinc, WSL

b. Dependent Variable: Pmax

Appendix 2.2: Linear ANOVA Output for Model-B

ANOVA[b]

Model		Sum of Squares	df	Mean Square	F	Sig.
1	Regression	69.447	2	34.723	23.778	.000[a]
	Residual	24.825	17	1.460		
	Total	94.272	19			

a. Predictors: (Constant), Hinc, WSL

b. Dependent Variable: Pmax

Appendix 2.3: Linear ANOVA Output for model-C

ANOVA[b]

Model		Sum of Squares	df	Mean Square	F	Sig.
1	Regression	56.086	2	28.043	19.906	.000[a]
	Residual	23.949	17	1.409		
	Total	80.035	19			

a. Predictors: (Constant), Hinc, WSL

b. Dependent Variable: Pmax

Appendix 2.4: Linear ANOVA Output for model-D

ANOVA[a]

Model		Sum of Squares	df	Mean Square	F	Sig.
1	Regression	71.310	2	35.655	23.104	.000[b]
	Residual	26.235	17	1.543		
	Total	97.545	19			

a. Dependent Variable: Pmax

b. Predictors: (Constant), Hinc, WSL

APPENDIX 3: The MRA outputs indicating values of coefficients b_0, b_1, b_2, b_3, b_4, b_5, b_6 and b_7 for model-A, model-B, model-C and model-D

Appendix 3.1: The MRA outputs indicating values of coefficients in model-A equation

Parameter Estimates

Parameter	Estimate	Std. Error	95% Confidence Interval	
			Lower Bound	Upper Bound
b0	-.199	3642615.523	-7936577.635	7936577.236
b1	-.413	3.461	-7.953	7.128
b2	4.536	121.849	-260.951	270.023
b3	8.205	8.959	-11.315	27.724
b4	-.306	3629321.619	-7907612.813	7907612.201
b5	-4.091E-008	1.679	-3.659	3.659
b6	-.306	1880834.156	-4097985.895	4097985.283
b7	-.004	27080.989	-59004.410	59004.401

Appendix 3.2: The MRA outputs indicating values of coefficients in model-B equation

Parameter Estimates

Parameter	Estimate	Std. Error	95% Confidence Interval	
			Lower Bound	Upper Bound
b0	-.210	3.699	-8.143	7.724
b1	-.712	2.547	-6.174	4.749
b2	8.448	1.368	5.514	11.381
b3	-.012	.514	-1.114	1.091
b4	-2.410	27.884	-62.215	57.395
b5	-.352	1.629	-3.845	3.141

Appendix 3.3: The MRA outputs indicating values of coefficients in model-C equation

Parameter Estimates

Parameter	Estimate	Std. Error	95% Confidence Interval	
			Lower Bound	Upper Bound
b1	785.578	19817849.891	-43178600.021	43180171.177
b2	6296.417	10945672.517	-23842275.292	23854868.126
b3	11.028	5.021	.087	21.968
b4	-788.010	19817850.665	-43180175.296	43178599.277
b5	1.000	7.773	-15.936	17.936
b6	-6288.528	10945632.376	-23854772.777	23842195.721
b7	.997	4.946	-9.778	11.773
b0	4.840	25.663	-51.075	60.754

Appendix 3.4: The MRA outputs indicating values of coefficients in model-D equation

Parameter Estimates

Parameter	Estimate	Std. Error	95% Confidence Interval	
			Lower Bound	Upper Bound
b0	20.305	7.739	3.706	36.903
b1	-11.232	5.948	-23.990	1.525
b2	18.270	1.955	14.078	22.463
b3	10.135	8.505	-8.108	28.377
b4	-9.519	2.418	-14.705	-4.334
b5	-22.143	7.889	-39.063	-5.223

APPENDIX 4: Table showing transducer number that recorded the highest impact pressures

Appendix 4.1: Table showing the transducer's number that recorded the highest impact pressure values for wall model-A at varying orientations

r-depth (d_o), m	90 degree		75 degree		60 degree		45 degree	
	Max impact pressure, kPa	Transducer number	Max impact pressure, kPa	Transducer number	Max impact pressure, kPa	Transducer number	Max impact pressure, kPa	Transducer number
0.55	9.522115	1	4.073415	1	4.182891	1	9.246618	4
0.45	6.892416	1	2.522509	1	2.70953	1	2.616477	1
0.35	3.959378	1	1.906572	1	1.8839	2	1.950963	1
0.25	1.993376	1	1.330072	1	1.395821	1	1.372058	1
0.15	1.103886	1	0.424224	1	0.65686	1	0.646771	1

Appendix 4.2: Table showing the transducer's number that recorded the highest impact pressure values for wall model-B at varying orientations

r-depth (d_o), m	90 degree		75 degree		60 degree		45 degree	
	Max impact pressure, kPa	Transducer number	Max impact pressure, kPa	Transducer number	Max impact pressure, kPa	Transducer number	Max impact pressure, kPa	Transducer number
0.55	9.086493	1	4.351666	1	4.515880	1	3.557555	4
0.45	7.129614	1	2.618300	1	2.947585	3	2.577247	6
0.35	4.137276	1	2.139615	1	1.895268	1	2.048114	1
0.25	2.070921	1	1.190554	1	1.313714	1	1.386698	1
0.15	0.903180	1	0.424224	1	0.647393	1	0.524576	1

Appendix 4.3: Table showing the transducer's number that recorded the highest impact pressure values for wall model-C at varying orientations

r-depth (d_o), m	90 degree		75 degree		60 degree		45 degree	
	Max impact pressure, kPa	Transducer number	Max impact pressure, kPa	Transducer number	Max impact pressure, kPa	Transducer number	Max impact pressure, kPa	Transducer number
0.55	3.046177	1	4.081995	1	4.444240	1	9.306123	6
0.45	2.505045	1	2.834655	1	2.864620	3	2.492506	3
0.35	1.342836	1	1.743352	1	1.938467	1	1.886867	3
0.25	0.684003	1	1.190554	1	1.164043	1	1.304591	1
0.15	0.291665	1	0.305625	1	0.574753	1	0.451593	1

Appendix 4.4: Table showing the transducer's number that recorded the highest impact pressure values for wall model-D at varying orientations

r-depth (d_o), m	90 degree		75 degree		60 degree		45 degree	
	Max impact pressure, kPa	Transducer number	Max impact pressure, kPa	Transducer number	Max impact pressure, kPa	Transducer number	Max impact pressure, kPa	Transducer number
0.55	9.254128	1	4.519941	1	4.429212	3	3.248101	5
0.45	7.143298	1	2.568124	1	3.069888	1	2.623519	4
0.35	4.141838	1	1.774425	1	1.965149	1	1.997938	1
0.25	1.975130	1	1.286345	1	1.248995	1	1.254415	1
0.15	0.962479	1	0.437908	1	0.565630	1	0.520015	1

APPENDIX 5: Magnitude of maximum impact pressures at each of the six transducers and the plots of vertical distribution of maximum impact for wall model-C

Appendix 5.1: Magnitude of maximum impact pressures obtained for each of the six transducers at varying initial reservoir depths for wall-C model

	Pmax for the vertical (kPa)					Pmax at angle 75 degree (kPa)				
Transducer Number	r-depth 0.55m	r-depth 0.45m	r-depth 0.35m	r-depth 0.25m	r-depth 0.15m	r-depth 0.55m	r-depth 0.45m	r-depth 0.35m	r-depth 0.25m	r-depth 0.15m
1	3.0461	2.5051	1.3428	0.6840	0.2916	4.0819	2.8347	1.7434	1.1906	0.3056
2	1.7020	0.9932	0.6514	0.3916	0.0497	3.8754	2.5980	1.7307	1.0805	0.2070
3	1.0853	0.8535	0.5082	0.1974	0.0148	3.0719	2.2259	1.5097	0.6396	0.0675
4	1.0857	0.7721	0.3363	0.1185	0.0201	2.8500	1.9745	1.1200	0.3376	0.1119
5	0.8485	0.5786	0.2297	0.0212	0.0152	2.4578	1.6284	0.7625	0.1792	0.1016
6	0.8031	0.5074	0.1609	0.0097	0.0202	2.3437	1.2493	0.5799	0.1536	0.1077

	Pmax at angle 60 degree (kPa)					Pmax at angle 45 degree (kPa)				
Transducer Number	r-depth 0.55m	r-depth 0.45m	r-depth 0.35m	r-depth 0.25m	r-depth 0.15m	r-depth 0.55m	r-depth 0.45m	r-depth 0.35m	r-depth 0.25m	r-depth 0.15m
1	4.4442	2.8646	1.9385	1.1640	0.5748	9.3061	2.3081	1.8657	1.3046	0.4516
2	3.2968	2.4440	1.7596	0.9737	0.2071	4.2308	2.4925	1.8869	1.1775	0.3381
3	3.1249	2.3701	1.6013	0.6785	0.0531	3.0648	2.3221	1.6394	0.7597	0.1396
4	2.9957	2.2001	1.2496	0.4864	0.0688	2.9056	2.2289	1.4128	0.6928	0.0832
5	2.3900	2.0431	0.9174	0.3615	0.0470	2.3805	1.9337	1.1043	0.5866	0.0881
6	2.1581	1.6252	0.7312	0.1261	0.0940	2.2479	1.5977	0.9788	0.3974	0.1536

Appendix 5.2: Plots of vertical distributions of maximum impact pressures for wall model-C in vertical form

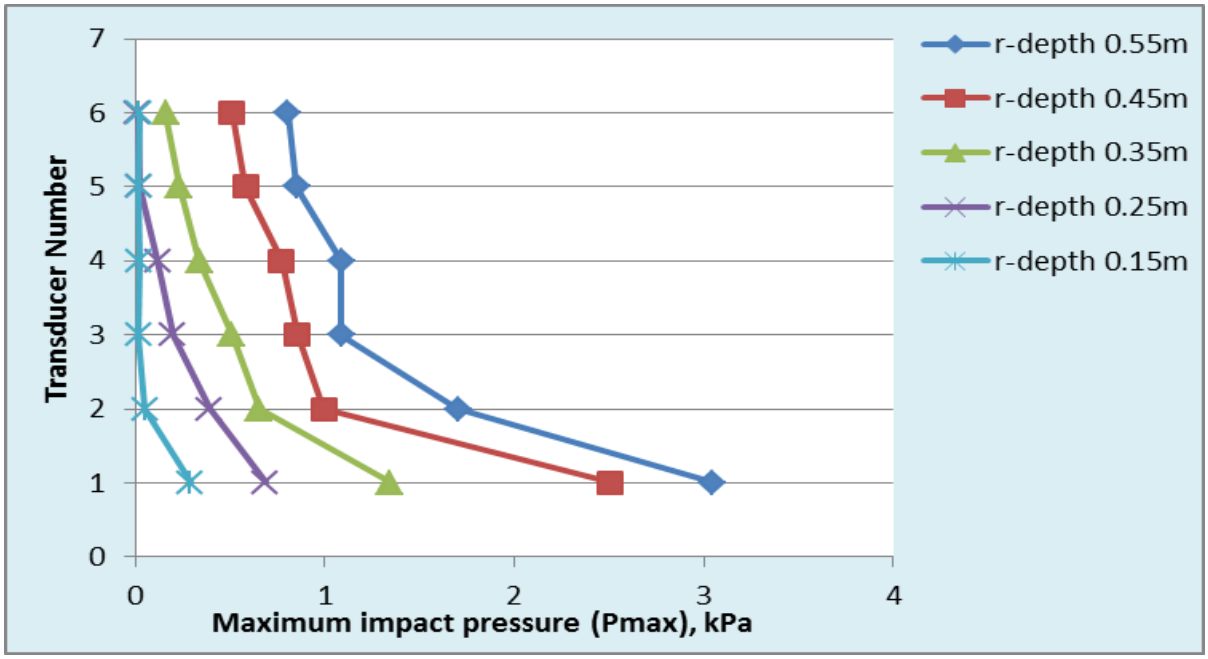

Appendix 5.3: Plots of vertical distributions of maximum impact pressures for wall model-C at 75 degree

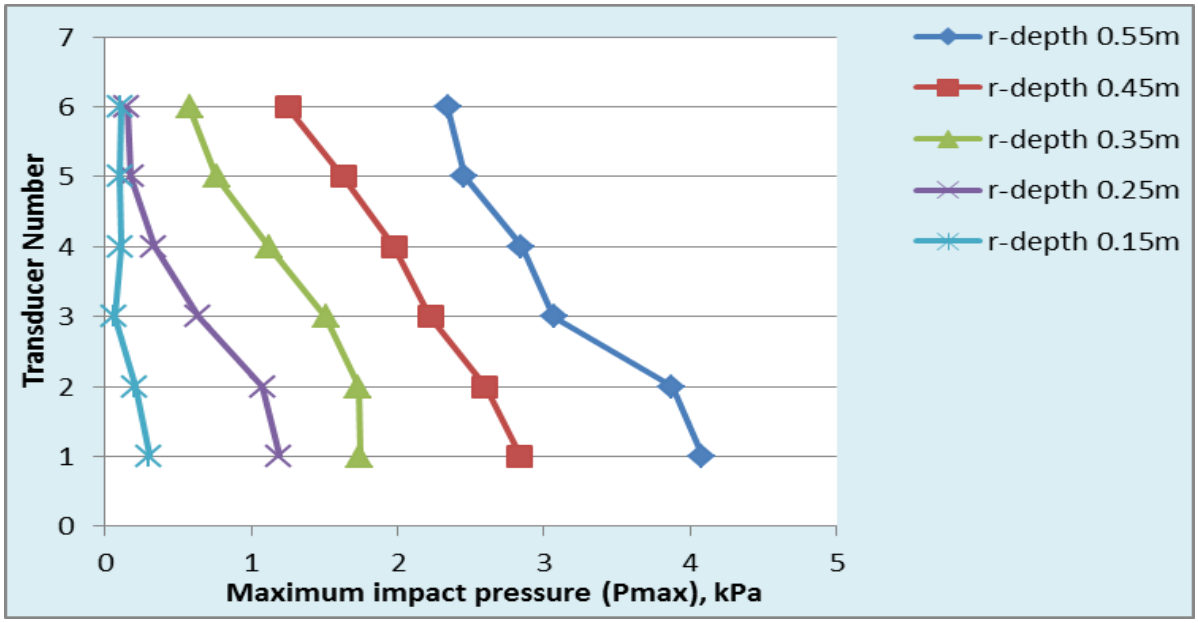

Appendix 5.4: Plots of vertical distributions of maximum impact pressures for wall model-C at 60 degree

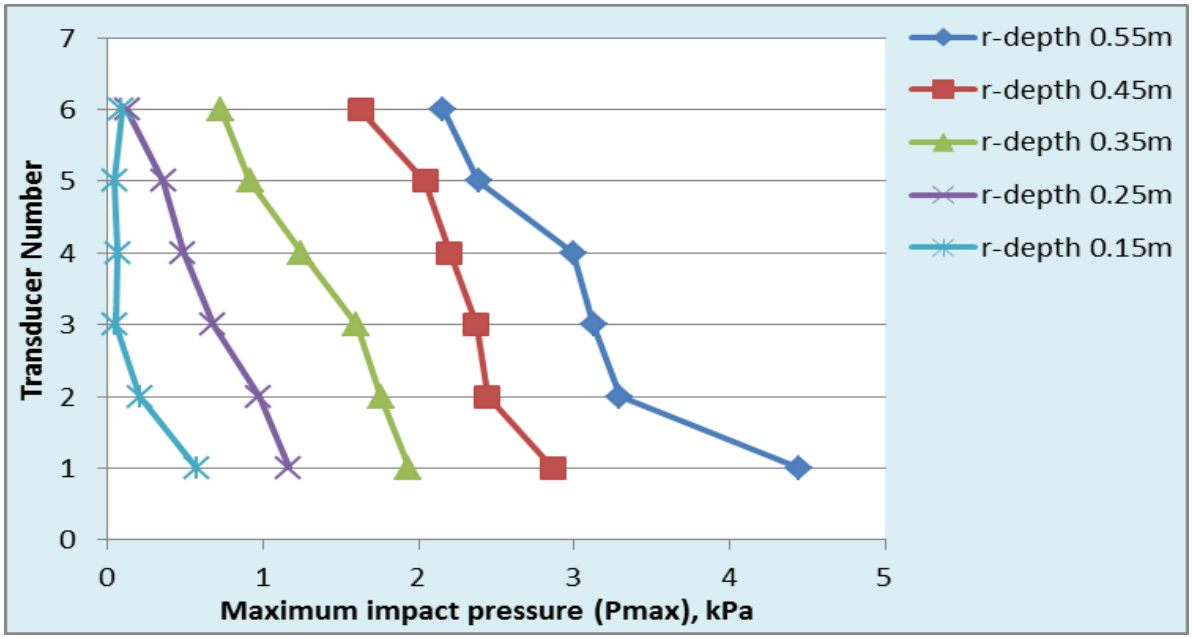

Appendix 5.5: Plots of vertical distributions of maximum impact pressures for wall model-C at 45 degree